Targeting endothelial cells to improve cancer therapy

Emma Louise Newport

Submitted in partial fulfilment of the requirements of the Degree of Doctor of Philosophy

April 2021

Adhesion and Angiogenesis Laboratory

Barts Cancer Institute

School of Medicine and Dentistry

Queen Mary University of London

Charterhouse Square

London EC1M 6BQ

United Kingdom

1 Statement of originality

I, Emma Louise Newport, confirm that the research included within this thesis is my own work or that where it has been carried out in collaboration with, or supported by others, that this is duly acknowledged below and my contribution indicated. Previously published material is also acknowledged below.

I attest that I have exercised reasonable care to ensure that the work is original, and does not to the best of my knowledge break any UK law, infringe any third party's copyright or other Intellectual Property Right, or contain any confidential material.

I accept that the College has the right to use plagiarism detection software to check the electronic version of the thesis.

I confirm that this thesis has not been previously submitted for the award of a degree by this or any other university.

Signature:

Date: 29/04/2021

2 Details of collaboration:

- Murine endothelial cell FAK kinase dead cytokine arrays were performed by Dr Delphine Lees from the Adhesion and Angiogenesis laboratory at Barts Cancer Institute, Queen Mary University of London, London, UK.
- Mass-Spectrometry data for the endothelial cell FAK kinase dead chapter were performed by Rita Pedrosa (Adhesion and Angiogenesis laboratory) and Pedro Casado (Cell Signalling and Proteomics lab).
- Marina Roy-Luzarraga, Adhesion and Angiogenesis laboratory, Barts Cancer Institute, Queen Mary University of London, London, UK, performed orthotopic pancreatic injection of TB32048 cells.
- ***29*** and ***29P*** were provided by the laboratory of Prof. Horst Kessler, Technische Universität München, Munich, Bayern, Germany.
- MTT assays on relative survival of A549 cells treated with ***29*** and gemcitabine *in vitro* were performed and included by kind permission of José Manuel Muñoz Félix, Barts Cancer Institute.

3 Details of relevant publications:

Demircioglu, F., Wang, J., Candido, J., Costa, A.S.H., Casado, P., de Luxan Delgado, B., Reynolds, L.E., Gomez-Escudero, J., **Emma Newport**, Rajeeve, V., Baker, A-M., Roy-Luzarraga, M., Graham, T.A, Foster, J., Wang, Y., Campbell, J.J., Singh, R., Zhang, P., Schall, T.J., Balkwill, F.R., Sosabowski, J., Cutillas, P.R., Frezza, C., Sancho, P., & Hodivala-Dilke, K. *Cancer associated fibroblast FAK regulates malignant cell metabolism*, in Nature Communications, 2020.

Emma Newport, Ana-Rita Pedrosa, Delphine Lees, Matthew Dukinfield, Edward Carter, Jesus Gomez-Escudero, Pedro Casado, Vinothini Rajeeve, Louise E Reynolds, Pedro Cutillas, Beatriz De Luxán Delgado, Kairbaan Hodivala-Dilke. *Elucidating the role of the kinase activity of endothelial cell focal adhesion kinase in angiocrine signalling and tumour growth* (Under re-review, *J. Pathol*)

4 Abstract

Antiangiogenic strategies have not provided the cancer control effects predicted from pre-clinical experiments. Obstacles include increasing hypoxia, reducing chemotherapy delivery and acquired resistance. Novel strategies to overcome these obstacles are thus warranted. In particular, exploiting endothelial cell-derived paracrine signalling (angiocrine signalling), manipulating blood vessel numbers and function whilst pursuing options of enhancing blood flow, chemo-delivery and reducing hypoxia become attractive possibilities. My PhD explores two such strategies:

Targeting angiocrine signalling to enhance chemosensitivity

Our laboratory's previously published work demonstrated that deletion of endothelial cell focal adhesion kinase (FAK) in mice with established subcutaneous tumour sensitised tumour cells to doxorubicin (Tavora, Reynolds, et al. 2014). This was through the alteration of endothelial cell signalling, known as angiocrine signalling. My experiments use *pdgfb-iCre^{ert};FAK$^{fl/fl}$;R26$^{K454R/K454R}$* mice, where kinase-dead endothelial cell FAK is expressed in tumour blood vessels *in vivo.* My results demonstrate that loss of EC-FAK kinase activity had no impact on the tumour growth of PBS treated, established subcutaneous B16F0 melanomas but was sufficient to reduce tumour growth in doxorubicin treated animals. This change in tumour growth occurs with no apparent effect on blood vessel density or doxorubicin delivery but reduced perivascular tumour cell proliferation and increased DNA damage and apoptotic area relative to blood vessel number *in vivo*. Additionally, loss of EC-FAK kinase activity and pharmacological FAK inhibition were both sufficient to affect doxorubicin-induced cytokine production *in vitro*. The results suggest that EC-FAK kinase activity is involved in altering cytokine production and in modulating chemosensitisation of tumour cells.

Testing the effect of a low dose of orally available vascular promotion agent 29P in enhancing chemosensitisation in pancreatic ductal adenocarcinoma.

Our laboratory previously published that increasing blood vessel density by treating mice with intraperitoneal injections of low doses of the cyclic Arg-Gly-Asp (RGD)-mimetic, Cilengitide, was sufficient to increase gemcitabine delivery and decrease hypoxia, thus reducing tumour growth in mouse models of pancreatic ductal adenocarcinoma (Wong et al. 2015). Here I tested the utility of a similar RGD-peptide ***29P*** that has been designed to be administered orally. I have carried out pilot *in vivo* experiments in various models

of PDAC, but due to technical difficulties, many of these data remain inconclusive. As part of dealing with these technical difficulties, I have also established a protocol for mouse pancreatic ductal adenocarcinoma

5 Acknowledgements

I would like to thank everyone who has helped me to make it through my PhD; it has been a huge challenge and has made me realise how wonderful the people around me are!

Firstly, thank you to my fantastic, inspiring supervisor, Kebs, for never-ending faith and support in and out of the lab and for creating such a positive, supportive lab group. I feel very lucky to have done my PhD in such a supportive environment.

I would like to thank the members of Kebs' group, Louise, Marina, Jose, Jesus, Rita, Gabi, Matt, Laura, Bea, Becca, Fevzi, Julie and Bruce. I feel so lucky to have been working with such a friendly, helpful and kind team over the last three and a bit years; thank you so much for all of your advice and friendly chats!

Thank you, Louise, for calmly pointing me in the direction of the best solutions to my disasters and panics. Thank you for helping me understand that I would probably survive a bad PCR!

Marina, thank you for being my lab big sister, for always being there through the blood, sweat and many tears of my PhD. Thank you for always being willing to take time out of the busiest days to dry my tears and tell me it would be okay.

Jesus, if you ever leave science, there is a great career out there for you as a motivational speaker. Thank you for your spontaneous lectures and funny but excellent advice!

Jose, thank you for sharing so much ***29P*** knowledge and advice and always being willing to help, talk through results and trek to the pharmacy with me.

Rita, thank you for all of your FAK expertise and willingness to share your beautiful protocols!

Laura, Alge and Katie, thank you for your hours of help with MRI, for your willingness to help troubleshoot at all hours for your constant patience.

Gabi and Bea, thank you for your never-ending patience and kindness and for always taking the time to help me in the lab.

Julie and Bruce, thank you for looking after my mice, for your great advice and incredible levels of organisation. I hope that some of your efficiency will rub off on me!

To ATS, thank you for always being willing to help out, whether arranged in advance or in a last-minute panic. Thank you for always being able to find the right screwdriver for an MRI and the right person to help with any problem.

To all of the members of Tumour Biology and Tumour Microenvironment, thank you for being so friendly and welcoming, sharing advice, reagents and weekend plans!

To Norah and all the donors and volunteers of the Barry Reed Cancer Research Fund, thank you for funding my PhD and for allowing me to do this work. Thank you for your interest in my work and for your support at the Barry Reed Cancer Research Fund events.

To my family, thank you for always supporting me, for always picking up the phone whatever time and letting me rant or cry when things went wrong and for being enthusiastic when things went right.

To Andy, thank you for your faith in me, for always finding me muddy fields when I needed them and for your ability to know when I desperately needed a funny animal video.

6 Contents

7 List of figures

8 List of tables

9 List of abbreviations

γH2AX-a variant of the H2A histone and marker of DNA damage

ΔΔCT-Delta delta cycle threshold

µl – Microlitre

129 Sv- inbred strain of agouti laboratory mouse

2-D-Two dimensional

3-D-Three dimensional

4-OHT-4-Hydroxytamoxifen

5-FU-5-Fluorouracil

A549- Human non-small-cell lung cancer cells

ABC- Strept (Avidin)–Biotin Complex

ABC transporter-ATP-binding cassette transporter

ACN Acetonitrile

ADMIDAS-Site adjacent to MIDAS

ANG1- Angiopoietin-1

ANG2-Angiopoietin-2

ANOVA – Analysis of Variance

APCs-Antigen presenting cells

APS – Ammonium Persulphate

Arf-ADP-Ribosylation factor

ATP-Adenosine triphosphate

B16F0 – Mouse melanoma cell line parental (C57bl6)

B2M – Beta 2 Microglobulin

BCA-bicinchoninic acid

Bregs-Regulatory B cells

BSA-Bovine Serum Albumin

C5-Complement component 5

C57Bl6J- Inbred strain of black laboratory mouse

CAFs-Cancer-Associated Fibroblasts

CAMs-Cell Adhesion Molecules

CATZ-Cathepsin X

CC3-Cleaved Caspase 3

CCL5-Chemokine (C-C motif) ligand 5

CCL7-Chemokine (C-C motif) ligand 7

CD4-Cluster of differentiation 4

CD8-Cluster of differentiation 8

CD31- Cluster of differentiation 31

CDA- Cytidine deaminase

cDNA – Complementary DNA

CFAH-Complement Factor H

chFAK-Chicken FAK

CNS-central nervous system

CNT3- Concentrative nucleoside transporter 3

CSCs- Cancer stem cells

CSL-CBF1, Suppressor of Hairless, Lag-1

CTLA4 Cytotoxic T-lymphocyte antigen 4

D218-Aspartate at position 218

D227-Aspartate at position 227

DAB- 3,3'-Diaminobenzidine

DAMPs-Danger/damage-associated molecular patterns

DAPI- 4',6-diamidino-2-phenylindole

DCK-Deoxycytidine kinase

DDT-Dichlorodiphenyltrichloroethane

DLL4Delta-like 4

DMEM – Dulbecco's Modified Eagle Media

DMSO – Dimethyl sulfoxide

DNA – Deoxyribonucleic acid

DT6066-KP pancreatic cancer cell line

E (number) – Embryonic day

EC-Endothelial Cell

ECL – Enhanced chemiluminescence

ECM-Extracellular Matrix

EDTA – Ethylenediaminetetraacetic acid

EGF-Epidermal growth factor

EMT- Epithelial-to-mesenchymal transition

ENT1- Equilibrative nucleoside transporter 1

ENT2- Equilibrative nucleoside transporter 2

EPC- Endothelial progenitor cell

EPR-Enhanced permeability and retention

ER-oestrogen receptor

ERT2- mutant form of the human oestrogen receptor

ES-embryonic stem

FACS-Fluorescence-activated Cell Sorting

FAK-Focal Adhesion Kinase

FAK-KO- Focal Adhesion Kinase knockout

FAK-KD- Focal Adhesion Kinase kinase-dead

FAT-Focal Adhesion Targeting

FDR-False discovery rate

FERM-4.1 Ezrin Radixin Moesin

FGF-Fibroblast growth factor

FGRS- FosB, Gfi1, Runx1 and Spi1

FOLFIRINOX- Folinic acid, 5-FU, Irinotecan and Oxaliplatin

FOXP3-Forkhead box P3

FWHM-full width at half maximum

GAPs-GTPase-activating proteins

GEFs-Guanine nucleotide exchange factors

GEM-Genetically Engineered Mouse

GFP-Green Fluorescent Protein

GM-CSF-Granulocyte-macrophage colony-stimulating factor

GO-Gene ontology

GT-Glanzmann thrombasthenia

GTPase-Guanosine triphosphatase

H and E- Hematoxylin and eosin

HCD-higher energy collisional dissociation

hDMEC- Human adult dermal microvascular Ecs

HEPES-4-(2-hydroxyethyl)-1-piperazineethanesulfonic acid

HEXB-Beta-hexosaminidase subunit beta

HIF- Hypoxia inducible factors

HPMEC- Human pulmonary endothelial cell

HS90A-Heat shock protein 90-alpha

Hr-Hour

HUVECs-Human umbilical vein ECs

IAM-Iodoacetamide

IC_{50}- Half maximal inhibitory concentration

ICD-Intracellular domain

iCre-improved Cre

Ig-Immunoglobulin

IgG- Immunoglobulin G

IMS- Methylated spirit industrial

IP-Intraperitoneal

Jag1-Notch Ligand Jagged-1

K454R- Mutation of lysine at position 454 to arginine

KD-Kinase Dead

KO-Knock Out

KP- *LSL-Kras$^{G12D/+}$;LSL-Trp53$^{R172H/+}$*

KPC- *LSL-Kras$^{G12D/+}$;LSL-Trp53$^{R172H/+}$*;Pdx-1-Cre

Kras-Kirsten Rat Sarcoma

ICAM- Intercellular Adhesion Molecule

iCre^{ert}-tamoxifen-inducible form of Cre recombinase

IFN-γ-Interferon-gamma

IFP-Interstitial fluid pressure

IL-1- Interleukin 1

IL-2-Interleukin-2

IL-4-Interleukin 4

IL-6-Interleukin 6

IL-17A-Interleukin 17A

IL-33-Interleukin 33

IP- IntraPeritoneal

IV – Intra-venous

LAP- Latency associated peptide

LC-liquid chromatography

LC-MS/MS- Liquid chromatography–mass spectrometry/mass spectrometry

LdCil – Low dose Cilengitide

LGR5-Leucine-rich G-protein-coupled receptor 5

LIMBS-Ligand-associated metal binding site

LoxP-locus of X-over P1

LP2-2 loxP sites

LSL-Lox-Stop-Lox

MaSCs-Mammary stem cells

M-CSF-Macrophage colony-stimulating factor

Mdm2- Mouse double minute 2

MDSCs-Myeloid-derived-suppressor cells

MGFs-mascot generic format files

MIDAS-Metal-ion-dependent adhesion site

ml – Millilitre

MLEC-Primary mouse lung endothelial cell

mFAK-Mouse FAK

mm – Millimetre

mM – Millimolar

MMPs-Matrix Metalloproteases

Mmu-Milli mass unit

MP-Membrane proximal

MRI-Magnetic Resonance Imaging

mRNA – Messenger ribonucleic acid

MS/MS-Tandem mass spectrometry

MTT – 3-(4,5-Dimethylthiazol-2-yl)-2,5-Diphenyltetrazolium Bromide

N-Cadherin-Neural Cadherin

NDS-Normal Donkey Serum

NETs-Neutrophil Extracellular Traps

NET-DNA-The DNA the makes up NETs

NK-Natural killer cells

NKT-Natural killer T cells

nM – Nanomolar

NSCLC-Non small cell lung carcinoma

OCT-Optimal Cutting Temperature compound

P (number)-Passage number of cells

P53- Tumor protein P53

PAK- p21-activated kinase

PanIn- Pancreatic intraepithelial neoplasia

PBS-Phosphate Buffered Saline

PCR-Polymerase Chain Reaction

PD-1-Programmed cell death protein 1

PDAC-Pancreatic ductal adenocarcinoma

PDGF-Platelet-derived growth factor

PD-L1-Programmed cell death ligand 1

PECAM- Platelet endothelial cell adhesion molecule

PGF- Platelet growth factor

Pgp-P-glycoprotein

$PI4,5P_2$- Phosphatidylinositol-4,5-bisphosphate

PIPKIγi2-phosphatidylinositol 4-phosphate 5-kinase Iγi2

PmT-Polyoma Middle T

Ppm-parts per million

PFS-Progression Free Survival

PSCs-Pancreatic stellate cells

PSI-Plexin-semaphorin-integrin

Pyk2-Protein tyrosine kinase 2

Q221-Glutamine at position 221

qPCR-Quantitative PCR

Rab-Ras-related in brain

RGD-Arg-Gly-Asp

Rgs5-G-protein signalling 5

RNA – Ribonucleic acid

RNA-seq – RNA-sequencing

ROI-Regions Of Interest

ROUT- Robust regression and outlier removal

RPM – Revolutions per minute

RS1-Transporter regulator 1

RT-Room Temperature

RT-qPCR-Quantitative Reverse Transcriptase Polymerase Chain Reaction

SAP-Serum amyloid P component

SCC-Squamous Cell Carcinoma

SCID-severe combined immunodeficient

Sem-Standard Error of the Mean

SH2-Src homology 2

sST2-soluble ST2

ST2-Interleukin 1 receptor-like 1

TAMs-Tumour Associated Macrophages

TB32048-KPC pancreatic cancer cell line

TFA-0.1 % Trifluoroacetic acid

TGF-β-Transforming growth factor-beta

TME-Tumour microenvironment

TE-Echo Time

TGFβ-Transforming growth factor β

TGFα -Transforming growth factor α

TH1-CD4+ T helper 1 cells

TH2- CD4+T helper 2 cells

TLCK-Tosyl-L-lysyl-chloromethane hydrochloride

TNF-α-Tumour Necrosis Factor α

TR-Repetition Time

Treg-Regulatory T cells

US-Ultrasound

V-CAM- Vascular cell adhesion protein

VE-cadherin-Vascular Endothelial Cadherin

VEGF-Vascular endothelial growth factor

VEGFR2-VEGF receptor 2

VPF- vascular permeability factor

VR2-VEGF-receptor 2

WT-Wildtype

w/v – Weight/Volume

XICs-Extracted ion chromatograms

Y194- Tyrosine 194

Y379- Tyrosine 379

Y861-Tyrosine 861

Y925-Tyrosine 925

10 Aims

1. **Establish whether the kinase activity of endothelial cell (EC) FAK is involved in doxorubicin induced angiocrine signalling and chemosensitisation in mouse models of cancer.**
    - Test the effect of endothelial cell FAK-kinase-dead mutation, using *pdgfb-iCre^{ert}; FAK$^{fl/fl}$; R26$^{K454R/K454R}$* mice, on tumour growth, with and without doxorubicin treatment, in the B16F0 model of mouse melanoma.
    - Examine the effect of the endothelial cell FAK-kinase-dead mutation on blood vessel numbers, blood vessel function and doxorubicin delivery.
    - Determine the effect of endothelial cell FAK-kinase-dead mutation on tumour cell proliferation, DNA damage and apoptosis.
    - Investigate the effect of FAK kinase inhibition on doxorubicin induced cytokine production of human pulmonary microvascular endothelial cells *in vitro*.

2. **Explore the utility of *29P* in combination with Gemcitabine in controlling pancreatic ductal adenocarcinoma in mice.**
    - Determine the best scheduling strategy for combination treatment of orally administered ***29P*** and gemcitabine mouse models of pancreatic ductal adenocarcinoma.
    - Explore the effect of ***29P*** treatment on tumour growth *in vivo*.

3. **Explore the use of murine pancreatic adenocarcinoma organoids for modelling pancreatic cancer *in vivo* and *in vitro***
    - Isolate and culture organoids from the tumours of KPC mice
    - Implant KPC organoids orthotopically into the pancreas of mice as a pilot of their use as an *in vivo* model of pancreatic cancer.

11 Introduction

11.1 Cancer and the tumour microenvironment

Cancer is an abnormal cell growth composed of a mixture of malignant and non-malignant cells with a non-cellular extracellular matrix (ECM) (Hanahan and Weinberg 2011). All malignant solid tumours are supported by a complex microenvironment, including blood vessels, immune cells and extracellular matrix (ECM). The tumour microenvironment (TME) is a highly complex body of cells interacting to support tumour growth. Despite therapies traditionally focusing on the cancer cells themselves, the crucial role of the cross-talk between cells in the TME and cancer cells is now widely recognised and increasingly the target of therapeutic intervention (Hui and Chen 2015). Features of the tumour microenvironment such as the level of hypoxia (Jing et al. 2019), immune cell infiltrate (Liu et al. 2017), blood vessel density (Wang, Xiong, et al. 2018; Tian et al. 2015), and expression of signalling proteins (Roy-Luzarraga and Hodivala-Dilke 2016; Wang 2017) can influence prognosis, progression and response to therapy making them promising drug targets (Wong et al. 2015; Wong, Bodrug, and Hodivala-Dilke 2016; Ramjiawan, Griffioen, and Duda 2017; Sunshine and Taube 2015; Jean et al. 2014).

11.1.1 The extracellular matrix of the tumour microenvironment

The extracellular matrix is a non-cellular network predominantly made up of collagens, proteoglycans, glycosaminoglycans, elastin, fibronectin and laminins (Theocharis et al. 2016). It acts as a physical scaffold for all the cells of the TME but, beyond this, also has a dynamic role in the development and spread of cancers (Balkwill, Capasso, and Hagemann 2012). The adhesion of cells to the ECM is an important stage in their movement in and out of the TME. There are also many chemokines and growth and angiogenic factors throughout the ECM that interact with cell surface receptors, further altering the properties of the TME (Frantz, Stewart, and Weaver 2010). Cancer-associated fibroblasts (CAFs) deposit substantial amounts of ECM making tumours generally stiffer than healthy tissues (Weigelt and Bissell 2008). The ECM is constantly changed and remodelled; matrix metalloproteases (MMPs) degrade the ECM proteins and are secreted and activated by malignant cells, tumour associated macrophages (TAMs) and CAFs. This remodelling by MMPs also releases chemokines and growth and angiogenic factors from the ECM (Balkwill, Capasso, and Hagemann 2012).

11.1.2 The lymphatic system in cancer

The lymphatic system is a system of vessels that transport antigen and antigen presenting cells (APCs) to lymph nodes where an adaptive immune response is mounted, the system also maintains fluid balance and carries lipid absorbed by the gut to the blood for circulation. However, it is also involved in cancer progression and metastasis as cancer cells can travel via lymph vessels to distant locations to form metastases. For this reason, lymph nodes are the most common sites in the body for solid tumour metastases. They are also predictive of poor prognosis (Padera, Meijer, and Munn 2016). It is thought that VEGF-C and VEGF-D produced by the tumour may increase the contraction of tumour proximal collecting lymphatic vessels resulting in increased lymph flow and promoting tumour cell transport to the lymph nodes (Zheng, Aspelund, and Alitalo 2014; Hoshida et al. 2006; Gogineni et al. 2013).

As in blood vessels (discussed later) the lymph vessels can be remodelled by tumours but when this is prevented, the metastasis to lymph nodes is reduced (Hoshida et al. 2006; Padera et al. 2008).

Through the lymph vessels, the primary tumour is able to promote the formation of a pre-metastatic niche in the lymph nodes so that when cancer cells reach them, they can rapidly form metastases. The ability to mount an immune response to the cancer cells is altered with pre-metastatic lymph nodes lacking lymphocytes(Padera, Meijer, and Munn 2016).

The enhanced permeability and retention (EPR) effect refers to the fact that certain types of molecules including nanoparticles, macromolecular drugs and liposomes typically accumulate more in tumour than normal tissue (Matsumura and Maeda 1986; Vasey et al. 1999). This difference is due to the pathophysiology of tumours compared to normal tissue. In normal tissue, low molecular weight drugs readily extravasate out of blood vessels while nanomedicines are too large to do so. In tumours, however, larger molecules are able to extravasate due to the larger gaps between endothelial cells. Therefore, more of these larger molecules accumulate. In addition, whereas in normal tissue, the lymphatic system drains accumulated molecules, in the tumour, there is minimal lymphatic drainage further increasing their accumulation in comparison to the situation in normal tissue (Torchilin 2011; Prabhakar et al. 2013; Maeda, Nakamura, and Fang 2013; Golombek et al. 2018).Desmoplasia

In wounded tissue, fibrosis, the deposition of connective tissue and proliferation of cells occurs, causing thickening and scarring of the tissue. This is important in the process of wound healing, although it can be extremely damaging when it is dysregulated (Henderson, Rieder, and Wynn 2020). Dvorak described cancer as the 'wound that does not heal' as it can have a constant production of fibrosis (Dvorak 1986). Chronic fibrosis diseases such as idiopathic lung fibrosis and epidermolysis bullosa are cancer risk factors for the tissues they impact (Guerra et al. 2017; Karampitsakos et al. 2017). The fibrosis surrounding a tumour, known as desmoplasia, is characterised by excessive production of ECM proteins and/or excessive proliferation of myofibroblast-like cells (Yen et al. 2002). It can vary between tumours from an excessive production of cells such as fibroblasts, vascular cells, and immune cells with minimal ECM to a dense, collagen-rich ECM with few cellular components, predominantly fibroblasts and myofibroblasts (DeClerck 2012). This results in a fibrous, dense tissue of both cellular and non-cellular elements surrounding the tumour. The ECM components typically include collagens, fibronectin, laminin and hyaluronan. Desmoplasia is also referred to as the desmoplastic reaction as it develops in response to signalling due to insults such as tumour development. Tumour epithelial cells and immune cells that infiltrate the desmoplasia signal through many different signalling molecules, including transforming growth factor β (TGFβ) and basic fibroblast growth factor (basic-FGF) to increase ECM deposition and platelet-derived growth factor (PDGF) to stimulate proliferation of myofibroblasts. Both the cellular and non-cellular components increase the pathogenesis of the tumour (Whatcott et al. 2012).

The desmoplastic reaction reduces the elasticity of the tumour, and this, in turn, increases the interstitial fluid pressure (IFP) of the microenvironment. Higher IFP hinders perfusion from the blood vessels reducing the delivery and, therefore, the efficacy of chemotherapeutics. For this reason, desmoplasia is significant in reducing chemotherapy efficacy in many tumour types (Heldin et al. 2004; Whatcott et al. 2012).

In tumours with dense desmoplasia such as breast and pancreatic, the proliferation of tumour cells imposes tensile forces on the surrounding ECM, which imposes forces on the tumour mass, constraining it. This increases the pressure and stored stress within the tumour and deforms structures within it, such as the blood and lymph vessels impairing the flow of fluid, increasing hypoxia and preventing the drainage of lymph. The interaction between the growing tumour increasing the pressure on the ECM and the ECM restricting the tumour growth creates tensile stress. This stress induces fibroblasts

to differentiate to myofibroblasts which, when activated, drive fibrosis, creating a feedback loop of increasing fibrosis and tensile stress (Kollmannsberger et al. 2018). The mechanical stress within the tumour also activates the Ret-β/catenin pathway in the tumour cells, a pathway which acts to increase tumour proliferation, invasion and epithelial-mesenchymal transition (EMT), leading to increased metastasis (Fernández-Sánchez et al. 2015).

Desmoplasia also triggers signalling cascades that increase resistance to chemotherapy; for example, non-cellular components of the desmoplasia stimulate the expression of the ATP-binding cassette (ABC) efflux transporter family of proteins. These transporters increase the efflux of drugs by tumour cells, and their presence increases drug resistance. The ABC transporters MDR1 or MRP1-6 allow cells to resist many hydrophobic chemotherapeutics such as doxorubicin, vinblastine, and paclitaxel by increasing their efflux out of the cell, thereby reducing the intracellular concentration (Borst et al. 1999). The binding of hyaluronan to its receptor (CD44) results in an increase in the MDR1 ABC transporter in breast, ovarian and pancreatic tumour cell lines through a Stat-3-mediated pathway (Bourguignon et al. 2008; Hong et al. 2009).

In pancreatic cancer, key regulators of the desmoplastic reaction are the pancreatic stellate cells (PSCs). PSCs are the primary source of fibrosis in pancreatic cancer stroma and interact with the cancer cells to produce a tumour microenvironment that favours growth and metastasis. When PSCs are activated in cancer, they undergo changes in their morphology and structure, allowing them to deposit ECM faster than it is degraded by the pancreas, meaning that the level of desmoplasia increases (Phillips 2012).

There is considerable variation in the levels of desmoplasia between tumour types. Pancreatic ductal adenocarcinoma (PDAC) is typically highly desmoplastic, with desmoplasia accounting for around 80 % of the tumour mass (Parente et al. 2018) and is typically hypovascularized (Katsuta et al. 2019). This high level of desmoplasia contributes to the challenges in treating it, and the level of desmoplasia correlates unfavourably with clinical outcome (Watanabe et al. 2003). PDAC is unusual in that, while many solid tumours are highly angiogenic, pancreatic cancer cells can secrete antiangiogenic factors, such as angiostatin and endostatin (Erkan et al. 2009). ECM deposition and pancreatic stellate cells further increase endostatin production by cancer cells, reducing the vasculature and contributing to a hypoxic microenvironment (Erkan et al. 2009; Ren et al. 2018).

In renal carcinomas, however, there is a range in levels of desmoplasia, papillary renal cell carcinoma usually has very low levels of desmoplasia, whereas medullary carcinoma typically has a pronounced desmoplastic reaction (Srigley and Delahunt 2009), but renal cell carcinomas tend to be highly vascularised (Zhang and Waxman 2013; Sciarra et al. 2008; Sawhney and Kabbinavar 2008).

11.1.3 Hypoxia in the tumour microenvironment

Most tumours have regions that are exposed, whether permanently or temporarily, to hypoxia due to the irregular vasculature causing insufficient blood supply (as discussed in more detail later) (Pouysségur, Dayan, and Mazure 2006).

This poor vasculature and high levels of hypoxia promote abnormal blood vessel development, increased desmoplasia and inflammation, each of which promotes tumour progression and resistance to therapy (Jing et al. 2019; Whatcott, Han, and Von Hoff 2015).

Late-stage cancers typically have hypoxic microenvironments leading to the activation of hypoxia-inducible factors (HIFs). Hypoxia has a substantial impact on both tumour cells and the other cells of the TME. Hypoxia promotes the expansion of more aggressive clones, leading to more lethal tumours from a heterogeneous population of tumour cells, which is associated with poor clinical outcome, the emergence of resistant clones, and the evasion of the immune system (Petrova et al. 2018; Vito, El-Sayes, and Mossman 2020).

The poor oxygenation of tumours also alters their metabolism, favouring glycolysis and lactic acid production. Lactic acid is acidic, and therefore, its excess production promotes an acidic microenvironment. Low intracellular pH of endosomes and lysosomes is thought to aid the activation of proteases assisting in metastasis. In addition, acidic pH blocks the activation of T-cells and therefore, neutralising the acidity of tumours has been effective in enhancing immunotherapy in subcutaneous mouse models of cancer (Pilon-Thomas et al. 2016).

11.1.4 The immune component of the tumour microenvironment

The immune system plays a vital role in the tumour microenvironment, with both tumour suppressive and pro-tumourigenic immune cells infiltrating to various degrees. The immune cell infiltration is strongly influenced by other ECM features, especially the level of hypoxia of the tumour (Petrova et al. 2018). Hypoxic tumour microenvironments are

thought to particularly favour immune tolerance, whereas the immune infiltrate of a normoxic TME is more tumour suppressive, although there is evidence that, under certain circumstances, hypoxia can induce immunogenic cell death (Vito, El-Sayes, and Mossman 2020). Examples of immune cells that play an important role in the tumour microenvironment are listed below.

11.1.4.1 T lymphocytes

There are a range of T lymphocyte populations within the TME with both pro-tumourigenic and tumour suppressive characteristics. CD8+ memory T cells are associated with a good prognosis; they have already come into contact with tumour antigens and have the capacity to kill tumour cells (Fridman et al. 2012). Hypoxic tumour microenvironments inhibit CD8+ T cell lysis of tumour cells contributing to a worsened prognosis in hypoxic tumours (Vuillefroy de Silly, Dietrich, and Walker 2016). CD8+ T cells are supported by CD4+ T helper 1 (TH1) cells which produce the cytokines interleukin-2 (IL-2) and interferon-gamma (IFN-γ) and are also associated with a good prognosis (Fridman et al. 2012). However, other CD4+ lymphocytes produce cytokines with a detrimental impact. T helper (TH2) cells support B cells by producing the cytokines IL-4, IL-5 and IL-13 and TH17 cells, produce the cytokines IL-17A, IL-17F, IL-21 and IL-22, which are associated with tissue inflammation. Both of these T cell populations are generally associated with increased tumour growth (Fridman et al. 2012; Balkwill, Capasso, and Hagemann 2012).

The forkhead box P3 (FOXP3) and CD25 expressing CD4+ T lymphocytes, regulatory T cells (Tregs), are most commonly associated with poor prognosis, and this has been documented in many cancer types (Bates et al. 2006; Curiel et al. 2004; Hiraoka et al. 2006; Balkwill, Capasso, and Hagemann 2012). These cells produce IL-10, transforming growth factor-beta (TGF-β) cell-mediated contact through cytotoxic T-lymphocyte antigen 4 (CTLA4), which cause an immunosuppressive phenotype by inhibiting the recognition and clearance of tumour cells by tumour suppressive immune cells (Campbell and Koch 2011; Balkwill, Capasso, and Hagemann 2012). However, in some cases, such as Hodgkin's Lymphoma, Tregs can have a tumour suppressive effect, correlating with improved prognosis (Fozza and Longinotti 2011; Koreishi et al. 2010; Tzankov et al. 2008).

11.1.4.2 B lymphocytes

B cells have both pro - and anti-tumourigenic responses. In certain breast and ovarian cancers, they are associated with a good prognosis (Coronella et al. 2001; Milne et al. 2009), but in mouse models, they inhibit the anti-tumour action of CD8+ T cells (Qin et al. 1998). The regulatory B cells (Bregs) produce the cytokine IL-10 and, in inflammation-induced skin cancer, they inhibit anti-tumour immune responses and increase tumour burden (Schioppa et al. 2011; Mauri and Bosma 2012). The pro-tumorigenic effects of Bregs seem to be due to their effect on other immune cells in lymphoid tissue or lymph nodes rather than through infiltration of the TME (Schioppa et al. 2011).

In clinical metastatic melanomas, the co-occurrence of tumour-associated CD8+ T cells and CD20+ B cells correlates with improved survival independent of all other clinical variables (Cabrita et al. 2020). The presence of tertiary lymphoid structures have been found to be predictive of improved survival and response to immune checkpoint blockade in melanoma and sarcoma (Cabrita et al. 2020; Petitprez et al. 2020; Helmink et al. 2020).

11.1.4.3 NK and NKT cells

Natural killer (NK) and natural killer T (NKT) cells are innate cytotoxic lymphocytes that infiltrate the tumour stroma but are not found in direct contact with the tumour cells (Balkwill, Capasso, and Hagemann 2012; Tachibana et al. 2005). They are often associated with improved prognosis (Balkwill, Capasso, and Hagemann 2012). Hypoxia is known to inhibit NK-mediated lysis (Solocinski et al. 2020).

11.1.4.4 Tumour-associated macrophages

Tumour-associated macrophages (TAMs) are broadly pro-tumourigenic and are observed at high levels in most human and mouse experimental cancers. They facilitate malignant cell migration, invasion, metastasis and angiogenesis (Qian and Pollard 2010; Balkwill, Capasso, and Hagemann 2012). Both pre-clinically and clinically, they are associated with poor prognosis (Bingle, Brown, and Lewis 2002). TAMs have different subpopulations, including invasion-associated TAMs, which are enriched for molecules involved in Wnt signalling promoting vascular remodelling. They also promote motility and intravasation in the surrounding tumour cells linking angiogenesis, Wnt signalling and tumour invasion (Ojalvo et al. 2010).

11.1.4.5 Myeloid-derived suppressor cells

MDSCs are a phenotypically diverse population of cells that expand dramatically under conditions of cancer, inflammation and infection. They have a strongly suppressive response to T-cell mediated cell killing (Gabrilovich and Nagaraj 2009). They have the capacity to differentiate into TAMs (Kusmartsev, Nagaraj, and Gabrilovich 2005) and to cause the development of Tregs (Huang et al. 2006) or the polarisation of macrophages into a TAM phenotype (Sinha et al. 2007).

11.1.4.6 Dendritic cells

Dendritic cells are antigen-presenting cells but are thought to be defective in the case of cancer. They do not stimulate a robust immune response to tumour antigens. Dendritic cells are particularly responsive to hypoxia and inflammation, and the high levels in the TME impair their function, some even suppressing T cell activity (Balkwill, Capasso, and Hagemann 2012).

11.1.4.7 Tumour-associated neutrophils

Tumour-associated neutrophils have been shown to promote angiogenesis (Nozawa, Chiu, and Hanahan 2006) and to enhance primary tumour growth in mouse models of cancer (Pekarek et al. 1995), they also lead to degradation of the ECM and immune suppression (Balkwill, Capasso, and Hagemann 2012). However, there is also evidence that a population of tumour-associated neutrophils can eliminate tumour cells in the early stages of metastasis (Granot et al. 2011) and inhibit TGF-β, further contributing to the tumour suppressive quality (Friedlander et al. 1995; Balkwill, Capasso, and Hagemann 2012).

Neutrophil extracellular traps (NETs) also have an important role in cancer. They are made up of chromatin filaments of DNA coated in granule proteins. They are a component of the innate immune system that functions to trap microorganisms (Brinkmann et al. 2004; McDonald et al. 2012; Fuchs et al. 2007). The DNA the makes up NETs (NET-DNA) has a role in promoting metastasis of cancer mouse models (Tohme et al. 2016; Cools-Lartigue et al. 2013; Cedervall, Zhang, and Olsson 2016). It is a chemoattractant for cancer cells. The NETs in liver and lungs attract cancer cells but rather than trapping them, the cells form metastases. In the clinical setting too, NETs are found to be abundant in liver metastases of breast and colon cancer patients. The level of NETs in the serum are also predictive of liver metastases in early-stage breast cancer (Yang et al. 2020; Nolan and Malanchi 2020).In fact, neutrophils have been identified as

the main driver of metastatic establishment in the pre-metastatic niche of the lung in mouse breast cancer models. By blocking the recruitment of neutrophils to the pre-metastatic niche of murine breast cancer models can reduce the development of metastases (Wculek and Malanchi 2015).

11.1.4.8 Cancer-associated fibroblasts

CAFs play an important role in the tumour microenvironment; their functions include matrix deposition and remodelling as well as contributing to immune escape of tumours through cytokine and chemokine secretion, recruitment and functional differentiation of innate and adaptive immune cells and preventing the function of infiltrating leukocytes (Sahai et al. 2020; Monteran and Erez 2019). Overall they promote cancer cell growth and invasion, and their interaction with tumour cells is important in cancer progression, making them a valuable drug target (Xing, Saidou, and Watabe 2010). They are strongly influenced by the conditions of the tumour microenvironment; for example, under conditions of hypoxia and low pH, they produce reactive oxygen species (ROS), which act as a mutagen, increasing the tumourigenicity of surrounding tumour cells (Xing, Saidou, and Watabe 2010; Yuan and Glazer 1998).

11.1.4.9 Cancer immunotherapy

Immunotherapy is the stimulation or suppression of specific immune cells or immune populations to treat cancer. This is a fast-developing field, and there is a diverse range of techniques for the manipulation of the immune system being developed. However, as many techniques focus on the activation or suppression of specific immune cells, a favourable immune microenvironment is essential, requiring the presence of tumour suppressive immune cells (Steven, Fisher, and Robinson 2016).

A commonly used technique is immune checkpoint blockade. Immune checkpoints are mechanisms to modulate the duration and intensity of an immune response, preventing activated T cells from causing excessive damage from inflammation and autoimmunity in surrounding healthy tissue. Checkpoint blockade is the pharmacological inhibition of checkpoint proteins making T cells more active and able to target cancer cells. Programmed cell death-1 (PD-1) is a protein found on the surface of T cells that promotes self-tolerance through its interaction with its ligand programmed cell death ligand 1 (PD-L1) on other cells. PD-L1 is highly expressed on many cancer cells promoting tolerance of the immune system. It is expressed in tumour cells in around 50 % of NSCLC (Steven, Fisher, and Robinson 2016), whereas in PDAC, reports vary on the level of expression (Lu

et al. 2017; Lutz et al. 2014). Directing antibodies against PD-1 or PD-L1 has been effective in improving the immune response against the tumour both as a single agent and in combination with other therapies (Sunshine and Taube 2015; Brahmer et al. 2010).

11.2 Blood vessel development in health and disease

11.2.1 Endothelial cells

Endothelial cells (ECs) are squamous cells with an apical-basal polarity, strongly connected by tight and adherens junctions (Medici and Kalluri 2012). These cells form the inner surface of blood and lymphatic vessels and are essential in the structure and remodelling of this network of vessels connecting the heart to all other organs allowing the exchange of nutrients (Adams and Alitalo 2007; Piera-Velazquez, Mendoza, and Jimenez 2016; Ursoli Ferreira et al. 2019). However, endothelial cells are highly diverse, with heterogeneity in cell morphology, function, gene expression, and antigen composition dependent on vessel size and growth conditions (Aird 2012). Endothelial cells are far from static structural cells forming conduits for blood and lymph. They regulate vascular permeability, maintaining fluid homeostasis and host defence by dynamic control of intercellular junctions (Sukriti et al. 2014) and regulating vascular tone through the release of relaxing and contracting factors that stimulate smooth muscle cell movement (Feletou, Tang, and Vanhoutte 2008). Their position, lining the blood vessels, puts endothelial cells at the interface between the immune and vascular systems (Sturtzel 2017). They transport immune cells, form a barrier against pathogens, regulate the recruitment of immune cells and control the extravasation of leukocytes at sites of inflammation through control of the adhesion molecules E-selectin, P-selectin, Intercellular Adhesion Molecule 1 (ICAM) or Vascular cell adhesion protein 1 (V-CAM) (Vestweber 2012). In addition, endothelial cells can signal in a paracrine fashion known as angiocrine signalling (Sturtzel 2017).

11.2.2 Angiocrine signalling

Beyond the roles of endothelial cells directly in vascular maintenance, endothelial cells' contact with the blood stream puts them in a position to sense signals from the blood and to deploy signals to the rest of the body. This paracrine and juxtracrine signalling occurs through angiocrine factors, a broad range of molecules that are secreted from endothelial cells, including stimulatory and inhibitory growth factors, chemokines,

cytokines, components of the extracellular matrix and exosomes (Rafii, Butler, and Ding 2016). They are produced by tissue-specific endothelial cells and have roles in guiding organ regeneration as well as maintenance of metabolism and homeostasis (Rafii, Butler, and Ding 2016). The release of these angiocrine factors is important in stimulating the differentiation of tissue-specific resident stem and progenitor cells to allow them to populate and regenerate a site of injury (Rafii, Butler, and Ding 2016).

11.2.2.1 Angiocrine signalling and cytokines

Angiocrine signalling by cytokine production is especially relevant to this thesis as the cytokine production of endothelial cells in response to doxorubicin is altered by FAK KO (Tavora, Reynolds, et al. 2014). Cytokines are defined as 'small secreted proteins released by cells have a specific effect on the interactions and communications between cells' (Zhang and An 2007). Cytokines have wide-ranging functions in cancer, both tumour suppressive and tumour promoting roles. Some cytokines have roles in the control of infection, inflammation and immunity and, through these, aid the host in suppressing the tumour. However, other cytokines have tumour promoting effects, acting to promote tumour growth and increase apoptosis resistance (Dranoff 2004). Cytokines rarely work in isolation but in concert with whole profiles of cytokines out of balance in cancer development (Dranoff 2004).

11.2.2.2 Juxtacrine signalling

Juxtacrine signalling is the communication between cells by proteins from one cell interacting with receptors on another cell without diffusion of signals. This may be by the protein on one cell-binding directly to the receptor on another, a receptor on one cell binding to a ligand on the ECM secreted by another cell or a signal transmitted from the cytoplasm of one cell to another through small conduits in the cell membranes (Gilbert and Sunderland 2000).

One of the most well-known examples of juxtacrine signalling is the Notch signalling pathway, which is important in a wide range of developmental processes across many organs and cell types, including hematopoiesis and somitogenesis vasculogenesis, and neurogenesis (Lasky and Wu 2005). Notch is a cell surface receptor with a single transmembrane domain; when a Notch receptor on one cell interacts with a Notch ligand, such as Delta (Delta-like in humans), on an adjacent cell, signalling is initiated. The interaction triggers the release of the Notch intracellular domain (ICD), freeing it to translocate to the nucleus. Within the nucleus, the ICD binds to the transcriptional

regulator CSL (CBF1, Suppressor of Hairless, Lag-1), displacing co-repressors previously bound to CSL and allowing the recruitment of co-activators. This leads to the activation of downstream signalling for a wide range of functions within the cell that has received the signal (Lasky and Wu 2005). For Notch signalling to be productive, the Notch much be on a neighbouring cell to the ligand. When the receptor and ligand are on the same cell, the activation is inhibited, controlling whether a cell will signal (when the ligand is more abundant than Notch) or receive signals (when Notch is more abundant than the ligand) (Sprinzak et al. 2010).

Notch signalling plays a role in several juxtacrine signalling mechanisms by endothelial cells. For example, in fetal development, juxtacrine Notch signalling by ECs is vital in specifying haematopoietic stem cells' development (Nguyen et al. 2014). Endothelial niche-derived angiocrine signals are essential for the direct conversion of adult ECs into haematopoietic cells. The minimal set of transcription factors required to that reprogram full-term human umbilical vein ECs (HUVECs) and human adult dermal microvascular ECs (hDMEC) into hematopoietic cells are FosB, Gfi1, Runx1 and Spi1 (collectively termed FGRS) (Sandler et al. 2014). However, when ECs are FGRS-transduced, they fail to convert to engraftable haematopoietic cells unless they are cultured in constant, direct contact with ECs. This is because angiocrine signalling through the Notch receptor is required in the differentiation of haematopoietic stem cells (Rafii, Butler, and Ding 2016; Sandler et al. 2014).

11.2.3 The blood vascular system

A vascular system composing a network of blood and lymphatic vessels that supply the organs with nutrients and remove waste products is common to all vertebrate life. Herein, we discuss the role of the blood vasculature network.

The blood vasculature comprises two hierarchically arranged systems, arterial (bringing oxygenated, nutrient-dense blood to the organs) and venous (returning nutrient-depleted blood and waste products to the heart). Within the venous system, vessels decrease in size as veins branch to venules, followed by capillaries. Similarly, in the arterial system, arteries branch to smaller arterioles before meeting the venous system with capillaries (Dudley 2012; Red-Horse and Siekmann 2019).

Blood vessels are composed of endothelial cells surrounded by and basement membrane with supporting mural cells (pericytes and smooth muscle cells) (Baluk, Hashizume, and McDonald 2005). In health, blood vessels are organised hierarchically from simple,

adaptable vessels up to more complex, highly stabilised vessels. The smallest blood vessels are capillaries, which are composed of a single layer of endothelial cells enabling easy transfer of metabolites and nutrients (Tucker, Arora, and Mahajan 2020). Capillaries are highly adaptable vessels stabilised by pericytes. In contrast, more established vessels are less adaptable and are supported by smooth muscle cells (Tucker, Arora, and Mahajan 2020).

Pericytes project finger-like processes that wrap around capillaries stabilising the smallest blood vessels and share the basement membrane with endothelial cells. In vascular development, pericytes are highly motile, allowing appropriate organisation on the developing vessel and adequate pericyte coverage of the endothelial cells. In fact, even in the adult brain, capillary pericytes of the adult mouse cortex have dynamic processes able to extend and retract over days, although their somata are immobile. In addition to this scaffolding role, their location on the capillaries enables them to communicate with endothelial cells through direct physical contact and paracrine signalling (Baluk, Hashizume, and McDonald 2005) as well as through gap junctions direct from endothelial cells to pericytes allowing the transfer of ions and small molecules (Bergers and Song 2005). In contrast, to capillaries, larger vessels such as arterioles and arteries are surrounded by smooth muscle cells, which encircle the endothelial cells providing stability and regulating vessel diameter through their expression of contractile proteins. Like pericytes, they can also signal to the endothelium through juxtacrine and paracrine signalling (Dudley 2012). In between pericytes and smooth muscle cells, there are mural cell types that have features of both pericytes and smooth muscle cells (Grant et al. 2019).

All blood vessels are also surrounded by a basement membrane, a form of extracellular matrix composed of collagen IV, laminin and fibronectin (Baluk et al. 2003). This provides additional support and stability and can also interact with integrins expressed on the EC surface to contribute to signalling (Dudley 2012; Hynes 2009).

In addition to the structural diversity dependent on vessel size and position within the hierarchical arrangement, vessels and their component cells are also highly specialised to their tissue and organ location. For example, the endothelium of the blood brain barrier is highly specialised to restrict the passage of solutes into the central nervous system, so it is densely populated with junctional proteins. Whereas the blood vessels that form the glomerulus of the kidney, a tuft of capillaries specialised to filter blood to

form urine, are much more porous (Dudley 2012). The surrounding basal membrane is also highly adaptive, complementing these blood vessels' roles in different organs. The basal membrane of the endothelium and the brain astrocytes merge at the interface between blood and brain, reinforcing the tight junction barrier formed by endothelial cells. The basal membrane at the blood brain barrier controls the transport of solutes between blood and brain. In the kidney, the basal membrane prevents plasma leakage into the urine. Still, the network of laminin and collagen is also thought to act as a selective filter controlling the porosity by selecting for size and charge of the proteins that pass through (Jayadev and Sherwood 2017).

There are many different mechanisms for blood vessel development and maintenance, creating this diversity of vascular structure. New blood vessel development is an essential process in vertebrate growth and maintenance, which are required to provide growing tissues with nutrients and oxygen. Blood vessels develop rapidly in embryonic growth, and their growth and repair are essential throughout adult life. However, in adult life, most new blood vessel development happens as in short-lived transitory phases necessary for wound repair (Tonnesen, Feng, and Clark 2000) and maintenance of the menstrual cycle (Maybin and Critchley 2015) but rarely persists for more than two weeks (Ribatti 2013). Growth factors and cell adhesion proteins orchestrate the diverse processes of blood vessel development and maintenance.

11.2.4 Growth factors in angiogenesis

Over 20 different growth factors drive the formation of new blood vessels by angiogenesis (Ucuzian et al. 2010; Hanahan and Weinberg 2011). Of these, basic fibroblast growth factor (basic-FGF) and vascular endothelial growth factor (VEGF-A) are most commonly studied.

Basic-FGF and VEGF-A are produced by many cell types, including tumour cells and stimulate angiogenesis. VEGF-A increases permeability and dilation of the existing blood vessels and degrades the ECM by upregulating the expression of matrix metalloproteases (MMPs) (enzymes responsible for degrading the ECM) to allow endothelial cell migration (Bergers et al. 2000). Basic-FGF also stimulates ECM degradation and endothelial cell proliferation (Presta et al. 2005). Inflammatory cytokines play a role in the ECM remodelling; for example, the cytokines Tumour Necrosis Factor (TNF)-α and interleukin (IL)-1 are produced by many tumour cells and tumour associated macrophages. These maintain the expression of basic-FGF and VEGF-A allowing continued ECM remodelling

but also stimulate ECM remodelling and production of MMPs in their own right (Francavilla, Maddaluno, and Cavallaro 2009). This ECM remodelling and basement membrane degradation allow endothelial tip cells to migrate and proliferate in the matrix extending the nascent blood vessel (Hillen and Griffioen 2007). To allow the blood vessels to grow, pro-angiogenic factors regulate the expression and function of adhesion molecules on endothelial cells.

11.2.4.1 Vascular endothelial growth factor (VEGF)

VEGF is a family of growth factors belonging to the PDGF family. VEGFs have diverse roles in the vasculature.

The VEGF family includes VEGF-A, VEGF-B, VEGF-C, VEGF-D and the placental growth factors (PlGF1, 2,3 and 4) and have diverse roles in blood and lymph vessel development. Among their functions, VEGF-A and platelet growth factor (PGF) are linked to tumour angiogenesis. VEGF-B is important in maintaining nascent blood vessels, VEGF C and D have roles in both angiogenesis and lymphangiogenesis, and VEGF-A and C control vascular permeability (Ramjiawan, Griffioen, and Duda 2017).

11.2.5 Cell adhesion molecules in tumour angiogenesis

Cell adhesion molecules (CAMs) are surface glycoproteins responsible for regulating interactions between a cell and the neighbouring cells or extracellular matrix (ECM). They respond to the tumour microenvironment; in angiogenesis, CAM expression is dynamically regulated in response to tumour growth to allow endothelial cells to leave a quiescent state and angiogenesis to commence (Francavilla, Maddaluno, and Cavallaro 2009). There are four main classes of CAMs: cadherins, selectins, Ig-CAMs and Integrins.

11.2.6 Sprouting angiogenesis

Angiogenesis is the formation of new blood vessels from pre-existing vessels and generally occurs in response to ischemia (Tahergorabi and Khazaei 2012). It occurs through two different pathways, sprouting and splitting (intussusceptive) angiogenesis. Sprouting angiogenesis was the first characterised and the best understood mechanism of angiogenesis.

Sprouting angiogenesis occurs in stages, beginning with enzymatic degradation of the capillary basement membrane followed by endothelial cell proliferation and directed migration. The endothelial cells then form into a tube and are stabilised by fusing and mural cell coating (Adair and Montani 2010).

Sprouting angiogenesis is triggered in response to poor perfusion, causing a high level of hypoxia in tissues. Under these conditions, parenchymal cells such as myocytes, hepatocytes, neurons and astrocytes have inadequate oxygen and metabolites for their functions and respond to the hypoxia by secreting VEGF-A. VEGF-A is the predominant inducer of hypoxia-induced angiogenesis (Adair and Montani 2010).

The blood vessel then begins to grow toward this VEGF-A gradient in a process controlled by tip and stalk cells. Tip cells are endothelial cells that are specialised to sense guidance cues in the environment and lead to the sprouting of new blood vessels. They have long, thin protrusions from their cell membranes known as filopodia. The filopodia have large numbers of the VEGF-A receptor VEGF receptor 2 (VEGFR2). VEGFR2 is the primary receptor for VEGF and is important in the regulation of endothelial migration and proliferation. Its expression on tip cells allows them to sense VEGF-A in the microenvironment and move in the direction of the VEGF-A gradient. The filopodia on tip cells also secrete proteolytic enzymes that digest areas of the ECM, creating a pathway for the growing blood vessel sprout (Small et al. 2002). Tip cells move forwards stimulated by interaction with VEGF-A; when VEGF-A binds to the VEGFR2 on tip cells, it stimulates the anchoring of filopodia to the substratum in the direction of the VEGF gradient. Once enough filopodia have anchored, actin filaments within them contract, pulling the tip cell towards the VEGF-A signal (Adair and Montani 2010).

The fate of endothelial cells, determining whether they progress to a tip or stalk phenotype, is controlled by cell-cell interaction through delta-notch. VEGF-A stimulates endothelial cells to upregulate their expression of the notch ligand delta-like 4 (DLL4). This upregulation in DLL4 sets the endothelial cells on a path to express a tip cell phenotype. The upregulation in DLL4, however, also leads to an activation of notch receptors in neighbouring cells. Notch receptor activation in these cells suppresses the expression of DLL4 and the production of VEGFR2, reducing the migratory behaviour. These cells become ‘stalk cells’.

Stalk cells in contrast, to tip cells, are not characterised by filopodia but are specialised to have a highly proliferative phenotype. They follow the tip cells, proliferating rapidly to allow the blood vessel to grow towards the gradient sensed by the tip cells (Dallinga et al. 2015). As the blood vessel grows, vacuoles develop in the stalk cells and join together to form a lumen for the nascent vessel. Once the lumen is fully formed, oxygenated blood can flow through perfusing the tissue. Eventually, when enough perfused vessels form,

the tissue becomes sufficiently oxygenated, and VEGF-A levels are reduced to baseline levels stopping the formation of new capillaries (Adair and Montani 2010).

Once the VEGF-A levels are reduced, the nascent capillaries can mature. The endothelial cell proliferation and migration of new capillaries are inhibited, and newly formed vessels fuse with others to stabilise the vascular tubes. Pericytes and vascular smooth muscle cells are then recruited to stabilise the vessel, and ECM is deposited around the edge (Tahergorabi and Khazaei 2012; Chien 2007). This ECM deposition causes mechanical signals, including shear stress, which further stabilises the vessel (Chien 2007). Pericytes are cells that stabilise capillaries and venules by wrapping around the endothelial cells that line them. In cancer, the level of VEGF is often high, meaning that vessels are not able to mature and stabilise effectively. Therefore, they are characterised by abnormal pericyte coverage and pericyte-endothelial cell interactions, leading to cancer progression and metastasis (Chen, Xu, and Hu 2016). In addition, pericytes have important signalling roles in altering tumour growth and metastasis (Wong et al. 2020; Armulik, Genové, and Betsholtz 2011; Raza, Franklin, and Dudek 2010; Ribeiro and Okamoto 2015). Vascular smooth muscle cells further stabilise larger blood vessels and allow vasoconstriction and dilation and contribute to extracellular matrix production (Bagher and Segal 2011).

In addition to VEGF mediated angiogenesis, sprouting angiogenesis can also be mediated by the angiopoietins angiopoietin 1 (ANG1) and angiopoietin 2 (ANG2) and their receptor Tie2. Tie2 is a tyrosine kinase receptor primarily expressed on endothelial cells (De Palma and Naldini 2011). ANG1 binds to Tie2, inducing its phosphorylation whereas ANG2 acts as an antagonist of ANG1/Tie2 (Adamis and Berman 2010). ANG1 is primarily expressed on mural cells such as smooth muscle cells and pericytes and act on endothelial cells to promote survival and quiescence of mature blood vessels. This pathway is antagonised by ANG2 which is secreted by endothelial cells in a context dependant manner. It is expressed in response to mediators of inflammation such as thrombin (Huang et al. 2002), as well as by hypoxic and tumour conditions. such as hypoxia (Kelly et al. 2003) and cancer (Sfiligoi et al. 2003; Hu and Cheng 2009; Akwii et al. 2019). By antagonising ANG1 mediated endothelial quiescence, ANG2 promotes angiogenesis (Augustin et al. 2009).

Outside of its effects in endothelial cells, Angiopoietin/Tie signalling in pericytes and macrophages also influences angiogenesis and the maturation of blood vessels. Deletion

of Tie2 in pericytes increases angiogenesis with reduced vessel maturation and increased tumour growth (Teichert et al. 2017). Some macrophages have been identified as expressing Tie2. Circulating macrophages have minimal Tie2 expression which is upregulated when they are in close contact with tumours causing them to differentiate into a subpopulation of perivascular macrophages (De Palma et al. 2003; De Palma et al. 2005; De Palma and Naldini 2011). These subpopulations of macrophages have been observed in several tumour models and are thought to promote angiogenesis through paracrine signalling. Intussusceptive (splitting) angiogenesis.

In contrast to sprouting angiogenesis, where new blood vessels form from mature ones, in splitting angiogenesis, a capillary is split to form two lumens from one; this is a faster process as it initially only requires reorganisation of the cells. In a process stimulated by angiopoietins, platelet-derived growth factor-B (PDGF-B), ephrins and EphB receptors (Burri, Hlushchuk, and Djonov 2004), the opposite walls of the capillary make contact within the lumen, in this 'contact zone'. ECs are reorganised to form two separate lumina with a 'core' in the middle. The vessels bilayer is perforated, allowing growth factors and cells to penetrate into the core, which fills with pericytes and fibroblasts. These cells lay down ECM for the new vascular network (Dimberg and Sund 2014).

11.2.6.1 Vasculogenesis

Vasculogenesis is the process whereby new blood vessels are formed from the endothelial progenitor cells, angioblasts (Tahergorabi and Khazaei 2012). This process occurs predominantly in embryonic growth. In mice, this process begins at embryonic day (E) 6.5 to 7. Clusters of angioblasts form with those at the perimeter differentiating to endothelial progenitors and those at the centre to hematopoietic cells (Lugano, Ramachandran, and Dimberg 2020). The angioblasts migrate distally into the yolk sac to form a primitive capillary network for the embryo, known as the primitive capillary plexus. This process is initially established by VEGF signalling activation (Dong and Yang 2018). Although vasculogenesis is predominantly a developmental mechanism of embryonic development, a version of this pathway is now thought to also be responsible for some capillary development in pathophysiological revascularisation in the adult (Heil and Schaper 2004). It can occur in adults post-ischemia or in tumours by the recruitment of endothelial progenitor cells (EPCs) to the tumour blood vessels (Lugano, Ramachandran, and Dimberg 2020). The mechanisms by which EPCs contribute to tumour vascular development are still poorly understood but thought to include both the direct incorporation of EPCs into the tumour vasculature and the use of EPCs as a

source of angiogenic factors (Tang, Feng, and Yao 2009). Under normal circumstances, the tumour has little dependence on vasculogenesis, but under specific pressures, such as radiotherapy, local angiogenesis may be impaired, leading to increased reliance on the recruitment of EPCs (Brown 2014).

11.2.6.2 Arteriogenesis

Arteriogenesis is the maturation, growth and remodelling of pre-existing arterioles to widen them and is generally triggered by physical stimuli such as shear stress due to arterial obstruction (Heil and Schaper 2004; Carmeliet 2000). This maturation of the blood vessels involves the recruitment of smooth muscles cells to the external wall to allow blood vessels to have the viscoelastic and vasomotor properties required of mature vessels to accommodate the plastic needs of tissue perfusion (Carmeliet 2000). This smooth muscle cell recruitment also stabilises the vessels, making them less likely to regress.

11.2.7 Dysregulation of blood vessel development

The precise regulation of vascular development is essential for healthy growth, and dysregulation of these processes is implicated in many diseases. For example, abnormal ocular neovascularization, a VEGF driven disease where new vessels sprout from existing ones within the retina and into the vitreous, is a leading cause of blindness (Campochiaro 2013; Yoo and Kwon 2013). Similarly, VEGF and local hypoxia may mediate atherosclerotic plaques' neovascularisation, contributing to their growth and rupture (Yoo and Kwon 2013). In contrast, though, a major limitation of tissue recovery in ischaemic diseases is insufficient angiogenesis (Herbert and Stainier 2011). In the case of cancer, angiogenesis stimulated by cancer cells promotes growth and progression to metastasis (Herbert and Stainier 2011). The development of a new vascular network is required to supply oxygen and remove waste products to the tumour allowing for the proliferation and metastatic spread of tumour cells. Therefore, angiogenesis is induced in tumour development but the blood vessels formed are highly disordered, and many are dysfunctional (Nishida et al. 2006).

11.2.7.1 Tumour vasculature

While transient angiogenesis is essential in healthy adult development, the dysregulation of angiogenesis and longer-term angiogenesis is associated with disease.

It is now understood that the dysregulation of angiogenesis in cancer contributes to the tumour microenvironment features. It is also now known that in addition to sprouting

angiogenesis which is typically the major contributor to blood vessel development in tumours, splitting angiogenesis, the recruitment of endothelial progenitor cells, vascular mimicry by tumour cells and the differentiation of cancer stem cells (CSCs) into ECs can all contribute to the disorganised vasculature of a tumour (Lugano, Ramachandran, and Dimberg 2020) **(Figure 11.1)**.

Just as differences can be seen in vasculature between different organs and tissues, abnormalities in endothelial cell, mural cell and basement membrane can be seen in the tumour microenvironment. Perhaps the most apparent difference in the vasculature is the chaotic growth and complete loss of the hierarchy of diameter, characterising healthy blood vasculature (Dudley 2012; Warren et al. 1978; Konerding et al. 1999). Tumour vessels do not fit into the classification of normal blood vessels, arterioles, capillaries and venules; even large vessels have very thin walls, pericyte coverage is incomplete and smooth muscle coating is rare (De Val and Black 2009). Whereas in healthy blood vessels, the endothelial cells are organised in uniform monolayer tubes with few cytoplasmic projections. The morphology of tumour endothelial cells is irregular in shape and size with multiple long, thin cytoplasmic projections. Chronically high VEGF stimulation is a major contributor to this abnormality. VEGF is a potent vasodilator known to increase interstitial pressure and promotes fluid leakage, small gaps and fissures and abnormal branching (Nagy, Dvorak, and Dvorak 2007).

These high VEGF-A levels, which are characteristic of most tumours, stimulate the production of tip-like filopodia that sprout outwards from the endothelial cells. Some of these sprouts may overlap with other endothelial cells or grow into the lumen. The changes in endothelial cell morphology lead to gaps between endothelial cells allowing fluid, fibrin and blood to leak into the surrounding tissue. The leakiness of tumour blood vessels also correlates with the histological grade and malignancy (Daldrup et al. 1998). These gaps in the vessel walls cause ‘blood lakes’ where extravasated erythrocytes pool at the tumour periphery (Hashizume et al. 2000; Dudley 2012) and can contribute to the formation of metastases as tumour cells can be trafficked in the bloodstream.

Tumour cells overlying the blood vessels compress vessels, creating strain and blood flow changes (Padera et al. 2004). This chaotic pattern of blood flow, in turn, causes the expression of flow-mediated transcription factors to be dysregulated, further altering endothelial cell shape, size and differentiation (De Val and Black 2009).

Pericyte coverage on tumour vessels is reduced compared to healthy blood vessels and are more loosely attached, contributing to vessel instability (Baluk, Hashizume, and McDonald 2005). The vessels are also fragile and leaky with abnormal blood flow, features that are thought to contribute to tumour growth and metastasis (Dudley 2012). Some tumour blood vessels are completely unperfused, and others have chaotic perfusion where the blood may flow in the reverse direction.

In addition to novel blood vessels, tumours can co-opt blood vessels from surrounding healthy tissue. This non-angiogenic mechanism, observed in a range of primary and metastatic cancers is considered an important mechanism for resistance to anti-angiogenic drugs (Kuczynski and Reynolds 2020). In some cases, the morphology, architecture and branching patterns of the vessels is maintained when they are co-opted (Kita, Itoshima, and Tsuji 1991; Bridgeman et al. 2017; Pezzella et al. 1997) but tumours can also remodel and deform them meaning that, like angiogenic tumour vessels, co-opted vessels may have abnormalities (Kuczynski et al. 2019). The proliferation of endothelial cells in co-opted vessels is typically lower than in angiogenic tumour vessels and more comparable to non-malignant tissue. In tumours with co-opted vessels, the tumour border is typically irregular with little or no desmoplastic reaction and no tumour capsule (Vermeulen et al. 2001; International Consensus Group for Hepatocellular 2009; Kuczynski et al. 2019). The tumours typically grow along pre-existing vessels connected to those they have co-opted (Kuczynski et al. 2019).

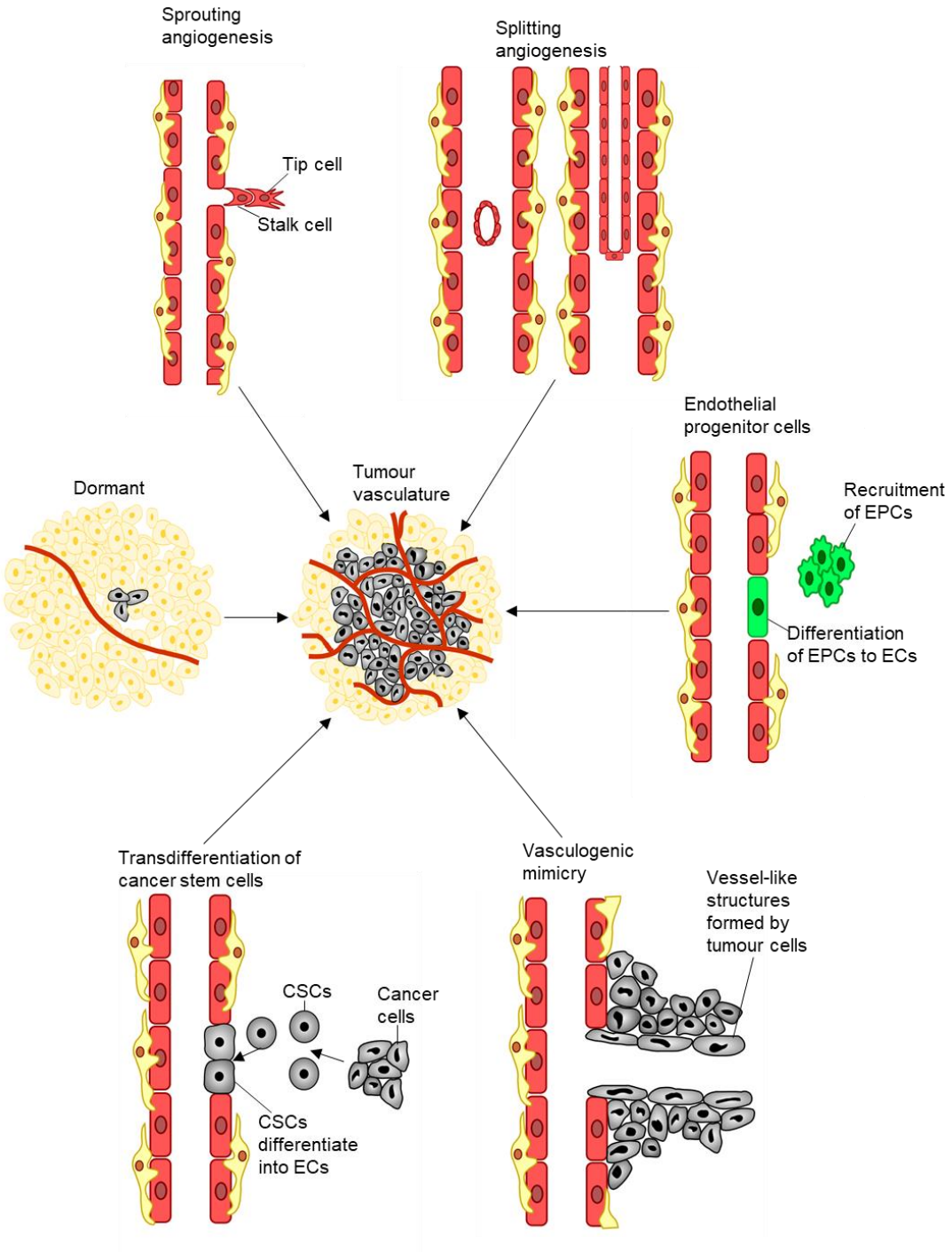

Figure 11.1 Development of tumour vasculature.

As a tumour develops, it upregulates blood vessel formation, predominantly through sprouting angiogenesis but splitting angiogenesis, the recruitment of endothelial progenitor cells (EPCs), vascular mimicry by tumour cells and transdifferentiation of cancer stem cells to ECs also play a role. Through these processes, dysregulated tumour vasculature occurs allowing tumour growth.

11.3 Integrins

11.3.1 Integrin structure

Integrins are a family of 24 heterodimeric receptors that mediate the interactions between cells and the ECM (Michael and Parsons 2020). They are formed from two type I transmembrane glycoproteins, the α and β subunits which each have several domains. The α and β subunits are non-covalently associated through flexible linkers. Each of the subunits has a single membrane-spanning helix and, in most cases, a short unstructured cytoplasmic tail. The extracellular parts of the α and β subunits are larger, roughly 700 and 1000 amino acids respectively and form elongated stalks with a globular ligand-binding head region (Danen 2000; Xiong et al. 2001; Campbell and Humphries 2011). These binding sites allow them to act as receptors for ligands in the extracellular space such as collagen IV and laminins in basement membranes, interstitial matrix (collagen I and fibronectin) and coagulating blood (fibrinogen and thrombospondin) (Hynes 2002) and have diverse roles controlling cell functions including proliferation, migration and cell motility (Paul, Jacquemet, and Caswell 2015). They bind to ligands through control of their conformation. The 24 different integrins are formed within the endoplasmic reticulum by the heterodimerisation of 18 α-integrin and eight β-integrin subunits. Post-translational modifications within the golgi apparatus, before they reach the cell surface, further increase the diversity of the integrins and enable them to perform all of their functions (Hynes 2002).

Integrins can be grouped by their ligand. This thesis will primarily address the RGD receptors that recognise Arg-Gly-Asp sequences of proteins, but integrins can also be collagen receptors, laminin receptors, and leukocyte-specific receptors. Furthermore, most integrins can fit into more than one of these categories and have several ligands (Paul, Jacquemet, and Caswell 2015; Hynes 2002; Legate, Wickström, and Fässler 2009).

The crystal structures of integrins have given valuable insight into the structure and ligand-binding site of integrins and show that the extracellular portion of integrin heterodimers have multiple domains (Takada, Ye, and Simon 2007; Xiong et al. 2002; Xiong et al. 2001; Xiao et al. 2004) **(Figure 11.2 A)**.

The α-chain comprises four highly conserved domains, a seven-bladed β-propeller, a thigh, and two calf domains. In addition, nine of the α chains found in vertebrates have an α-I domain of roughly 200 amino acids inserted into the β-propeller between blades two and three, which have ligand-binding function when present (Xie et al. 2010; Larson

et al. 1989). The I domain comprises five β-sheets surrounded by seven α helices. The lower side of the last three to four blades of the β-propeller contain Ca^{2+} binding domains which face away from the ligand-binding surface. The Ca^{2+} binding at these sites influences ligand binding (Oxvig and Springer 1998; Humphries, Symonds, and Mould 2003; Campbell and Humphries 2011).

The thigh and calf domains of the α-chain have similar immunoglobulin-like β-sandwich folds (Xiong et al. 2001). There are two main interdomain flexibility regions, the linker between the β-propeller and the thigh and the 'genu' or 'knee' at the bend between the thigh and the calf domain. The knee on the α-subunit close to a similar bend on the β subunit so that the whole integrin can extend and bend by hinging at the knees. Whereas the other domains of the α-chain have relatively rigid structures, I domains, in integrins that have them, show conformational changes, which are essential for regulating binding affinity (Xiong et al. 2001; Campbell and Humphries 2011).

The β-subunit has seven domains with complex, flexible interactions. It is generally more flexible than the α subunit (Xie et al. 2010). It consists of a β-tail domain linking the transmembrane domain to four cysteine-rich epidermal growth factor (EGF) modules, the links between all of which are relatively plastic, especially between EGF1 and EGF2, which is the β knee. The EGF region is linked to a plexin-semaphorin-integrin (PSI) domain, a hybrid domain and a β-I domain. There are conformational changes that can occur in the β-I hybrid regions. The β-I transitions from a "closed" to an "open" conformation when the α7-helix of the β-I domain moves toward the hybrid domain, which causes the hybrid domain to swing out by roughly 60° (Xiao et al. 2004; Campbell and Humphries 2011).

The metal-ion-dependent adhesion site (MIDAS) domain is a crucial Mg^{2+} binding site in the I domain of integrins. Ligand binding occurs through coordination with this ion. The βI domain contains an Mg^{2+} coordinating MIDAS and a site adjacent to MIDAS (ADMIDAS) binding an inhibitory Ca^{2+} ion. This ADMIDAS site binds the Mn^{2+} ion leading to a conformational change resulting in an active form of the integrin (Humphries, Symonds, and Mould 2003).

The crystal structure of αvβ3 bound to a cyclic RGD peptide shed light on the role of the MIDAS. The binding site of αvβ3 is a shallow crevice between the α and β chains with only the Arg and Asp side chains of the RGD peptide slightly berried and the rest of the peptide exposed to the water (Xiong et al. 2002). Divalent cations play a critical role in

this interaction. The binding site is composed of the β propeller domain of αv chain, the I-like domain of the β chain and the hybrid domain of β3. A divalent cation at the MIDAS site in the I like domain contacts the Asp of the RGD peptide. The MIDAS site is only occupied by the divalent ion when it is in its RGD-liganded state, but no ion is seen in the crystal structure of the unliganded integrin.

The role of MIDAS in ligand binding is slightly different in integrins that have an I domain on the α chain. In this case, the MIDAS can capture a divalent ion whether or not a ligand is bound (Emsley et al. 2000; Shimaoka et al. 2003; Shimaoka et al. 2002).

There are two other divalent cation binding sites on β3 integrin, called ADMIDAS (adjacent to MIDAS) and LIMBS (ligand-associated metal binding site). The ADMIDAS is 8 Å from the MIDAS and can be occupied by either an Mn^{2+} or a Ca^{2+} ion, whether or not a ligand is present (Xiong et al. 2002). The LIMBS, which is 6 Å from the MIDAS, captures an Mn^{2+} ion when an RGD peptide is present. These are thought to have a role in controlling ligand binding; for example, binding of a Ca^{2+} ion to the ADMIDAS site causes a shift in shape that decreases occupancy. An increase in affinity for RGD correlates with reduced Ca^{2+} availability and lack of Ca^{2+} binding, whereas Ca^{2+} binding to the ADMIDAS stabilizes integrins in the low affinity, closed conformation (Xia and Springer 2014; Craig et al. 2004).

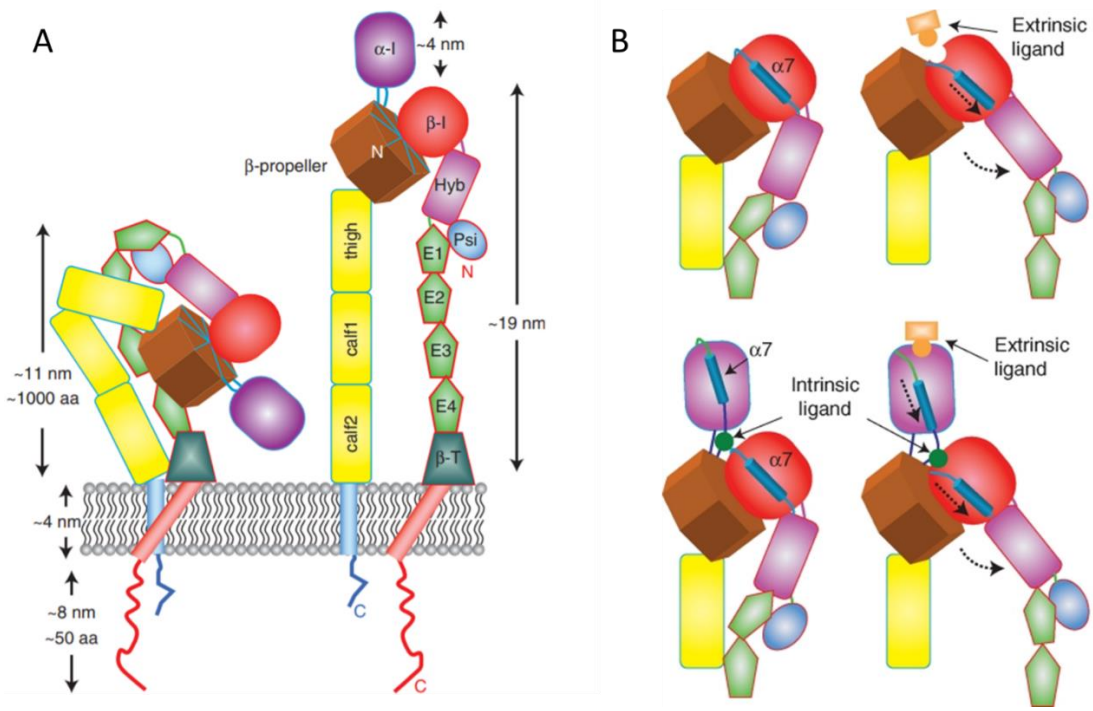

Figure 11.2 Integrin structure and allosteric binding sites adapted from Campbell and Humphries 2011

(A) Cartoon representation of bent and upright conformations of αxβ2 integrin showing α and β subunits in the bent (left) and upright (right) conformations and approximate dimensions. (B) Cartoon showing the movement of the α7 helix in the I domains and the swing-out of the hybrid domain. The top pair show the closed and open conformations of an integrin with no α-I domain. The lower pair represent the closed and open conformation of an integrin with an α-I domain showing allosteric activation. The intrinsic ligand is a glutamate.

11.3.2 Integrin activation

The precise regulation of integrins is crucial for many cellular processes. For example, platelet aggregation is controlled by the integrin αIIbβ3 (Wagner et al. 1996), and its rapid activation at a wound is required for blood coagulation and haemostasis (Shattil, Kashiwagi, and Pampori 1998). However, when the integrin is activated inappropriately, it can cause a platelet thrombus to block a blood vessel resulting in stroke or myocardial infarction (Ginsberg 2014).

11.3.2.1 Allosteric functions of integrins

Regulation of integrin activation is complex and happens in several different ways. The affinity of integrins for their ligands is highly dependent on allosteric regulation, which means that the binding of one ligand influences the activity or affinity for another ligand of the integrin through a conformational change (Manninen 2015). Although integrin conformation was initially thought to be limited to the bent (inactive) and extended (active) forms, it is now believed to be more complex with intermediate conformations induced by allosteric binding that have different ligand affinities (Campbell and Humphries 2011; Zhu, Zhu, and Springer 2013). Two common examples of allosteric activation of integrin activation are 'inside out' and 'outside-in activation discussed below, whereby an intracellular or extracellular signal respectively induces a change in integrin conformation, altering the affinity for the binding of another ligand. These signalling mechanisms are discussed below.

In addition, the affinity of an integrin for its ligand can be influenced by the binding of molecules to other sites. For example, the affinity of the αI domain for ligand-binding is allosterically regulated by the βI domain, its homologue in the β-subunit. In integrins with no αI domain, the βI domain has closed and open states whose conformation is controlled but the movement of an α7 helix allowing binding of extrinsic ligands when in the open conformation (Xiao et al. 2004; Luo, Carman, and Springer 2007) **(Figure 11.2 B; top panel)**. In integrins with an αI domain, similar conformational changes are seen and allosterically regulated. When integrin ligands, such as the RGD motif, bind to the integrin with the βI domain in an open state, the Mg^{2+} ion of the MIDAS coordinates with the Asp side chain of the ligand. In integrins with an αI domain, the MIDAS of the βI domain may bind an intrinsic ligand, thought to be an invariant glutamine residue on the α chain (Xie et al. 2010). This binding of an intrinsic ligand causes a shift in the α7 helix moving the βI domain to an open conformation **(Figure 11.2; bottom panel)**. Evidence for this comes from the fact that the αI domain's flexibility observed through

crystal structures would allow these interdomain interactions (Xie et al. 2010) and that when the glutamine is mutated, integrin activation is abolished (Huth et al. 2000; Alonso et al. 2002).

11.3.3 Inside-out activation of integrins

The precise control of integrin activation by inside-out activation is through the binding of cytoplasmic proteins. One of them is talin, a cytoskeletal protein that binds to the β tails of most integrins (Calderwood, Shattil, and Ginsberg 2000). In response to signals received by a diverse range of cellular receptors depending on the specific integrin to be activated, talin is recruited to the cytoplasmic end of the integrin β subunit (Watanabe et al. 2008). Talin binds to the integrin β-tail through a unique interaction with the membrane-proximal (MP) region of the integrin at a specific NPxY motif (Calderwood et al. 2002). This talin binding allows competition between a conserved lysine on the talin and an aspartic acid on the α chain of the integrin, which is essential to disrupt an α/β salt bridge on the integrin which maintains the integrin in the inactive conformation (Wegener et al. 2007; Anthis et al. 2009) **(Figure 11.3; left panel)**. The cleavage of this cytoplasmic salt bridge between subunits causes dissociation and reorganisation of the transmembrane helices, straightening the integrin at the knee and generating a high-affinity binding integrin **(Figure 11.3; central panel)**. Talin also binds to actin and to many cytoskeletal and signalling proteins meaning that it directly links activated integrins to signalling and cytoskeletal systems (Critchley and Gingras 2008). This also leads to multimerisation in focal adhesions (Mas-Moruno et al. 2016; Nieberler et al. 2017).

Inside-out integrin signalling can also be controlled by other proteins such as phosphatidylinositol 4-phosphate 5-kinase Iγi2 (PIPKIγi2) and Phosphatidylinositol-4,5-bisphosphate ($PI4,5P_2$) which are especially important in cell migration (Sun et al. 2013). $PI4,5P_2$ causes a confirmational change in talin allowing its head domain to tether to $PI4,5P_2$ enriched membranes. This exposes a previously hidden integrin binding interface which allows integrins to cluster (Saltel et al. 2009; Sun et al. 2013). The FERM domain of talin also binds to a NPxY motif on integrin beta chain's cytoplasmic domain which allows inside-out activation of the integrin (Saltel et al. 2009; Sun et al. 2013; Wegener et al. 2007). Through interaction with talin, PIPKIγi2 produces regions of high $PI4,5P_2$ density which are necessary for the formation of focal adhesion and allow epithelial cells to migrate by adhesion to the ECM (Sun et al. 2013; Ling et al. 2002; Di Paolo et al. 2002; Durand et al. 2016). In contrast to $PI4,5P_2$, PIPKIγi2 competes with integrins for talin binding, however, talin However, there is an additional talin binding domain on the beta

chain of integrins and talin is a homodimer, therefore, it is thought that talin and PIPKIγi2 can simultaneously bind to talin creating a single complex to regulate formation of focal adhesions as cells migrate (Thapa et al. 2012; Saltel et al. 2009; Sun et al. 2013).

11.3.4 Outside-in activation of integrins

In addition to 'inside-out' signalling initiated by the cleavage of intercellular salt bridges, integrins also have an 'outside-in signalling mechanism and are therefore considered bi-directional signalling proteins (Shattil, Kim, and Ginsberg 2010; Legate, Wickström, and Fässler 2009; Mas-Moruno et al. 2016). For 'outside-in signalling, conformational changes in the resting state integrins and multimerization are induced by binding to ECM ligands external to the cell. This binding of ECM ligands induces conformational changes in the structure of integrins, provokes dissociation of the transmembrane helices, and contributes to clustering into multimers, thereby transducing signals to the cell. The formation of multimers allows stronger binding in focal adhesions. Ligands can bind to the integrins in their resting state but for the signal to be transduced requires dissociation of the transmembrane helices of the integrins and subsequent multimerization (Gottschalk and Kessler 2004) **(Figure 11.3; right panel)**. In cell adhesion, integrins can mediate the transmission of force from focal adhesions to ECM proteins, a process known as mechanotransduction (Geiger, Spatz, and Bershadsky 2009). This may result in strengthening adhesions and enhanced cytoskeletal linkages (Ross et al. 2013).

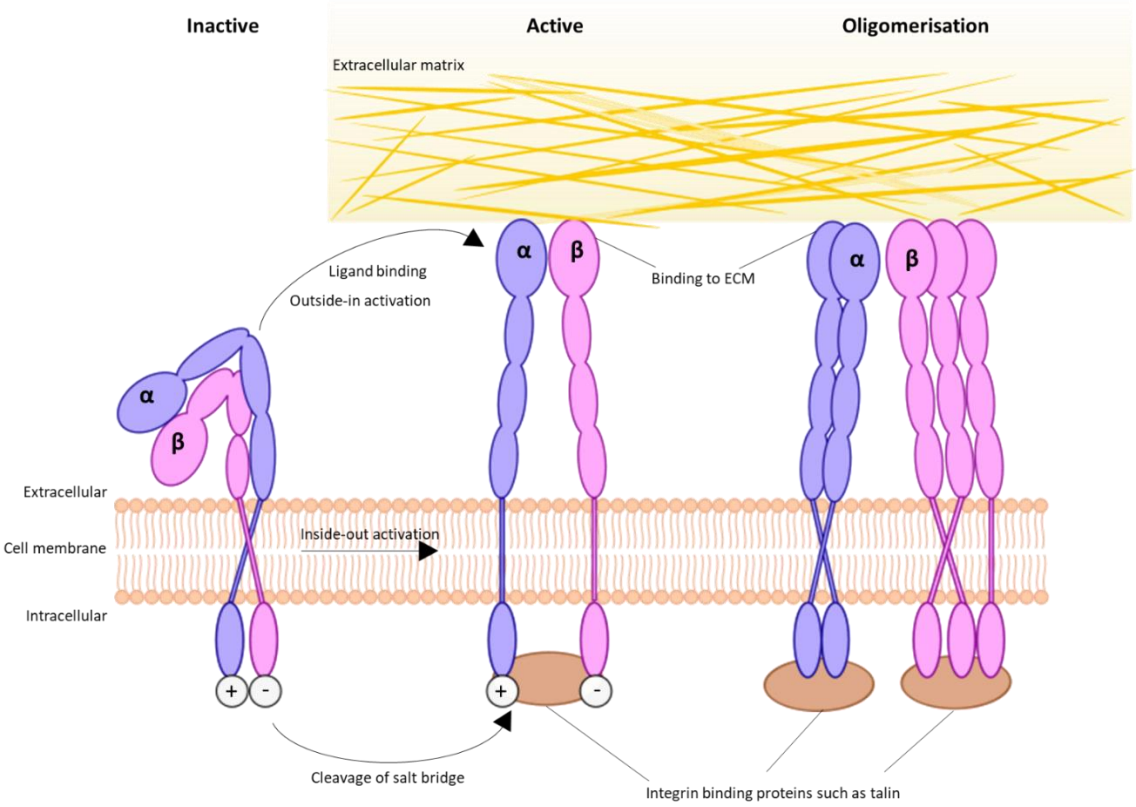

Figure 11.3 Schematic of integrin activation

Integrins in the bent resting conformation have low affinity for their ligands in the ECM. Inside-out signalling involves disruption of an intracellular salt bridge between the α and β cytoplasmic subunits. This salt bridge cleavage induces the dissociation of the transmembrane helices and subsequent reorganisation generating a high affinity binding integrin, plus multimerization in focal adhesions. Conformational changes of the resting integrin state are induced by the integrin binding of ECM ligands causing stronger binding at the focal adhesions. The outside-in signalling also requires integrin oligomerisation (Mas-Moruno et al. 2016).

11.3.5 Integrin function and RGD binding

The Arg-Gly-Asp (RGD) motif is a highly conserved minimal integrin recognition site that was first identified in 1984 in fibronectin (Pierschbacher and Ruoslahti 1984). However, it is also present in other ECM proteins such as vitronectin (Suzuki et al. 1985), von Willebrand factor (Plow et al. 1985), osteopontin (Oldberg, Franzén, and Heinegård 1986), and laminin (Grant et al. 1989). Of the 24 human integrin subtypes known to date, eight integrin dimers (αvβ1, αvβ3, αvβ5, αvβ6, αvβ8, α5β1, α8β1, and αIIbβ3) recognise the RGD motif in ECM proteins, and many of these interactions have roles in cancer and metastasis (Schittenhelm et al. 2013; Nieberler et al. 2017).

The mechanism of molecular activation and bidirectional signalling in integrins was unclear for a long time, but the structure of the extracellular domain of αvβ3 in the absence or presence of Cilengitide was solved in 2001 (Xiong et al. 2001; Xiong et al. 2002). This data led to the discovery that the extracellular domains of αvβ3 have a resting state where the integrin head groups are bent towards the cell membrane. When a ligand binds, the structure rearranges at the hinge region of each subunit by a mechanism known as a 'switchblade'.

'Inside-out signalling' is initiated by intracellular signals by inducing talin binding and kindlin to the cytoplasmic domains of integrin β subunits. This activates the integrin allowing ligands to bind (Shen, Delaney, and Du 2012; Tadokoro et al. 2003; Moser et al. 2008). 'Outside-in signalling' is between the ligands and the integrin, allowing the cell to sense and react to the extracellular environment (Ginsberg, Partridge, and Shattil 2005; Legate, Wickström, and Fässler 2009). Depending on the ligand-integrin interaction, outside-in signalling can induce cell spreading, retraction, migration, proliferation or survival (Shen, Delaney, and Du 2012).

Because integrin-mediated cell attachment is involved in regulating and controlling cell growth, migration, differentiation, and apoptosis, the role of the RGD sequence is a topic of considerable research. The RGD binding subfamily of integrins is believed to play an important role in cancer progression and metastasis (Nieberler et al. 2017). Drugs based on the RGD structure are under investigation for thrombosis, osteoporosis, and cancer (Ruoslahti 1996).

Although several integrins bind RGD motifs, there are differences in their specificity **(Figure 11.4)**. The integrin αIIbβ3, which is expressed on platelets, is highly specific to adhesive proteins, such as fibrinogen/fibrin, prothrombin and plasminogen. Although,

like many other integrins, it recognises RGD, the motif must be in an extended conformation. αIIbβ3 specifically recognises ligands with a distance of 0.7–0.9 nm between the positively charged arginine residue and the carboxyl group of aspartate (Müller, Gurrath, and Kessler 1994).

When the motif is kinked, however, the ligands tend to bind to other integrins such as αvβ3 and α5β1, but there is further specificity within these ligands with kinked RGD motifs. For example, both αvβ3 and α5β1 integrins bind kinked RGD motifs, but differences in the binding mode of the arginine side chain differentiate between ligands for each integrin.

In αvβ3, the guanidine group of arginine on the RGD motif binds to the aspartate at position 218 (D218) of the α-subunit of αvβ3, forming a bidentate salt bridge in a side-on interaction between the RGD and the integrin (Nagae et al. 2012).

In α5β1 integrins, there is a side-on interaction between the guanidine group of arginine on the RGD motif and the aspartate at position 227 (D227) of the α-subunit of α5β1. However, in addition to this side on interaction, there is also an end on interaction with the glutamine at position 221 (Q221) of the α-subunit of α5β1 (Nagae et al. 2012; Kapp et al. 2017).

Therefore, the integrins are selective for different integrins as specific ligands will interact side-on with the αv-pocket, but sterical hindrance does not allow them to also bind end on so they have a much lower affinity for α5β1 integrins but still have a high affinity for αvβ3 integrin. In contrast, those ligands that can perform both side on and end-on binding have a high affinity for α5β1 integrins (Kapp et al. 2016; Kapp et al. 2017).

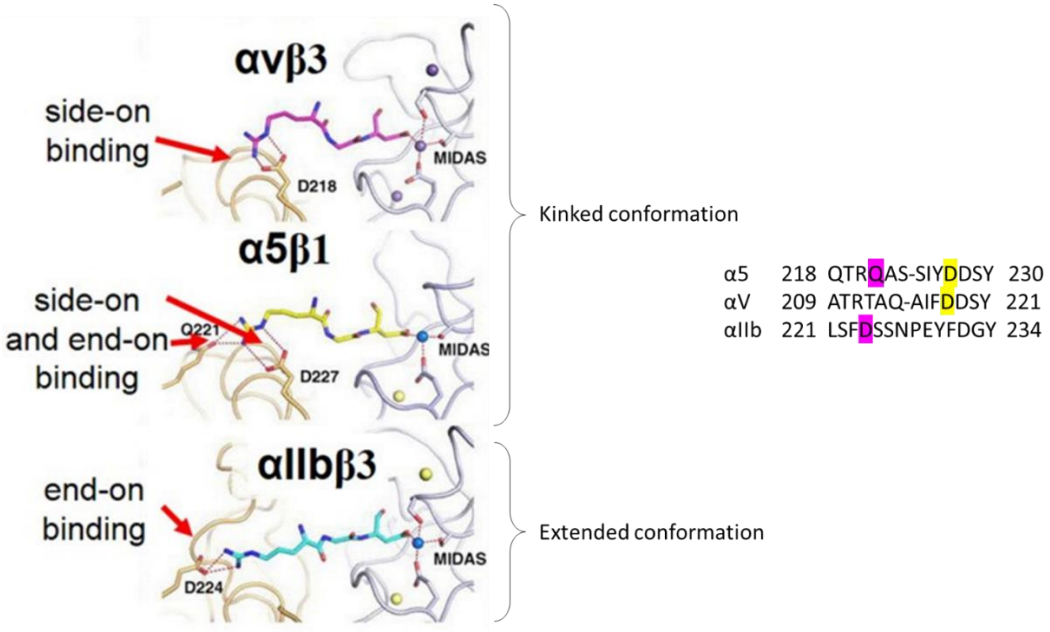

Figure 11.4 RGD binding sensitivity in kinked and extended conformation adapted from Kapp 2017

Crystal structures of α5β1 (top), αvβ3 (middle), and αIIbβ3 (bottom) in complex with RGD ligands.

11.3.6 Transdominant inhibitory functions of integrins

Rapid changes in integrin affinity for extracellular ligands is essential for the development and function of multicellular animals (Calderwood et al. 2004). When an integrin is occupied, this can alter the conformation of the extracellular domain and function of other integrins and also lead to the partition of the occupied integrins into focal adhesions (Díaz-González et al. 1996). This is dependent on interactions between the cytoplasmic tail of the integrin beta subunit and the cytoskeletal protein talin. The crosstalk between integrins and other integrins or receptors is important across diverse cellular processes such as adhesion, spreading, migration, clot retraction, proliferation, and differentiation. Transdominant inhibition is one form of integrin crosstalk and is the process where a ligand binding to one integrin inhibits the activation of another integrin. This is due to competition for talin.

These transdominant inhibitory effects are important to consider in the pharmacological inhibition of integrins. For example, in the case of αIIβ3 integrin, antagonists have successfully been used to directly inhibit adhesive functions with anti-platelet effects (Ley et al. 2016; Robinson and Hodivala-Dilke 2011; Dukinfield et al. 2019). In addition, Cilengitide has transdominant inhibitory functions at low dose, altering αvβ3 signalling to enhance recycling of VEGF-receptor 2 (VR2), allowing increased VEGF stimulated angiogenesis as discussed in more detail later (Reynolds et al. 2009)

11.3.7 The regulation of integrin/GFR function by endocytosis

Trafficking of integrins through endocytosis has a role in regulating their function (Hynes 2002; Caswell and Norman 2006; Pellinen and Ivaska 2006). Integrins undergo constant cycles of endocytosis and re-exocytosis (recycling to the surface) to control the availability of integrins on the plasma membrane. For some integrins, the majority of those at the surface can be removed within 30 minutes, but as they are slow to degrade, with a half-life of 12-24 hours (Lobert et al. 2010; Paul, Jacquemet, and Caswell 2015; Tiwari et al. 2011), most integrins are recycled to the surface (Paul, Jacquemet, and Caswell 2015; Bridgewater, Norman, and Caswell 2012).

The transit of integrins through the endolysosomal system is controlled by Ras-related in brain (Rab) and ADP-ribosylation factor (Arf) family guanosine triphosphatase (GTPases). Their action, in turn, is controlled by cycles of GTP binding catalysed by guanine nucleotide exchange factors (GEFs) and guanosine triphosphate (GTP) hydrolysis catalysed by GTPase-activating proteins (GAPs). The Rab GTPases are responsible for

recruiting effector proteins which regulate cargo sorting, the binding of motor proteins and tethering, docking and fusion events (Zhen and Stenmark 2015). The Arfs are responsible for recruiting coat proteins that control vesicle budding and have roles in regulating phospholipid signalling and linking to motor proteins (Donaldson and Jackson 2011; Hsu, Bai, and Li 2012). Integrins can interact directly with some Rab and Arf GTPase effectors as well as some Rab proteins allowing highly specific integrin traffic (Caswell and Norman 2006; Bridgewater, Norman, and Caswell 2012; De Franceschi et al. 2015).

For example, integrin trafficking is essential for several different modes of cell migration. In migrating neutrophils, integrins are internalised at the rear of the cell and recycled to the leading edge (Lawson and Maxfield 1995; Pierini et al. 2000). Similarly, when cells divide, vesicular integrins move from the site of division (the cleavage furrow) to the leading edge allowing the daughter cells to move apart and redistribute (Pellinen et al. 2008). However, in other cell types, such as epithelial cells and invasive cancer cells, much of the turnover of adhesion complexes (leading to integrin internalisation) happens towards the rear of the cell. In migrating epithelial cells, α5β1-integrin containing vesicles are trafficked along microtubules to the rear allowing the cell to orient itself and move towards guidance cues (Theisen, Straube, and Straube 2012). When cancer cells migrate through the ECM, active α5β1 integrin is endocytosed from the front of the cell, sorted in Rab25 endosomes and eventually, recycled back to the rear of the cell to enable forward movement of the trailing end (Dozynkiewicz et al. 2012).

11.3.8 Clustering of integrins at focal contact sites

Focal adhesions are contact sites of cells to the surrounding ECM through transmembrane protein integrins. Integrins cluster at focal adhesions, and then structural and signalling proteins are recruited, such as kinases and phosphatases. They allow integrins to transduce physical forces into chemical responses within the cell (McCloskey 2011). Forces concentrate in the focal adhesion sites stimulate dimerization of integrins and recruitment of focal adhesion proteins such as paxillin, talin, and vinculin, connecting the focal adhesion to microfilaments and indirectly to microtubules and intermediate filaments. Forces applied to integrins also produce a stress-dependent increase in focal adhesion assembly mediated by small GTPase and Rho. Although integrins lack enzymatic activity, the forces applied to them activate many of the proteins with enzymatic activity at the focal adhesions leading to integrin-associated signalling cascades (McCloskey 2011). Integrin-mediated activation of Src and FAK, for example,

can regulate Rho GTPases, which then regulate the organization of actin cytoskeleton (Mitra, Hanson, and Schlaepfer 2005; Mitra and Schlaepfer 2006; Lu and Wang 2014).

FAK (discussed in more detail later) was one of the first integrin signalling molecules to be identified. It acts as a phosphorylation-regulated signalling scaffold and is important in the cross-talk between growth-factor signalling and integrins as well as adhesion turnover, Rho-family GTPase activation and cell migration (Mitra, Hanson, and Schlaepfer 2005). It has a C-terminal focal-adhesion-targeting (FAT) domain that interacts with paxillin and talin. When integrins cluster, FAK is autophosphorylated, generating docking sites for SH2 domain-containing proteins such as Src, which are in turn activated and phosphorylate FAK to promote its kinase activity and interaction with other proteins (Harburger and Calderwood 2009).

11.3.9 αvβ3 integrin

αvβ3 is a promiscuous integrin binding to many different ligands; this promiscuity may be important in situations such as wound healing where the ECM is constantly changing, so function is more important than specificity (Alday-Parejo, Stupp, and Rüegg 2019). αvβ3 integrin expression is important in angiogenesis and present on all angiogenic endothelial cells; however, angiogenesis can be stimulated by two separate integrin signalling pathways which depend on different αv integrins αvβ3 and αvβ5 (Weis and Cheresh 2011). These pathways differ in their activation of the Ras/Raf/MEK/Erk pathway in blood vessels with the αvβ3 involving p21-activated kinase (PAK) whereas αvβ5 activates FAK and Src kinase (Weis and Cheresh 2011; Hood et al. 2003). αvβ3 integrin is involved in angiogenesis stimulated by the angiogenic factors basic-FGF, TNF-α and IL8 and is only present on growing blood vessels such as tumour, wound and inflammation vasculature, making it an interesting drug target (Hillen and Griffioen 2007; Brooks, Clark, and Cheresh 1994). αvβ3 recognises RGD containing proteins such as the ECM components vitronectin, fibronectin, fibrinogen and osteopontin. αvβ3 mediated signalling allows endothelial cell migration as it permits endothelial cells to bind to vitronectin, fibrinogen or osteopontin (Senger and Perruzzi 1996). In addition, proteolytically active MMP-2 on the surface of angiogenic blood vessels permits cell-mediated collagen degradation, so allows migration of tip cells (Brooks et al. 1996). αvβ3 has roles in sustaining growth factor-induced ERK signalling (Eliceiri et al. 1998), regulating the expression of COX-2 for activation of the small GTPases RAC-1 and Cdc-42 required for endothelial cell migration (Dormond, Lejeune, and Ruegg 2002). αvβ3 provides pro-survival signals making cells bound to vitronectin apoptosis-resistant by

activating signalling cascades such as FAK-PI3K-Akt, ERK (Wang and Milner 2006) and NF-kB (Scatena et al. 1998).

Integrin αvβ3 is a marker of human breast-tumour associated blood vessels and was therefore investigated in 1995 for its role in human angiogenesis and breast tumour growth (Brooks et al. 1995). Using severe combined immunodeficient (SCID) mice, they created a mouse/human chimeric model. Human, full-thickness neonatal skin was transplanted into the mouse. Once healed, the human breast carcinoma cell line MCF-7PB, which was shown by Fluorescence-activated Cell Sorting (FACS) to be cells αvβ3-negative, was injected intradermally. This tumour induced a human angiogenic response as measured by vascular cell immunoreactivity with the monoclonal antibodies LM609 and P2B1 against human αvβ3 and CD31, respectively. Tumour bearing animals were injected intravenously with mAb LM609, an antagonist of αvβ3. The antibody either prevented tumour growth or markedly reduced tumour cell proliferation within the microenvironment of the human skin. The tumours treated with anti-αvβ3 antibody significantly reduced blood vessel density and appeared considerably less invasive than tumours in control animals. This suggested that αvβ3 plays a significant role in human angiogenesis and breast tumour growth and that antagonists to αvβ3 may provide an effective antiangiogenic approach for the treatment of human breast cancer.

The β3 integrins are involved in many different physiological and pathological processes. As well as its roles in angiogenesis and tumour progression, αvβ3 also has roles in implantation, placentation and bone remodelling. The other member of the β3 subfamily of integrins comprises αIIbβ3 has roles in platelet aggregation and thrombosis. In addition to these integrin specific processes, the human bleeding disorder Glanzmann thrombasthenia (GT) is caused by defective genes for either the αIIb or the β3 subunit. In healthy platelets, their stimulation activates surface αIIbβ3, inducing platelet aggregation. In the case of GT, however, there is a severe reduction or complete lack of platelet aggregation in response to physiological antagonists that would normally induce it. GT patients who have defects αIIb have deficiencies in αIIbβ3 integrin, and those with a defective β3 gene have deficiencies in both αIIbβ3 and αvβ3 integrin (Coller, Seligsohn, and Little 1987). Patients with either of the faulty genes show similar phenotypes clinically, most notably, mucocutaneous haemorrhage. Therefore, it was essential to develop a mouse model in order to be able to further study β3 integrins.

The β3-integrin gene was disrupted in embryonic stem (ES) cells by homologous recombination creating three clones with the correct homologous recombination. These ES cells were injected into C57BL/6 blastocysts and transferred into pseudopregnant females. When the litters from each of these clones were crossed with wildtype C57BL/6 females, chimaeras from two of the clones had germline transmission producing heterozygous litters. These heterozygotes were intercrossed, creating viable, fertile homozygous β3-null mice (Hodivala-Dilke et al. 1999).

These mice accurately model the features of GT with defective platelet aggregation and clot retraction, prolonged bleeding times, and cutaneous and gastrointestinal bleeding. Implantation into the uterine wall is not affected by the mutation, but placental defects occur and lead to foetal mortality. In addition, postnatal haemorrhage leads to anaemia and reduced survival (Hodivala-Dilke et al. 1999). This model demonstrates the critical role of β3 integrin in healthy physiology and wound repair and facilitated the study of the physiological and pathological functions of β3 integrin. This model also helped further research into the role of αvβ3 integrin in cancer and unveiled the clinically important transdominant inhibitory response of β3 integrin inhibition. It was previously thought that αvβ3 and αvβ5 were likely to be critical modulators of angiogenesis as they are expressed in vascular sprouts, and their inhibition suppresses neovascularization and tumour growth (Brooks, Clark, and Cheresh 1994; Brooks et al. 1994; Brooks et al. 1995). However, using the β3 null mouse and a dual β3 and β5 knockout model, it was demonstrated that these animals support tumorigenesis and, in fact, have enhanced tumour growth. In fact, the tumours in these models have enhanced angiogenesis compared to WT animals which suggested that neither αvβ3 nor αvβ5 integrin is essential for neovascularization. The angiogenesis in response to hypoxia and VEGF were also increased in the absence of β3 integrins. Although the expression and function of other integrins did not appear to be altered, the levels of VR2 were enhanced in β3 null cells (Reynolds et al. 2002).

11.3.10 αvβ5 integrin

Integrin αvβ5 is also constitutively expressed on vascular endothelium but in contrast to αvβ3, which is required for basic-FGF/TNF-α stimulated angiogenesis, αvβ5 integrin function is necessary for angiogenesis induced by VEGF or transforming growth factor α TGF-α requires (Friedlander et al. 1995; Weis and Cheresh 2011). While in many ways, the role of αvβ5 is similar to that of αvβ3, VEGF, acting through αvβ5, promotes vascular permeability while basic-FGF in the αvβ3 pathway does not (Weis et al. 2004; Criscuoli,

Nguyen, and Eliceiri 2005). As increased permeability promotes metastasis, this suggests αvβ5 may promote the formation of metastases (Avraamides, Garmy-Susini, and Varner 2008).

11.3.11 αvβ6 integrin

αvβ6 integrin is an epithelial-specific integrin that has been the target of significant research. It is not expressed in healthy adult epithelial cells but is upregulated in wound healing and cancer. It is a receptor for a number of ECM proteins, including fibronectin, vitronectin, tenascin and an RGD motif on the latency-associated peptide (LAP) of TGF-β. It has roles in invasion, inhibiting apoptosis, regulation of MMP expression in the matrix and TGF-β1 activation, and it is thought to promote cancer progression (Bandyopadhyay and Raghavan 2009).

11.3.12 αIIbβ3 integrin

As previously mentioned, αIIbβ3 integrin is a platelet specific integrin involved in aggregation. Although it is not expressed on endothelial cells or pericytes, it still has a role in angiogenesis.

Platelets are small, anuclear blood cells that function to react to form blood clots in response to bleeding from blood vessel injury (Laki 1972). Under normal physiological conditions, circulating platelets do not interact with vessel walls, but in response to vascular injury or activation of the endothelial cells exposing the underlying ECM, platelets start to adhere, leading to thrombus formation. The initial platelet adhesion occurs through the of formation transient bonds between glycoproteins on the platelets and endothelial cells (Ruggeri 2002). This initial transient adhesion slows down the platelets, but they need to quickly form stable adhesions in order to activate and form a thrombus. This process is through the interaction of integrins (Kisucka et al. 2006), and this rapid appearance of platelets at vascular injury sites is thought to trigger angiogenesis (Pinedo et al. 1998).

11.3.13 Other integrins with roles in angiogenesis and cancer

Many other integrins have been shown to have essential roles in angiogenesis and cancer, including αvβ1, αvβ8, and α5β1. αvβ1 and αvβ8, like αvβ6 bind to the RGD motif of LAP and activate TGF-β1 *in vitro*, they are thought to also have a role in TGF-β activation *in vivo*. αvβ8 has also been shown to be expressed by murine Tregs, and when knocked out, the Itgb8−/− T-regs fail to activate TGF-β1 *in vitro* and *in vivo*, while the transfer of wildtype Tregs would rescue colitis, transfer of Itgb8−/− T-regs completely

fails to do so (Worthington et al. 2015). Therefore, inhibition of αvβ8 is being investigated for its potential to block immunosuppression in cancer (Stockis et al. 2017).

α5β1 and its ligand fibronectin are upregulated on tumour blood vessels, increasing angiogenesis. α5β1 integrin has been shown to mediate both metastasis and angiogenesis invasion (Yao, Veine, and Livant 2016).

11.3.14 Integrin inhibition in cancer treatment

Integrins, especially the αv family, are involved in cancer cell functions, including proliferation, survival, migration, invasion, and metastasis. Integrins also have roles in the tumour microenvironment that promote progression and metastasis, such as tumour angiogenesis, remodelling the matrix and recruiting immune and inflammatory cells. Therefore, integrins are a compelling target for cancer therapy. Inhibition of integrin αvβ3/αvβ5 and α5β1 showed promising results preclinically but have had mixed results in clinical trials (Alday-Parejo, Stupp, and Rüegg 2019). For example, the level of integrin α5β1 and its ligand fibronectin are upregulated in human tumour biopsies (Kim et al. 2000) and have important roles in angiogenesis which increase tumour growth *in vivo*. Antibody, peptide and novel nonpeptide antagonists of α5β1 can block angiogenesis that is induced by multiple factors but have little effect on VEGF induced angiogenesis in murine and chick embryo models. They have also been shown to inhibit angiogenesis in human tumour xenografts in mice. (Kim et al. 2000). The targeted peptide inhibitor of activated α5β1, Ac-PHSCN-NH2 (PHSCN), was developed to exploit these effects. It was used in phase I clinical trials to impede both metastatic invasion and neovascularization of breast cancers to the bone, which is a very common complication of breast cancer. When used as a monotherapy, PHSCN prevented disease progression for up to 14 months (Yao, Veine, and Livant 2016). As many integrins recognise the RGD motif, the development of inhibitors to target this sequence gave great hope, especially for the ability to inhibit tumour angiogenesis (Curley, Blum, and Humphries 1999; Alday-Parejo, Stupp, and Rüegg 2019).

One such inhibitor was RGD competitive αVβ3/αVβ5 Cilengitide, developed as an anti-angiogenic anti-cancer drug but with disappointing results clinically (Stupp et al. 2014; Chinot 2014).

11.3.15 Cilengitide

Cilengitide is an αvβ3/αvβ5 integrin-specific RGD-mimetic cyclic peptide (Yamada et al. 2006; Nisato et al. 2003b), an inhibitor of angiogenesis that was developed in the early

90s by spatial screening (Mas-Moruno, Rechenmacher, and Kessler 2010; Stupp et al. 2014). It is a selective αvβ3 and αvβ5 integrin inhibitor, and phase two clinical trials suggested that, as a single agent, it had anti-tumour activity in recurrent glioblastoma and in combination with standard temozolomide chemoradiotherapy, it was effective in newly diagnosed glioblastoma (Nabors et al. 2012). However, phase three clinical trials showed that the addition of Cilengitide to temozolomide chemoradiotherapy gave no improvement to survival, so the clinical trials were discontinued (Stupp et al. 2014). In addition to the problems commonly faced with anti-angiogenic treatments, Cilengitide faced an additional problem. At very low concentrations, it is pro-angiogenic (Reynolds et al. 2009), meaning that it is likely to have had both anti- and pro-angiogenic effects clinically. While this caused Cilengitide to fail clinical trials as an antiangiogenic drug, its pro-angiogenic features may be advantageous if exploited in the correct setting, and we later discuss the repurposing of this drug.

11.4 Focal Adhesion Kinase (FAK)

11.4.1 Focal adhesion kinase

Focal adhesion kinase (FAK) is a 125kDa non-receptor tyrosine kinase that is ubiquitously expressed in the majority of cell types where it has roles in motility, adhesion, survival, growth, invasion and sensing rigidity in the environment (Lechertier and Hodivala-Dilke 2012; Brami-Cherrier et al. 2014). It is over expressed in many cancers, both solid and non-solid (Sulzmaier, Jean, and Schlaepfer 2014; Vita 2010), and is, therefore, a promising drug target.

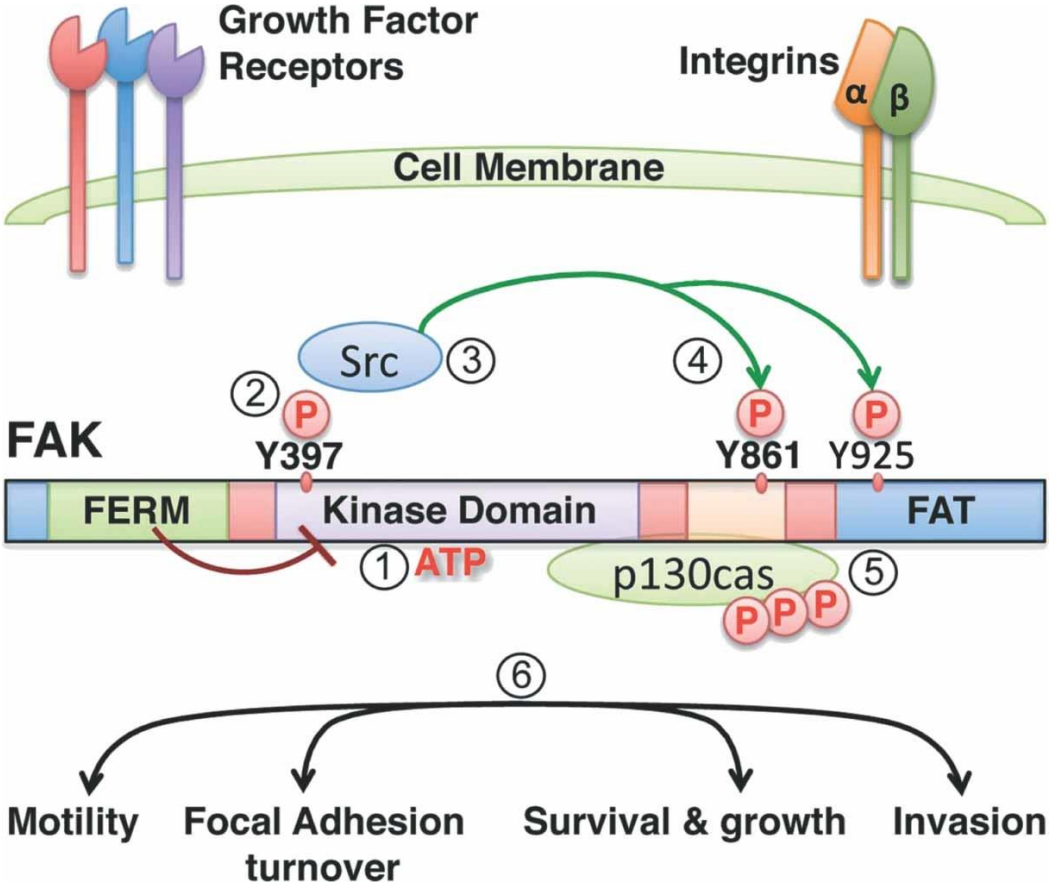

Figure 11.5 FAK structure and function.

FAK consists of a tyrosine kinase between two non-catalytic domains; the 4.1 ezrin radixin moesin (FERM) domain and the focal adhesion targeting (FAT) domain. FAK is maintained in an inactive form until activated in the following sequence of events: (1) clustered integrins of ligand-bound growth factors produce signals that bind to the FERM domain releasing the autoinhibitory interaction between FERM and the kinase domain, this allows ATP to bind, activating FAK, (2) FAK then autophosphorylates tyrosine (Y) 397 (3) which increases the affinity of Src homology 2 (SH2) allowing Src to bind, (4) Src transphosphorylates FAK at several sites including the key residues Y861 and Y925, (5) phosphorylation at Y861 allows p130cas to bind and phosphorylate itself, (6) activated FAK signalling has downstream effects on changing cell morphology and behaviour allowing changes in survival, growth, invasion, motility and behaviour and focal adhesion turnover. Figure from Lechertier T and Hodivala-Dilke K., Journal of Pathology, 2012.

11.4.2 Focal Adhesion kinase structure

FAK consists of a tyrosine kinase between two non-catalytic domains; the 4.1 ezrin radixin moesin (FERM) domain and the focal adhesion targeting (FAT) domain. FAK receives activating signals which bind to the FERM domain leading to tyrosine 194 (Y194) and tyrosine 397 (Y397) phosphorylation, increasing the affinity for Src homology 2 (SH2) allowing Src to bind. This increases the kinase activity of Src, initiating the formation of an active FAK-Src complex phosphorylating the FAT domain and allowing the binding of downstream signalling proteins (Zhou et al. 2015; Lawson and D Schlaepfer 2013) **(Figure 11.5)**.

FAK's control of cell motility, invasion, survival and EMT are kinase-dependent, but FAK also has kinase-independent roles; its scaffolding functions influence cell survival and breast cancer stem cell proliferation (Sulzmaier, Jean, and Schlaepfer 2014; Luo et al. 2013). Inhibitors of both the kinase domain and scaffolding functions of FAK mechanism have been developed and tested preclinically and clinically (Yoon et al. 2015). It is important to understand whether the mechanism is kinase-dependent to be able to target endothelial cell FAK for chemotherapy sensitivity *in vivo*. Pfizer's PF-573,228, like most FAK inhibitors, is an adenosine triphosphate (ATP)-competitive kinase inhibitor. It is highly specific to FAK kinase (Mabeta 2016) with an IC_{50} of 4nM for FAK and >1000 nM for Protein tyrosine kinase 2 (Pyk2) (Slack-Davis et al. 2007). Concentrations of PF-573,228 that reduced phosphorylation of FAK Tyr397 in REF-52 and PC3 cells inhibited migration suggesting focal adhesion turnover was inhibited but had no effect on growth or apoptosis. Importantly, mice lacking platelet FAK have a platelet aggregation defect which PF-573,228 recapitulates on human platelets *in vitro,* so could have deleterious effects clinically and failed to pass preclinical testing (Jones et al. 2009; Schultze and Fiedler 2011). The kinase inhibitors PF-562,271 and defactinib inhibit both FAK and Pyk2 kinase (Gerber et al. 2020; Roberts et al. 2008). PF-562,271 inhibits FAK and Pyk2 activity with IC_{50}s of 1.5 nM and 14 nM, respectively and inhibits tumour growth in a range of xenograft models (Chauhan and Khan 2021; Roberts et al. 2008). It also reduces invasion and metastasis in pancreatic ductal adenocarcinoma (PDAC) and optical window chamber (Canel et al. 2010; Stokes et al. 2011) *in vivo* models. It was generally well-tolerated in phase I clinical trial of patients with head and neck, prostatic and pancreatic cancer but did not progress to phase II or III (Schultze and Fiedler 2011). Defactinib, which is a highly potent inhibitor of both FAK Pyk2 (IC_{50}=0.6nM for both kinases (Shimizu et al.

2016), is well tolerated clinically with few adverse effects reported, so it has progressed to phase II clinical trials (Jones et al. 2015; Gerber et al. 2020; Fennell et al. 2019). In phase II trials, defactinib was moderately active in Kras mutant non-small cell lung carcinoma but, as a maintenance therapy, it did not meet the clinical trial outcome (Gerber et al. 2020). However, preliminary results of a phase I/Ib ovarian cancer trial of defactinib with paclitaxel demonstrated the potential of defactinib (Patel et al. 2014).

In contrast, to the kinase inhibitors are protein scaffold inhibitors such as Y11 and Y15 (Cure FAKtor). These inhibit the autophosphorylation of FAK at Y397 and have been shown to reduce cell viability in a variety of cancer cell lines (Yoon et al. 2015).

11.4.3 The *Pdgfb-iCre^{ert}* model

As constitutively active FAK mutations are embryonically lethal, to be able to study the effects of FAK mutation in adult mice, an inducible model is required. This problem is common to many molecular mechanisms in vascular biology, and therefore, Claxton et al. (Claxton et al. 2008) developed a system for creating inducible, endothelial-specific mutant mice.

To develop this model, they used Cre recombinase, tyrosine recombinase enzyme derived from the P1 bacteriophage, which catalyses a recombination event between two DNA recognition sites known as locus of X-over P1 (LoxP sites). LoxP sites are 34 base pair recognition sites made up of two 13 bp palindromic sequences flanking an 8bp spacer region. The product of Cre-mediated recombination at these sites depends on the location and orientation of the loxP sites. When separate DNA species contain loxP sites, the DNA can be fused when Cre cuts at the loxP sites. When DNA sequences contain two loxP sites, the DNA in between is described as ‘floxed’ and will be excised by Cre-recombinase in a process that does not require any accessory proteins or additional cofactors (such as ATP) (Nagy 2000; Abremski and Hoess 1984).

Cre recombinase was derived from a bacteriophage; mammalian codon usage was applied to it so that Cre expression was improved in three mammalian cell lines tested. In addition, as Cre is derived from prokaryotes, it contains a large number (65) 5'-cytosine-phosphate-guanine-3 (CpG) dinucleotides which, in mammals, can cause epigenetic silencing (Jabbari and Bernardi 2004; Tycko 2000). Therefore, the number of CpG repeats was reduced. This improved Cre gene is known as iCre (Shimshek et al. 2002) **(Figure 11.6 A)**.

Tamoxifen is a selective oestrogen receptor modulator commonly used to treat and prevent oestrogen receptor (ER) positive breast cancer (NIH 2021). The iCre was fused with a mutant form of the human oestrogen receptor (ERT2) that does not respond to naturally occurring oestrogen but is responsive to the tamoxifen metabolite 4-hydroxytamoxifen (OHT). This created a tamoxifen-inducible form of Cre recombinase, known as iCre^{ert} **(Figure 11.6 B)**.

In order to make transgenic mice that express this tamoxifen-inducible Cre specifically in endothelial cells, *Pdgfb* was used as it is predominantly expressed in the endothelial cells (Hellstrom et al. 1999). This was done by using a phage artificial chromosome (PAC) containing the *Pdgfb* gene to develop *Pdgfb-iCre^{ert}* mice **(Figure 11.6 C)**. PAC is a DNA construct derived from the P1 bacteriophage that can carry up to 300 kb of DNA and be used for Cre-lox recombination (Yarmolinsky and Hoess 2015; Sternberg 1990). The PAC containing genomic sequences up and downstream of the *Pdgfb* gene was used to create the transgenic mice by pronuclear injection. This contained all of the regulatory sequences required to drive the iCre$^{ert.}$ When there is no 4-Hydroxytamoxifen (OHT) present, iCre^{ert} remains sequestered by HSP90 in the cytoplasm of the cell. However, when OHT is administered, iCre^{ert} translocates to the nucleus, where it mediates recombination at loxP sites (Claxton et al. 2008).

To test the efficiency of the tamoxifen-induced iCre recombinase, they used ROSA26-lacZ reporter and found that, in newborn animals, recombination occurred in the majority of capillary and small vessel endothelial cells in most organs, including the central nervous system (CNS). In adult mice, the recombination was also widespread across capillaries of skeletal muscle, heart, skin, and gut, but in the central nervous system, only a subpopulation of the total endothelial cells was labelled. To test whether the recombination would also occur in implanted cells, they used a subcutaneous tumour model and found that recombination activity in all tumour blood vessels. Therefore, the *Pdgfb-iCre^{ert}* mice became a valuable tool to manipulate endothelial cell biology in postnatal mice and to study tumour angiogenesis.

As discussed in more detail for endothelial cell FAK kinase-dead model, the *Pdgfb-iCre^{ert}* mice allow different mutations to be put under the control of the *Pdgfb* promoter **(Figure 11.6 D)**. This means that when tamoxifen induces the Cre recombinase activity, the mutations become active in endothelial cells (Claxton et al. 2008).

For example, the *FAK$^{fl/fl}$* mouse has two loxP sites (LP2) flanking the exon that codes for FAK protein. This enables *FAK*-deletion under the control Cre (McLean et al. 2004), and therefore, crossing this mouse with the *Pdgfb-iCre^{ert}* mouse puts FAK expression under the control of the *Pdfgb*-driven Cre production and tamoxifen-induced Cre activity in endothelial cells only (Tavora et al. 2010).

The *Pdgfb-iCre^{ert}* model can also be used for more complex manipulation of FAK, including the FAK the series of FAK knockin (KI) models produced by Tavora et al. (Tavora, Batista, et al. 2014). In these models, mutant FAK is knocked in in the endothelial cells on Tamoxifen induction. The mutant FAK is either kinase-dead, has tyrosines Y397 or Y861 sites replaced with phenylalanine (Y397F or Y861F), making them unphosphorylatable or a mutant Y397E resulting in a continuously active Y397 (Tavora, Batista, et al. 2014).

The *Pdgfb-iCre^{ert};FAK$^{fl/fl}$;R26 FAK$^{K454R/K454R}$* model, which renders endothelial cells FAK-kinase dead under the temporal control of tamoxifen, is discussed further in the methods section.

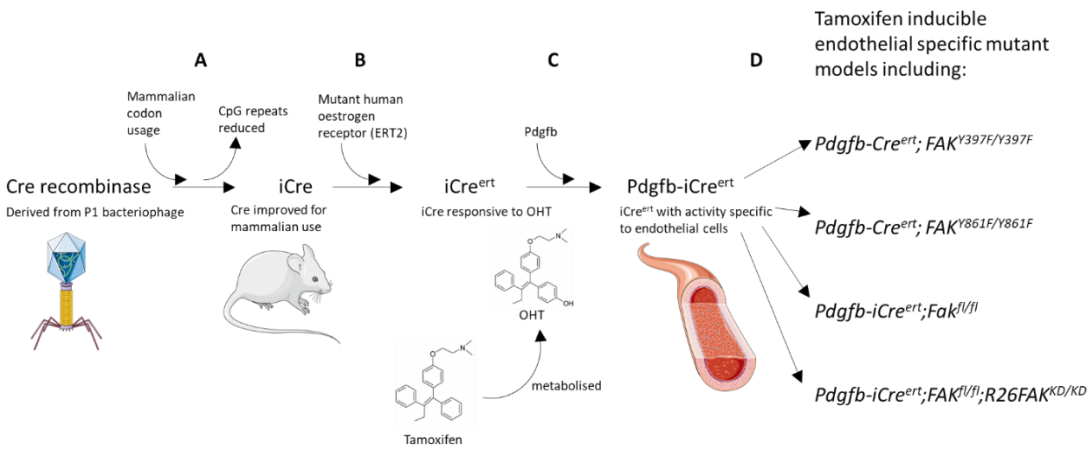

Figure 11.6 *Pdgfb-iCre^{ert}* model development

The *Pdgfb-iCre^{ert}* model was developed by (A) adapting phage *Cre* recombinase to *iCre* for mammalian use, (B) adapting *iCre* to *iCre^{ert}* to enable *Cre* activation only after exogenously administered tamoxifen that is metabolised OHT, (C) making *iCre^{ert}* endothelial specific under the *Pdgfb* promotor. (D) This model can then be used to make a range of mutations endothelial specific and tamoxifen inducible with examples given. These are examples of crosses using the *Pdgfb-iCre^{ert}* mice that we have generated in our lab (Tavora et al. 2010; Tavora, Batista, et al. 2014).

11.4.4 Phosphorylation of endothelial cell FAK

The expression of FAK in endothelial cells is vital for angiogenesis initiation (Tavora et al. 2010; Weis et al. 2008), but the level of differential phosphorylation at Y397 and Y861 also regulate tumour angiogenesis (Tavora et al. 2010; Weis et al. 2008; Tavora, Reynolds, et al. 2014). The phosphorylation of FAK Y397 is crucial developmentally.While FAK-null mice die at embryonic day 8.5, animals with FAK Y397 deleted by linker domain truncation mutation survive little longer, dying at E13.5-E14.5 (Corsi et al. 2009) and animals with Y397 substituted with a non-phosphorylatable phenylalanine (Y397F) die by E11.5 (Heim et al. 2017) this is due to the essential role of FAK Y397phosphorylation in angiogenesis making it a requirement for development *in utero*.

FAK Y397 phosphorylation also plays a major role in cancer development. The small-molecule inhibitor 1-(2-hydroxyethyl)-3, 5, 7-triaza-1-azoniatricyclo [3.3.1.13,7] decane; bromide named Y11 was developed through computer modelling of FAK. It binds to the N-terminal of FAK, targeting the Y397 site, specifically and significantly decreasing FAK Y397 autophosphorylation. *In vitro*, it reduces viability and clonogenicity while increasing apoptosis and detachment of cancer cell lines. In mice with colon cancer cell xenografts, it reduces Y397-FAK autophosphorylation correlating with reduced tumour growth (Golubovskaya et al. 2012). Therefore, FAK Y397 autophosphorylation is considered a target for cancer therapy.

Tumour growth and angiogenesis are reduced in inducible *pdgfb-iCre^{ert} ECCre+; FAK$^{Y397F/Y397F}$* mutant mice which have the tyrosine residue 397 mutated to a phenylalanine preventing normal phosphorylation at this site. In contrast, in *ECCre+;FAKY$^{861F/Y861F}$* mice, where the mutation is at Y861, there is an initial reduction in angiogenesis but is restored later in end-stage tumours, and overall tumour growth is not affected. FAK-Y397F ECs have increased levels of the expression of angiogenesis regulator Tie2, reduced Vegfr2 expression, decreased activation of integrin β1, and disruption of downstream FAK/Src/PI3K(p55)/Akt signalling. Whereas FAK-Y861F ECs have both decreased levels of Vegfr2 and Tie2 expression and enhanced β1 integrin activation. Mutations preventing Y397 or Y861 from being phosphorylated both regulate Vegfr2 and Tie2 expression and β1 integrin activation but in contrasting ways. Therefore, it was hypothesised that the differential phosphorylation of FAK regulates sensitivity to angiogenic growth factors through an inside-out signalling cascade. The exact mechanism by which this differential regulation is controlled is not known however, in the FAK-Y397F animals, Src binding to FAK and all subsequent phosphorylation is

impaired **(Figure 11.5)**. In contrast, in the FAK-Y861F animals, the autophosphorylation of FAK at Y397 is not impaired meaning that Src binding to FAK is not affected but Src phosphorylation of Y861 and anything downstream of this is affected **(Figure 11.5)**. In addition to phosphorylating FAK-Y861, Src also phosphorylates FAK-Y925 once bound to FAK. Therefore, in the FAK-Y861F animals, where Src binding is intact, it may be expected that Y925 phosphorylation is not affected. However, in practice, phosphorylation of FAK-Y925, is much reduced in FAK-Y861F mice compared to wildtype animals. The reason for this is unknown but suggests that a downstream effect of Y861 phosphorylation impacts the phosphorylation of FAK-Y925 by Src. For example, it may be that the phosphorylation of FAK-Y861 causes a conformational change in FAK opening up the structure to facilitate Y925 phosphorylation. (Pedrosa et al. 2019). It is currently unclear how this differential phosphorylation controls the expression of surface receptors such as Tie. However, FAK activity regulates the recycling, degradation and surface expression of integrins thereby controlling its activation (Thomas et al. 2010; Alanko et al. 2015; Nader, Ezratty, and Gundersen 2016; Alanko and Ivaska 2016; Pedrosa et al. 2019). Therefore, it is hypothesised that FAK may control the surface expression of receptors of Vegfa and ANG2 through a similar control of recycling and degradation. Alternatively, the differences in Tie2 and Vegfr2 expression may be a result of differences in β1 integrin activation. Adhesion mediated by FAK and integrins is known to influence the surface expression of proteins (Lebrun et al. 2000) so the differences in Tie2 and Vegfr2 expression may be due to adhesion mediated by β1 integrin (Pedrosa et al. 2019). The differential control of Tie2 expression may be important in the maturation of blood vessels as reduced endothelial cell Tie2 expression correlates with decreased vascular perfusion and function (Tsai and Lee 2009). Kinase and non-kinase functions of FAK.

The kinase-dependent roles of FAK are activated by autophosphorylation of Y397. Most functions of FAK in cancer, including cell motility, invasion, cell survival and transcriptional events promoting epithelial-to-mesenchymal transition (EMT), are kinase-dependent (Sulzmaier, Jean, and Schlaepfer 2014). However, many roles of FAK are also supplemented by kinase-independent roles. For example, mammary stem cells (MaSCs) and progenitor cells are essential for the healthy development and maintenance of mammary glands but may also become mammary cancer stem cells. Loss of the kinase activity of FAK in embryonic mammary epithelial cells decreases alveologenesis and proliferation of luminal progenitor cells. Reduced numbers of luminal progenitors

suppressed tumorigenesis and formation of mammary cancer stem cells in a mouse model of breast cancer (Luo et al. 2013).

In addition, FAK is also known to have scaffolding functions which are kinase-independent and influence cell survival and the proliferation of breast cancer stem cell proliferation (Sulzmaier, Jean, and Schlaepfer 2014).

11.4.4.1 Nuclear functions of FAK

In addition to its cytoplasmic kinase roles, nuclear FAK also has essential roles. It promotes the ubiquitination and subsequent degradation of *p53*, leading to the growth and proliferation of cancer cells. It also regulates the expression of the transcription factor GATA4 and the cytokine interleukin 33 (IL-33), reducing inflammatory responses and promoting immune escape (Zhou, Yi, and Tang 2019). FAK mediation of cell survival combines nuclear and scaffolding roles in the nucleus, using its FERM domain, where it acts as a scaffold binding both *p53* and the E3 ubiquitin ligase mouse double minute 2 (Mdm2). This allows the ubiquitination and degradation of *p53*, leading to enhanced cell survival (Cance and Golubovskaya 2008; Lim et al. 2008).

11.4.5 Focal Adhesion kinase in tumour and stromal cells

Originally, most work on FAK focused on mechanisms for chemotherapy resistance in tumour cells with important roles in cancer cell survival, anoikis resistance (Kim et al. 2012; Reddig and Juliano 2005), proliferation, migration, invasion and metastasis (Tai, Chen, and Shen 2015). However, it is now accepted that in the tumour microenvironment FAK has a strong influence on cancer; it is required for motility of TAMs, which suppress tumour cell attack by T cells and natural killer (NK) cells, stimulates angiogenesis and increases invasiveness, migration, and metastasis (Noy and Pollard 2014). FAK is also involved in the regulation of CAFs, which secrete chemokines and growth factors enabling cancer development via a protumour microenvironment for cancer, endothelial, and inflammatory cells (Kalluri and Zeisberg 2006).

11.4.6 Endothelial cell FAK

Deletion of endothelial cell FAK in *Tie-Cre* 2 mice results in embryonic lethality between e10.5 and e11.5. Before any other defects are apparent at e9.5, the capillaries and inter-capillary spaces in yolk sacs dilate, suggesting an endothelial cell defect (Braren et al. 2006). Similarly, a global knock-in kinase-dead mutation is lethal at embryonic day 9.5 with vascular defects (Lim, Chen, et al. 2010), demonstrating that FAK has a role in blood vessel morphogenesis, cell polarity and motility (Roy-Luzarraga and Hodivala-Dilke

2016), and the kinase domain is responsible for the control of many endothelial cell processes.

Endothelial cells form a vascular barrier between the blood and tissue by forming cell-cell adhesive interactions. Many soluble molecules can disrupt this barrier function, which often increases tissue damage in cancer and ischaemic reactions. For example, in cancer, leaky blood vessels cause the release of fibrin, attracting the materials required to create new blood vessels; it also causes an increased interstitial pressure which adds to the difficulty in drug delivery (Weis and Cheresh 2005). VEGF signalling promotes permeability in a FAK dependent manner; it stimulates the activation of FAK into an open conformation which localises to the VE cadherin cell-cell junctions so that the FERM domain of FAK binds to the cytoplasmic tail of VE-cadherin in the endothelial cell. FAK then phosphorylates β catenin on tyrosine Y142, allowing VE-cadherin to dissociate from β-catenin, breaking down the endothelial cell junction (Chen et al. 2012).

11.4.7 FAK in metastasis

Metastasis requires tumour cell intravasation into blood or lymph vessels and extravasation at the metastatic site (Chiang and Massagué 2008); therefore, compromising the barrier function of endothelial cells facilitates metastasis as it enables extravasation. Inhibition of FAK has been demonstrated to prevent both tumour growth and metastasis. FAK inhibition prevents the migration of tumour cells across endothelial cell barriers and prevents the extravasation of tumour cells and the metastasis of melanoma from dermal to lung (Jean et al. 2014).

11.4.8 FAK-regulated immune responses

FAK also has a role in the regulation of immune responses in the TME, promoting tumour immune evasion. In syngeneic mouse model of squamous cell carcinoma (SCC), the kinase activity of nuclear FAK regulates the production of chemokines and cytokines. This control of the immune component is through nuclear FAK binding to transcription factors and their upstream regulators within the chromatin. This interaction increases the production of chemokine (C-C motif) ligand 5 (CCL5), IL-33 and a soluble, secreted form of the IL-33 receptor interleukin 1 receptor-like 1 (ST2) called soluble ST2 (sST2). IL-33 forms a complex with FAK which interacts with chromatin modifiers to induce NF-κB activation which promotes transcription of chemokines including CCL5, thereby further increasing the CCL5 production. The production of CCL5 leads to recruitment of Tregs and depletion of CD8+ T cells in the TME. CD8+ T cell activity is inhibited allowing immune evasion in tumours with high levels on nuclear FAK. In FAK-positive SCC cells, there is a significant increase in IL-33 and CCL5 levels, but there was no difference in their production in normal keratinocytes. In addition, treatment of mice in this model with the FAK kinase inhibitor VS-4718 induces CD8+ T cell production and Treg depletion promoting an anti-tumour immune response (Serrels and Frame 2016; Serrels et al. 2015; Kurmasheva et al. 2017; Serrels et al. 2017).The vascular niche and chemoresistance

The vascular niche is a microenvironment created by the blood vessels and surrounding cells. In addition to the angiocrine signalling of endothelial cells stimulated by DNA damaging therapies, there are additional pro-tumorigenic signals that can come from the vascular niche. For example, VEGF-A activation of endothelial cells signals leukaemic cells to proliferate at higher rates and increases adhesion of the leukaemic cells to endothelial cells. In addition, the activated endothelial cells increase the chemotherapy resistance of the leukaemic cells (Poulos et al. 2014). Cao et al. (Cao et al. 2014) suggest a mechanism for the promotion of aggressive cancers by endothelial cells. They propose that in lymphoma, B cell lymphoma cells activate FGFR1 to produce FGF-4. This upregulates the Notch ligand Jagged1 (Jag1) on nearby endothelial cells. The endothelial cells upregulate Jag1 expression inducing the expression of Notch2-Hey1 in the lymphoma cells. This crosstalk allows the growth of the more aggressive CD44+IGF1R+CSF1R+ phenotypes of lymphoma cells. They demonstrate that deletion of Fgfr1 or Jag1 in endothelial cells or impairing Notch2 signalling made lymphomas less aggressive and increased survival. Therefore, the vascular niche is a valuable target in cancer therapy.

In addition, the endothelial cells are involved in the creation of a chemoresistant niche in response to genotoxic therapy. In a model of Burkitt's Lymphoma, IL-6 and Timp-1 are released from the thymus in response to DNA damage. This creates a chemo-resistant niche promoting lymphoma cell survival and eventual relapse (Gilbert and Hemann 2010). Small molecule inhibition of cytokine-induced signalling can help to mitigate this response, enhancing chemotherapeutic efficacy. Gilbert et al. show that the IL-6 release results from p38 MAP Kinase activation in tumour-associated endothelial cells immediately after DNA damage and occurs in treated human endothelial and hepatocellular carcinoma cells, suggesting it is a constant response. This rapid cytokine release in the thymus precedes cellular senescence induction, promoting sustained cytokine release in cultured cells (Acosta et al. 2008; Coppé et al. 2008; Kuilman et al. 2008; Wajapeyee et al. 2008). Therefore, in addition to their anti-cancer effects, genotoxic drugs can have an opposing effect, inducing pro-survival signalling in select anatomical sites so that there is a reservoir of minimal residual disease that eventually fuels tumour relapse (Gilbert and Hemann 2010).

11.4.9 Pyk2

Pyk2 is the closest paralogue of FAK (Corsi et al. 2006; Naser et al. 2018) and can often compensate for FAK, including during pharmacological inhibition of FAK (Sieg et al. 1998; Weis et al. 2008). Pyk2 has a similar structure and function to FAK, sharing a high degree of sequence homology, especially at the N-terminus and kinase domain (Kanner, Aruffo, and Chan 1994; Avraham et al. 1995; Sasaki et al. 1995). Similar to FAK, Pyk2 has an autophosphorylation site, which can serve as a Src SH2-domain binding site when it is phosphorylated (Dikic et al. 1996). Both proteins are also involved in signalling to the actin cytoskeleton, although only FAK typically localizes to focal adhesions (Sasaki et al. 1995; Astier et al. 1997; Guan 1997).

However, its distribution in tissues differs; FAK is ubiquitously expressed, whereas Pyk2 is predominantly expressed in the brain, osteoclasts, macrophages and lymphocytes (Beinke et al. 2010). Where they are co-expressed, there may be redundancy as both perform similar roles; however, in certain situations, their roles can differ and even contrast. Their activation differs in that FAK is primarily activated in response to integrin activation, whereas Pyk2 may be activated by stress, calcium flux or ligation of B and T cell receptors (Avraham et al. 2000). Furthermore, they contrast in that while FAK activation promotes cell survival and cell cycle progression, Pyk2 activation generally inhibits both cell cycle progression and survival (Xiong and Parsons 1997; Chauhan et al.

Therefore, although in many cases, dual inhibition of FAK and Pyk2 may be helpful to achieve the therapeutic effects desired, in specific tissues and circumstances where FAK and Pyk2 have contrasting roles, specific inhibition of FAK or Pyk2 in isolation may be more helpful (Naser et al. 2018).

In the case of endothelial cells, Pyk2 has also been reported to be expressed and, in some circumstances, may compensate for FAK (Weis et al. 2008). However, when FAK expression is heterozygous in endothelial cells, Pyk2 expression and phosphorylation levels do not change, demonstrating that it does not compensate for this reduction in FAK levels (Kostourou et al. 2013).

11.5 Angiocrine signalling / EC-FAK regulating chemosensitivity

We have previously shown that targeting endothelial cell FAK can sensitise tumours to DNA damaging therapies, reducing their growth and increasing survival (Tavora, Reynolds, et al. 2014) **(Figure 11.7)**. *Pdgfb-iCre^{ert};Fak$^{fl/fl}$* mice are an inducible model of endothelial cell-specific FAK deletion, and administration of tamoxifen generates *ECFAK^{KO}* (FAK deleted) and *ECFAK^{WT}* (expressing normal FAK) mice. Inducible deletion of FAK in mice with established subcutaneous B16F0 melanoma or CMT19T lung carcinoma tumours sensitised them to doxorubicin or irradiation, respectively reducing the tumour growth compared to controls. Consistent with this, FAK deletion decreased proliferation and increased the level of apoptosis in the tumours of doxorubicin or irradiation treated mice compared to similarly treated *ECFAK^{WT}* mice. This demonstrated for the first time that EC-FAK regulates chemosensitivity. FAK-KO endothelial cells stimulated with doxorubicin had less NF-κB activity than similarly treated WT endothelial cells suggesting FAK has a role in activating the NF-κB pathway, which controls cellular processes such as cytokine production and cell survival. FAK-KO ECs treated with doxorubicin produce less NF-KB dependent endothelial cytokines, suggesting that FAK regulates resistance to DNA damaging therapy by angiocrine signalling. FAK-WT ECs treated with doxorubicin create a pro-tumourigenic microenvironment through cytokine production via FAK.

This is an important study as chemotherapy resistance can lead to increased cancer progression (Hansen, Woods, and Read 2017). To use endothelial cell FAK to target chemotherapy resistance, we must understand the mechanism so that the most appropriate inhibitor can be used.

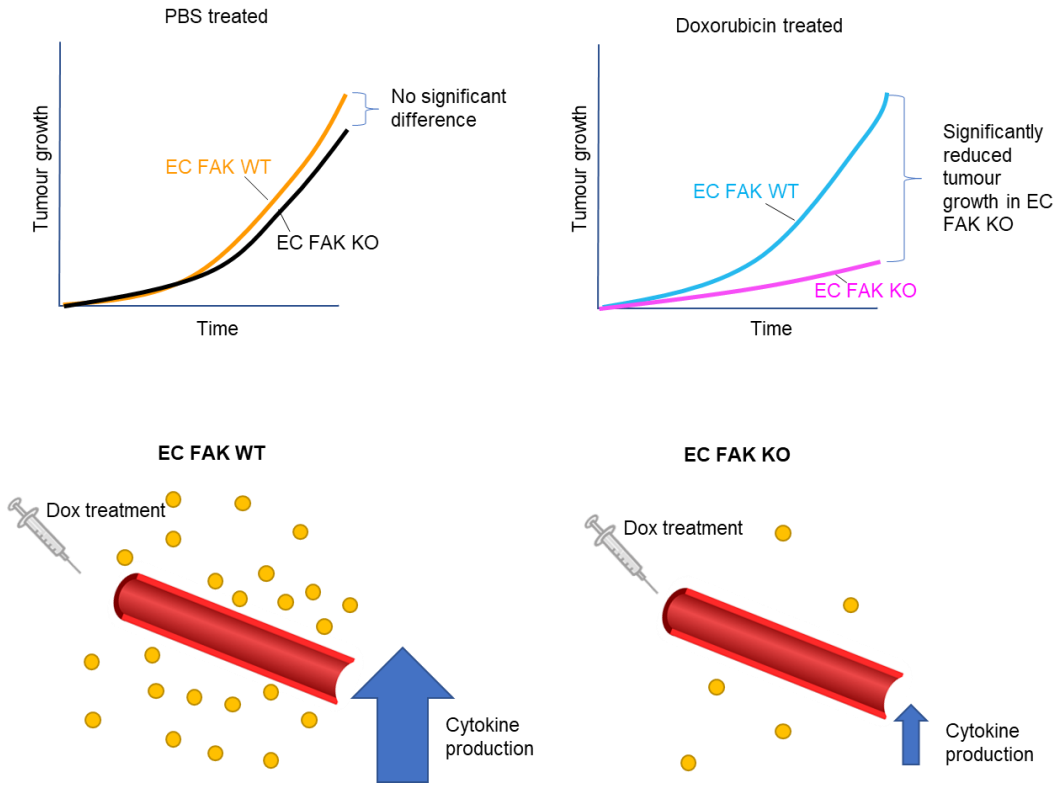

Figure 11.7 Endothelial cell FAK KO sensitises tumours to DNA damaging therapy

Pdgfb-iCre^{ert}*; Fak*$^{fl/fl}$ and control mice were injected subcutaneously with 1 million B16F0 melanoma cells (day 0). From day 7 onwards, they were given tamoxifen (Tam.) to generate EC-FAK^{KO} and EC-FAK^{WT} mice respectively. No significant difference in tumour volume was found between untreated EC-FAK^{KO} and EC-FAK^{WT} mice. However, when treated with doxorubicin (dox.) the tumour growth in EC-FAK^{KO} animals was significantly reduced compared to EC-FAK^{WT}. In WT cells *in vitro*, there was an upregulation of cytokine production with doxorubicin treatment which was significantly muted in EC-FAK^{KO} cells suggesting that an altered cytokine profile was responsible for the change in doxorubicin response *in vivo*. (From Tavora et al. 2014).

11.5.1 EC-FAK as a biomarker

Endothelial cell FAK is associated with tumour promotion; in the pre-metastatic phase, it mediates hyperpermeability of the lung, allowing metastatic cells to home more easily to foci (Hiratsuka et al. 2011). In ovarian carcinomas, there is an increase in FAK expression in both tumour cells and the associated blood vessels; the overexpression of phosphorylated FAK Y397 in the vasculature of these tumours is predictive of poor prognosis (Stone et al. 2014). In addition, the tumour associated ECs of invasive ovarian carcinoma have significantly increased levels of FAK (Lu et al. 2007). In astrocytic tumours, high levels of microvascular endothelial cell FAK are associated with grade III and IV tumours but not grade I and II (Haskell et al. 2003).

In breast cancer, the level of endothelial cell FAK correlates with the molecular sub-type and prognosis of invasive cancers. Low endothelial cell FAK expression correlates with luminal A subtype, and higher endothelial cell FAK correlates with the worse prognosis non-luminal A tumours. The study also suggests that high endothelial cell FAK correlates with aggressive triple-negative and basal-like breast cancers (Alexopoulou et al. 2014). In fact, of a cohort of 82 women with locally advanced breast cancer, high levels of EC-pY397-FAK correlated with high Ki67, higher tumour category, higher lymph node category and higher tumour node metastasis stage. Out of 21 patients with high EC-pY397-FAK expression, none had a pathologic complete response compared to 11 of 61 patients with high EC-pY397-FAK. In addition, both high EC-pY397-FAK expression and high blood vessel density were associated with reduced five-year, relapse-free survival in this cohort (Roy-Luzarraga et al. 2020).

11.6 Pancreatic ductal adenocarcinoma (PDAC)

Pancreatic ductal adenocarcinoma is the fourth leading cause of cancer-related death worldwide, the overall five-year survival recorder in 2019 was less than 8 % (Orth et al. 2019; Siegel, Miller, and Jemal 2019), and its incidence is expected to increase in the US and Europe over the next ten years (Quante et al. 2016; Rahib et al. 2014; Orth et al. 2019) https://www.cancerresearchuk.org/health-professional/cancer-statistics/statistics-by-cancer-type/pancreatic-cancer#heading-Zero. At diagnosis, 80-90 % of patients already have locally advanced, non-resectable PDAC or distant metastases meaning they are not candidates for surgery (Gillen et al. 2010; Werner et al. 2013). Chemotherapy is a common first-line treatment in patients with non-resectable or borderline-resectable tumours. This includes gemcitabine, capecitabine or 5-fluorouracil

(5-FU) as a monotherapy or in combination. Additionally, the combination of folinic acid, 5-FU, irinotecan and oxaliplatin (FOLFIRINOX) can almost double median survival in patients with metastatic cancer compared to gemcitabine alone (Conroy et al. 2011) but is associated with more toxicity so cannot be used in elderly patients (Gourgou-Bourgade et al. 2013).

The vascular promotion element of my thesis will focus on developing the technique for the treatment of PDAC. PDAC is notoriously difficult to treat and is expected to become the most common cause of cancer-related death in the US by 2030 (Rahib et al. 2014). PDAC progression begins with non-invasive precursor lesions called pancreatic intraepithelial neoplasia (PanIN). These are generally under five millimetres and are the result of proliferation and metaplasia of the ductal epithelium in the pancreas (Yu et al. 2018). PanIN progresses from PanIN-1 to PanIN-3 before becoming PDAC. Pan-IN 1 lesions are made up of columnar epithelial cells with round, basally oriented nuclei. PanIN-2 lesions have a more complex morphology than PanIN-1, the nuclei begin to lose polarity, and there is more variation in nuclear size. PanIN-3 lesions have higher dysplasia and are architecturally complex. The nuclei are enlarged, irregular in size and poorly orientated. From PanIN-3, lesions may progress to PDAC; at this stage, the irregular structure invades out of the pancreatic lobular structure (Hruban, Maitra, and Goggins 2008).

The TME is thought to be a major contributor to the challenges in PDAC treatment (Murakami et al. 2019). PDAC TME is characterised by a dense, fibrous stroma making the tumour highly drug-resistant. In addition, pancreatic cancer creates an immunosuppressive tumour microenvironment evading the host immune system, stellate cells, ECM and immune cells, especially CAFs, interact with the tumour cells controlling their growth, invasion and metastasis. In addition, they release cytokines which further enhance tumour growth (Murakami et al. 2019).

Pancreatic cancer is highly hypoxic, which promotes a fibrotic reaction, further increasing the ECM component of the TME. This hypoxia is thought to have a role in signalling resulting in invasion and metastasis and is increasingly being viewed as an indicator of pancreatic cancer malignancy and a target for therapy (Yuen and Díaz 2014). A significant cause of the hypoxic microenvironment is that pancreatic cancer is also, importantly, characterised by hypervascularity, which is thought to limit the access to the TME of tumour suppressive immune cells. In fact, patients with high expression of cluster of

differentiation 31 (CD31) have greater overall survival than those with low CD31 expression (Katsuta et al. 2019). Therefore, the manipulation of the blood vessel density in pancreatic cancer is a possible target for drug development.

11.7 Therapeutic manipulation of the tumour vasculature

11.7.1 The rationale behind the development of antiangiogenic drugs for the treatment of cancer

The presence of blood vessels in cancer was first reported over 100 years ago and was promoted as an important feature of cancer research over the last 40 years (Goldmann 1907; Algire et al. 1945; Carmeliet and Jain 2000). In 1939, Ide et al. suggested that the growth of new blood vessels was stimulated by factors released by tumour cells, and in 1945, Algire and Chalkley showed that tumours could cause continuous capillary growth by the host (Ribatti 2008). Using a transparent chamber implanted into cat skin, they observed vasoproliferation in response to wound or implantation of normal or neoplastic tissues. The vasoproliferative response induced by tumour tissues was observed earlier and was more substantial than the response to normal tissue or a wound, suggesting a close involvement of tumours with the vascular network (Algire et al. 1950). Melwin and Algire (1956) added to this that while the implantation of normal tissues induced a vasoproliferative response in the host, this never extended to the implanted tissue and was only present if the implant was less than 50 µm away. In contrast, implanted tumour tissue induced the formation of new blood vessels penetrating into the implant and had a much greater range (Merwin and Algire 1956).

In 1963, Folkman and Becker perfused canine thyroid glands with haemoglobin substitutes maintaining them for up to two weeks. They injected them with mouse melanoma cells and found that tumours developed but never grew beyond one to two millimetres and were never vascularized (Folkman, Long, and Becker 1963). However, when these tumours were transplanted into host mice, they became vascularized and grew to volumes exceeding $1cm^3$. This research showed for the first time that a tumour growing on a perfused organ where neovascularization does not occur is limited to 1-2 mm^3. In contrast, in a live host, where neovascularization does occur, the tumour grows rapidly, thus linking the absence of neovascularization with severely restricted tumour growth (Folkman, Long, and Becker 1963).

In 1971, Folkman published the hypothesis that tumour growth depends on angiogenesis; therefore, inhibition of angiogenesis could be used therapeutically (Folkman 1971). In this article, he coined the term 'anti-angiogenesis', meaning the restriction of new blood vessel recruitment to a tumour. He predicted that if the continuous recruitment of new capillaries to the tumour could be prevented, it would be restricted to 1-2mm^3.

Since this significant discovery, extensive research has proven Folkman's hypothesis (Folkman and Hochberg 1973; Gimbrone et al. 1973; Gimbrone et al. 1974; Ausprunk, Knighton, and Folkman 1974, 1975; Knighton et al. 1977; Brem et al. 1976).

Since Judah Folkman's 1971 publication *Tumor Angiogenesis: Therapeutic Implications* declaring that tumours are angiogenesis dependent, there has been interest in therapeutically manipulating tumour vasculature (Folkman 1971; Carmeliet and Jain 2000). Folkman showed preliminary evidence that without recruiting new capillaries to a solid tumour, it cannot grow beyond a few millimetres. He stated that an unknown diffusible factor was responsible for stimulating endothelial cell proliferation in the host capillaries (Cao and Langer 2008). He hypothesised that if this unknown factor could be blocked, a tumour could remain in a dormant state with no angiogenesis and possibly no metastasis and thus introducing the concept of anti-angiogenesis. Over the following decades, the 'unknown factor' was discovered to be a combination of fibroblast growth factor (FGF), vascular endothelial growth factor (VEGF), also known as vascular permeability factor (VPF), platelet-derived growth factor (PDGF) and angiopoietin families (Cao et al. 2004; Stacker et al. 2001; Folkman and Klagsbrun 1987; Rajabi and Mousa 2017; Dvorak et al. 1995).

11.7.2 Anti-angiogenesis as a therapeutic strategy for cancer therapy

From the time that Judah Folkman showed the necessity of angiogenesis in cancer growth, many promising anti-angiogenic therapies were developed. Angiogenesis inhibitors may be direct (acting on endothelial cells) or indirect (acting on tumour or stromal cells) (Rajabi and Mousa 2017). Direct inhibitors inhibit the proliferation and migration of vascular endothelial cells in response to angiogenic factors (Rajabi and Mousa 2017). For example, endostatin is a naturally occurring direct inhibitor of angiogenesis that prevents microvascular endothelial cells from responding to pro-angiogenic stimuli such as bFGF and VEGF (Folkman 2006; Abdollahi et al. 2003). A recombinant endostatin (Endostar) has been used clinically for the treatment of stage

IIIB and IV NSCLC patients who had a life expectancy under three months. Patients were treated with a standard chemotherapy regimen of vinorelbine and cisplatin with or without the addition of Endostar. Those given the triple combination had significantly enhanced response rate and median time to progression compared to chemotherapy alone (Sun et al. 2005). Indirect inhibitors may block the production or activity of pro-angiogenic proteins; for example, Bevacizumab, the first FDA approved anti-angiogenic treatment, is an IgG1 humanized monoclonal antibody which neutralises VEGF-A (Diaz et al. 2017; Quick et al. 2014). Bevacizumab has had some success in clinic including in patients with colorectal cancer and lung cancer (Cohen et al. 2007; Lauro et al. 2014). Bevacizumab was initially approved for use in combination with paclitaxel for patients with metastatic HER-2 negative breast cancer who had not received chemotherapy. This approval was based on a 5.5 month increase in progression free survival (PFS). However, the drug has severe, common side effects including high blood pressure, numbness, increased risk of infection and increased bleeding. Therefore, an increase in median PFS without improved overall survival or quality of life does not provide meaningful clinical benefit to the patients (Sasich and Sukkari 2012; CRUK 2019).With all anti-angiogenic treatments, there are problems caused by the pruning of blood vessels, these contribute to adverse effects which can be severe as in the case of Bevacizumab. In addition, the pruning of blood vessels can have effects that promote tumour growth and progression. Anti-angiogenesis increases hypoxia, accelerating tumour progression through a number of mechanisms such as increases in migration and inflammation and a more stem-like cell phenotype as well as increased resistance to chemo and radio therapy (Ramjiawan, Griffioen, and Duda 2017; Jain et al. 2018; Jain 2005). Some studies also suggest that after anti-angiogenesis, there is a reduction in drug delivery (Ma et al. 2001; Jain and Stylianopoulos 2010; Wang and Zhu 2016), and the tumour microenvironment is more immunosuppressive (Wang and Zhu 2016). In addition, anti-angiogenesis may also affect wound healing and blood pressure (Rajabi and Mousa 2017; Chen and Cleck 2009; Belcik et al. 2012).

Avastin,

11.7.3 Vascular normalisation as a therapeutic strategy for cancer therapy

To counter some of the problems associated with anti-angiogenesis, Rakesh J. Jain introduced the concept of vascular normalisation in 2005 (Jain 2005), using lower doses of anti-angiogenic drugs to ‘normalise’ tumour vasculature. Vascular normalisation has successfully reduced hypoxia and increased delivery and efficacy of cytotoxic agents by

increasing pericyte coverage, which improves vessel stabilisation, reducing vascular permeability and leakiness (Cooke et al. 2012; Meng et al. 2015).

Normalising tumour vasculature makes the tumour microenvironment more immuno-permissive by reducing levels of Tregs and regulatory B cells and enhancing the levels of the M1 macrophages and activation of T-cells CD8+ T cells (Hung et al. 2013). For example, a low dose of the VEGFR2 inhibitor DC101 in combination with a mitomycin C vaccine led to higher CD4+ and CD8+ cell infiltration, lower levels of Myeloid-derived-suppressor cells (MDSCs) and Tregs. It resulted in decreased hypoxia, breast cancer cell proliferation and increased survival (Huang et al. 2012).

Vascular normalisation often limited by most of the strategies being temporary, meaning that it is hard to use them in combination with other therapies such as immunotherapy (Wong, Bodrug, and Hodivala-Dilke 2016). Therefore, both the ability to lengthen it are important in the therapeutic benefit of vascular normalisation.

There are methods being developed to lengthen the window of vascular normalisation, the simplest being through modulation of the dose of anti-angiogenic agent. For example, lower doses of anti-VEGF drugs correlate with an increased length of vascular normalisation window (Jain 2013). High doses cause the pruning of vessels to take place too quickly, impairing response to other therapies and increasing hypoxia resulting in a shortened normalisation window (Huang et al. 2012). In addition, high doses increase the deposition of the ECM, promoting infiltration of immunosuppressive immune cells such as MDSCs and Tregs (Huang et al. 2012). Low doses, however, increase the window of normalisation, delaying the onset of negative side effects and inducing a better distribution of functional blood vessels throughout the tumour (Huang et al. 2012). A clinical trial using 15 mg/kg bevacizumab in non-small cell lung cancer showed the drug decreased perfusion and uptake of docetaxel (Stylianopoulos et al. 2012); similarly, in a breast cancer clinical trial, the same dose gave no benefit in overall survival (Brufsky et al. 2011) . Murine models suggest that this poor response may have been because the dose was too high (Chauhan et al. 2012; Huang et al. 2012), and retrospective clinical trials demonstrate that, in glioblastoma patients, low dose bevacizumab treatment had a better outcome than higher doses (Lorgis et al. 2012; Levin et al. 2015). Therefore, careful monitoring of the dose of anti-angiogenic treatment can be used to increase the window of vascular normalisation.

Another way to improve the vascular normalisation window is through modulation of the ANG2-Tie2 axis, which plays a vital role in tumour angiogenesis (Li, Zhang, and Hong 2020; Rigamonti et al. 2014). ANG2 is a proangiogenic cytokine, the receptor for which, Tie2 is predominantly expressed on vascular endothelial cells. ANG2 induces vascular destabilisation, promoting tumour progression and metastasis. Inhibition of ANG2 promotes pruning of blood vessels and improves vascular normalisation by preventing the loss of contact between endothelial and smooth muscle cells (Mazzieri et al. 2011; Falcón et al. 2009). Inhibition of ANG2 significantly reduced tumour growth, the blood vessel uniformity and pericyte coverage were increased, and the endothelial sprouting decreased (Falcón et al. 2009). Furthermore, Park et al. demonstrated that inhibition of both VEGFRs and ANG-2 increased the normalisation window and reduced tumour proliferation compared to either single inhibition (Park et al. 2016).

Genetic modification to interfere with the signalling pathways involved in angiogenesis can also be used to lengthen the window. One gene that has an important role in the abnormal growth of tumour blood vessels is G-protein signalling 5 (Rgs5) (Manzur, Hamzah, and Ganss 2009; Ganss 2015). Disrupting this gene in tumour burdened mice resulted in normalised vasculature with mature pericytes, reduced vascular leakiness and enhanced oxygenation. There was enhanced infiltration of effector immune cells to the tumour as well as increased animal survival (Hamzah et al. 2008). Therefore, the Rgs5 gene could be a promising target to promote lengthened vascular normalisation windows. However, the mechanism is currently unclear, making its targeting in humans challenging (Li, Zhang, and Hong 2020).

11.7.4 Vascular promotion as a therapeutic strategy for cancer therapy

There are many problems associated with low blood vessel density; intratumoral hypoxia is common in solid tumours and promotes tumour progression, malignancy, and resistance to therapy (Yuen and Díaz 2014). Drug delivery and anti-tumour immune responses are also reduced.

In PDAC, increased vascularity and vessel maturity is associated with more prolonged overall survival. A cohort of 185 PDAC patients was divided into high or low expression of CD31 mRNA from RNA sequencing data from The Cancer Genome Atlas (TCGA). Higher CD31 mRNA expression indicates that there are more vascular endothelial cells and was associated with significantly better overall survival. In the high CD31 expression group, there were also increased markers of vascular stability and anti-tumour immune

response (Katsuta et al. 2019). This increased survival may be due to changes in hypoxia, which is a key determinant of progression, metastasis and immune infiltration in pancreatic cancer (Yuen and Díaz 2014). This highlights that, in contrast to anti-angiogenic therapy, increasing blood vessel density and maturity may offer therapeutic benefit in pancreatic cancer.

As the drug Cilengitide, originally developed as an anti-angiogenic, had been identified as having vascular promoting qualities at low doses, work in our laboratory aimed to exploit the proangiogenic property of low dose Cilengitide by using it as a vascular promoting agent (Wong et al. 2015) **(Figure 11.8)**. Low dose Cilengitide in combination with gemcitabine and verapamil, a calcium channel blocker that reduces the efflux of nucleoside analogues such as gemcitabine and can increase vessel diameter (Bergman et al. 2003; Kaelin et al. 1982). The triple combination of low dose Cilengitide/gemcitabine and verapamil increased blood vessel density, leakiness of blood vessels and gemcitabine delivery to mouse non-small cell lung cancer or pancreatic adenocarcinomas resulting in reduced tumour volume and enhanced overall survival. They demonstrate across four models, subcutaneous Lewis Lung carcinoma, experimental metastasis of human non-small-cell lung cancer cells (A549), orthotopic pancreatic DT6066 model and the *LSL-Kras$^{G12D/+}$;LSL-Trp53$^{R172H/+}$;Pdx-1-Cre* (KPC) spontaneous PDAC model, that tumour volume is reduced in the triple combination compared to placebo or chemotherapy alone. They also show that the tumour hypoxia is reduced with less desmoplasia, and gemcitabine delivery to other organs is not affected. In addition, blood vessel density has since been shown to be indicative of survival in human PDAC. PDAC is known for its hypovascularity, and addition of the anti-angiogenic drug Bevacizumab to standard chemotherapy does not improve outcome. Therefore, it was hypothesized that increasing vascularity might improve outcome. PDAC patients were classified into high or low CD31 expression using mRNA levels from RNA-seq data. Those with high expression of CD31 had significantly better overall survival. In these patients, the immune response-related pathways were also significantly higher than in the low CD31 group (Katsuta et al. 2019).

Cilengitide was initially developed as an RGD-mimetic antagonist of αvβ3 integrin to be used as an anti-angiogenic drug in cancer at maximally tolerated doses (5–50 mg/kg) (Buerkle et al. 2002; Brooks, Clark, and Cheresh 1994; Nisato et al. 2003a; Maubant et al. 2006; Nabors et al. 2007). However, at low doses (ldCil, 50 μg/kg in vivo or 2 nm in vitro), Cilengitide enhances pathological angiogenesis without any apparent change in

quiescent vasculature. Mechanistically, it was found that, at low doses, ldCil does not act as an antagonist of αvβ3 integrin. Therefore, it has no effect on cell adhesion or migration. Instead, it alters αvβ3 signalling to enhance the activation and recycling of the major pro-angiogenic receptor VR2 through a transdominant inhibition model (Reynolds et al. 2009). Pharmacological inhibition of VR2 with the inhibitor DC101 suppressed both the ability of nanomolar inhibitor concentrations to promote VEGF-mediated angiogenesis *ex vivo* and tumour growth and angiogenesis *in vivo*. Therefore, the upregulation of VEGFR2 function was found to be essential for αvβ3/αvβ5 inhibitors to enhance VEGF-mediated angiogenesis, tumour growth and tumour angiogenesis (Reynolds et al. 2009).

In addition to this role in enhancing the recycling of VR2, ldCil also sensitises cells to gemcitabine through αvβ5 integrin (Wong et al. 2015). Wong et al found that ldCil increased gemcitabine efficacy; therefore, the expression of transporters and enzymes involved in the action of gemcitabine were tested. The equilibrative nucleoside transporters 1 and 2 (ENT1 and ENT2) and concentrative nucleoside transporter 3 (CNT3) are Gemcitabine transporters. The enzymes deoxycytidine kinase (DCK) and cytidine deaminase (CDA) are the rate-limiting metabolizing enzyme and catabolizing enzyme, respectively, for CNT3. Therefore, ENT1, ENT2, CNT3, and DCK are expected to increase gemcitabine efficacy and CDA to reduce it. ENT1 and 2 were already known to be regulated by hypoxia (Eltzschig et al. 2005; Morote-Garcia et al. 2009), and this was shown in the case of ldCil treatment. In fact, in sections from both LLC subcutaneous tumours and pancreatic tumours from KPC mice, there was increased expression of ENT1, ENT2, CNT3, and DCK and reduced levels of CDA in tumours from animals treated with ldCil/Ver/Gem^{75}. Levels of transporter regulator 1 (RS1), which is known to control CNT3 activity (Errasti-Murugarren et al. 2012), were found to be elevated in tumour cells from ldCil/Gem^{75} treated animals. siRNA depletion of β5-integrin was sufficient to decrease RS1 levels depletion of β3-integrin had no effect suggesting that β5 was responsible for this regulation of gemcitabine sensitivity.

In addition, ldCil has a direct effect on CNT3; pharmacological inhibition of CNT3 did not affect the survival of ldCil-treated cells without gemcitabine. However, in the ldCil/Gem75 treated cells, cell survival was rescued, suggesting that ldCil enhances gemcitabine transport into the cell by CNT3 (Wong et al. 2015).

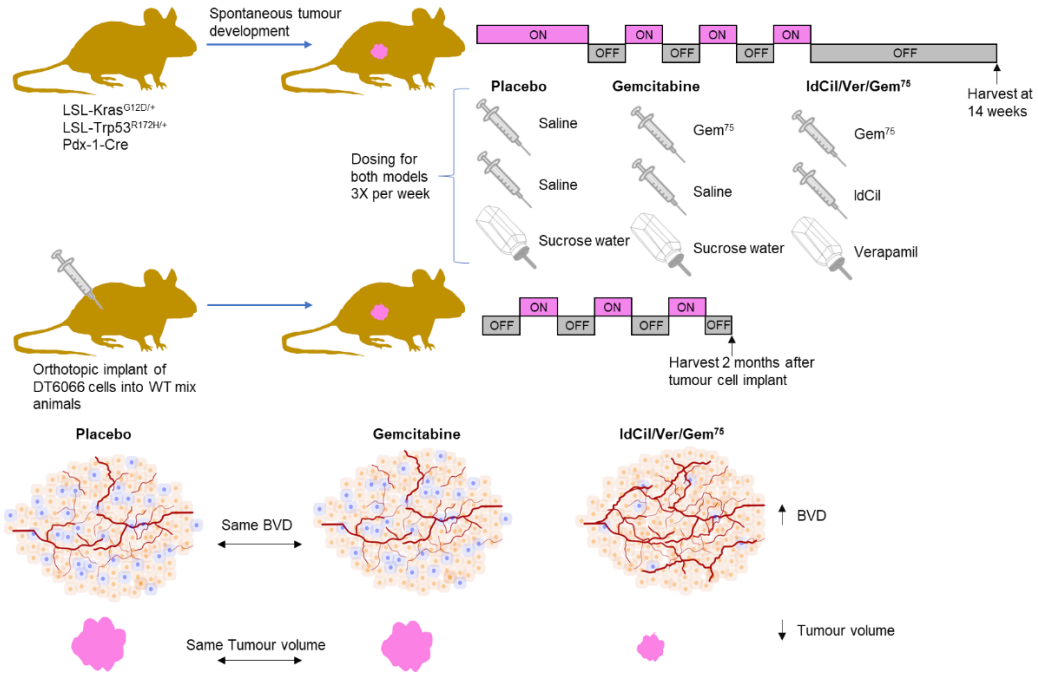

Figure 11.8 Vascular promotion in combination with chemotherapy reduces tumour growth

Animals were given the combination treatment of low dose Cilengitide, Verapamil and low dose (75mg/kg) Gemcitabine, low dose gemcitabine alone or placebo. The dosing strategy for KPC and DT6066 injected animals is indicated by pink and grey boxes. Within each tumour model, the blood vessel density was similar between placebo and gemcitabine animals but was increased in the triple combination treated mice. Blue cells represent areas of hypoxia, there is a similar level of hypoxia in placebo and gemcitabine treated animals but reduced hypoxia in the triple combination. The tumour volume was also similar between placebo and gemcitabine but was reduced in the triple combination treated mice. (From Wong et al. 2015).

11.7.5 29P

Having failed clinical trials in the past and as an off-patent drug, Cilengitide is now less commercially viable and is limited by not being orally available. ***29P*** is an orally available analogue of Cilengitide; an inactive prodrug cleaved in the serum of the blood to the active drug ***29***. At low doses, ***29*** has many of the vascular promoting effects of low dose Cilengitide (Weinmuller et al. 2017).

In the early 1990s, it was discovered that, by making a peptide with an RGD sequence cyclic and inserting a D-amino acid, the affinity and selectivity for receptors was increased compared to linear peptides (Aumailley et al. 1991; Pierschbacher and Ruoslahti 1984). This method was used to optimise Cilengitide (cyclo(RGDf(NMe)V), which has a subnanomolar affinity for αvβ3 (IC 50=0.6nM) but also has a residual affinity for αvβ5 and αvβ1 (Mas-Moruno, Rechenmacher, and Kessler 2010). However, to improve properties such as oral availability, affinity, and selectivity, a library of N-methyl cyclic hexapeptides were developed and tested for their permeability in the human colon epithelial cell line, Caco-2. Caco-2 permeability does not correlate with any single characteristic of the peptides, such as the number of N-methylations, the number of external NH groups or lipophilicity, but for some of the peptides, it was high, suggesting the presence of an active transporter. The ones with the highest Caco-2 permeability were chosen as templates; these were peptides with two-fold N-methylation at the positions 1,5, 1,6, 3,5, 5,6.

The binding affinity to RGD-binding integrin subtypes of 24 of these RGD-containing hexapeptides was tested, and those with high affinity for integrin αvβ3 and low affinity for α5β1 were selected. This was different from linear peptides because these usually have unselective binding affinity to other RGD integrins such as αvβ5, αvβ6, αvβ8 and αvIIβ3. The alanine residues flanking the RGD site were replaced with other residues as previous studies showed aromatic residues could improve the affinity and selectivity of the peptide (Bochen et al. 2013). One of the resulting peptides was ***29,*** which has a subnanomolar affinity for αvβ3, αvβ8 and α5β1 comparable to Cilengitide but an increased affinity for αvβ6. Because of its high affinity and selectivity for αvβ3, ***29*** was chosen to be modified into the prodrug ***29P***. ***29*** is the active form of the agent.

The structure of ***29P*** is given in (Weinmuller et al. 2017), and IP status for ***29P*** is currently being pursued with Queen Mary University Innovations **(Figure 11.9)**.

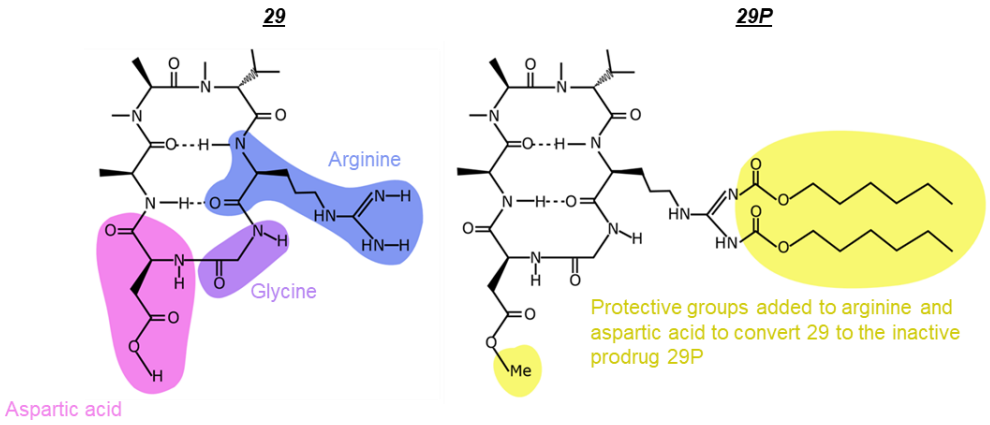

Figure 11.9 *29* and *29P* structure

Showing the structure of RGD mimetic ***29*** (left) with arginine (blue), glycine (purple) and aspartic acid (pink) highlighted and (right) ***29P*** with protective lipophilic residues highlighted in yellow.

12 Materials and methods

12.1 Mice

All animals were kept according to the UK Home Office regulations. Health screens were carried out quarterly in accordance with FELASA guidelines for health monitoring of rodent colonies to confirm their free status of known pathogens in accordance with FELASA screens for all animals bred in-house. No clinical signs were detected. Mice were housed in groups of 4-6 animals per individually ventilated cage. They were kept in a 12-hr light-dark cycle (06:30-18:30 light; 18:30-06:30 dark), the temperature was maintained at 21±1 °C with relative humidity of 40-60 %. All cages contained a 1-1.5 cm layer of animal bedding and with environmental enrichment, including cardboard box-tunnel and crinkled paper nesting material. Animals had access to food and water *ad libitum*.

12.1.1 *Pdgfb-iCre^{ert};FAK$^{fl/fl}$;R26 FAK $^{K454R/K454R}$* mice

Our laboratory developed a mouse model with for tamoxifen-inducible, endothelial cell specific kinase-dead FAK knock-in and simultaneous endogenous mouse FAK knockout (*Pdgfb-iCre^{ert};FAK$^{fl/fl}$;R26FAK$^{K454R/K454R}$*). This was done by generating a kinase-dead mutant from chicken FAK cDNA constructs by mutation of lysine (AAA) at position 454 to arginine (AGA) to disrupt the ATP binding site (Provided by Margaret Frame's Laboratory, Glasgow UK) (Hildebrand, Schaller, and Parsons 1993). This mutation is denoted K454R **(Figure 12.1 A)**. The mutant sequence was preceded by a STOP codon flanked by loxP sites and then targeted to the Rosa26 locus creating a tamoxifen-inducible Cre-activating kinase-dead knock-in mutant. The constructs were electroporated into embryonic stem cells, confirmed positive clones were injected into blastocysts and transferred to pseudopregnant mice and pups were born 18 days later. High percentage chimaeras were crossed with C57bl6 mice. *Platelet-derived growth factor b* (*Pdgfb*) is predominantly expressed by endothelial cells (Hellstrom et al. 1999), and the tamoxifen-inducible Cre recombinase activity under the *Pdgfb* promotor has been shown to be endothelial cell-specific (Claxton et al. 2008). *R26FAK$^{K454R/K454R}$* mice were bred with endothelial cell-specific *Pdgfb-iCre^{ert}; FAK$^{fl/fl}$* mice (Tavora et al. 2010) to generate *Pdgfb-iCre^{ert}; FAK$^{fl/fl}$; FAK$^{K454R/K454R}$* mice (Tavora, Batista, et al. 2014).

Treatment of *Pdgfb-iCre^{ert}; FAK$^{fl/fl}$; FAK$^{K454R/K454R}$* mice with tamoxifen activates *Cre* in endothelial cells, knocking in the mutant kinase-dead chicken FAK and simultaneously

knocking out endogenous mouse FAK **(Figure 12.1 B)**. These mice are referred to as *ECCre+; FAK$^{KD/KD,}$* and *Pdgfb-iCre^{ert}*-negative litter mates where the endogenous mouse FAK remained expressed and mutant chicken FAK not expressed, are referred to as *ECCre-; FAK$^{KD/KD}$*. The model has previously been published (Alexopoulou et al. 2017).

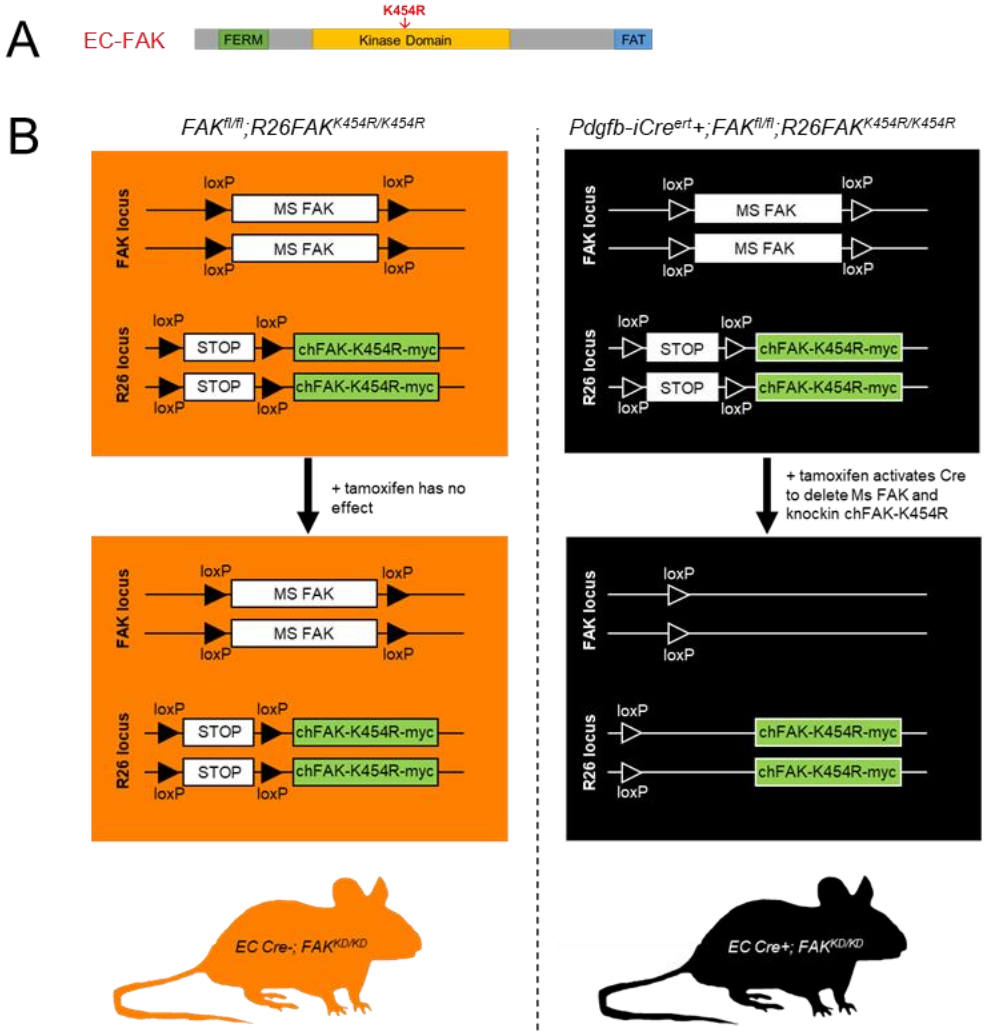

Figure 12.1 Generation of endothelial cell FAK KD mice

(A) The K454R mutation in chicken FAK renders it kinase dead. (B) In *Pdgfb-iCre^{ert}+;FAK$^{fl/fl}$;R26 FAK$^{K454R/K454R}$* mice tamoxifen administration activates *Cre* in ECs and induces simultaneous EC-FAK deletion and Rosa 26-driven mutant *FAK$^{K454R/K454R}$ (FAK-KD)* expression (*EC Cre+; FAK$^{KD/KD}$*). Knockin-mutant is myc-tagged. Tamoxifen has no effect on FAK expression in *FAK$^{fl/fl}$;R26 FAK$^{K454R/K454R}$* mice (*EC Cre-; FAK$^{KD/KD}$*).

12.1.2 LSL-Kras$^{G12D/+}$;LSL-Trp53$^{R172H/+}$;Pdx-1-Cre (KPC) mice

KPC mice were originally developed by Hingorini et al. (Hingorani et al. 2005) and spontaneously develop pancreatic tumours at approximately four months. Histology characterising features of this colony at the time of this thesis is given in Appendix II, chapter 22.2.

12.1.3 WT mice

WT mix mice were bred in house from a cross of C57bl6 and 129sv. Female C57bl6J mice were bought from Charles River at six weeks to be used at 7-8 weeks.

12.2 Breeding schemes

12.2.1 Breeding scheme for *Pdgfb-iCre^{ert};FAK$^{fl/fl}$;R26-FAK$^{K454R/K454R}$* and expected Mendelian ratios

The *Pdgfb-iCre^{ert}+;FAK$^{fl/fl}$;R26-FAK$^{K454R/K454R}$* colony was maintained by crossing *Pdgfb-iCre^{ert}+;FAK$^{fl/fl}$;R26-FAK$^{K454R/K454R}$* mice with *FAK$^{fl/fl}$;R26-FAK$^{K454R/K454R}$* mice. *Pdgfb-iCre^{ert}+;FAK$^{fl/fl}$;R26-FAK$^{K454R/K454R}$* mice are hemizygous for *cre*-insertion. The expected Mendelian ratios of the litters weaned are 1:1, *Pdgfb-iCre^{ert}+;FAK$^{fl/fl}$;R26-FAK$^{K454R/K454R}$* mice*: FAK$^{fl/fl}$;R26-FAK$^{K454R/K454R}$* mice **(Figure 12.2)**.

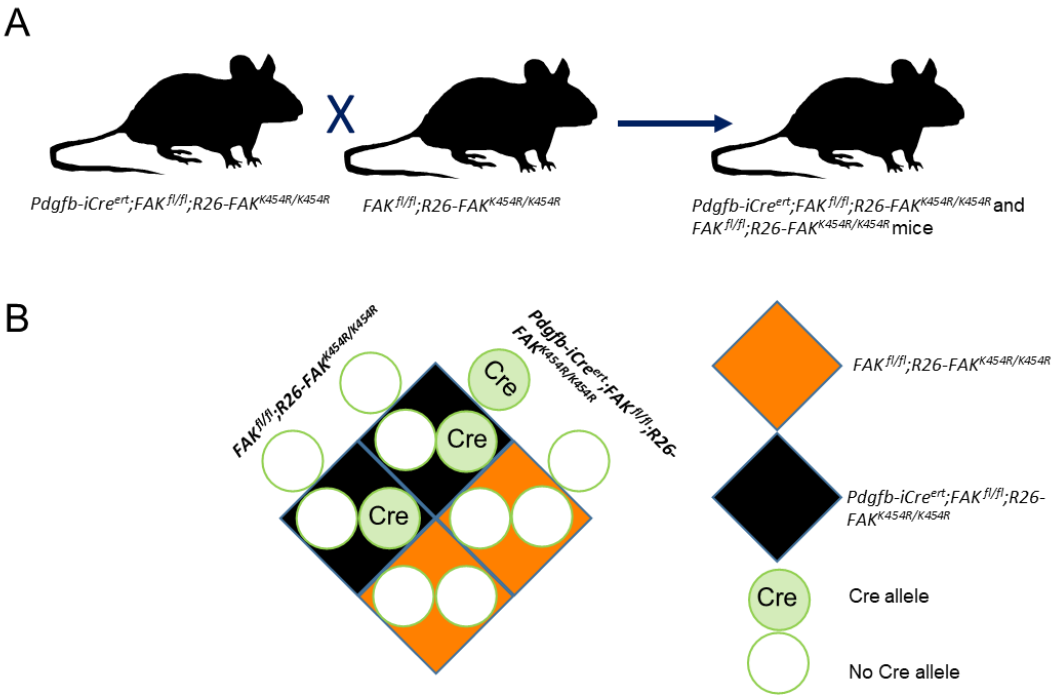

Figure 12.2 *Pdgfb-iCre^{ert};FAK $^{fl/fl}$;R26-FAK$^{K454R/K454R}$* mice breeding scheme and expected Mendelian ratios

(A) Breeding scheme for *Pdgfb-iCre^{ert};FAK$^{fl/fl}$;R26 FAK$^{K454R/K454R}$* mice. (B) Predicted mendelian ratios for *Pdgfb-iCre^{ert}+;FAK$^{fl/fl}$;R26-FAK$^{K454R/K454R}$* mice (orange) and *FAK$^{fl/fl}$;R26-FAK$^{K454R/K454R}$* mice (black). Presence of *Cre* insert is indicated in pale green.

12.2.2 Sex and genotype ratios of animals weaned from the *Pdgfb-iCre^{ert};FAK$^{fl/fl}$;R26 FAK$^{K454R/K454R}$* colony

All animals weaned were genotyped by PCR as described in *Materials and Methods*. To further characterise the colony, the sex and genotype ratios were calculated from 400 weaned mice. The genotype ratio was skewed towards slightly more *FAK$^{fl/fl}$;R26 FAK$^{K454R/K454R}$* mice than *Pdgfb-iCre^{ert}+;FAK$^{fl/fl}$;R26 FAK$^{K454R/K454R}$* (231:169) **(Figure 12.3 A)**. However, the sex ratios of male animals compared to female animals weaned was almost equal (205:195) **(Figure 12.3 B)**.

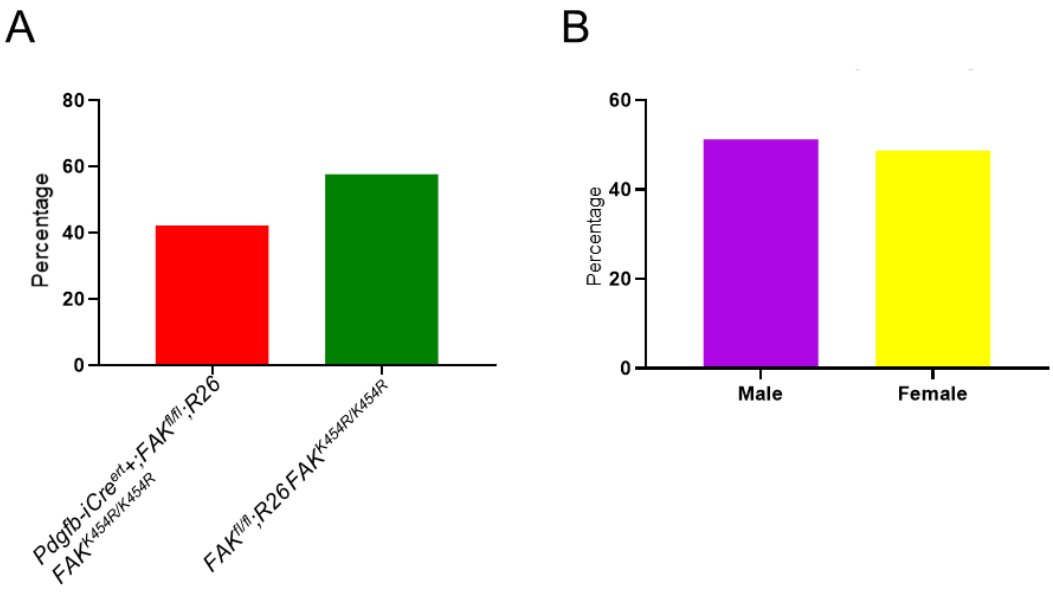

Figure 12.3 Characterisation of the EC FAK KD colony

(A) Ratio of *FAK$^{fl/fl}$;R26 FAK$^{K454R/K454R}$* : *Pdgfb-iCre^{ert}+;FAK$^{fl/fl}$;R26 FAK$^{K454R/K454R}$* weaned mice out of 400 animals. (B) Ratio of male : female *Pdgfb-iCre^{ert};FAK$^{fl/fl}$;R26 FAK$^{K454R/K454R}$ mice* weaned out of 400 animals.

12.2.3 Breeding scheme and expected Mendelian ratios for KPC mice

The LSL-*Kras*$^{G12D/+}$;LSL-*Trp53*$^{R172H/+}$;*Pdx-1-Cre* (KPC) colony was maintained through the breeding of two founder colonies LSL-*Kras*$^{G12D/+}$;LSL-*Trp53*$^{R172H/+}$ and *Pdx-1-Cre*. The *Pdx-1-Cre* colony was maintained on a pure C57bl6J background. Two *Pdx-1-Cre* animals were crossed, resulting in litters of *Pdx-1-Cre* animals **(Figure 12.4 A)**, they are homozygous mutant, and therefore all offspring are expected to be homozygous mutant for *Pdx-1-Cre* **(Figure 12.4 B)**. The LSL-*Kras*$^{G12D/+}$;LSL-*Trp53*$^{R172H/+}$ colony was maintained on a C57Bl6/129sv background. Breeding pairs were set up with two LSL-*Kras*$^{G12D/+}$;LSL-*Trp53*$^{R172H/+}$ animals and LSL-*Kras*$^{G12D/+}$;LSL-*Trp53*$^{R172H/+}$ offspring were kept for further breeding **(Figure 12.4 C)**. As the animals in the breeding pairs were heterozygous for both the *Kras* and *P53* mutation, there were several different genotypes in the predicted litters **(Figure 12.4 D)**. The LSL-Kras$^{G12D/G12D}$ animals (1/4 total) die *in utero* and are therefore not in the predicted weaned animals. Of the remaining animals, 1/3 are *LSL-Kras*$^{G12D/+}$*;LSL-Trp53*$^{R172H/+}$ and are kept for further breeding; the remaining genotypes are culled. From the litters of the LSL-Kras$^{G12D/+}$;LSL-Trp53$^{R172H/+,}$ and *Pdx-1-Cre* colonies, a 129sv *LSL-Kras*$^{G12D/+}$*;LSL-Trp53*$^{R172H/+}$ animal is crossed with a C57Bl6J *Pdx-1-Cre* mouse to produce KPC mice which spontaneously develop pancreatic tumours **(Figure 12.4 E)**. The *Kras* and *P53* mutations in the *LSL-Kras*$^{G12D/+}$*;LSL-Trp53*$^{R172H/+}$ colony are heterozygous, and the *Pdx-1-Cre* colony they are crossed with does not contain either of these mutations; therefore, ¼ of the offspring are predicted to carry both mutations heterozygously. The *Pdx-1-Cre* colony is a homozygous mutant for *Pdx-1-Cre*; therefore, all offspring are expected to carry this mutation heterozygously. Therefore, ¼ of the offspring of this cross are expected to be *LSL-Kras*$^{G12D/+}$*;LSL-Trp53*$^{R172H/+}$*;Pdx-1-Cre* (KPC), the remaining animals are culled are genotypes are confirmed **(Figure 12.4 F)**.

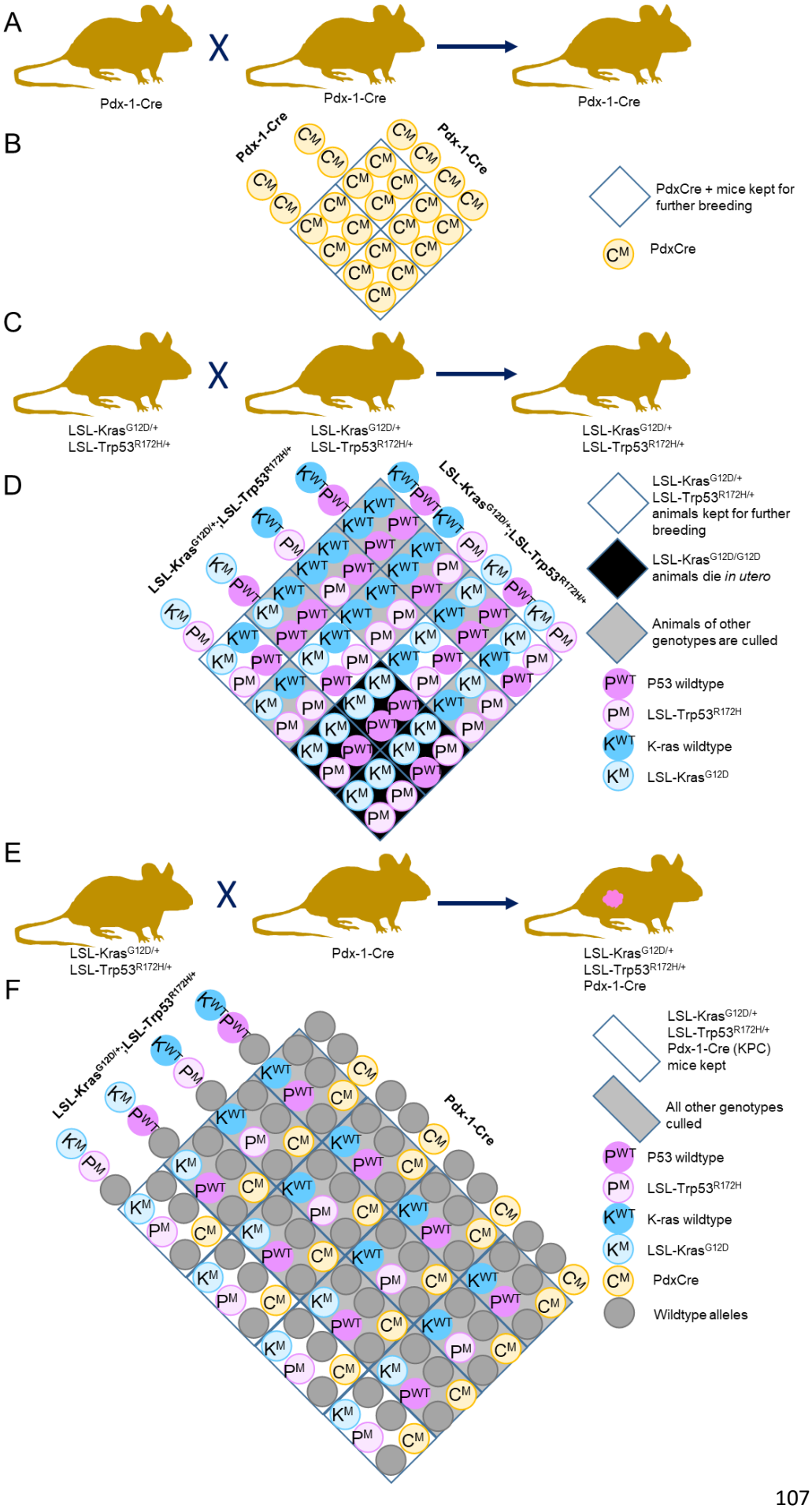
A
Pdx-1-Cre
X
Pdx-1-Cre
Pdx-1-Cre
B
Pdx-1-Cre
Pdx-1-Cre
PdxCre + mice kept for further breeding
PdxCre
C
LSL-Kras G12D/+
LSL-Trp53 R172H/+
X
LSL-Kras G12D/+
LSL-Trp53 R172H/+
LSL-Kras G12D/+
LSL-Trp53 R172H/+
D
LSL-Kras G12D/+;LSL-Trp53 R172H/+
LSL-Kras G12D/+;LSL-Trp53 R172H/+
LSL-Kras G12D/+ LSL-Trp53 R172H/+ animals kept for further breeding
LSL-Kras G12D/G12D animals die in utero
Animals of other genotypes are culled
P WT P53 wildtype
P M LSL-Trp53 R172H
K WT K-ras wildtype
K M LSL-Kras G12D
E
LSL-Kras G12D/+
LSL-Trp53 R172H/+
X
Pdx-1-Cre
LSL-Kras G12D/+
LSL-Trp53 R172H/+
Pdx-1-Cre
F
LSL-Kras G12D/+;LSL-Trp53 R172H/+
Pdx-1-Cre
LSL-Kras G12D/+ LSL-Trp53 R172H/+ Pdx-1-Cre (KPC) mice kept
All other genotypes culled
P WT P53 wildtype
P M LSL-Trp53 R172H
K WT K-ras wildtype
K M LSL-Kras G12D
C M PdxCre
Wildtype alleles

Figure 12.4 KPC breeding strategy and expected Mendelian ratios

Breeding the KPC colony requires two founder colonies, the *Pdx-1-Cre* and *LSL-Kras$^{G12D/+}$;LSL-Trp53$^{R172H/+}$* (A) Breeding scheme for the *Pdx-1-Cre* colony (B) Expected mendelian ratios for the *Pdx-1-Cre* colony (C) Breeding scheme for the *LSL-Kras$^{G12D/+}$;LSL-Trp53$^{R172H/+}$* colony (D) Expected mendelian ratios for the *LSL-Kras$^{G12D/+}$;LSL-Trp53$^{R172H/+}$* colony (E) Breeding scheme for the *LSL-Kras$^{G12D/+}$;LSL-Trp53$^{R172H/}$Pdx-1-Cre* colony (F) Expected mendelian ratios for the *LSL-Kras$^{G12D/+}$;LSL-Trp53$^{R172H/}$;Pdx-1-Cre* colony. *Pdx-1-Cre* alleles are indicated with pale orange circles, *LSL-Kras^{G12D}* in pale blue, *LSL-Trp53^{R172H}* in pale purple, Kras WT in dark blue, *P53* WT in dark purple and other WT alleles in grey.

12.3 Sequencing

The gDNA was amplified with the primers 397mut fw2 (nt519-541) CCT TGA AAT CAG GAG ATC CTA CG and 397mut rev (nt1902-1921) GCC GCT CAC CGT TCT CAA TC in a mix of 2ul gDNA, 0.2ul each primer (primers kept at 100 µM), 50 µl MegaMixBlue (Microzone). PCR conditions were: 94 °C 3' (94 °C 30" / 55.2 °C 30" / 72 °C 1'30") x36cc 72 °C 5' / 16 °C. 20 µl was loaded on a 2 % agarose gel to check amplification (amplicon predicted size = 1403). The PCR product was prepared for sequencing by the WHRI Genome centre: 3 µl of PCR product was with of incubated with 3 µl the ExoSap using the following conditions:

37 °C for 40 minutes, 80 °C for 15 minutes, 4 °C for 5 minutes to remove primers and dNTPs. 5 µl of the product was combined with 5 µl of primer (GCA CCA TCC TTA ACC ATT GC) with a concentration of 5uM (5 pmol/µl) and sequenced by Eurofins using Bigdye terminator v3.1 cycle sequencing kit.

The data were analysed by comparison with the WT chicken FAK sequence using the NIH Blasting tool available at: https://blast.ncbi.nlm.nih.gov/Blast.cgi?PAGE_TYPE=BlastSearch&PROG_DEF=blastn&BLAST_PROG_DEF=blastn&BLAST_SPEC=GlobalAln&LINK_LOC=BlastHomeLink confirming that the sequence was consistent apart from a K454R point mutation.

12.4 Genotyping

12.4.1 Genomic DNA extraction

12.4.1.1 Genomic DNA extraction for Cre PCR (Pdgfb-iCre^{ert};FAK $^{fl/fl}$;R26 FAK $^{K454R/K454R}$ colony)

Earsnips were digested overnight in 100 µl tail buffer (10 mM Tris-HCL (pH 8.5), 10 mM EDTA, 100 mM NaCl and 0.2 % SDS) with 0.1 mg/ml proteinase K. 100 µl isopropanol was added to precipitate DNA and the plates centrifuged at 2600rpm for 30 minutes. The supernatant was removed by inverting the plate, and the pellet dried at 56 °C for 1-2 hours. The pellet was then resuspended in 200 µl TE buffer (10 mM Tris-HCL (pH 7.5) and 1 mM EDTA) and incubated at RT for two hours before use.

12.4.1.2 Genomic DNA extraction for KPC PCR

For KPC PCR, a long DNA extraction was performed. 360 µl tail buffer supplemented with 15 µl 10 mg/ml proteinase K. The sample was incubated overnight at 55 °C, vortexed for

10 seconds and centrifuged at 14,000 rpm for 30 s at RT. 125 µl NaCl (5M) was added, and the sample vortexed for 10 s the centrifuged for five minutes (14,000 rpm, RT). 375 µl of the middle phase were added to 250 µl isopropanol in a clean tube which was vortexed for 10 s and centrifuged for 10 minutes (14,000 rpm, RT). The supernatant was discarded and 500 µl 70 % ethanol added to the tube before centrifuging again for 5 minutes (14,000 rpm, RT). The ethanol was removed, and the tubes dried in an oven at 55 °C for 1 hour. The DNA was then resuspended in 100µl of sterile, nuclease-free dH_2O and pipetted up and down to mix.

12.4.2 PCR reactions

Genetically modified mice were bred in house and genotyped by PCR or by Transnetyx®.

12.4.3 Genotyping for the *Pdgfb-iCre^{ert};FAK$^{fl/fl}$;R26FAK$^{K454R/K454R}$* colony

In order to confirm the genotype of the *Cre* inducible kinase-dead mouse model (*Pdgfb-iCre^{ert};FAK$^{fl/fl}$;R26FAK$^{K454R/K454R}$*) for both *in vivo* work and for making mouse lung endothelial cells, a *Cre* PCR was performed as follows:

1.5 µl genomic DNA was added to 12 µl DreamTaq Green PCR (2x) (LifeTechnologies), 12 µl nuclease-free water and 0.3 µl primer mix (*Cre* Forward, *Cre* Backward, β2 microglobulin Forward, β2 microglobulin backward in a 1:1:1:1 ratio) **(Table 12.1 A and B)**. To confirm the animals were all *FAK$^{fl/fl}$, LP2 PCR* was performed with 1.5µl DNA added to 24µl total MasterMix (MegaMix-Blue (Microzone)), and 0.3µl total primer mix (LP2as, LP2h, LP2s 1:1:1) all animals were LP2 positive **(Table 12.1 C and D)**.

A

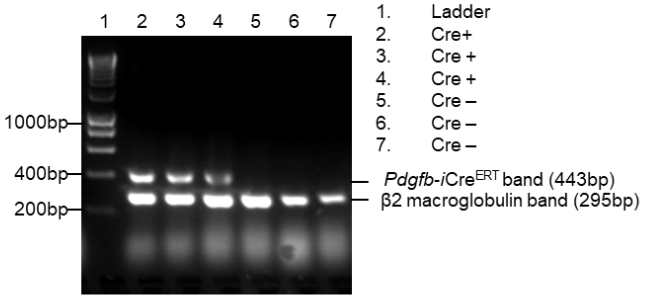

B

Target	Primers	Sequence	Conditions	Product
Cre	Cre Forward	5'-GCCGCCGGGATCACTCTC-3'	94° 4 min 94° 30s 65° 80s 72° 60s 34 cycles 70°10 min 4° Infinite	β2 microglobulin band at 295bp Cre band at 443bp.
	Cre Backward	5'-CCAGCCGCCGTCGCAACT-3'		
	β2 microglobulin Forward	5'-CACCGGAGAATGGGAAGCCGAA-3'		
	β2 microglobulin backward	5'-TCCACACAGATGGAGCGTCCAG-3'		

C

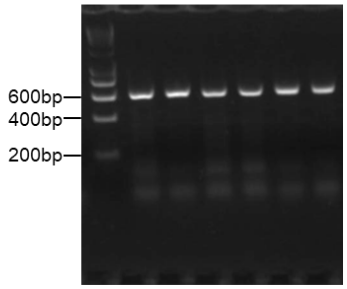

Product size: LP2 697 bp and wild-type 429 bp.
Note: all samples here are LP2 positive where LP2 is 697bp.

D

Target	Primers	Sequence	Conditions	Product
FAKfl/fl	LP2 as	5'-TTAATAAGACCAGAGGACTCAGC-3'	94° 3 min 94° 45s 56° 45s 72° 1 min 36 cycles 70° 5 min 4° Infinite	LP2 band at 697 bp wild-type band at 429 bp.
	LP2 h	5'-GGAAGAAGCTTGTATACTGTATG-3'		
	LP2s	5'-ATTGTGCTATACTCACATTTGGA-3'		

Table 12.1 *Pdgfb-iCre^{ert};FAK$^{fl/fl}$;R26FAK$^{K454R/K454R}$*

(A) Representative Cre and β2 macroglobulin control PCR. (B) Primer sequences and thermocycler cycle for Cre PCR (C) Representative LP2 PCR. (D) Primer sequences and thermocycler cycle for LP2 PCR.

12.4.3.1 KPC PCR

KPC mice harbour the mutations *LSL-Kras$^{G12D/+}$;LSL-Trp53$^{R172H/+}$;Pdx-1-Cre* causing them to spontaneously develop pancreatic tumours. These animals were genotyped for *Kras*, *P53* and *Pdx-1-Cre*, as described in **Table 12.2** or were genotyped out of house by Transnetyx® (Cordova, Tennessee, USA). For *Kras^{G12D}* genotyping, the reaction mix was made up of 10 µl AccuStart II PCR Supermix P/N 84229, 2 µl of each primer (final concentration 2 µM), 2 µl template DNA and 4 µl nuclease-free water. For *Trp53* genotyping, the reaction mix was made up of 17 µl MegaMix Blue (Microzone), 2 µl each primer (final concentration 2 µM) 2 µl template DNA. For *Pdx-1-Cre* genotyping, the reaction mix contained 5 µl DreamTaq Green, 5 µl nuclease free water, 2µl of each primer (final concentration 2 µM) and 2 µM template DNA.

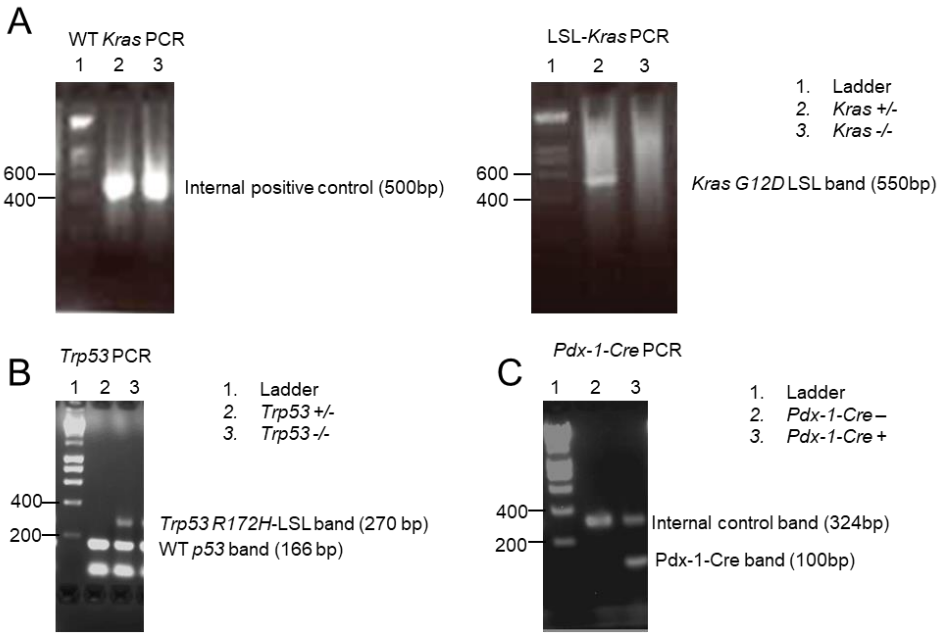

D

Target	Primers		Conditions	Product
Kras G12D LSL	Forward LSL primer	5'-GTC GAC AAG CTC ATG CGG G-3'	95° 5 min 94° 30s 62° 30s 72° 1min 40 cycles 72° 2min	Kras G12D LSL 550bp
	Reverse WT primer	5'-CGC AGA CTG TAG AGC AGC G -3'		
***Kras* WT**	Forward WT primer	5'- CCA TGG CTT GAG TAA GTC TGC - 3'		Kras WT 500bp
	Reverse WT primer	5'-CGC AGA CTG TAG AGC AGC G -3'		
Trp53 R172H	*Trp53* WT forward	5'-TTA CAC ATC CAG CCT CTG TGG-3'	95° 5 min 94° 30s 61° 30s 72° 1min 35 cycles 72° 2min	Trp53 WT 166 bp Trp53 R172H-LSL 270 bp
	Trp53 WT reverse	5'-CTT GGA GAC ATA GCC ACA CTG-3'		
	Trp53 R172H F-LSL	5'-AGC TAG CCA CCA TGG CTT GAG TAA GTC TGC A-3'		
Pdx-1-Cre	Cre_olMR1084	5'-GCG GTC TGG CAG TAA AAA CTA TC-3'	95°C 5 min 94°C 30s 51.7°C 1 min 72°C 1 min 40 cycles 72°C 2 min	PdxCre 100bp Internal control 324bp
	Cre_olMR1085	5'-GTG AAA CAG CAT TGC TGC TGT CAC TT-3'		
	olMR7338 (control)	5'-CTA GGC CAC AGA ATT GAA AGA TCT-3'		
	olMR7339 (control)	5'-GTA GGT GGA AAT TCT AGC ATC ATC C-3'		

Table 12.2 KPC genotyping.

(A) Representative PCR of the internal positive control for *Kras* (left) and *Kras* $^{G12D\ LSL}$. (B) Representative PCR of *Trp53* ^{R172H} and WT *P53*. (C) Representative PCR of *Pdx-1-Cre* and internal positive control. (D) Primer sequences and thermocycler cycle.

12.5 RT-qPCR

12.5.1 Mouse and Chicken FAK rt-qPCR

EC-WT and EC-FAK KD cells were isolated, sorted and grown to 75 % confluency in a T75 flask as subsequently described; they were washed three times in sterile PBS. PBS was aspirated off, and 350 µl of RLT lysis buffer (Qiagen) with 1:100 β-mercaptoethanol was added for 1 minute before scraping the cells on ice. This lysate was stored at -80 °C or used immediately for RNA extraction.

12.5.2 RNA extraction for RT-qPCR

On a sterile bench, 350µl nuclease-free 70 % ethanol was added to the lysate and mixed well by pipetting up and down ten times, followed by vortexing. 700 µl of the sample was added to an RNeasy spin column, a centrifuge was cleaned with 70 % ethanol, and the sample centrifuged for 30s at 12,000 rpm. The flow-through was discarded by inversion and tapping onto a clean paper towel, and 350 µl buffer RW1 (Qiagen) was added to the column and centrifuged for 30s at 12,000rpm, the flow-through was discarded and 10 µl DNAse digestion solution in RDD buffer (10 µl DNAse:70 µl RDD buffer) was added to the column and incubated at RT for 15minutes. A further 350 µl buffer RW1 was added to the column and centrifuged for 30s at 12,000 rpm; the flow-through was discarded. 500 µl buffer RPE (Qiagen) (1:4 RPE concentrate: ethanol) was added to the column and centrifuged for 1 minute at 14,000 rpm, the flow-through was discarded, and the RPE was repeated but centrifuging for two minutes. The column was then centrifuged for 1 minute at 14,000 rpm in a dry tube to dry the membrane. The column was placed in a collection tube, and 40 µl nuclease-free water was added and incubated on the membrane for 1 minute at RT. The column was centrifuged for 1 min at 14,000 rpm to precipitate the RNA into the tube; this was either store at -80 °C or used immediately to synthesise cDNA.

12.5.3 RNA purity assessment

The absorbance of RNA at 260/280 and 260/230 nm was read with a Spectrophotometer (NanoDrop, Wilmington, US). The ratio of absorbance at 260/280 was expected to be >1.8, indicating pure RNA free of contaminating protein and phenol, and the 260/230 ratio was expected to be in the range of >2.0, indicating the RNA is free from EDTA, carbohydrates and phenol, a secondary measure of nucleic acid purity. The RNA concentration was also measured using the Spectrophotometer and used to calculate the volume required for 600 ng RNA.

12.5.4 Reverse Transcription

The RNA was reverse transcribed to cDNA with a high-capacity cDNA Reverse Transcription kit (Applied Biosystems). 600 ng RNA diluted to a total volume of 14.2 µl in nuclease-free water were added to the reagents listed in **Table 12.3**.

Component	Volume (µl)
10x RT buffer	2.0
25x dNTP mix	0.8
10x RT random primers	2.0
Multiverse reverse transcriptase	1.0

Table 12.3 RNA reverse transcription mix.

These were run in a thermocycler with the conditions listed in **Table 12.4**.

	Temperature (°C)	Time (minutes)
Step 1	25	10
Step 2	37	120
Step 3	85	5
Step 4	4	Infinite

Table 12.4 Thermocycler conditions for RNA reverse transcription.

The resultant cDNA was either used immediately for qPCR or stored at -20 °C.

12.5.5 RT-qPCR for mouse and chicken FAK

A qPCR plate was set up with six wells of each cDNA sample, three wells were loaded with mFAK and GAPDH primers and three wells with cFAK and GAPDH control primers in a master mix as described in **Table 12.5**. The plate was covered in an adhesive qPCR plate cover and centrifuged.

Component	Volume (μl)
TaqMan mastermix (PE Applied Biosystems)	10
FAM tagged gene of interest primer (mFAK/chFAK)	1.0
VIC tagged housekeeping gene primer (GAPDH)	1.0
cDNA (at least 2.5ng)	8.0

Table 12.5 Taqman mix components for mouse/chicken FAK qPCR.

The samples were run on a StepOnePlus™ Real-Time PCR System for 40 cycles as described in **Table 12.6** with the primer sequences listed in **Table 12.7**.

	Temperature (°C)	Time
Step 1	60	10 minutes
Step 2	95	10 minutes
Step 3 and 4 (40 cycles)	95	15 seconds
	60	60 seconds

Table 12.6 Thermocycler conditions for RT-qPCR.

Taqman primers	Assay ID (Thermofisher Taqman)
GAPDH (mouse)	Mm99999915_g1
FAK (mouse)	Forward: GGCGTTGCCATCAATACCA Probe: AAGGCATGCGGACACA Reverse: GGTGTATGTGTCTTCCTCATCGAT
FAK (chicken)	Forward: CAACAGCAAGAGATGGAAGAAG ATC Probe: ACGATTCCTGGTAATGAA Reverse: 5′-CCGTCCTCCCGTTCAATG-3′

Table 12.7 Taqman RT-qPCR primers.

The qPCR machine was set up to measure quantitation comparative CT with Taqman reagents at standard speed. Plate layout was set up within the software with sample name, FAM chicken or mouse FAK and VIC GAPDH.

12.5.6 RT-qPCR for IL-6

RT-qPCR for IL-6 was performed using Sybr Green using the following master mix listed in **Table 12.8**.

	Volumes (µl)
Syber Green mix	6.65
cDNA (at least 2.5ng)	0.27
H_2O	6.4

Table 12.8 RT-qPCR mix for IL-6.

To this, 1.1 µl of 2 µM qPCR primer for IL6 or B-actin were added to separate wells with *B-actin* used as the housekeeping gene. Syber green primer sequences are listed in **Table 12.9**.

Syber Green Primers	**Primer sequence 5'-3' (SYBR)**
IL6	Forward primer : CTGCAAGAGACTTCCATCCAGTT Reverse primer : GAAGTAGGGAAGGCCGTGG
B-actin	Forward: CACAGCTTCTTTGCAGCTCCTT Reverse: TCAGGATACCTCTCTTGCTCT

Table 12.9 Sybr green primers for IL6 qPCR.

The samples were amplified for 40 cycles as described for mFak and chFAK RT-qPCR.

12.5.7 RT-qPCR analysis

Analysis was performed using the ABI Prism 7500 Sequence Detection system Instrument and software (Applied Biosystems). An RQ value was calculated using the $2^{(-\Delta\Delta ct)}$ method.

12.6 Tumour growth methods

12.6.1 Tumour growth and doxorubicin treatment (B16-F0 melanoma)

Unless otherwise stated, 1 X 10^6 Mouse melanoma (B16-F0, ATCC; mycoplasma free) cells were injected subcutaneously in the flank of *Pdgfb-iCre^{ert} +; FAK $^{fl/fl}$ R26 FAK $^{K454R/K454R}$* mice and control *FAK $^{fl/fl}$ R26 FAK $^{K454R/K454R}$* mice. Tumours were measured daily

with callipers, and once the tumour volume exceeded 100 mm^3, the mice were injected intraperitoneally (IP) with 100 µl of 10 mg/ml tamoxifen (Sigma, T5648) diluted in 10 % ethanol in corn oil (Acros Organics 405435000) to induce deletion of the endothelial-cell FAK kinase domain. 24 hours after the first tamoxifen injection, mice were given another tamoxifen injection and were fed with tamoxifen-containing diet (TAM400, Harlan) in the hopper in addition to a mash of 25 % tamoxifen diet (ENVIGO TT.55125IC), 75 % regular diet (Prolab 5P00) in water. This diet was continued to the end of the experiment to maintain *Cre* activity. 24 hours after the second tamoxifen injection, mice began three consecutive IP injections of 6 mg/kg of doxorubicin (Seacross Pharmaceuticals Ltd PL41013/0003) or 100 µl PBS as a negative control 24 hours apart. Calliper measurements were made daily, and animals were culled when tumours reached the maximum size allowed by UK Home Office regulations, were sick, had ulcerated tumours or had reached ten days of treatment. After the relevant ante-mortem procedure, tumours were dissected and either dehydrated in sucrose and PFA as described for blood vessel perfusion or fixed in PFA and embedded in paraffin as described for Doxorubicin delivery.

12.6.2 Tumour growth for immunostaining (B16F0 melanoma)

For Ki-67 and CC3 immunostaining, 1 X 10^5 Mouse melanoma (B16F0, ATCC; mycoplasma free) cells were injected subcutaneously into each flank of *Pdgfb-iCre^{ert} +;FAK $^{fl/fl}$ R26 FAK $^{K454R/K454R}$* mice and control *FAK $^{fl/fl}$ R26 FAK $^{K454R/K454R}$* mice. Tumours were measured daily with callipers, and once the volume of one tumour exceeded 100 mm^3, the mice were recruited in cohorts and injected intraperitoneally (IP) with 100 µl of 10 mg/ml tamoxifen (Sigma, T5648) diluted in 10 % ethanol in corn oil (Acros Organics 405435000) to induce deletion of the endothelial-cell FAK kinase domain. 24 hours after the first tamoxifen injection, mice were given another tamoxifen injection and were fed with tamoxifen-containing diet (TAM400, Harlan) in the hopper in addition to a mash of 25 % tamoxifen diet (ENVIGO TT.55125IC), 75 % regular diet (Prolab 5P00) in water. This diet was continued to the end of the experiment to maintain Cre activity. 24 hours following the second tamoxifen injection, mice began three consecutive IP injections of 6 mg/kg of doxorubicin (Seacross Pharmaceuticals Ltd PL41013/0003) or 100 µl PBS as a negative control 24 hours apart. Mice were culled 48 hours after the final PBS or doxorubicin treatment.

12.6.3 Orthotopic pancreatic tumour cell injection

TB32048 cells (derived from murine KPC tumours) were grown in DMEM (Gibco 4.5g/L glucose 41966-029) supplemented with 1 % P/S and 10 % FBS to 70 % confluency (P6). 50 C57Bl6 mice were shaved the day before surgery. Mice were anesthetised with isoflurane and 1.5 l/minute O_2, the skin cleaned with a swab of chlorohexidine (Vetasept XHG025) and given 30 µl injectable anaesthetic subcutaneously into the neck. The skin was cut on the left side of the animal, just below the bottom of the ribs and parallel to them. Using clean scissors, the skin was separated from the peritoneum. The spleen was then visible through the peritoneum an incision of roughly 8 mm in the same orientation as the skin incision, was made in the peritoneum directly over the spleen. The spleen was then lifted through to the outside of the peritoneum bringing the pancreas with it. 1 x 10^3 TB32048 cells in 10 µl 1:1 PBS: Matrigel® (Growth factor reduced Corning 336230) were injected into the tail of the pancreas with a 10 µl Hamilton syringe. The peritoneum was sutured, the skin clipped, and the mouse was put into recovery.

DT6066 (KP derived murine pancreatic cancer cell line) cell injection was performed as for TB32048 but using 1 x 10^6 cells in 40 µl PBS with no Matrigel; treatment schedules are described in the results.

12.7 Mouse treatment and drugs

12.7.1 Drugs

Gemcitabine (Fresenius-Kabi, 38mg/ml) was purchased as a liquid from Barts Hospital pharmacy and given by intraperitoneal injection at 75 mg/kg body weight in saline (100 µl). The gemcitabine was stored at room temperature until it was opened; once opened, it was stored at 4 °C and used within one month. *In vitro* doses are described in the text. ***29P*** was provided by Horst Kessler (Munich, Germany). ***29P*** was stored at a concentration of 4.2 X 10^{-5} M in saline (0.9 % NaCL in water) at -20 °C. Animals were grouped by weight with a maximum weight difference of 2 g in each group. On the day of treatment, the ***29P*** was thawed on ice and diluted in saline to a concentration so that 200 µl would be a dose of 250 µg/kg for a mouse of average weight in the group. For example, for a group of mice with average weight of 20g, 137 µl of ***29P*** stock would be diluted to a total volume of 200 µl. This dose was given by oral gavage as described in the text. ***29P*** doses were calculated based on how much of the deprotected drug ***29*** is available in the blood and adjusted to be comparable to optimal Cilengitide doses (data

not shown). Mice were given an equal volume of saline by oral gavage or by intraperitoneal injection as placebo controls for ***29P*** and gemcitabine, respectively.

Doxorubicin (Seacross Pharmaceuticals Ltd PL41013/0003) was also purchased from Barts Hospital pharmacy. It was kept at 4 °C, used within 48 hours of opening and was administered, undiluted, *in vivo* IP at 6 mg/kg or *in vitro* as described in the text.

EC FAK deletion in the Tamoxifen *Pdgfb-iCre^{ert} +; FAK $^{fl/fl}$ R26 FAK $^{K454R/K454R}$* model was achieved *in vivo* with IP injection of tamoxifen (10 mg/ml). Tamoxifen preparation: 500 mg of tamoxifen (T5648-5G Sigma) was dissolved in 5 ml of 100 % ethanol at 37 °C for 30 min. This solution was mixed with 45 mL of corn oil (Sigma C8267) and vortexed for 2 min. 500 µl aliquots were stored at -20 °C prior to use.

12.8 *In vivo* imaging methods

12.8.1 Magnetic resonance imaging (MRI)

Mice were imaged by MRI under general anaesthetic (isoflurane) on day 20. Once mice were fully anaesthetised, they were placed in the MRI on a heated bed. They were given a constant supply of isoflurane (~2 %) which maintained their breathing at a regular rhythm, approximately 28-50 breaths per minute measured by a pressure-sensitive pad. Gating was also employed to image between breaths so that artefacts due to movement were minimised. Eyes were kept hydrated with eye gel (lubrithal 321/00/12/PUVPT, Dechra). A T2 scan was carried out using Paravision 6.0.1 software, and a Bruker ICON 1T MRI with a repetition time (TR) of 2671 ms and echo time (TE) of 84 ms. 11 slices were obtained with a thickness of 0.75 mm and a slice gap of 0.25 mm. Each slice contains 110 X 110 pixels, with a resolution of 0.27 X 0.27 mm, corresponding to a field of view of 30 X 30 mm. An estimate of the tumour volume was obtained by drawing 3-D regions of interest (ROI) using VivoQuant software (version 3.5) (inviCRO, Boston, USA).

12.8.2 Ultrasound (US)

Mice were shaved, placed on a heat pad at 39 °C, anaesthetised with isoflurane; the hair was then removed with hair removal cream, and the skin washed. Ultrasound gel was applied to the transducer, and the MS550S transducer applied to the mouse. The presence of a tumour was confirmed visually using Vevo2100 software.

12.9 Immunostaining protocols

Tumours were prepared for immunostaining by three separate methods: (1) snap freezing in liquid nitrogen and maintained at -80 °C: (2) sucrose dehydration or by (3) fixing in 4 % formaldehyde (Fisherchem F/1501/PB08) for 24 hours before transferring to 70 % ethanol.

1. For snap-frozen tumours, the piece of tumour was wrapped in foil and submerged in liquid nitrogen until solid. They were stored at -80 °C, and frozen tumours were sectioned at 6 µm.
2. For sucrose dehydration, tumours were fixed in 4 % PFA with a tumour to fixative volume ratio of at least 1:10, 4 % sucrose in PBS for 1 hour at 4 °C and then dehydrated in 15 % sucrose in PBS overnight at 4 °C. The tumours were then frozen in moulds in cryomartrix (OCT) (ThermoScientific, 6769006), cooled on dry ice and then kept at -80 °C. They were sectioned at -20 °C to 6 µm sections.
3. For formalin fixation, tumours were fixed in 4 % formaldehyde with a tumour to fixative volume ratio of at least 1:10 overnight. The formaldehyde was then replaced with 70 % ethanol. Fixed tumours were embedded in paraffin in the histology department, and 4 µm sections prepared.

12.9.1 Haematoxylin and eosin (H and E) staining

H and E staining was performed by BCI histology service on a g Leica Autostainer XL. Formalin-fixed; paraffin-embedded sections were deparaffinised in 3 changes of xylene (X/0200/17, Fisher) 3 minutes each. They were rehydrated in 2 changes of 100 % Methylated spirit industrial (IMS; M/445/17, Fisher), one change of 90 % IMS and one of 70 % IMS three minutes each, followed by 2 minutes washing in tap water. The sections were then dipped in haematoxylin (Haematoxylin Gill III, Leica, 3801542E) for 3.5 minutes and washed again in running tap water for 4 minutes. They were dipped in 1 % acid alcohol for 20 s and washed in running tap water for 3 minutes before dipping in eosin (Leica 3801601E) for 6 minutes. The slides were washed again in running tap water before dehydrating in 70 % IMS (1.5 minutes), 90 % IMS (2 minutes), 100 % IMS (three changes, two minutes each) and three changed of 2 minutes in xylene before mounting in DPX.

12.9.2 Ki-67

Paraffin-embedded sections were deparaffinised in two changes of xylene, 5 minutes each, then hydrated in two changes of 100 % ethanol for 3 minutes each, 80 %, 70 %, 50

% ethanol for 1 minute each and washed in distilled water. Sodium citrate buffer (10 mM sodium citrate, 0.05 % tween 20, pH 6) was heated in the microwave (full power) for six minutes. The slides were added and boiled for 10 minutes, the sodium citrate was topped up and slides boiled for a further 10 minutes, then cooled for 20 minutes. Sections were washed twice in PBS-tween 20 (0.01 %) for 2 X 2 minutes, blocked for 60 minutes in 5 % goat serum in PBS at room temperature, then incubated overnight at 4 °C with rat anti-endomucin (Santa-Cruz sc-65495) and rabbit anti-Ki-67 (Abcam Ab16667) both 1:100 in 5 % goat serum in PBS. They were washed in PBS-tween 2 X 5 minutes then incubated with secondary antibodies, goat anti-rabbit 488 (Invitrogen A11008) and goat anti-rat 546 (Invitrogen A11081). Sections were washed in PBS 2 X 3 minutes and once in 1 in 50,000 DAPI in PBS (5 minutes). They were dipped in water and mounted in pro-long gold antifade (Thermofisher Scientific P36930). The percentage of nuclei that were Ki-67 positive within 50 µm of blood vessels were quantified. Tumour sections were analysed using the Zeiss Axioplan microscope, and images were captured using an LSM 710 confocal microscope.

12.9.3 Cleaved caspase 3 (CC3)

Sucrose dehydrated, frozen tumour sections fixed in 4 % sucrose/PFA were air-dried, washed in PBS for 10 minutes and blocked in 5 % goat serum in PBS (1 hr, RT). After a further wash in PBS, they were incubated overnight at 4 °C with endomucin antibody (Sc-65495 Santa Cruz) and rabbit anti-cleaved caspase 3 (Cell Signalling, 9661), both diluted 1:100 in 0.5 % goat serum in PBS. They were washed in PBS 2X 5 minutes then incubated with secondary antibodies-goat anti-rabbit 488 (Invitrogen A11008) and goat anti-rat 546 (Invitrogen A11081). Sections were washed in PBS 2 X 3 minutes and once in 1 in 50,000 DAPI in PBS (5 minutes). They were dipped in water and mounted in pro-long gold antifade (Thermofisher Scientific P36930).

12.9.4 γ H2AX staining

γ H2AX staining was performed on sections of PFA fixed, sucrose dehydrated tumours frozen in optimal cutting temperature compound (OCT). The sections were thawed and air-dried at room temperature for 30 minutes, rehydrated in PBS for 5 minutes in a humidified chamber and permeabilised for 3 minutes 0.5 % TritonX-100 in PBS. Sections were blocked in 5 % bovine serum albumin (BSA) (SIGMA Life Science-A8022-500G) in PBS at RT for 1 hr. Sections were incubated overnight in 5 % BSA in PBS with 1 in 100 γ H2AX (Cell Signalling Phospho-Histone H2A.X (Ser139) 2577S) and 1 in 200 endomucin

(Sc-65495 Santa Cruz) at 4 °C. After 3 x 5-minute washes in PBS, the sections were incubated for 1 hr at RT in 5 % BSA in PBS with 1 in 100 goat anti-rat 546 (Invitrogen A11081) and 1 in 100 goat anti-rabbit 488 (Invitrogen A11008). They were washed 2 X 5 minutes in PBS, followed by 15 minutes in 1 in 10,000 DAPI in PBS, a 5-minute wash in 0.1 % TritonX-100 in PBS, and 5 minutes distilled water. Sections were mounted in Prolong Gold antifade (Life Technologies P36930) followed by a coverslip (VWR International, Catalogue no. 631-0135).

12.9.5 Blood vessel perfusion

When mice reached the experimental endpoint, they were warmed in a hot box to dilate the blood vessels then injected with 100 µl undiluted biotinylated tomato lectin (Vector Laboratories b-1175) via the tail vein 10 minutes before killing to analyse blood vessel perfusion. Tumours were halved, half was formalin-fixed, half fixed in 4 % paraformaldehyde, 4 % sucrose in PBS for 1 hour and then dehydrated in 15 % sucrose in PBS overnight. Tumours were then frozen in moulds in OCT (ThermoScientific 6769006), cooled on dry ice and then kept at -80 °C and sectioned at -20 °C (6 µm thick sections). Cryosections were air-dried, washed in PBS then incubated in 3 % H_2O_2 in methanol in the dark for 30 min. They were washed twice in PBS, followed by 0.1 % triton in PBS. Sections were blocked in 2 % BSA, 5 % heat-inactivated goat serum, 0.1 % tween 20 in PBS in a humidified chamber for 1 hour. Slides were incubated at 4 °C with endomucin ((V7C7) SC-65495 SantaCruz Biotechnology) (1/100) for 1 hr, then washed in PBS tween and incubated for 1 hour with anti-rat- 488 (Invitrogen A-11006) and streptavidin 568 (Thermofisher S11226). Slides were washed in PBS, incubated with DAPI for 3 minutes and mounted in Prolong Gold (Life Technologies).

12.9.6 Endomucin staining

Paraffin-embedded sections were de-waxed, antigen retrieval was performed by microwaving (5 minutes full power, 10 minutes half power) in sodium citrate buffer (10 mM sodium citrate (Fisher Chemical S/3280/60), 0.05 % Tween 20 (11 TWEEN201 MP BIOMEDICALSCAS Number 9005-64-5), pH 6) and washed in PBS. Endogenous peroxidase was blocked with 3 % hydrogen peroxide in MeOH for 10 minutes, washed in PBS and blocked for 1 hour in 3 % BSA (Sigma Aldrich A8022-500G), 0.3 % Triton X (Alfa Aesar A16046) in PBS at room temperature. They were stained for endomucin (Endomucin V.7C7 SC-65495 Santa-Cruz Biotechnology) 1/500 in 3 % BSA at 4 °C overnight. They were washed in PBS for 10 minutes before incubation with biotinylated secondary to rat anti-

rat IgG (BA-4001 Vector laboratories) at a 1/200 dilution in PBS. After a further PBS wash, the slides were incubated in strept (avidin)–Biotin Complex (ABC) (Vectastain Vector PK-6100) reagent for 40 minutes. After washing in PBS, the slides were stained with DAB reagent for 10 minutes, and the reaction stopped with ddH2O. A counterstain of haematoxylin (Haematoxylin solution Sigma Aldrich MHS16-500 ml) was applied for two minutes, and excess washed off with tap water. Samples were dehydrated in increasing concentrations of EtOH followed by xylene. The slides were mounted with DPX mounting medium for histology (Sigma 06522-500 ml).

12.9.6.1 Blood vessel density (BVD) counts

Blood vessels were counted from endomucin stained sections. Unless otherwise stated, BVD counts were done on representative fields of view, excluding necrotic areas (identified by histological observation) and tumour periphery regions. For DAB-stained blood vessels, sections were scanned on a Pannoramic 250 High Throughput Scanner, 3D Histech Ltd and counted on the screen with Case Viewer V2.4.0.119028, 3D Histech Ltd. For fluorescent sections, the blood vessels were counted down the microscope on a Zeiss Axioplan microscope, and representative images were captured using Axiovision Rel.4 software. The first set of blood vessel density counts for vascular promotion experiments were performed counting only vessels with a visible lumen as detailed in the text. This was as an indication of vessels that were likely to be perfused. However, while this gives some indication of which vessels may be perfused, results are impacted by where the blood vessel has been sectioned and give no indication of leakage. Therefore, after this initial experiment, all blood vessels were counted whether or not a lumen was visible but the animals were perfused with biotinylated lectin to allow further perfusion analysis if differences were observed in the blood vessel numbers. They were not size-matched, but correlation coefficients were calculated to confirm that there was no correlation between size and BVD in the tumours quantified.

12.9.7 Myc-tag staining

Myc-Tag (FAK) staining was performed on tumours that were fixed in 4 % PFA, 4 % sucrose in PBS for 1 hr at 4 °C, with rotation, then transferred to a 15 % sucrose in PBS overnight at 4 °C. The next day fixed tumours were embedded in OCT on dry ice and frozen at -80 °C. 10 µm sections were cut. For staining, sections were allowed to dry for 30 minutes at RT and re-hydrated and permeabilised in PBS for 5 minutes, followed by 0.5 % triton-X-100 in PBS for 3 minutes at RT. Sections were then blocked for 1 hr at RT

with a blocking solution of 5 % donkey serum (NDS, Sigma), 0.2 % BSA (Sigma), 0.3 % TritonX-100 and 0.05 % NaN_3 (Sigma) in PBS. They were incubated for 30 minutes at 37 °C with anti-mouse Myc-Tag (9B11) Alexa 488 conjugated antibody (#2279- Cell Signalling Technologies) and rat anti-Pecam (#550274 from BD Pharmingen) and left overnight at 4 °C. Slides were then washed in PBS 3 times for 5 minutes and incubated with secondary Alexa Fluor-594 anti-rat antibody (Invitrogen, Paisley, UK) for 1 hr at RT. Slides were washed in 0.1 % triton-100 in PBS 3 times 5 minutes each, followed by a 5 minutes wash in PBS and subsequently rinsed in distilled water and mounted with Prolong Gold antifade reagent with DAPI (Life Technologies).

12.9.8 Doxorubicin delivery

Mouse melanoma (B16F0, ATCC; mycoplasma free) cells (grown as described in *materials and methods* 12.10.2) were injected subcutaneously in the flank of *Pdgfb-iCre^{ert} +; FAK $^{fl/fl}$ R26 FAK $^{K454R/K454R}$* mice and control *FAK $^{fl/fl}$ R26 FAK $^{K454R/K454R}$* mice and treated as previously described (Tavora et al. 2010). To assess doxorubicin delivery to the tumours, the mice were given a high dose, slow IV injection of doxorubicin (20 mg/kg) for 1 minute, 5 minutes before euthanasia. The mice were perfused with 4 % paraformaldehyde to fix tumours at room temperature, which were removed and fixed overnight in 4 % paraformaldehyde at 4 °C, then transferred to 70 % ethanol. Tumours were paraffin-embedded, and sections were deparaffinized and rehydrated with ethanol. They were mounted with prolong-gold with DAPI and imaged with the Zeiss Axioplan microscope. Images were captured using Axiovision Rel.4 software.

12.10 Cell culture and *in vitro* cell survival

12.10.1 Endothelial cell culture

12.10.1.1 Mouse lung endothelial cell (MLEC) culture

MLECs were isolated from *Pdgfb-iCre^{ert} +;FAK $^{fl/fl}$;R26 FAK $^{K454R/K454R}$* or *FAK $^{fl/fl}$;R26 FAK $^{K454R/K454R}$* adult mice as described previously. After a positive sort with rat anti-ICAM2 antibody (Serotec, MCA 2295EL) and sheep anti-rat IgG magnetic beads (Dynabeads) as described (Reynolds and Hodivala-Dilke 2006), cells were immortalised with polyoma middle T (PmT) virus by incubating them over two consecutive days for four h with supernatant from GgP+E packaging cells (May et al. 2005). Cells were grown in flasks coated with collagen, fibronectin and gelatin in MLEC Media (Reynolds and Hodivala-Dilke 2006) supplemented with 500 nM 4-hydroxytamoxifen (4-OHT). Cells from *Pdgfb-*

iCre^{ert} +;FAK $^{fl/fl}$;R26 FAK $^{K454R/K454R}$ were termed FAK^{KD} ECs, and those from *FAK $^{fl/fl}$;R26 FAK $^{K454R/K454R}$* mice were termed WT ECs. The cells were then transfected with a green fluorescent protein alone (GFP) or GFP with Cre (to maintain Cre expression in vitro, which was otherwise lost) plasmid and cultured in coated flasks in MLEC media.

T75 flasks for MLECs were coated in 5ml 15 µg/ml vitronectin (Vitrogen Cohesion, Palo Alto, CA) and 5 µg/ml fibronectin (Sigma, UK) in 0.1 % gelatin for 30 minutes before plating cells. Once confluent, they were washed twice in PBS and dissociated with 2.5 ml 0.25 % Trypsin-EDTA (Gibco 25200-072). 10 ml MLEC medium was added to the flask, and the cells spun down for 5 minutes at 1200 rpm. The supernatant was discarded, and the cells resuspended in MLEC and plated into 5 T75s.

12.10.1.2 Human pulmonary endothelial cell (HPMEC) culture

Cryopreserved HPMECs (Promocell C-12281) were purchased at passage four. T75 flasks were prepared by coating with 5ml sterile 0.2 % gelatin for 20 minutes at 37 °C and removed immediately before use. Cells were grown to confluency in basal medium (Promocell C-22020) supplemented with Growth Medium MV Supplement Mix (Promocell C-39225). Once confluent, cells were passaged by removing medium, washing twice in PBS and aspirating before adding 3 ml 0.25 % Trypsin-EDTA (Gibco 25200-072) and incubating at 37 °C until cells detached. The trypsin was inactivated with 10 ml Ham's F12 (Gibco) with 20 % FBS (Gibco), and the cells centrifuged for 3 minutes at 1200 rpm. The medium was removed, and the cells resuspended in culture medium and plated into five coated flasks in 10 ml medium. Cells were used at 90-100 % confluency.

12.10.2 B16F0 melanoma cell culture

B16F0 melanoma cells were cultured in DMEM supplemented with 10 % FBS and passaged in 3 ml 0.25 % Trypsin-EDTA (Gibco 25200-072) when 70 % confluent. For subcutaneous injection, they were passaged 24 hours before injection so that they were in an exponential growth phase on the day of the experiment. Immediately before injection, the cells were washed twice in 10 ml PBS and trypsinised in 3 ml 0.25 % Trypsin-EDTA. The cells were incubated at 37 °C until they detached (roughly 2 minutes), the trypsin was then inactivated with 10 ml DMEM supplemented with 10 % FBS. The cells were centrifuged (1200 rpm, 5 minutes), and the supernatant discarded. Cells were resuspended in 1 ml PBS and passed through a 40 µm cell strainer, they were then

counted and diluted in PBS to a concentration of 1 million cells in 100 µl. This suspension was kept on ice and mixed between injections.

12.10.3 Pancreatic cancer cell culture

12.10.3.1 TB32048 and DT6066

TB32048 cells were cultured in DMEM supplemented with 10 % FBS, 1 % P/S and passaged in 3 ml 0.25 % Trypsin-EDTA (Gibco 25200-072) when 70 % confluent.

DT6066 cells were a gift from Professor David Tuveson (2010) and were cultured and passaged as described for TB32048 cells.

12.10.4 Gemcitabine resistant DT6066 cells

The gemcitabine resistant DT6066 cells were a gift from Dr Lewis Stevens and Dr Ping Pui Wong. They were produced by continuously culturing the DT6066 cell line with gemcitabine. The cells were treated as for other pancreatic cancer cells, but 24 hours after thawing, the medium was replaced with medium supplemented with 2000nM gemcitabine to maintain the pressure for gemcitabine resistance.

12.10.5 Crystal violet assays

For Crystal violet assays, cells were treated as described in the text. At the end of treatment, the medium from cells and washing them twice in PBS. They were then stained in 0.5 % in 100 % MeOH for 3 hours at RT. The crystal violet was then removed, and the plates washed in copious amounts of tap water. The plates were then inverted in an incubator at 37 °C until dry. Dry plates were imaged on a Chemidoc™ imager by transillumination and quantified in the intensity of the stain quantified in ImageJ.

12.10.6 MTT assays

Cell viability assays were performed with 3-(4,5-Dimethylthiazol-2-yl)-2,5-Diphenyltetrazolium Bromide (MTT). 10,000 A549, TB32048 or DT6066 cells were plated per well of a 96 well plate in DMEM medium supplemented with 10 % FBS and 1 % P/S. 24 hours after plating, the cells were treated with gemcitabine and ***29*** at concentrations of 0, 25, 50, 75 or 100 nM gemcitabine and 0, 0.2, 2 or 20 nM ***29*** as described in the figure. 48 hours after initial drug treatment, the cells were treated again by removing the medium and replacing it with fresh, drug-containing medium. After a further 48 hours, the MTT assay was performed by removing the medium and replacing it with 500 µg/ml MTT in complete medium. Cells were incubated with MTT in medium at 37 °C for 90 minutes before removing and solubilising the formazan in 50µl DMSO per well. The

absorbance was measured spectrophotometrically at 570nm. Relative survival values were calculated by dividing the absorbance value in drug-treated cells by the average absorbance value for the untreated cells and multiplying by 100.

12.11 Cytokine arrays

12.11.1 Cytokine arrays (kinase-dead cells)

Immortalised *FAK^{KD}* and *WT* endothelial cells were grown in normal MLEC media to confluency in a T75. The cells were treated with 125 nM Doxorubicin (Seacross Pharmaceuticals Ltd PL41013/0003) or an equal volume of PBS. After 44 hr, the media was changed to OptiMem with the same doxorubicin treatment for a further 4 hr. Whole-cell lysates were extracted, and mouse cytokine arrays (Proteome Profiler ARY006, R&D Systems) were processed according to the manufacturer's instructions.

12.11.2 Cytokine arrays with human cells (kinase inhibitor)

Human pulmonary microvascular endothelial cells (Promocell) were grown to 80 % confluency and treated with 5 µM of the FAK inhibitors PF-573,228 (*Pfizer*), PF-562,271 (*Pfizer*) or defactinib (*Verastem*) and 250 nM Doxorubicin for 48 h. DMSO was used as a control for FAK inhibitors as they were suspended in DMSO, and PBS was used as a control for doxorubicin. Cells were lysed in RIPA buffer and 250 µg loaded onto a human XL cytokine array (R & D Biosystems ARY022B). The array was performed as in the manufacturer's instructions.

12.12 Mass spectrometry methods

Samples for mass spectrometry were prepared by Dr Rita Pedrosa and Liquid chromatography–mass spectrometry/mass spectrometry (LC-MS/MS) for proteomics, phospho-proteomics or secretomics run and analysed by Pedro Casado and Vinothini Rajeeve under the supervision of Pedro Cutillas. Methods are described below.

12.12.1 Phosphoproteomics, Proteomics and secretomics

Primary endothelial cells from the lungs of *Pdgfb-iCre+;FAK$^{fl/fl}$* and *Pdgfb-iCre-;FAK$^{fl/fl}$* mice were isolated as described for FAK-KD ECs and in (Reynolds and Hodivala-Dilke 2006). Cells were washed twice with ice-cold phosphatase inhibitor (1 mM Na_3VO_4, 1 mM NaF) supplemented PBS. They were lysed in urea buffer (8 M Urea in 20 mM (4-(2-hydroxyethyl)-1-piperazineethanesulfonic acid) HEPES at pH 8.0) supplemented with the phosphatase inhibitors Na_3VO_4 (1 mM), NaF (1 mM), β-glycerol-phosphate (1 mM) and

$Na_4P_2O_7$ (2.5 mM). The resultant lysates were centrifuged for 10 minutes, 20,000 g, 4 °C and the supernatant transferred to fresh, low protein binding tubes. The protein concentration was quantified using a Pierce bicinchoninic acid (BCA) assay (23225) and 160 µg of protein per sample diluted in 400 µl in urea buffer. Samples were sequentially incubated at 24 °C, shaking with 10 mM Dichlorodiphenyltrichloroethane (DDT) for 1 hr and 16.6 mM Iodoacetamide (IAM) for 30 minutes. The urea concentration was diluted to 2 M by adding 1.2 mL of 20 mM HEPES (pH 8.0), 90 µL of conditioned trypsin beads (50 % slurry of Tosyl-L-lysyl-chloromethane hydrochloride (TLCK)-trypsin (Thermo-Fisher Scientific, 20230) conditioned with three washes of 20 mM HEPES at pH 8.0) were added to samples before overnight incubation with shaking at 37 °C. The trypsin beads were removed by centrifugation at 2,000 g, 5 °C for 5 minutes and 140 µg of the digested protein was used for phosphoproteomics, 20 µg for proteomics.

The samples were desalted using Carbon C18 Top tips (Glygen, TT2MC18). The tips were activated with 100 µL of elution solution (70 % Acetonitrile (ACN), 0.1 % Trifluoroacetic acid (TFA)) and equilibrated twice with 200 µL of wash solution (1 % ACN, 0.1 % TFA). The samples were loaded, and columns washed twice with 200 µL of wash solution. For phosphoproteomics, the phosphopeptides were eluted four times with 50 µl of glycolic acid solution 1 (1 M glycolic acid in 50 % ACN, 5 % TFA) and subjected to phosphoenrichment. For proteomics, the peptides were eluted four times with 50 µL of elution solution; they were dried in a speed vacuum and stored at -80 °C. In all of the steps, column spin tips were centrifuged at 2,000 g, 5 °C for 5 min.

The phosphopeptides were enriched using TiO_2 beads (Capital HPLC ltd, 5020-75010). Desalted samples were diluted in glycolic acid solution (1 M glycolic acid in 80 % ACN, 5 % TFA) to a final volume of 500 µL and incubated for 5 minutes with 50 µL of titanium bead solution (500 µg/ml TiO_2 beads in 1 % TFA). The samples were then centrifuged at 1,500 rpm, RT for 3 min and two-thirds of the supernatant was transferred to fresh tubes. The pellets of TiO_2 beads were resuspended in the remaining third of the supernatant and packed into empty spin tips (Glygen, TT2EMT) by centrifugation. The two-thirds of the supernatants collected previously were run through the TiO_2 loaded spin columns by centrifugation. TiO_2 beads were washed by centrifugation with 100 µL of the glycolic solution, followed by ammonium acetate solution (100 mM ammonium acetate in 25 % ACN) and finally twice with neutral solution (10 % ACN). The TiO_2 beads were centrifuged four times with 50 µL of phosphopeptide elution solution (5 % NH_4OH) to elute the phosphopeptides. All centrifugations were done at 1,500 rpm, RT. Phosphopeptide

solutions were frozen on dry ice for 15 min, then dried in a speed vac and stored at -80 °C.

The phosphopeptide pellets were then re-suspended in 7 µL of reconstitution buffer (20 fmol/µl enolase in 3 % ACN, 0.1 % TFA) and 5 µl injected into the LC-MS/MS platform. The liquid chromatography (LC) system (Dionex UltiMate 3000 RSLC) used mobile phases A (3 ACN: 0.1 % FA) and B (100 % ACN; 0.1 % FA). Peptides were trapped in a µ-pre-column (Thermo Fisher Scientific, 160454) and then separated in an analytical column (EASY-SPRAY RSLC C18 2 µM, 50 CM X 75 µM, #ES803). The parameters used were: 3 % to 23 % B gradient for 90 min and a flow rate of 0.25 µL/min. Samples shuffled to randomise them before loading to run on the LC-MS/MS system. The peptides were infused into the online connected Q-Exactive Plus system via an Easy Spray Source as they eluted from the nano-LC system (Thermo Fisher Scientific). The instrument operated a 2.1 s duty cycle consisting of acquisition of a full scan survey spectra (375-1,500 m/z) with a 70,000 full width at half maximum (FWHM) resolution. This was followed by a data-dependent acquisition process where the 15 most intense ions were selected for HCD (higher energy collisional dissociation) and tandem mass spectrometry (MS/MS) scanning (200-2,000 m/z) with a resolution of 17,500 FWHM. A 30 s dynamic exclusion period was enabled with an exclusion list with a 10 ppm mass window. Overall duty cycle generated chromatographic peaks with a base of approximately 30 s, which allowed the construction of extracted ion chromatograms (XICs) with at least 10 data points. The peptide pellets produced for proteomics analysis were resuspended in reconstitution buffer (0.5 µg/µL), and 2 µL of the resultant solution were injected into the LC-MS/MS platform. Samples were run in a 120 minute gradient (3 % to 23 % B) with the rest of the LC-MS/MS parameters as described for phosphoproteomics analysis.

12.12.2 Mascot Daemon automated peptide identification from MS data.

Mascot Distiller v2.7.1.0 generated Peak list files (mascot generic format files; MGFs) from RAW data. The Mascot search engine (v2.5) was used to match data stored in MGF files to specific peptides by searching against the SwissProt Database (uniprot_sprot_2014_08.fasta) with a false discovery rate (FDR) of ~1 %. The parameters for MS scans were set to: 2 trypsin missed cleavages, mass tolerance of ± 10 ppm for MS/MS scans, ± 25 mmu. carbamidomethyl Cys as a fixed modification, PyroGlu on N-terminal Gln, oxidation of Met and phosphorylation of Ser, Thr and Tyr as variable modifications. Pescal software (developed in house; Barts Cancer Institute) was used to quantify label-free peptides as indicated in (Casado and Cutillas 2011; Cutillas and

Vanhaesebroeck 2007), and XICs for all the identified peptides across all samples were constructed with a ±7 ppm mass window and ±2 min retention time window. Peak areas were calculated for all XICs and missed datapoints, given an intensity value equal to the minimal value obtained in the assessed sample divided by 10. The intensity values calculated for each peptide were normalized to total sample intensity. Phosphorylation of Ser, Thr and Tyr were not considered in Mascot searches for proteomics analysis. Protein amount was inferred from quantitative data for all peptides identified in the same protein.

12.12.3 Secretomics

For secretomics analysis, the medium was collected, and BSA removed using an Albumin Depletion and Low Abundance Protein Enrichment Kit (AlbuVoid™). The protein concentration was quantified using a BCA kit and 50 µg diluted in elution buffer (AlbuVoid™) to a final volume of 50 µl. 50 µl of 4 M urea in 20 mM pH 8.0 HEPES was added to the protein to suspend it in a final concentration of 2 M Urea. The sample volume was increased to 1 mL by addition of 2 M urea in 20 mM pH 8.0 HEPES, 80 µL of conditioned trypsin beads (50 % slurry of TLCK-trypsin conditioned with three washes of 20 mM pH 8.0 HEPES) and samples were incubated at 37 °C overnight with shaking. The trypsin beads were removed by centrifugation at 2,000 g, 5 °C for 5 min, and samples were desalted with Carbon C18 Top tips as described for proteomics. The proteins present in the secretome pellets were identified and quantified as described for proteomics analysis. A serum-supplemented, phenol red-free, MLEC medium sample that was not exposed to ECs was also subjected to BSA removal, processed for MS analysis as for EC exposed samples; this was used as an internal control for medium proteins not secreted by ECs. All secreted proteins considered in the analysis were presented as an average amount across samples higher than in the reference sample not exposed to cells.

12.12.4 Bioinformatics

Volcano plots and heatmaps were constructed in R (v3.6.1) within the RStudio (v1.1.463) environment using the package “ggplot2” for volcano plots and the base R function “heatmap” for heatmaps. Unpaired two-tailed Student’s t-tests were used to determine statistical differences in phosphopeptide or protein abundance between conditions and considered significantly different if $p > 0.05$. Gene ontology (GO) enrichment between conditions was determined using David bioinformatics software

(https://david.ncifcrf.gov/). For all phosphoproteins or proteins significantly changed under the study conditions, enrichment was determined. All of the identified phosphoproteins or proteins were used as background, and a Modified Fisher's Exact Test was used to determine the significance of enrichment. From this analysis, GOs were considered significantly enriched if $p < 0.05$.

12.12.5 Data availability

The mass spectrometry proteomics data are available in the ProteomeXchange Consortium via the PRIDE (Perez-Riverol et al. 2019). The identifiers are PXD019728 and 10.6019/PXD019728. The sample names for each RAW file in the PRIDE database are listed in **Table 22.1** Sample details linked to the RAW submitted to PRIDE Mass Spectrometry database.

12.13 Organoid methods

12.13.1 General preparation for organoid production

Matrigel® matrix (Corning) is a reconstituted basement membrane which is extracted from Engelbreth-Holm-Swarm (EHS) mouse tumour. It contains a mix of laminin, collagen IV, entactin and heparan sulfate proteoglycan, and growth factors that naturally occur naturally in EHS tumour. The proteins have functional domains which can interact with laminin, collagen IV, and heparin-binding protein, forming the structural organisation of the Matrigel®. At temperatures of 22 °C to 37 °C, there is adequate energy for the formation of bonds which solidify the Matrigel, but at 4 °C, there is not enough energy to maintain these bonds, so the Matrigel® becomes liquid.

Therefore, to work with Matrigel in organoid production, it is important to be able to maintain a low temperature until the organoids are plated, at which point, they must be quickly warmed to 37 °C.

12.13.1.1 Hot water flask

In advance of any organoid production or passage, a hot water bottle was prepared by filling a T175 flask with sterile water supplemented with a water bath anti-fungal agent. This flask was closed tightly, sealed with parafilm and stored in a tissue culture incubator at 37 °C at least six hours in advance of any organoid work. Organoids were always plated on top of this flask to rapidly warm the Matrigel to 37 °C.

12.13.1.2 Tissue culture plastics

Pipette tips and tubes to be used for organoid passage were stored at -20 °C to ensure Matrigel® remained liquid. 24 and 96 well plates for organoid culture were warmed in a tissue culture incubator at 37 °C at least six hours prior to use.

12.13.2 R-spondin conditioned media

R-Spondin conditioned media was produced from Cultrex® R-spondin1 (Rspo1) Cells (Trevigen 3710-001-K). The cells were cultured in Advanced DMEM/F12 (ThermoFisher 12634010) supplemented with 12 % FBS (Gibco) and 1 % Pen/Strep with 100 mg/ml with 100 mg/ml zeocin selection reagent (Thermofisher R25001). Once confluent, cells were split into six T175 flasks; five of these were grown in culture medium without zeocin and the sixth with zeocin for selection; this was the flask that was maintained for further culture or freezing of the cells. Once the five flasks without zeocin were confluent, the cells were washed in PBS and the medium replaced with 50 ml mouse splitting medium (Advanced DMEM/F12, supplemented with 1 % Pen/strep, 1 % HEPES and 1 % GlutaMax supplement). The cells were cultured for one week, then the conditioned media was centrifuged for 5 minutes at 300 RCF, and the supernatant filtered through a 0.2µm filter. R-spondin media activity level was tested by demonstrating enhanced Wnt activity of Wnt conditioned media when R-spondin conditioned media. The R-spondin is added to the medium in order to activate Wnt pathways. This is through leucine-rich G-protein-coupled receptor 5 (LGR5) which binds to R-spondin to modulate Wnt signalling (Wang, Wang, et al. 2018).

12.13.3 Wnt conditioned media

Wnt-3a-conditioned media was produced from L Wnt-3A cells (ATCC CRL-2647). The cells were cultured in a culture medium (DMEM, high glucose, GlutaMAX, pyruvate (Thermofisher 10569010), with 12 % FBS (Gibco) and 1 % pen/strep) with 125 µg/ml zeocin selection reagent. Once a T175 flask was confluent, the cells were passaged into six T175 flasks, one was maintained with zeocin as the selection flask, and the remaining flasks were cultured in culture medium without zeocin as the conditioning flasks. Once confluent, these cells were passaged and maintained for a further week in culture medium without zeocin. The conditioned media was centrifuged for five minutes at 300 RCF and the supernatant filtered through a 0.2µm filter.

12.13.4 Plasmid expansion

The plasmids, FOPflash (12457 Addgene) and TOPflash (12456 Addgene), were bought as bacterial stabs. They were streaked onto Ampicillin agar plates (100 µg/mL ampicillin) with an inoculating loop and incubated overnight (37 °C) to produce single colonies. Single colonies were picked off plates using sterile pipette tips; each single colony was dropped into 5 ml liquid broth with 100 µg/ml ampicillin in a 25 ml tube with a lid loosely attached. This was incubated overnight at 37 °C to grow the culture. Once the bacteria had grown in liquid broth, 500 µl of this was mixed with 500 µl 50 % glycerol and frozen at -80 °C in cryovials. The remaining stock was used for a miniprep to extract the plasmid.

12.13.5 Miniprep

A miniprep was performed using the QIAprep® Spin Miniprep Kit (QIAgen 27104) on bacterial cultures to extract the plasmid.

The bacterial-culture was pelleted by centrifugation at 8000 rpm 1–5 ml (6800 x g) for three minutes at room temperature and resuspended in 250 µl Buffer P1 in a microcentrifuge tube. 250 µl Buffer P2 was added and mixed by inversion until the solution became clear, for no more than five min. 350 µl Buffer N3 was added and mixed by inversion, then centrifuged for 10 minutes at 13,000 rpm (17,900 x g). 800 µl of the supernatant was pipetted into a QIAprep 2.0 spin column and centrifuged at 13,000 rpm (~17,900 x g) for 30–60 s; the flow-through was discarded. The QIAprep 2.0 spin column was washed by adding 500µl buffer PB, centrifuging for 30–60 s at 13,000 rpm (~17,900 x g) and discarding the flow-through, washed again with 750µl buffer PE and then dried by centrifuging at 13,000 rpm (~17,900 x g) for 1 minute to remove residual wash buffer. The DNA was eluted by adding 50 µl Buffer EB (10 mM TrisCl, pH 8.5) to the QIAprep 2.0 spin column, let stand for 1 min, and centrifuging 13,000 rpm (~17,900 x g) for 1 min. The resulting eluate was stored at -20 °C.

12.13.6 HEK cell culture for TopFlash assay

HEK cells used for TopFlash assay were cultured as described for pancreatic cancer cell culture.

12.13.7 TopFlash Assay

To test the R-spondin activity of conditioned medium, a TopFlash assay was carried out to ensure it enhanced Wnt-3A activity. Two transfection mixes were prepared as follows:

TOP tube	Volume
DMEM (with glucose (4.5 g/l), L-glutamine and sodium pyruvate)	37.6 µl
X-treme Gene 9 Transfection reagent (Sigma-Aldrich 06365779001)	2.4 µl
TOP plasmid (1 µg/µl)	0.5 µl
Renilla plasmid (100 ng/µl)	0.5 µl

Table 12.10 TOP transfection mix.

FOP tube	Volume
DMEM (with glucose (4.5 g/l), L-glutamine and sodium pyruvate)	37.6 µl
X-treme Gene 9 Transfection reagent (Sigma-Aldrich 06365779001)	2.4 µl
FOP plasmid (1 µg/µl)	0.5 µl
Renilla plasmid (100 ng/µl)	0.5 µl

Table 12.11 FOP transfection mix.

Each tube was mixed by pipetting and incubated at room temperature for 20 minutes. Meanwhile, a confluent T75 flask of HEK293T cells was split as previously described. The cells were counted, and 204000 cells suspended in 7.2 ml HEK culture medium. The TOP transfection mix was added to one of these tubes and the FOP transfection mix to the other. 600 µl of the TOP transfection mix were pipetted into wells of a 24 well plate to give 12 wells with 17, 000 cells per well. This was repeated with the FOP transfection mix into separate wells of the plate, and the plates placed in a tissue culture incubator at 37 °C for 24 hours.

Medium to be tested was warmed to 37 °C and 3.6 ml of each condition prepared as follows:

Negative control	Base Wnt-3A culture medium (DMEM+ GlutaMAX, pyruvate, 10 % FBS, 1 % p/s)
Wnt-3A conditioned medium	50 % Wnt 3A conditioned medium, 50 % Base Wnt-3A culture medium
R-Spondin and Wnt-3A Conditioned medium	50 % R-Spondin conditioned medium, 50 % Wnt 3A conditioned medium

Table 12.12 Media conditions for R-Spondin testing.

600 µl of each prepared medium were pipetted gently on top of the HEK culture medium for the appropriate wells so that three TOP and three FOP transfected wells were treated with each medium without detaching the cells. The cells were returned to the incubator for 24 hours.

Passive lysis buffer was prepared as directed (Promega Dual luciferase® Reporter Assay System E1910) and warmed to room temperature.

12.13.8 Media production

12.13.8.1 Mouse wash medium

Mouse wash medium was composed of 500 ml DMEM with glucose (4.5 g/l), L-glutamine, sodium pyruvate, 5 ml Penicillin/Streptomycin (1X) and 5 ml FBS (1 %).

12.13.8.2 Mouse digestion medium

The mouse digestion medium was composed of 200 ml mouse wash medium with 0.125 mg/ml Collagenase Type XI (Sigma-Aldrich C9407-1G) and 0.125 mg/ml dispase (ThermoFisher 17105041).

12.13.8.3 Mouse splitting medium

Mouse splitting medium was made with 485 ml Advanced DMEM/F12, 5 ml HEPES (10mM), 5 ml Penicillin/Streptomycin (1X) and 5 ml GlutaMAX (1X). This medium can be stored for up to four weeks.

12.13.8.4 Mouse organoid feeding medium

The culture medium was based on Advanced DMEM/F12 (ThermoFisher 12634010) supplemented with B27 (ThermoFisher 17504044), 1.25 mM N-Acetylcysteine (Sigma-Aldrich A9165-5G), 10 nM gastrin I (human) (TOCRIS 3006), 500 nM A 83-01 (TOCRIS 2939) and the growth factors: 50 ng/ml EGF recombinant mouse protein (Peprotech AF-100-15), 100 ng/ml Recombinant Murine Noggin (Peprotech 250-38), 100 ng/ml Recombinant human FGF-10 (Peprotech 100-26), 10 mM Nicotinamide (Sigma-Aldrich N0636-100G) and 10 % R-Spondin-conditioned media produced as described above. When organoids were first isolated, thawed or dissociated to single cells, the medium was supplemented with 10.5 µM of the Rho-kinase inhibitor Y-27632 (Sigma-Aldrich Y0503-5mg). This complete mouse organoid feeding medium was kept for up to two weeks.

12.13.9 Isolation of organoids from mouse pancreatic tumours

Organoids were produced using the Tuveson method as detailed in (Huch et al. 2013). A hot water flask, mouse wash medium and mouse digestion medium were prepared in advance as described. Aliquots of Matrigel® and DNAse (Sigma-Aldrich D5025-150KU) were thawed on ice, and mouse organoid feeding medium with Rho-kinase inhibitor warmed to 37 °C.

The mouse was culled by cervical dislocation immediately followed by decapitation to drain the blood onto a piece of tissue. In a tissue culture hood, the mouse's fur was sprayed with ethanol and the mouse skinned using one set of sterile dissection tools. The peritoneum was opened to expose the intestines and pancreas. Using a second set of clean dissection tools, the tumour was dissected out without disrupting the intestines to maintain sterility. The tumour was quickly dipped in ethanol and moved to a petri dish on ice, where it was minced quickly and added to a 15 ml tube of mouse wash medium on ice. The tumour pieces were allowed to settle to the bottom of the tube and the medium and fat aspirated off until ~1 cm remained, including all of the tumour pieces.

10 ml mouse digestion medium was added to the tumour and incubated at 37 °C with agitation for 2-4 hours, depending on the size of the tumour. The tumour pieces were pipetted up and down to break them down and allowed to settle by gravity. 8.5 ml of the supernatant were transferred to a new tube. If there was a very large pellet, 8.5 ml wash medium was added, and the tube returned to 37 °C incubation with agitation for a second digest. The supernatant was centrifuged at 1000 rpm (200 RCF) for five minutes

at 4 °C. The supernatant was aspirated, and the pellet resuspended in 1 ml TypLE Express (ThermoFisher 12605010) with 1 µl 10 mg/ml DNAse. This was incubated at 37 °C with gentle agitation for 10 minutes before adding 10 ml mouse splitting medium to the digest. This was centrifuged at 1000 rpm (200 RCF) for five minutes at 4 °C.

The medium was aspirated, and the organoids resuspended in Matrigel and plated as described for organoid passage. Rho-kinase inhibitor was added to the mouse organoid feeding medium until it began to change colour, at which point it was replaced with medium without Rho-kinase inhibitor.

12.13.10 Passaging of mouse organoids

In advance of any organoid passage, mouse organoid feeding medium, mouse splitting medium were prepared as described previously. A hot water flask and 24 well plate were maintained at 37 °C, and plasticware for passage were pre-cooled as previously described. Matrigel was thawed on ice (1 ml takes 1-2 h), mouse complete organoid medium was warmed to 37 °C, and a 15 ml flacon tube of mouse splitting medium was cooled on ice.

The medium was aspirated from the organoids to be passaged, and 1 ml ice-cold mouse splitting medium was pipetted harshly with the pipette tip touching the base of the 24 well plate at a 45° angle 4-5 times onto each Matrigel dome to disrupt it. This was repeated to suspend all organoids to be passaged in mouse splitting medium, and up to 10 organoid domes were combined in a 15 ml tube of ice-cold mouse splitting medium. The organoids in splitting medium were centrifuged at 1500 rpm (250 RCF) for five minutes at 4 °C. The medium was aspirated slowly using a 10 ml pipette and changing to a P200 for the last few hundred µls. The organoid pellet was resuspended in 50 µl Matrigel® per new dome to be plated, keeping both the pellet and Matrigel® on ice throughout and being careful not to reduce bubbles. Keeping the organoids on ice, the culture plate was removed from the incubator and placed on a hot water flask in the hood. The organoids were gently pipetted up and down again without forming bubbles. 50 µl of the suspension was taken into the pipette, and the tip touched to the base of the 24 well plate. While lifting the pipette slowly upwards, the suspension was expelled, repeating until all of the organoids were plated. The 24 well plate was returned to an incubator at 37 °C on the hot water flask allowing the Matrigel to harden for 5-15 minutes.

500µl pre-warmed mouse organoid feeding medium was then added to each dome, pipetting gently down the outside edge of each well. Organoids were returned to the incubator for 2-4 days until medium changed colour, at which point it was replaced.

12.13.11 Freezing organoids

To freeze organoids, they were suspended in splitting medium and pelleted as described for passaging organoids. The medium was aspirated, removing the final ~200 µl with a P200 and resuspended in 500 µl recovery cell culture freezing medium (Corning 354253) per cryovial (1-3 domes per cryovial). The cryovials were labelled and frozen in a freezing chamber at -80 °C for 24 hours before transferring to liquid nitrogen.

12.13.12 Thawing organoids

Hot water flask, mouse splitting medium, mouse organoid feeding medium, Matrigel and plastics were prepared as described previously. The cryovial containing organoids was thawed rapidly in a 37 °C water bath. They were transferred to a 15 ml falcon tube of ice-cold mouse splitting medium and centrifuged at 1000 rpm (200 RCF) for five minutes at 4 °C. The medium was aspirated, carefully removing the last ~200 µl with a P200. The organoids were resuspended in Matrigel® (50 µl per dome, 1-3 domes per pellet depending on the size of pellet) and plated as described for organoid passage. Mouse organoid feeding medium was supplemented with Rho-kinase inhibitor for 2-4 days until organoids started to grow and the media began to change colour; at this point, the media was replaced with mouse organoid feeding medium without Rho-kinase inhibitor.

12.13.13 Generating single cells from organoid cultures

To generate single cells from organoids, a 2 mg/ml dispase solution was prepared in mouse splitting medium (weighing at least 20 mg dispase each time for accuracy). The dispase was dissolved and the solution filtered through a 0.2 µm filter. The medium was removed from the domes to be harvested and replaced with 500 µl dispase solution. Each Matrigel® dome was broken up by pipetting up and down with a P1000 before returning the plate to an incubator at 37 °C for 10 minutes. Up to eight wells of dispase/organoid suspension were combined in a 15 ml falcon tube, and the wells washed in a further 1 ml dispase solution which was added to the 15 ml tube. 1 µl 10 mg/ml DNAse solution was initially added to the tube; however, if DNA precipitation was noticed (cells clumping together in strings), this volume was increased as required. The solution was incubated at 37 °C for 10 minutes with agitation and then centrifuged at 1000 rpm (200 RCF) for 3 minutes at 4 °C. The supernatant was removed, leaving a small

amount to avoid losing the pellet, and replaced with 1 ml TrypLE Express before centrifuging again as before. The supernatant was removed, leaving a little to avoid losing the pellet, and 1-4 ml TrypLE Express was added dependent on pellet size (one for one or two domes, four for up to 12 domes) with 2 µl 10 mg/ml DNAse I stock per ml TrypLE Express. The solution was pipetted up and down 20 times to resuspend the cells and incubated at 37 °C with agitation for five minutes, then pipetted up and down 20 times again. If stringy clumps of cells were visible, 2-8 µl DNAse was added, and the solution mixed again by pipetting. The cells were checked under the microscope, and if they were all dissociated, they were centrifuged at 1000 rpm (200 RCF) for 3 minutes; if not, they were returned to 37 °C until dissociated, which took up to 35 minutes. Once centrifuged, the majority of the supernatant was removed, and the cells washed twice in 5 ml splitting medium, centrifuging and removing the majority of the supernatant at each wash.

12.13.14 Orthotopic transplant of organoids into the pancreas

To orthotopically implant organoids into the pancreas, a single cell suspension was performed on organoids from mixed background (C57bl6 / 129sv) animals. The cells were counted and resuspended in a mix of 50 % Matrigel®, 50 % mouse splitting medium at 250,000 cells per 40 µl. Animals were injected with organoids as detailed for orthotopic implant of TB32048 cells.

12.13.15 Plating organoids for biotherapeutics experiments

To plate organoids in a 96 well plate for therapeutics experiments, a clear 96 well culture plate was pre-cooled at -20 °C. A 50 % Matrigel®, 50 % PBS solution was made at 4 °C and 30 µl added to each well of the plate on ice. The plate was centrifuged at 200 RCF for 1 minute at 4 °C before incubating at 37C for 20 minutes to harden. A single-cell suspension of organoids was prepared and resuspended in 90 % mouse organoid feeding medium (with Y-27632 Rho kinase inhibitor) and 10 % Matrigel® to a final concentration of 20 cells/µl. 100µl (2000 cells) were plated into each well on top of the Matrigel® bed.

12.14 Statistical analysis

Results are presented as mean ± s.e.m unless otherwise stated, and n numbers are stated in figure legends. Unless otherwise stated, statistical analyses were performed in Graphpad Prism. For each dataset, outliers were excluded by robust regression and outlier removal (ROUT) with the false discovery rate, Q, set to 1 %, meaning that fewer

than 1 % of the values identified as 'statistically significant' (outliers) are false positives, the remaining values (over 99 %) are true outliers (Motulsky and Brown 2006). For bar charts, a Shapiro-Wilke normality test was performed on the datasets. For comparison of two datasets, both of which were normally distributed, a student's T-test was performed, and when either dataset was not, a Mann-Witney U test was performed. For comparison of three or more datasets with a single independent variable, a one-way ANOVA was performed with Tukey's multiple comparison if all datasets were normally distributed or Kruskal Wallis multiple comparisons if not all datasets were normally distributed. A two-way ANOVA was performed to compare three or more datasets with two independent variables.

For comparison of cytokines in the FAK-KD endothelial cell cytokine array, a chi-squared analysis was performed to compare the number of cytokines upregulated by more than 25 %, downregulated by more than 25 % or unchanged.

Statistical significance was reported as appropriate. $P < 0.05$ was considered statistically significant. The level of statistical significance was reported ns, $P > 0.05$, * $P \leq 0.05$, ** $P \leq 0.01$, *** $P \leq 0.001$ and **** $P \leq 0.0001$.

For tumour growth curves, data were analysed using the mixed model linear regression, with a random effect to take into account the fact that repeated observations on the same animal can be correlated with each other (Diggle et al. 2002). Tumour growth for all animals was analysed with the outcome variable as the logarithm of relative change in tumour volume from day 1. Similar results (not shown) also were observed when using the untransformed relative change, when using absolute volume or using the logarithm of absolute volume as the outcome variable. For each case, the results of significance tests were the same for all endpoints. This was the case whether analysis was restricted to animals with at least five days of observations or to animals with at least six days of observations. Regression coefficients were retransformed after analysis to be presented as average daily percentage increases.

Other statistical analyses are reported within the text.

12.15 Ethics

All procedures were approved by our local animal ethics committee at the Queen Mary University of London and were executed in accordance with UK Home Office regulations.

13 Results I: Targeting angiocrine signalling to enhance chemosensitivity

13.1 Endothelial cell FAK deletion sensitises subcutaneous B16-F0 melanomas to doxorubicin

Work from our laboratory previously demonstrated that loss of endothelial cell FAK in established B16F0 tumours did not affect angiogenesis but did enhance the sensitivity of tumour cells to doxorubicin, and this reduced tumour growth. Mechanistically loss of EC-FAK reduced doxorubicin-stimulated cytokine production, thus altering the angiocrine profile of ECs (Tavora, Reynolds, et al. 2014). Here I have determined the role of the kinase activity of EC-FAK specifically in doxorubicin-stimulated cytokine production and sensitivity to doxorubicin *in vivo*.

13.2 Deletion of EC-FAK reduces angiocrine response to doxorubicin

Our group has previously demonstrated a sensitising effect of endothelial cell FAK deletion on malignant cell growth *in vivo*. This corresponded with a reduced cytokine response to doxorubicin in FAK-KO cells *in vitro* compared to EC-WT cells. Therefore, we wanted to fully understand the molecular changes in endothelial cells in response to doxorubicin and how these are impacted by FAK deletion. In experiments performed by Dr Rita Pedrosa and Dr Pedro Casado, the proteomic, phosphoproteomic and secretomics changes in FAK KO vs WT EC treated or not with doxorubicin were compared. Primary lung ECs were isolated from *Pdgfb-iCre+;FAK$^{fl/fl}$* and *Pdgfb-iCre-;FAK$^{fl/fl}$* mice. Both genotypes of cells were treated with tamoxifen *in vitro* to activate Cre in the ECs derived from *Pdgfb-iCre+; FAK$^{fl/fl}$* mice but not in *Pdgfb-iCre-; FAK$^{fl/fl}$*, generating FAK KO and WT ECs, respectively **(Appendix Figure 22.1 A)**. FAK KO and WT ECs were treated for 48 hours with 250 nM doxorubicin or PBS before harvesting cell lysates for proteomics and phosphoproteomics and conditioned medium for secretomics **(Figure 13.1 A)**. At baseline (untreated cells), the expression of several proteins were altered by the FAK KO mutation, with the expression of more proteins downregulated than upregulated, affecting intrinsic processes such as cell proliferation **(Figure 13.1 B; Appendix Figure 22.1 B)**. Proteomic, phosphoproteomic and secretomics analysis revealed that the number of proteins with a significant change in expression after doxorubicin treatment was much greater in the EC-WT than EC-FAK KO condition for each analysis. For all three

analyses, the number of proteins with expression levels significantly changed by doxorubicin was at least four times greater in EC-WT than EC-FAK KO, with the number of upregulated secreted proteins changing from almost 100 to close to baseline levels in EC-WT cells **(Figure 13.1 C)**. Doxorubicin is a DNA damaging agent; therefore, it was unsurprising that there was an enrichment in DNA-damage repair phospho-proteins in doxorubicin treated WT ECs. However, this was seen to a much lesser extent in FAK KO ECs **(Appendix Figure 22.1 D).**

The secretome profiles of proteins from conditioned medium of WT and FAK-KO ECs showed significant changes in EC-WT cells treated with dox compared to PBS but not necessarily changed by doxorubicin treatment in EC-FAK KO cells **(Figure 13.1 D)**. Presentation of secretomics data in volcano plots further demonstrates that that doxorubicin treatment increases the expression of many secreted proteins in WT ECs, but their levels remain close to baseline in EC-FAK KO ECs **(Figure 13.1 E)**. This reduction in the response to doxorubicin was also seen, although to a lesser extent, in the phosphopeptides **(Appendix Figure 22.1 C).**

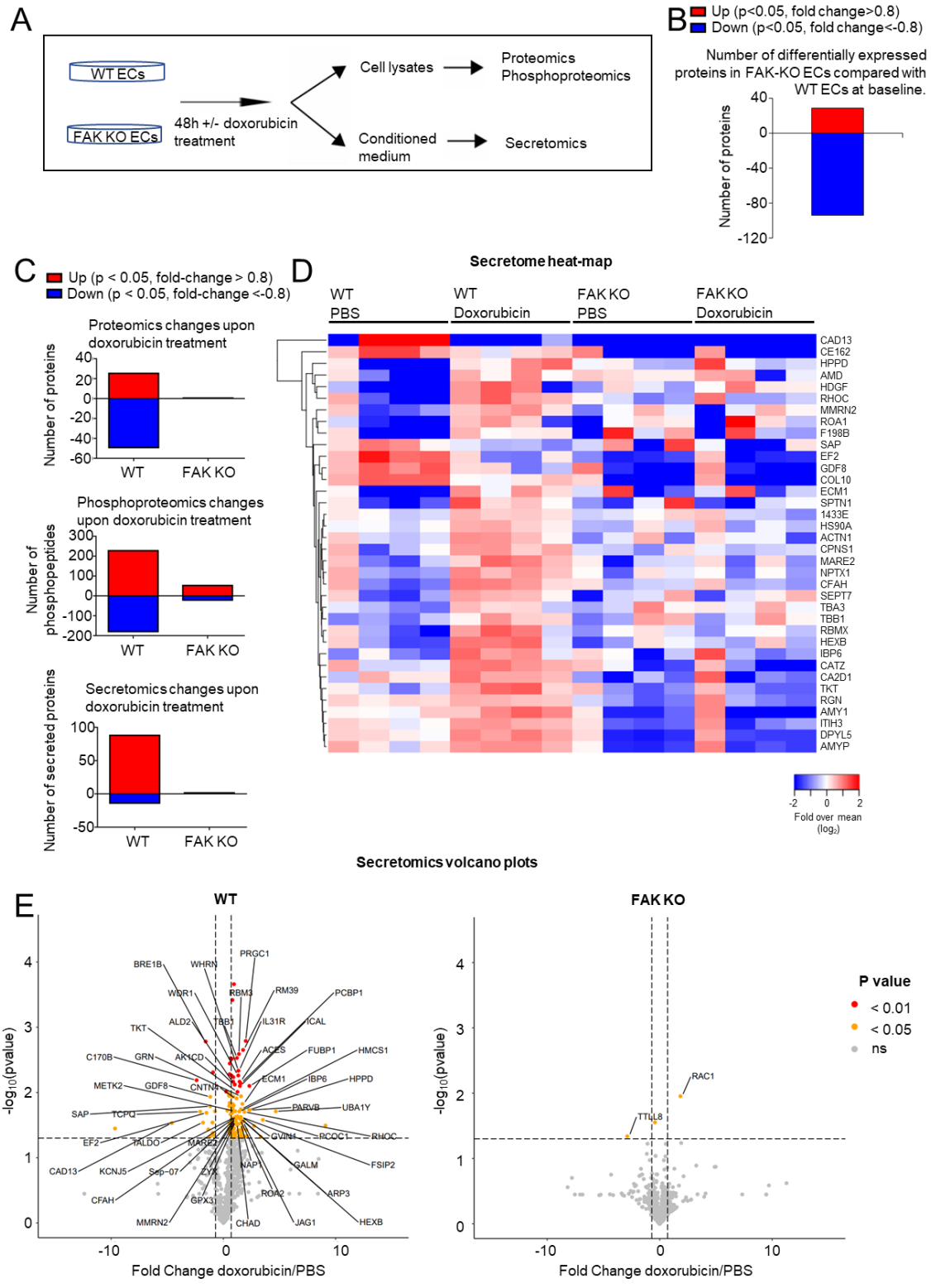
A
WT ECs
FAK KO ECs
48h +/- doxorubicin treatment
Cell lysates
Proteomics
Phosphoproteomics
Conditioned medium
Secretomics
B
Up (p<0.05, fold change>0.8)
Down (p<0.05, fold change<-0.8)
Number of differentially expressed proteins in FAK-KO ECs compared with WT ECs at baseline.
Number of proteins
C
Up (p < 0.05, fold-change > 0.8)
Down (p < 0.05, fold-change <-0.8)
Proteomics changes upon doxorubicin treatment
Number of proteins
Phosphoproteomics changes upon doxorubicin treatment
Number of phosphopeptides
Secretomics changes upon doxorubicin treatment
Number of secreted proteins
WT
FAK KO
D
Secretome heat-map
WT PBS
WT Doxorubicin
FAK KO PBS
FAK KO Doxorubicin
Fold over mean (log2)
Secretomics volcano plots
E
WT
FAK KO
-log10(pvalue)
Fold Change doxorubicin/PBS
P value
< 0.01
< 0.05
ns

Figure 13.1 Cellular protein, phosphoprotein and secreted protein analysis identify that doxorubicin treatment effects are reduced significantly in FAK-null endothelial cells.

(A) Experimental plan: WT and FAK-KO primary ECs were treated for 48 h with doxorubicin or PBS. Lysates from these cells were processed for proteomics and phosphoproteomics analysis and conditioned medium from the cells for secretomics analysis. (B) The numbers of cellular proteins that showed significant changes in expression in FAK-KO EC vs FAK-WT ECs were determined. Red bars, up-regulation and blue bars, down-regulation. (C) Numbers of cellular proteins, phosphopeptides or secreted proteins that showed significant changes in expression were identified in FAK-WT and FAK-KO ECs after doxorubicin treatment. Red bars, up-regulation and blue bars, down-regulation. (D) Heatmap: protein changes in the conditioned medium secretome of WT and FAK-KO ECs before and after doxorubicin treatment. Heatmap colour codes for fold change over mean across all samples in Log 2 scale. (E) Volcano plots illustrate secretomic changes caused by doxorubicin treatment in WT and FAK-KO ECs. Red dots, $p<0.01$, yellow dots, $p<0.05$ and grey circles non-significantly changed proteins. Independent biological replicates were performed (5 independent WT and 4 independent FAK-KO EC cell preparations),. All preparations were generated from 3 mice. For the secretomics study, 4 independent cell preps were used for WT and FAK-KO ECs and each prep was pooled from 3 mice. Data generated by Dr Rita Pedrosa and Dr Pedro Casado-Izquierdo.

13.3 *Pdgfb-iCre+;FAK$^{fl/fl}$;R26 FAK$^{K454R/K454R}$* mice can be induced by tamoxifen to express K454R mutant chicken FAK in endothelial cells rendering them kinase-dead

Our observation that deletion of endothelial cell FAK increases malignant cell sensitivity to doxorubicin could be useful clinically. However, FAK inhibition targets specific functions of FAK, most commonly the kinase domain. Therefore, it was important to establish whether the kinase domain of FAK is responsible for the sensitising property of endothelial cell FAK KO. We employed a tamoxifen-inducible endothelial cell FAK kinase-dead model (*Pdgfb-iCre;FAK$^{fl/fl}$;R26 FAK$^{K454R/K454R}$*) to establish the role of the kinase domain in this sensitising effect. As described in *Materials and Methods*, a K454R mutation renders FAK kinase-dead **(Figure 12.3 A)**. When Cre is activated by exogenous tamoxifen in *Pdgfb-iCre+;FAK$^{fl/fl}$;R26 FAK$^{K454R/K454R}$* animals, mouse FAK is deleted, and the kinase-dead chicken FAK is expressed, whereas in the Cre – animals, the mouse FAK remains expressed **(Figure 12.3 B)**.

13.4 Sequencing *Pdgfb-iCre+;FAK$^{fl/fl}$;R26 FAK$^{K454R/K454R}$* mouse DNA confirmed the presence of the K454R mutation

The *Pdgfb-iCre^{ert};FAK $^{fl/fl}$ R26 FAK $^{K454R/K454R}$* mouse DNA was also sequenced to confirm that the kinase domain is disabled by mutation of the ATP binding site in lysine (AAA) position 454 to arginine (AGA) (K454R) **(Figure 13.2)**. The mutation was confirmed in all *Pdgfb-iCre^{ert};FAK $^{fl/fl}$ R26 FAK $^{K454R/K454R}$* mice **(Figure 13.2 A)**. The sequencing chromatogram shows some background, but the true peaks are still clear **(Figure 13.2 B)**.

A

```
Query         ------------------------------------------------------------
Sbjct  961    GCTGGTGCACCTGAGCCTCTGACAGTGACAGCACCATCCTTAACCATTGCAGAGAATATG  1020
Query  6      ----------------GATACTGCCGACTGGTGAATGGAGCCACGCAATCTTTTATTATC  49
                              ||||||||||||||||||||||||||||||||||||||||||||
Sbjct  1021   GCTGACTTGATAGACGGATACTGCCGACTGGTGAATGGAGCCACGCAATCTTTTATTATC  1080
Query  50     AGGCCACAGAAAGAAGGTGAAAGAGCTTTACCATCAATACCAAAGCTGGCCAACAATGAG  109
              ||||||||||||||||||||||||||||||||||||||||||||||||||||||||||||
Sbjct  1081   AGGCCACAGAAAGAAGGTGAAAGAGCTTTACCATCAATACCAAAGCTGGCCAACAATGAG  1140
Query  110    AAGCAAGGAGTAAGGTCGCACACAGTCTCTGTATCAGAAACAGATGACTATGCAGAGATA  169
              ||||||||||||||||||||||||||||||||||||||||||||||||||||||||||||
Sbjct  1141   AAGCAAGGAGTAAGGTCGCACACAGTCTCTGTATCAGAAACAGATGACTATGCAGAGATA  1200
Query  170    ATAGATGAAGAAGATACTTATACAATGCCATCAACCAGAGATTATGAAATTCAAAGGGAG  229
              ||||||||||||||||||||||||||||||||||||||||||||||||||||||||||||
Sbjct  1201   ATAGATGAAGAAGATACTTATACAATGCCATCAACCAGAGATTATGAAATTCAAAGGGAG  1260
Query  230    AGAATTGAACTGGGGCGCTGCATTGGTGAAGGACAGTTTGGAGATGTGCACCAAGGAATT  289
              ||||||||||||||||||||||||||||||||||||||||||||||||||||||||||||
Sbjct  1261   AGAATTGAACTGGGGCGCTGCATTGGTGAAGGACAGTTTGGAGATGTGCACCAAGGAATT  1320
Query  290    TACATGAGTCCGGAAAATCCAGCTATGGCTGTAGCAATCAGAACATGTAAAAACTGCACC  349
              |||||||||||||||||||||||||||||||||||| ||||||||||||||||||||||
Sbjct  1321   TACATGAGTCCGGAAAATCCAGCTATGGCTGTAGCAATCAAAACATGTAAAAACTGCACC  1380
Query  350    TCAGACAGCGTTAGAGAAAAGTTCCTACAAGAAGCCTTAACAATGCGTCAGTTTGATCAT  409
              ||||||||||||||||||||||||||||||||||||||||||||||||||||||||||||
Sbjct  1381   TCAGACAGCGTTAGAGAAAAGTTCCTACAAGAAGCCTTAACAATGCGTCAGTTTGATCAT  1440
Query  410    CCTCACATTGTGAAGCTCATTGGAGTTATTACAGAAAACCCAGTGTGGATAATCATGGAG  469
              ||||||||||||||||||||||||||||||||||||||||||||||||||||||||||||
Sbjct  1441   CCTCACATTGTGAAGCTCATTGGAGTTATTACAGAAAACCCAGTGTGGATAATCATGGAG  1500
Query  470    CTCTGTACACTTGGAGAGTTGAGATCGTTTCTGCAAGTAAGAAAATTCAGCTTGGACCTG  529
              ||||||||||||||||||||||||||||||||||||||||||||||||||||||||||||
Sbjct  1501   CTCTGTACACTTGGAGAGTTGAGATCGTTTCTGCAAGTAAGAAAATTCAGCTTGGACCTG  1560
Query  530    GCCTCCCTCATCCTCTACGCTTACCAGCTTAGCACAGCACTTGCTTACCTAGAGAGCAAA  589
              ||||||||||||||||||||||||||||||||||||||||||||||||||||||||||||
Sbjct  1561   GCCTCCCTCATCCTCTACGCTTACCAGCTTAGCACAGCACTTGCTTACCTAGAGAGCAAA  1620
Query  590    AGATTTGTACATAGAGATATTGCTGCTAGGAACGTGCTGGTATCTGCCACTGACTGTGTG  649
              ||||||||||||||||||||||||||||||||||||||||||||||||||||||||||||
Sbjct  1621   AGATTTGTACATAGAGATATTGCTGCTAGGAACGTGCTGGTATCTGCCACTGACTGTGTG  1680
Query  650    AAATTGGGTGACTTTGGCTTATCCCGATACATGGAAGACAGTACTTACTATAAAGCTTCC  709
              ||||||||||||||||||||||||||||||||||||||||||||||||||||||||||||
Sbjct  1681   AAATTGGGTGACTTTGGCTTATCCCGATACATGGAAGACAGTACTTACTATAAAGCTTCC  1740
Query  710    AAAGGAAAGTTACCTATCAAATGGATGGCTCCAGAGTCAATCAACTTCCGACGGTTTACC  769
              ||||||||||||||||||||||||||||||||||||||||||||||||||||||||||||
Sbjct  1741   AAAGGAAAGTTACCTATCAAATGGATGGCTCCAGAGTCAATCAACTTCCGACGGTTTACC  1800
Query  770    TCAGCAAGCGATGTGTGGATGTTTGGTGTGTGTATGTG----------------------  807
              ||||||||||||||||||||||||||||||||||||||
Sbjct  1801   TCAGCAAGCGATGTGTGGATGTTTGGTGTGTGTATGTGGGAGATCCTGATGCATGGGGTA  1860
Query         ------------------------------------------------------------
```

Mutant

WT

B

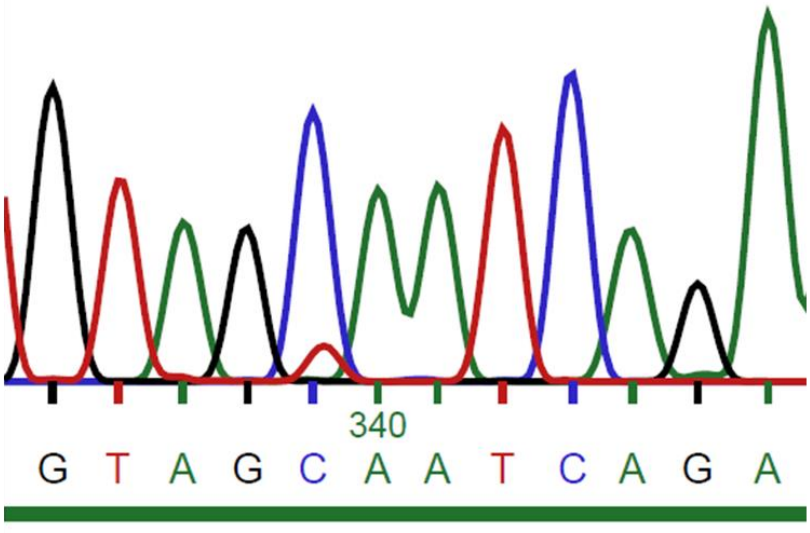

Figure 13.2 EC Cre;FAK$^{KD/KD}$ mouse sequencing confirmed K454R mutation in all mice

Sanger sequencing result of *Pdgfb-iCre^{ert};FAK$^{fl/fl}$;R26FAK$^{K454R/K454R}$* mice confirming mutation of the ATP binding site lysine (AAA) position 454 to arginine (AGA) (K454R). (A) Typical sequencing result aligned to a WT murine FAK sequence indicating the K454R mutation (red box). (B) Sequencing chromatogram showing the K454R mutation in a typical *Pdgfb-iCre^{ert};FAK$^{fl/fl}$;R26FAK$^{K454R/K454R}$* mouse.

13.5 Myc-Tag was expressed in *EC Cre+; FAK$^{KD/KD}$* mice but not *EC Cre-; FAK$^{KD/KD}$* mice *in vivo* and *in vitro*, EC-FAK KD MLECs expressed increased chicken FAK and reduced mouse FAK compared to EC-WT

The K454R FAK kinase-dead mutation is myc-tagged. This is a mutant form of myc that is not detectable endogenously. Therefore, to confirm that tamoxifen activation was successful *in vivo,* and the animals were true *EC Cre+; FAK$^{KD/KD}$* and *EC Cre-; FAK$^{KD/KD}$*, tumour sections from both genotypes were immunostained for myc-tag. *Cre+; FAK$^{KD/KD}$* mice were myc-tag positive whilst *EC Cre-; FAK$^{KD/KD}$* were myc negative **(Figure 13.3 A)**. *In vitro*, knockin of mutant chicken FAK and knockout of mouse FAK specific to the endothelial cells was tested by qPCR. Endothelial cells and all other non-selected non-endothelial cells were isolated from the lungs of *EC Cre+; FAK$^{KD/KD}$* and *EC Cre-; FAK$^{KD/KD}$* mice. The levels of mouse and chicken FAK from endothelial cells and non-endothelial cells from both *EC Cre+; FAK$^{KD/KD}$* and *EC Cre-; FAK$^{KD/KD}$* mice were measured by qPCR. The relative quantity of mRNA was plotted relative to the level EC *Cre*- endothelial cells. There was no significant difference in mouse FAK levels mRNA in non-endothelial cell populations from both genotypes. However, in the endothelial cells, there was significantly reduced levels of mouse FAK and increased chicken FAK in *Cre* + EC **(Figure 13.3 B)**.

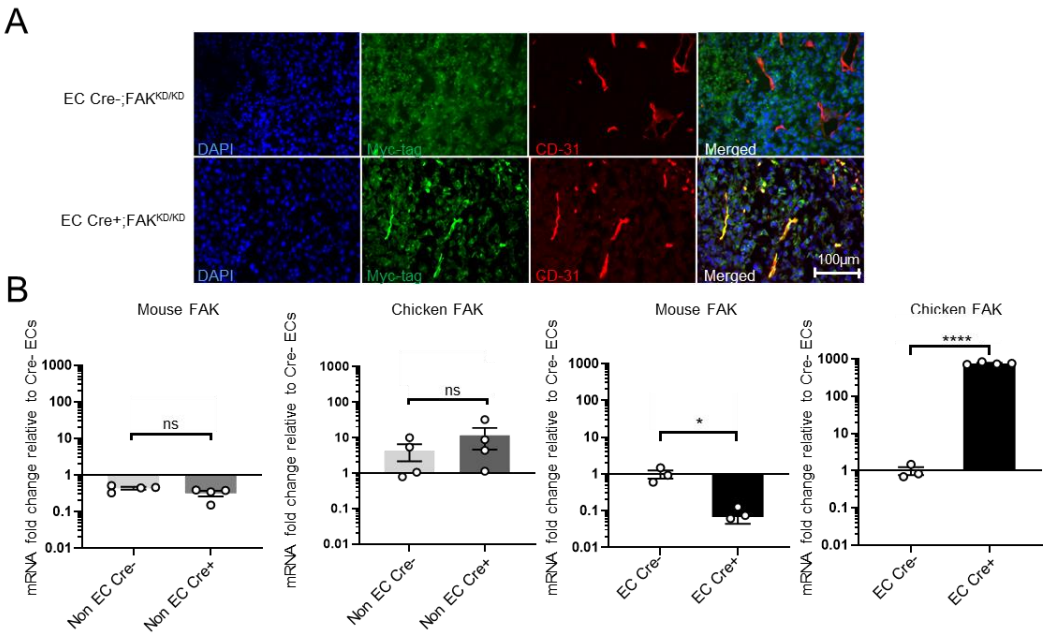

Figure 13.3 Activation of the EC FAK KD mutation

(A) Myc-tag is only detected in ECs found in tumours grown in EC Cre+; $FAK^{KD/KD}$ mice but not ECs in tumours grown in EC Cre-; $FAK^{KD/KD;}$ Myc-tag (green) and CD-31 (red). Data are analysed with a one-way ANOVA. ns, not significant. Scale bar, 100 µm. (B) RT-qPCR showing the level of mouse and chicken FAK mRNA in EC Cre + and EC Cre – cells as well as cells that were not sorted as EC. N=4 independent cell preps per genotype, each cell prep was from a single mouse.

13.6 The Endothelial-cell FAK kinase-dead mutation modestly sensitises cancer cells to doxorubicin *in vivo*.

Endothelial cell FAK KO sensitises tumours to doxorubicin *in vivo* to reduce tumour growth (Tavora, Reynolds, et al. 2014). Therefore, tumour growth curves were created to establish whether endothelial cell FAK kinase dead mutation had the same impact or not. *EC Cre+; FAK$^{KD/KD}$* and *EC Cre-; FAK$^{KD/KD}$ mice* were implanted subcutaneously with 1 X 10^6 B16F0 melanoma cells. When tumours reached, 100 mm^3 mice began treatment as shown **(Figure 13.4 A)**. Animals were culled ten days after the start of treatment or earlier if tumours reached the size limit or ulcerated or mice showed signs of signs of distress, according to the humane endpoint established in our animal project license. In PBS treated animals, tumour growth curves were similar for *EC Cre+; FAK$^{KD/KD}$* and *EC Cre-; FAK$^{KD/KD}$* animals **(Figure 13.4 B; represented as fold change in appendix Figure 22.2)**. In the doxorubicin treated animals, however, in the raw tumour growth curves, there appeared to be subtly reduced tumour growth in the *EC Cre+; FAK$^{KD/KD}$* compared to *EC Cre-; FAK$^{KD/KD}$* animals **(Figure 13.4 C; represented as fold change in appendix Figure 22.2)**. As the animals were culled at different time points, statistical comparison by ANOVA was not possible. However, the percentage of tumours that exceeded the mean volume for PBS treated *EC Cre-; FAK$^{KD/KD}$* (571mm^3, orange line) was lower in doxorubicin treated *EC Cre+; FAK$^{KD/KD}$* (56 %) than the other treatment groups (100 %, 100 %, 77 % for PBS treated *EC Cre-; FAK$^{KD/KD}$* and *EC Cre+; FAK$^{KD/KD}$* and doxorubicin treated *EC Cre-; FAK$^{KD/KD}$* respectively suggesting a reduction in tumour growth in the doxorubicin treated *EC Cre+; FAK$^{KD/KD}$*.

The exponential slope of each individual tumour growth curve was calculated, and the percentage change in exponential slope with doxorubicin treatment relative to the average exponential slope for doxorubicin treated animals were plotted for each genotype. This showed that in the *EC Cre+; FAK$^{KD/KD}$* animals, there was significantly more reduction in exponential tumour growth with doxorubicin treatment than in the *EC Cre+; FAK$^{KD/KD}$* animals demonstrating a sensitisation to doxorubicin in the *EC Cre+; FAK$^{KD/KD}$* animals **(Figure 13.4 D).**

Finally, the data tumour growth curves were analysed by mixed-model linear regression as described in materials and methods. The change in tumour volume, as expected, increased significantly with time ($p<0.001$). Additionally, the rate of change in tumour volume (gradient of the increase) was significantly altered by treatment and genotype

($p<0.001$). The highest gradient was observed in PBS treated *EC Cre-; FAK$^{KD/KD}$* mice, and the lowest gradient in doxorubicin treated *EC Cre+; FAK$^{KD/KD}$* mice. **Figure 13.4 F** shows the estimated daily percentage increases in tumour volume and their 95 % confidence intervals for the four groups. Although the tumour growth in both *EC Cre+; FAK$^{KD/KD}$* and *EC Cre-; FAK$^{KD/KD}$* mice was reduced by doxorubicin treatment compared to PBS, there was no difference in tumour growth between genotypes with PBS treatment, but with doxorubicin treatment, tumour growth in *EC Cre+; FAK$^{KD/KD}$* mice was significantly less than in *EC Cre-; FAK$^{KD/KD}$* mice. This further confirmed the sensitisation to doxorubicin in *EC Cre+; FAK$^{KD/KD}$* mice and confirmed that the kinase domain of FAK is involved in the chemosensitisation effect of endothelial cell FAK targeting observed by (Tavora, Reynolds, et al. 2014).

No difference in percentage survival to legal tumour limit was observed between the treatment groups **(Figure 13.5)**.

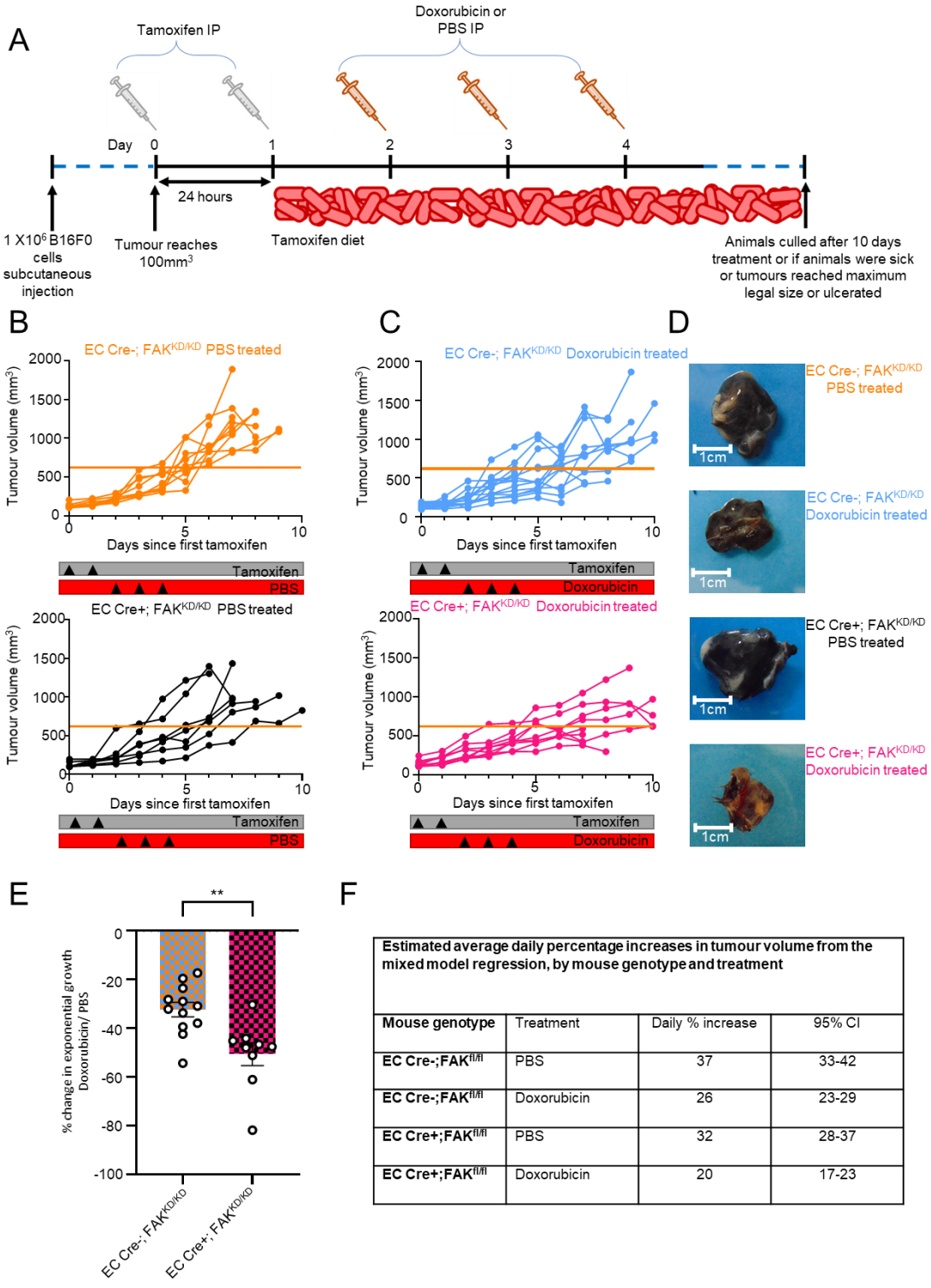

F

Estimated average daily percentage increases in tumour volume from the mixed model regression, by mouse genotype and treatment

Mouse genotype	Treatment	Daily % increase	95% CI
EC Cre-;FAK$^{fl/fl}$	PBS	37	33-42
EC Cre-;FAK$^{fl/fl}$	Doxorubicin	26	23-29
EC Cre+;FAK$^{fl/fl}$	PBS	32	28-37
EC Cre+;FAK$^{fl/fl}$	Doxorubicin	20	17-23

Figure 13.4 Tumour growth curves

(A) Schematic of experimental design and dosing schedule. (B and C) Tumour growth curves in PBs or doxorubicin treated EC Cre-; $FAK^{KD/KD}$ and EC Cre+; $FAK^{KD/KD}$ mice. Bars represent treatment timelines. Orange horizontal line indicates the mean tumour volume in PBS treated EC Cre-; $FAK^{KD/KD}$ mice. (D) Representative images of tumours at 4 days after the final PBS or doxorubicin injection. (E) The exponential tumour growth of PBS and Doxorubicin treated EC Cre-; $FAK^{KD/KD}$ and EC Cre+; $FAK^{KD/KD}$ mice. Exponential slope of the tumour growth curves analysed with students t-test. **P ≤ 0.01. The numbers of mice recruited to the experiment were 11, 10, 11 and 11 mice with one tumour per animal for EC Cre-; $FAK^{KD/KD}$ PBS treated, EC Cre+; $FAK^{KD/KD}$ PBS treated, EC Cre-; $FAK^{KD/KD}$ doxorubicin treated and EC Cre+; $FAK^{KD/KD}$ doxorubicin treated respectively. However, mice that did not complete the treatment or survived at least one day post treatment were excluded from the exponential slope analysis, n=9, 8, 7 or 6 mice each with one tumour for EC Cre-; $FAK^{KD/KD}$ PBS treated, EC Cre+; $FAK^{KD/KD}$ PBS treated, EC Cre-; $FAK^{KD/KD}$ doxorubicin treated and EC Cre+; $FAK^{KD/KD}$ doxorubicin treated respectively. (F) Estimated average daily percentage increases in tumour volume from the mixed model regression, by mouse type and treatment showing percentage the daily increase and 95 % confidence limits. Average daily increase in tumour volume. Data were analysed by mixed model linear regression, with a random effect for animal, to take into account the fact that repeated observations on the same animal can be correlated with each other (Diggle et al. 2002). Average daily increase in tumour volume was significantly lower in doxorubicin-treated EC Cre+; $FAK^{KD/KD}$ compared with doxorubicin treated EC Cre-; $FAK^{KD/KD}$ mice. P<0.001

13.7 Survival to 10 days was not impacted by genotype or treatment

The majority of the animals became sick, had to be culled due to ulcerated tumours or as tumours had reached the home office legal limit according to our licence. There was, however, no difference in animal survival up to 10 days between the treatment groups **(Figure 13.5)**. This is not surprising for such a short time course of treatment and the limitations of the experimental model.

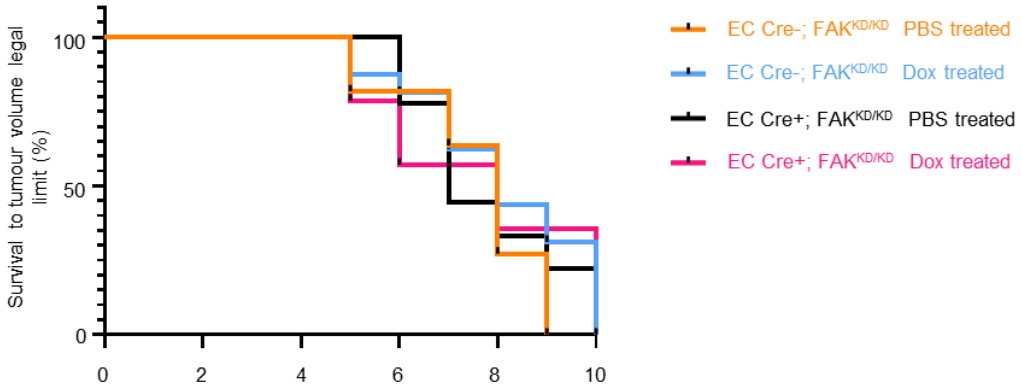

Figure 13.5 Kaplan Meier curve of percentage survival to maximum legal tumour volume limit in each treatment group over time showing no significant differences.

Log-rank (Mantel-Cox) test (P=0.3916). N=11, 7, 13 and 11 for EC Cre-; $FAK^{KD/KD}$ PBS treated, EC Cre+; $FAK^{KD/KD}$ PBS treated, EC Cre-; $FAK^{KD/KD}$ doxorubicin treated and EC Cre+; $FAK^{KD/KD}$ doxorubicin treated respectively.

13.8 Blood vessel density, perfusion and doxorubicin delivery are not impacted by activation of the endothelial cell FAK KD mutation

To ascertain the reason for increased doxorubicin sensitivity in *EC Cre+; FAK$^{KD/KD}$* compared to *EC Cre-; FAK$^{KD/K}$* mice, blood vessel density, perfusion and doxorubicin delivery were quantified. For analysis of blood vessel density, sections were stained for endomucin **(Figure 13.6 A),** and the numbers of blood vessels/mm^2 tumour section were calculated. There was no difference in blood vessel density between any of the treatment groups, implying the tumour growth phenotype was not a result of any changes in angiogenesis between the genotypes. However, more important than blood vessel density is perfusion; for a tumour cell to proliferate, it must be close enough to a perfused blood vessel for the diffusion of nutrients and oxygen, but many tumour blood vessels are poorly perfused (Forster et al. 2017). To check whether there were differences in blood vessel perfusion, mice were perfused with biotinylated lectin. There were no differences in blood vessel perfusion between the groups **(Figure 13.6 B)**. Therefore, any differences in sensitivity to doxorubicin are unlikely to be due to any differences in blood vessel development.

In addition, to check whether there were any differences in drug delivery by the blood vessels, doxorubicin delivery to the tumour was measured. We exploited the auto-fluorescent property of doxorubicin to measure doxorubicin delivery into the tumour with a high dose injection in an ante-mortem procedure. Doxorubicin is auto-fluorescent with emission signal at 595 nm upon excitation with a 470 nm laser and is therefore visible in green down a fluorescent microscope (Shah et al. 2017). Tumour sections from *EC Cre+; FAK$^{KD/KD}$* and *EC Cre-; FAK$^{KD/KD}$* mice showed similar intensity of doxorubicin autofluorescence, showing that doxorubicin delivery was the same. Therefore, differences in doxorubicin delivery were not likely to be the cause of reduced tumour growth in doxorubicin treated *EC Cre+; FAK$^{KD/KD}$* mice **(Figure 13.6 C)**.

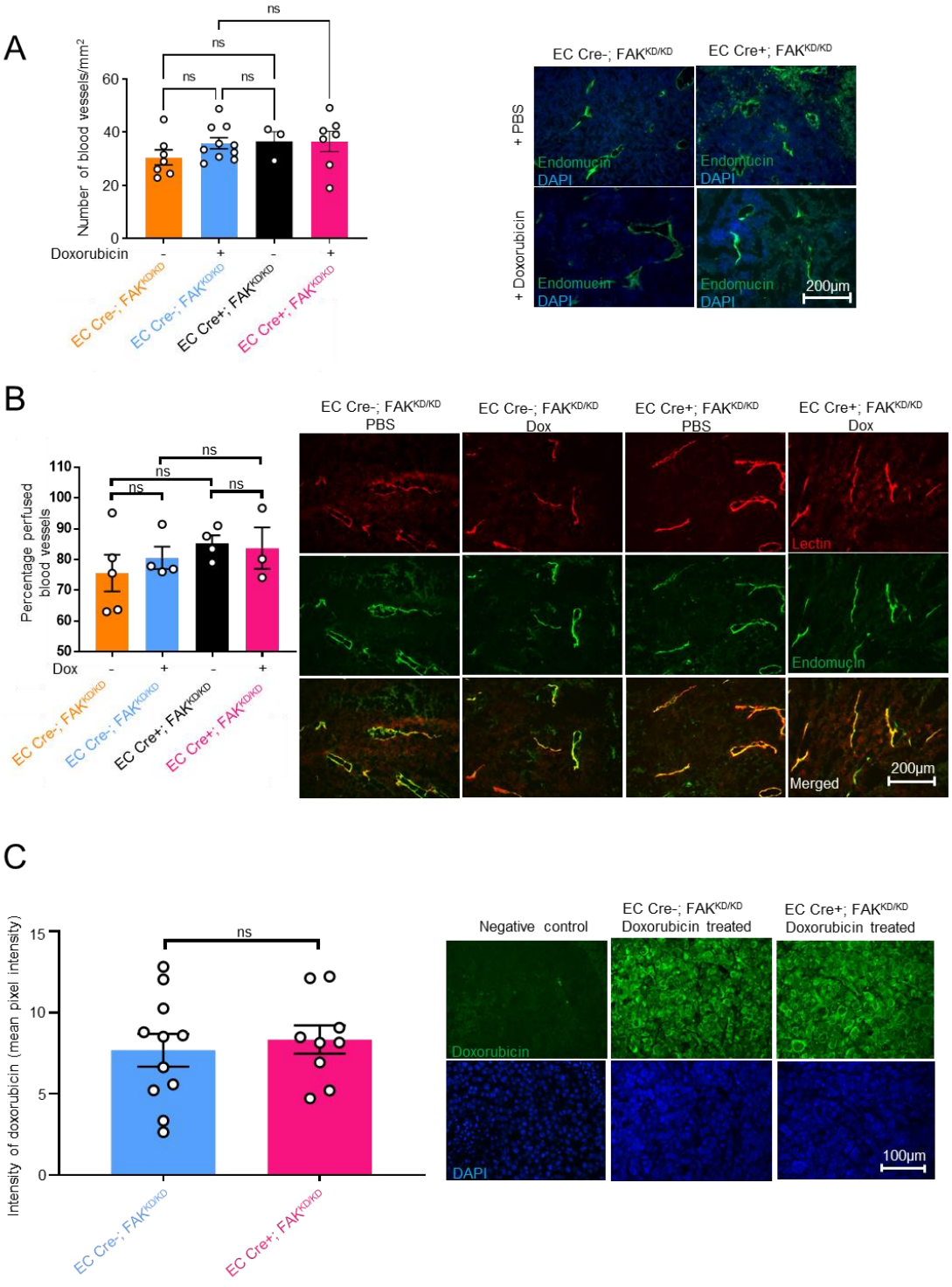
A
Number of blood vessels/mm²
ns
Doxorubicin
EC Cre-; FAKKD/KD
EC Cre-; FAKKD/KD
EC Cre+; FAKKD/KD
EC Cre+; FAKKD/KD
EC Cre-; FAKKD/KD
EC Cre+; FAKKD/KD
+ PBS
+ Doxorubicin
Endomucin
DAPI
200µm
B
Percentage perfused blood vessels
Dox
EC Cre-; FAKKD/KD PBS
EC Cre-; FAKKD/KD Dox
EC Cre+; FAKKD/KD PBS
EC Cre+; FAKKD/KD Dox
Lectin
Endomucin
Merged
200µm
C
Intensity of doxorubicin (mean pixel intensity)
Negative control
EC Cre-; FAKKD/KD Doxorubicin treated
EC Cre+; FAKKD/KD Doxorubicin treated
Doxorubicin
DAPI
100µm

Figure 13.6 Blood vessel density, perfusion and doxorubicin delivery were not affected by deletion of the kinase domain of FAK.

B16F0 tumour sections from EC Cre+; FAK$^{KD/KD}$ and EC Cre-; FAK $^{KD/KD}$ mice treated with doxorubicin or PBS. (A) Blood vessel density. Bar chart shows mean number of blood vessels per mm^2 ± s.e.m, n= 7, 5, 4 and 3 tumours from independent mice for EC Cre-; FAK $^{KD/KD}$ PBS treated, EC Cre-; FAK $^{KD/KD}$ doxorubicin treated, EC Cre+; FAK $^{KD/KD}$ PBS treated, and EC Cre+; FAK $^{KD/KD}$ doxorubicin treated respectively, for each tumour, 10 fields from 1 section were quantified. Images show representative fields of endomucin staining (green) with DAPI as a nuclear marker. (B) Blood vessel perfusion. Bar chart shows the percentage perfused blood vessels ± s.e.m, n= 7, 5, 4 and 3 tumours from independent mice reduced to n= 5, 4, 4 and 3 after exclusion of outliers by ROUT, Q=1 % for EC Cre-; FAK $^{KD/KD}$ PBS treated, EC Cre-; FAK $^{KD/KD}$ doxorubicin treated, EC Cre+; FAK $^{KD/KD}$ PBS treated, and EC Cre+; FAK $^{KD/KD}$ doxorubicin treated respectively. For each tumour, 10 fields from 1 section were quantified. Images show representative fields of lectin (red) and endomucin (green). (C) Doxorubicin delivery. Bar chart shows mean percentage of tumour area positive for doxorubicin delivery ± s.e.m. n = 11 tumours from independent mice, EC Cre-; FAK $^{KD/KD}$ and 9 tumours for EC Cre+; FAK $^{KD/KD}$, for each tumour, 15 fields from 1 section were quantified. Representative images of auto-fluorescent doxorubicin are given, white line shows positive area. NS, not significant (P > 0.05) analysed with a student's t-test. Scale bar in A and B 200 µm, C, 100 µm.

13.9 48 hours after the final treatment, Perivascular cellular proliferation is reduced and apoptosis and DNA damage increased in doxorubicin-treated *EC Cre+; FAK$^{KD/KD}$* subcutaneous B16F0 melanomas

To check whether there were any differences in perivascular proliferation, apoptosis or perivascular DNA damage, immunostaining was performed on tumours harvested 48 hours after the last treatment. *EC Cre+; FAK$^{KD/KD}$* and *EC Cre-; FAK$^{KD/KD}$* were injected subcutaneously with 5 X 10^5 B16F0 melanoma cells. They were treated as for tumour growth curves but harvested 48 hours after the final PBS or doxorubicin treatment **(Figure 13.7 A)**.

Sections from tumours that had been treated with PBS or doxorubicin 48h before harvest were stained for Ki-67, an indicator of proliferation. There was a significant reduction in Ki-67 expression between PBS and doxorubicin treated *EC Cre+; FAK$^{KD/KD}$* mice. Therefore, although there are no changes in doxorubicin delivery, blood vessel density or perfusion, there is significantly less proliferation in doxorubicin treated than PBS treated *EC Cre+; FAK$^{KD/KD}$* mice **(Figure 13.7 B)**. In the *EC Cre-; FAK$^{KD/KD}$* mice, however, there was no difference in proliferation with doxorubicin treatment.

Sections from this experiment were also stained for CC3, a marker for apoptosis and the CC3 positive area per blood vessel number was quantified. Apoptosis per blood vessel was significantly increased in doxorubicin treated *EC Cre+; FAK$^{KD/KD}$* mice compared to either doxorubicin treated *EC Cre-; FAK$^{KD/KD}$* mice or PBS treated *EC Cre-; FAK$^{KD/KD}$* mice. In *EC Cre-; FAK$^{KD/KD}$* animals, however, there was no difference in the level of apoptosis with doxorubicin treatment compared to PBS **(Figure 13.7 C)**.

Similarly, 48 hours after the last treatment, there were no differences in the level of perivascular DNA damage (indicated by nuclear γH2AX) between *EC Cre-; FAK$^{KD/KD}$* and *EC Cre+; FAK$^{KD/KD}$* mice treated with PBS. In doxorubicin treated animals. However, there was an increase in DNA damage in *EC Cre+; FAK$^{KD/KD}$* mice treatment compared to *EC Cre-; FAK$^{KD/KD}$* mice **(Figure 13.7 D)**.

Taken together, these data suggest that without treatment, tumours in *EC Cre+; FAK$^{KD/KD}$* and *EC Cre-; FAK$^{KD/KD}$* mice have similar levels of proliferation, apoptosis, and DNA damage. In doxorubicin treated animals, however, while the *EC Cre-; FAK$^{KD/KD}$* mice have

little response, *EC Cre+; FAK$^{KD/KD}$* mice are sensitised to the treatment showing reduced proliferation and increased levels of apoptosis and DNA damage.

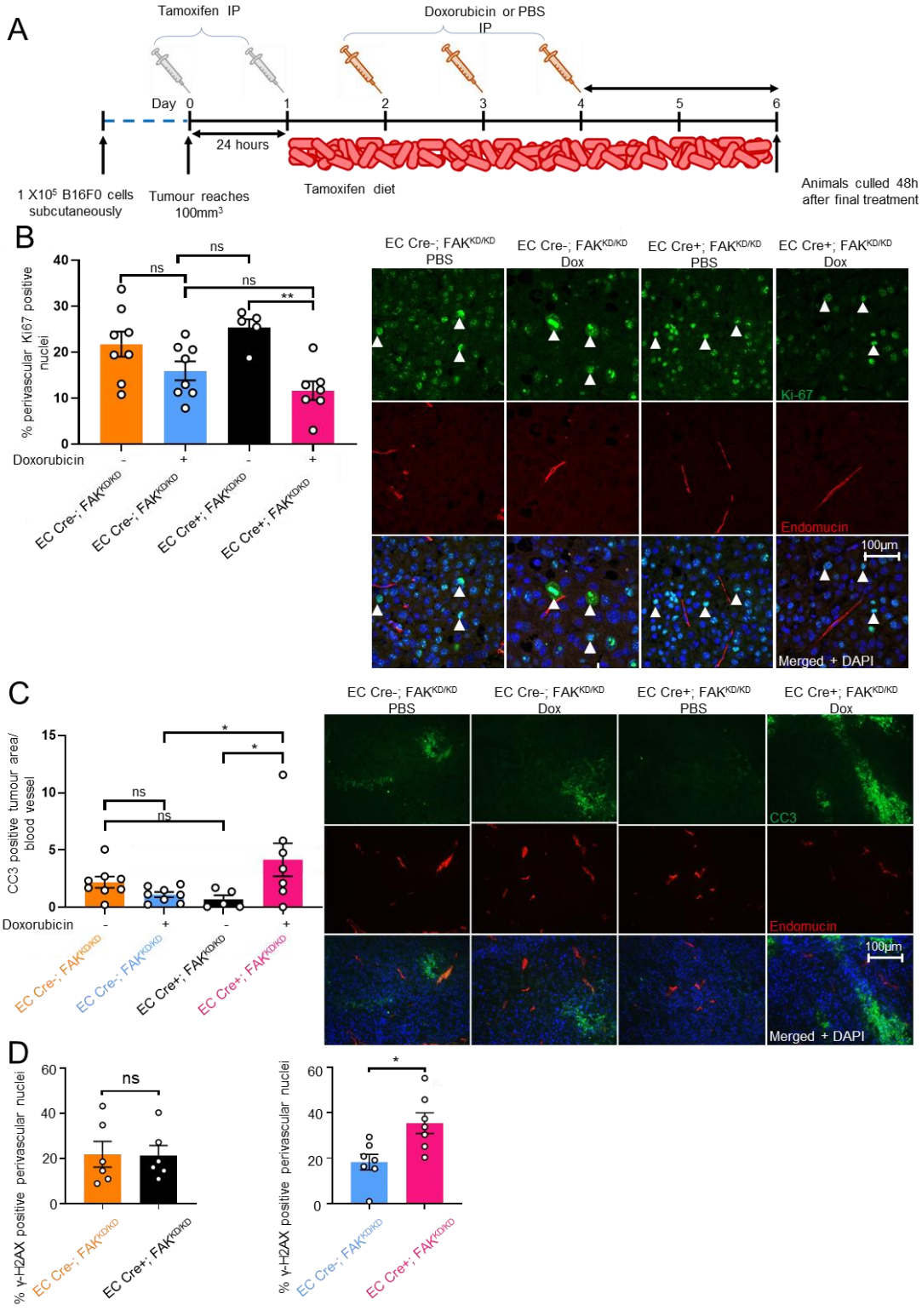
A
Tamoxifen IP
Doxorubicin or PBS IP
Day 0
1
2
3
4
5
6
24 hours
1 X10⁵ B16F0 cells subcutaneously
Tumour reaches 100mm³
Tamoxifen diet
Animals culled 48h after final treatment
B
% perivascular Ki67 positive nuclei
ns
**
Doxorubicin
EC Cre-; FAKKD/KD
EC Cre+; FAKKD/KD
Ki-67
Endomucin
100µm
Merged + DAPI
C
CC3 positive tumour area/ blood vessel
*
CC3
D
% γ-H2AX positive perivascular nuclei

Figure 13.7 Targeting the kinase domain of endothelial-cell FAK sensitises tumour cells to DNA damaging therapy *in vivo*.

B16F0 tumour sections from EC Cre+; $FAK^{KD/KD}$ and EC Cre-; $FAK^{KD/KD}$ mice treated with doxorubicin or PBS. (A) The percentage of perivascular tumour cells that were Ki-67-positive. N= 8, 8, 5 and 7 tumours from independent mice for EC Cre-; $FAK^{KD/KD}$ PBS treated, EC Cre-; $FAK^{KD/KD}$ doxorubicin treated, EC Cre+; $FAK^{KD/KD}$ PBS treated, and EC Cre+; $FAK^{KD/KD}$ doxorubicin treated respectively. 1 tumour per mouse, 15 fields were quantified from one section per animal. Representative images of staining for Ki-67, endomucin and DAPI as a nuclear marker. (B) Tumour apoptosis was assessed as the area of CC3 staining relative to the number of blood vessels. N numbers were 8, 8, 6 (reduced to 5 by exclusion of outliers ROUT, Q=1 %) and 7 for EC Cre-; $FAK^{KD/KD}$ PBS treated, EC Cre-; $FAK^{KD/KD}$ doxorubicin treated, EC Cre+; $FAK^{KD/KD}$ PBS treated, and EC Cre+; $FAK^{KD/KD}$ doxorubicin treated respectively. 1 tumour per mouse, 15 fields were quantified from one section per animal. Representative images of staining for CC3, endomucin and DAPI as a nuclear marker. (C) DNA damage was assessed as the % of H2A histone family member X (γ-H2AX positive nuclei. N=6, 8 (reduced to 7 by exclusion of outliers by ROUT, Q=1 %), 6 and 7 for EC Cre-; $FAK^{KD/KD}$ PBS treated, EC Cre-; $FAK^{KD/KD}$ doxorubicin treated, EC Cre+; $FAK^{KD/KD}$ PBS treated, and EC Cre+; $FAK^{KD/KD}$ doxorubicin treated respectively. 1 tumour per mouse, 15 fields were quantified from one section per animal. Representative images of staining for γ-H2AX, endomucin and DAPI as a nuclear marker. Bar charts show quantitation of sections taken 48 h post cessation of treatment. (A and B) Data are analysed with a one-way ANOVA. ns, not significant ($P > 0.05$), *$P < 0.05$ **$P \leq 0.01$. (C) Analysed with a student's t-test *$P < 0.05$ Scale bar, 100 µm.

13.10 Knockin of the FAK kinase-dead mutation in ECs leads to a reduction in cytokine production in response to doxorubicin

Cytokine production by endothelial cells is known to influence tumour growth (Balkwill 2009; Edwardson, Parissenti, and Kovala 2019; Galdiero, Marone, and Mantovani 2018; Aliper et al. 2014; He et al. 2010). Tavora et al. (Tavora, Reynolds, et al. 2014) showed that cytokine production of WT endothelial cells was increased by doxorubicin treatment, while in FAK-null endothelial cells, this response was much reduced (Tavora, Reynolds, et al. 2014). This suggested a possible role for the change in cytokine signalling in the increased *in vivo* sensitivity to doxorubicin in EC FAK^{KO} mice. Therefore, we wanted to know whether the response of EC-FAK-KD cells to doxorubicin was similar to that of FAK-null endothelial cells. Therefore, Dr Delphine Lees for our laboratory, prepared immortalised WT and FAK KD endothelial cells as described in **(Figure 13.8 A)** and ran a cytokine array to establish the cytokine response to doxorubicin in each cell type. Although this was only one array (one membrane with two dots per sample for each cytokine), it demonstrated that while the expression of many cytokines was upregulated in response to doxorubicin treatment in WT ECs, cytokine production was much reduced in FAK-KD endothelial cells to close to baseline expression **(Figure 13.8 B and C)**. Plotting the number of cytokines that were upregulated more than 25 % (red), downregulated more than 25 % (blue) or unchanged (grey), there were significantly more unchanged in the FAK KD than WT ECs **(Figure 13.8 D).** Therefore, the effect on the response to doxorubicin treatment of rendering endothelial cells kinase-dead was similar to the effect in FAK KO endothelial cells.

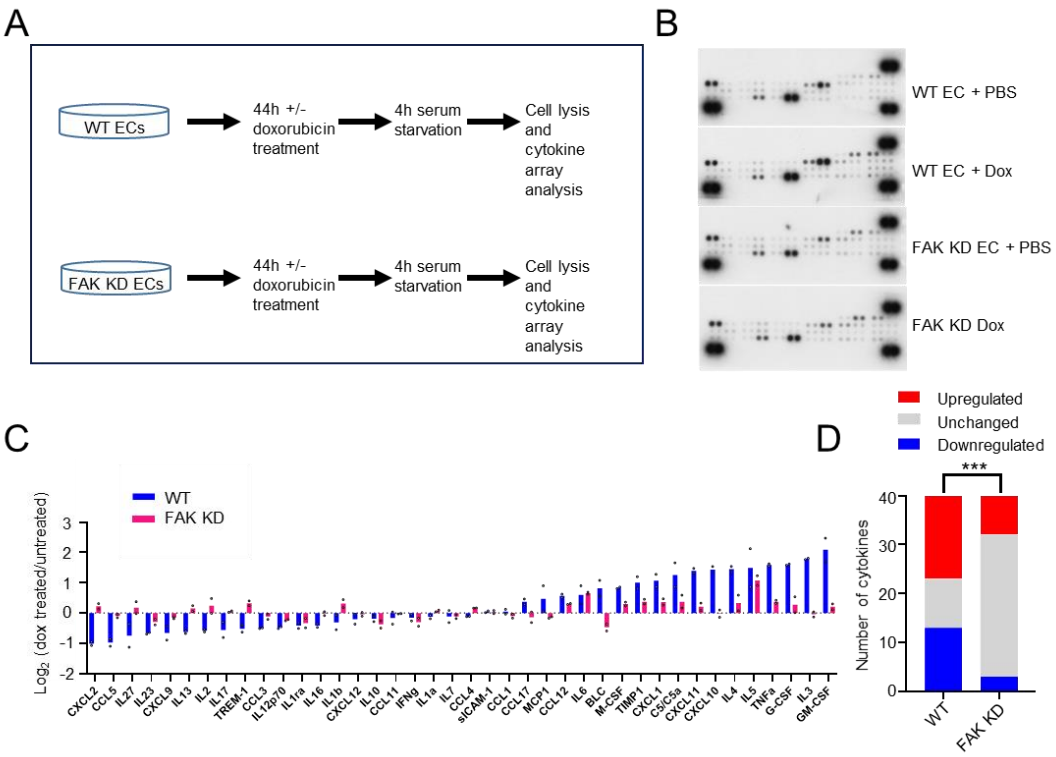

Figure 13.8 Genetic inactivation of FAK in ECs leads to a downregulation of cytokine production after Dox treatment.

(A) Method outline. (B) Whole cytokine array membranes for EC-WT and EC-FAK KD MLECs treated with doxorubicin or PBS. (C) Quantitation of fold difference in cytokine expression between doxorubicin-treated and non-treated EC-WT and EC-FAK KD MLECs (n=1 experiment, bars represent average of 2 dots on the array). (D) Number of cytokines upregulated or downregulated by > 25 % in EC-WT and EC-FAK KD cells on doxorubicin treatment. Red bars represent number of up-regulated cytokines after doxorubicin treatment. Blue bars represent down-regulated number of cytokines after doxorubicin treatment. Grey bars represent number of cytokines whose expression did not change after doxorubicin treatment. Analysed by chi squared, **** P <0.0001.

13.11 Pharmacologically rendering endothelial cell FAK kinase dead *in vitro* leads to a downregulation in cytokine production in response to doxorubicin treatment

As genetically rendering murine endothelial cells kinase-dead appeared to reduce their cytokine response to doxorubicin treatment, we wanted to establish whether this effect could be replicated in human cells with pharmacological FAK kinase inhibition. Human pulmonary microvascular endothelial cells were grown to confluency and treated for 48 hours with or without 5 µM FAK kinase inhibitors PF-573,288, PF-562,271 or defactinib and 250 nM doxorubicin **(Figure 13.9 A)**. Initially, the PF-573,288 inhibitor was tested and, while in the controls, there was an upregulation in the production of most cytokines with doxorubicin treatment, there was much reduced cytokine production in response to doxorubicin in PF-573,288 treated cells **(Figure 13.9 B and C)**. The effects of PF-562,271 and defactinib were then tested in a second experiment. Consistent with the PF-573,288 experiment, when no inhibitor was used, the cells increased their cytokine production in response to doxorubicin. There was generally a downregulation in cytokine response with doxorubicin treatment in inhibitor-treated cells compared to baseline **(Figure 13.9 D-F)**. More significant differences were recorded with defactinib than PF-562,271 treatment, but the reduction in doxorubicin-induced cytokine production was consistent across all three inhibitors and the genetically kinase-dead cells.

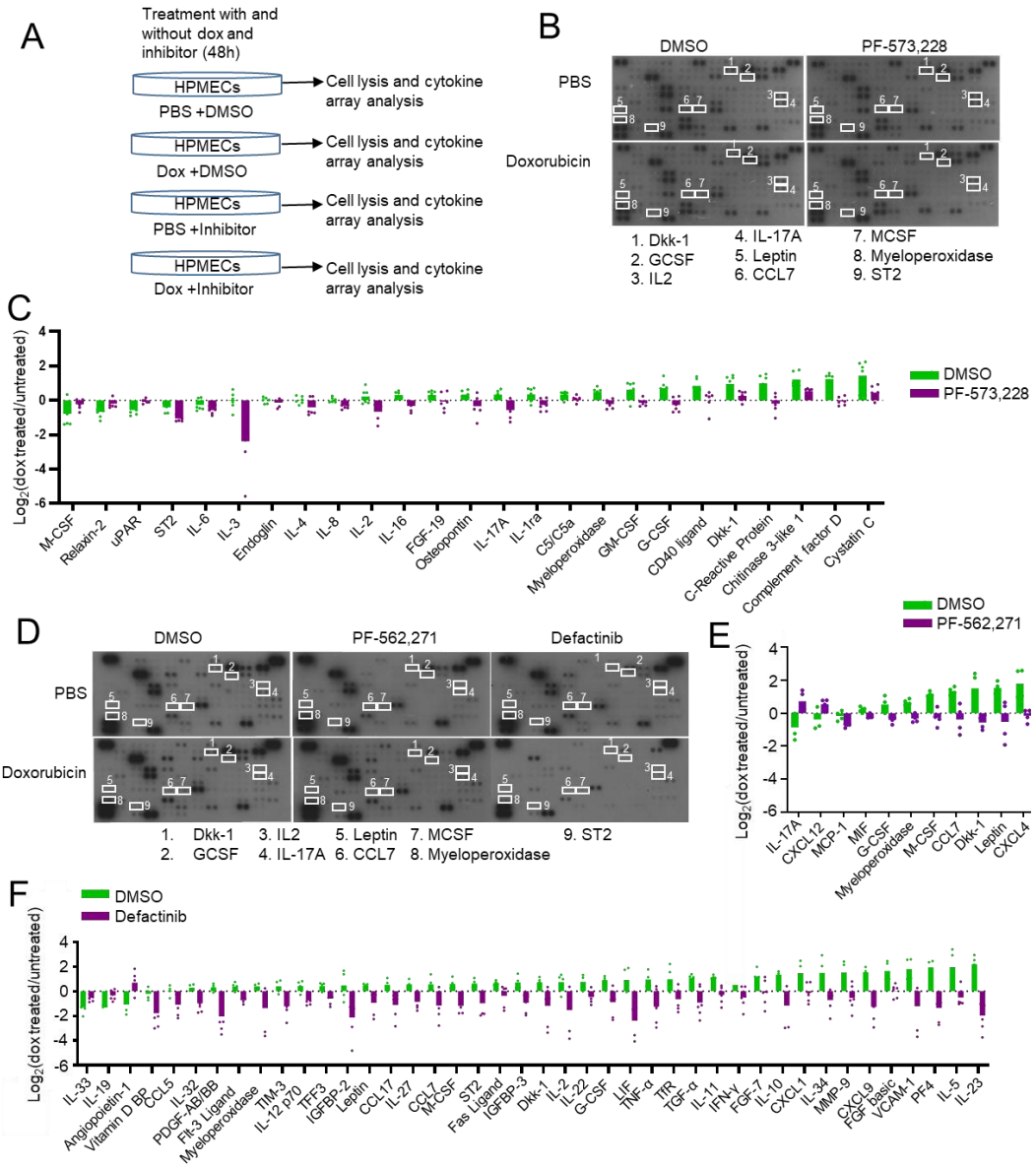
A
Treatment with and without dox and inhibitor (48h)
HPMECs
PBS +DMSO
Cell lysis and cytokine array analysis
HPMECs
Dox +DMSO
Cell lysis and cytokine array analysis
HPMECs
PBS +Inhibitor
Cell lysis and cytokine array analysis
HPMECs
Dox +Inhibitor
Cell lysis and cytokine array analysis
B
DMSO
PF-573,228
PBS
Doxorubicin
1. Dkk-1
2. GCSF
3. IL2
4. IL-17A
5. Leptin
6. CCL7
7. MCSF
8. Myeloperoxidase
9. ST2
C
Log2(dox treated/untreated)
DMSO
PF-573,228
M-CSF
Relaxin-2
uPAR
ST2
IL-6
IL-3
Endoglin
IL-4
IL-8
IL-2
IL-16
FGF-19
Osteopontin
IL-17A
IL-1ra
C5/C5a
Myeloperoxidase
GM-CSF
G-CSF
CD40 ligand
Dkk-1
C-Reactive Protein
Chitinase 3-like 1
Complement factor D
Cystatin C
D
DMSO
PF-562,271
Defactinib
PBS
Doxorubicin
1. Dkk-1
2. GCSF
3. IL2
4. IL-17A
5. Leptin
6. CCL7
7. MCSF
8. Myeloperoxidase
9. ST2
E
DMSO
PF-562,271
Log2(dox treated/untreated)
IL-17A
CXCL12
MCP-1
MIF
G-CSF
Myeloperoxidase
M-CSF
CCL7
Dkk-1
Leptin
CXCL4
F
DMSO
Defactinib
Log2(dox treated/untreated)
IL-33
IL-19
Angiopoietin-1
Vitamin D BP
CCL5
IL-32
PDGF-AB/BB
Flt-3 Ligand
Myeloperoxidase
TIM-3
IL-12 p70
TFF3
IGFBP-2
Leptin
CCL17
IL-27
CCL7
M-CSF
ST2
Fas Ligand
IGFBP-3
Dkk-1
IL-2
IL-22
G-CSF
LIF
TNF-α
TfR
TGF-α
IL-11
IFN-γ
FGF-7
IL-10
CXCL1
IL-34
MMP-9
CXCL9
FGF basic
VCAM-1
PF4
IL-5
IL-23

Figure 13.9 Pharmacological inactivation of FAK in ECs leads to a downregulation of cytokine production after Dox treatment.

(A) Method outline. (B) Representative cytokine array membranes for HPMECs with and without PF-573,228 FAK kinase inhibition and doxorubicin treatment, commonly regulated cytokines are labelled. (C) Waterfall plot of all cytokines whose response to doxorubicin was significantly regulated by PF-573,228 treatment. (D) Representative cytokine array membranes for HPMECs with and without PF-562,271 and defactinib FAK kinase inhibition and doxorubicin treatment, commonly regulated cytokines are labelled. (E) Waterfall plot of all cytokines whose response to doxorubicin was significantly regulated by PF-562,271 treatment. (F) Waterfall plot of all cytokines whose response to doxorubicin was significantly regulated by defactinib treatment. Waterfall plots shown as $\log_2$ (doxorubicin treated/untreated) cytokine levels, waterfall plots are represented as the fold-change against the -log of the P-value.

13.12 The overall impact of the three FAK kinase inhibitors PF-573,228, PF-562,271 and defactinib on cytokine production in response to doxorubicin was consistent

To summarise the cytokine response, volcano plots were produced for control cells and each inhibitor. These demonstrated that in the cells used as a control for PF-573,228 treatment **(Figure 13.10 A)**, there were many cytokines significantly upregulated (red) and downregulated (blue) with doxorubicin treatment compared to baseline levels. The effect of the PF-573,228 on response to doxorubicin, however (doxorubicin response in PF-573,228 treated cells relative to doxorubicin response in control cells) was overall one of downregulation **(Figure 13.10 B).** This can be seen in the number of up-or downregulated cytokines in response to doxorubicin in the control and PF-573,228 treated cells. With PF-573,228, fewer cytokines are upregulated and more downregulated in response to doxorubicin **(Figure 13.10 C)**. For the cells used as a control for PF-562,271 and defactinib, the overall cytokine response was similar to the control cells in 14.14 A, with many cytokines significantly up-or downregulated in response to doxorubicin compared to baseline **(Figure 13.10 D)**. The effect of both PF-562,271 and defactinib was a downregulation in the cytokine production in response to doxorubicin but with more significant changes recorded in defactinib treated than PF-562,271 treated cells **(Figure 13.10 E and F)**. Similar to PF-573,228, these results can be further summarized by plotting the number of cytokines up and downregulated compared to baseline. For both inhibitors, the number of cytokines significantly upregulated in response to doxorubicin is reduced, and the number downregulated increased, but this effect was much more pronounced in defactinib, where more than 30 cytokines were significantly downregulated by doxorubicin treatment **(Figure 13.10 G)**.

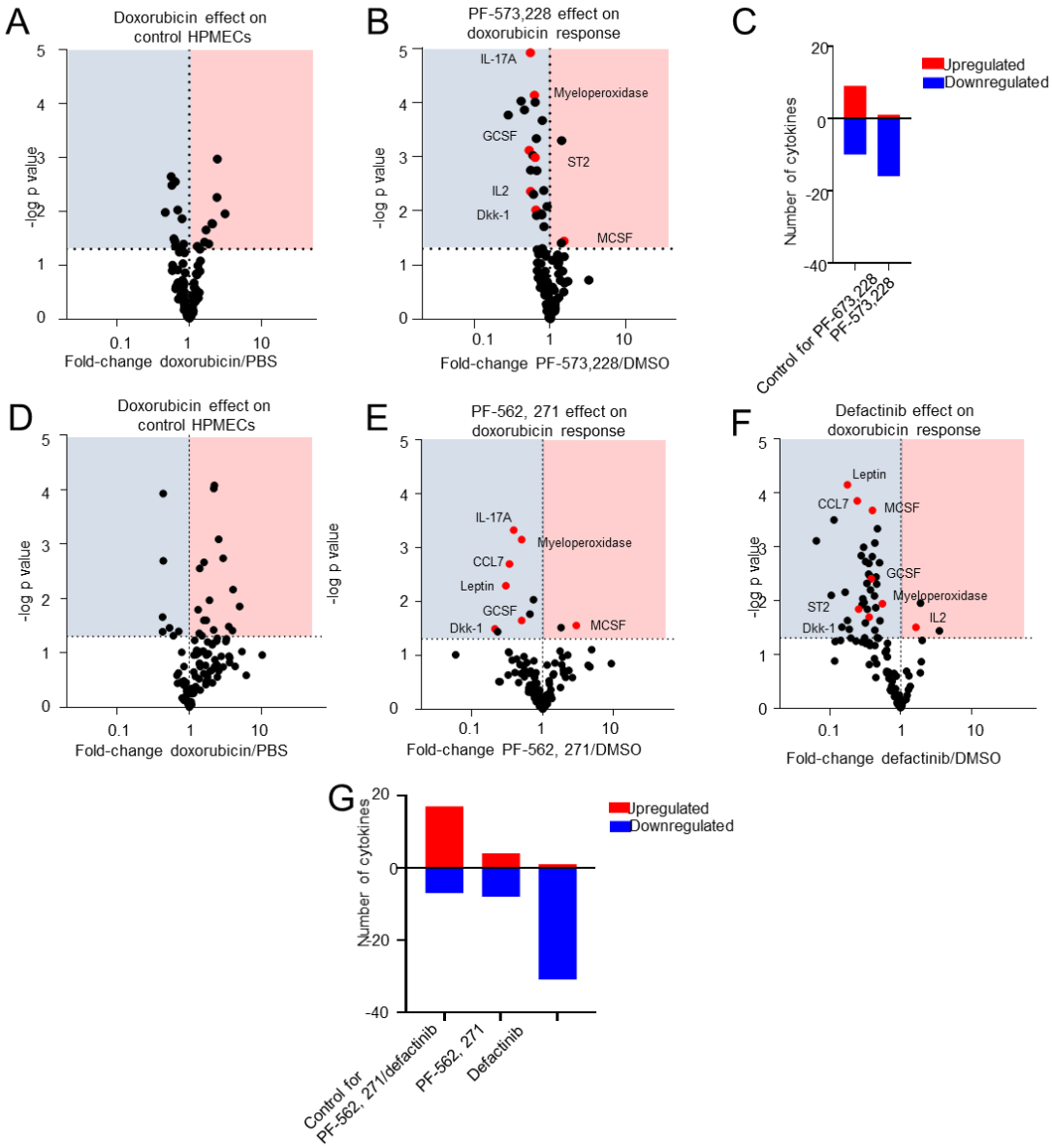
A
Doxorubicin effect on control HPMECs
-log p value
Fold-change doxorubicin/PBS
B
PF-573,228 effect on doxorubicin response
IL-17A
Myeloperoxidase
GCSF
ST2
IL2
Dkk-1
MCSF
-log p value
Fold-change PF-573,228/DMSO
C
Upregulated
Downregulated
Number of cytokines
Control for PF-573,228
PF-573,228
D
Doxorubicin effect on control HPMECs
-log p value
Fold-change doxorubicin/PBS
E
PF-562, 271 effect on doxorubicin response
IL-17A
Myeloperoxidase
CCL7
Leptin
GCSF
Dkk-1
MCSF
Fold-change PF-562, 271/DMSO
F
Defactinib effect on doxorubicin response
Leptin
CCL7
MCSF
GCSF
ST2
Myeloperoxidase
Dkk-1
IL2
-log p value
Fold-change defactinib/DMSO
G
Upregulated
Downregulated
Number of cytokines
Control for PF-562, 271/defactinib
PF-562, 271
Defactinib

Figure 13.10 Pharmacological inactivation of FAK in ECs leads to a downregulation of cytokine production after Dox treatment.

(A) Fold-change in cytokine expression levels with doxorubicin/PBS treatment in control HPMECs used for PF-573, 228 comparison. (B) The effect of PF-573,228/PBS treatment on cytokine expression levels in doxorubicin treated cells, red dots indicated cytokines significantly regulated by more than one inhibitor. For PF-573,228 cytokine arrays, n=3 control and 3 treated cytokine array membranes (6 dots per condition) each membrane represents an independent cell sample. (C) Number of cytokines significantly regulated by doxorubicin treatment in control or PF-573,228 treated HPMECs. Red bars represent number of up-regulated cytokines after doxorubicin treatment. Blue bars represent down-regulated number of cytokines after doxorubicin treatment. (D) Second experiment. Fold-change in cytokine expression levels with doxorubicin/PBS treatment in control HPMECs for PF-562,271 and defactinib comparison. (E) The effect of PF-562,271 treatment on cytokine expression levels in doxorubicin treated cells, red dots indicated cytokines significantly regulated by more than one inhibitor. (F) The effect of defactinib treatment on cytokine expression levels in doxorubicin treated cells. For PF-573,271 and defactinib cytokine arrays, n=2 control and PF-573, 271 treated and 3 doxorubicin treated cytokine array membranes (4, 4 and 6 dots per condition respectively) each membrane represents an independent cell sample. (G) The number of cytokines significantly up regulated or downregulated by doxorubicin treatment in control, PF-562, 271 treated and defactinib treated HPMECs. Red bars represent number of up-regulated cytokines after doxorubicin treatment. Blue bars represent down-regulated number of cytokines after doxorubicin treatment.

13.13 Cytokines whose production in response to doxorubicin was significantly altered by more than one inhibitor have broad roles in the innate immune response

There was a general trend towards reducing cytokine production in response to doxorubicin in inhibitor-treated compared to control cells. For many of the cytokines, more than one inhibitor caused an altered response to doxorubicin **(Figure 13.11)**. Of the cytokines whose response to doxorubicin was significantly altered by more than one of the inhibitors, several have roles in the innate immune system. For example, chemokine (C-C motif) ligand 7 (CCL7) is a chemoattractant for monocytes (Liu et al. 2018), macrophage colony-stimulating factor (M-CSF) promotes differentiation of monocytes into macrophages, and myeloid cell growth factor (Ushach and Zlotnik 2016) and interleukin 17A (IL-17A) is associated with infiltration of MDSCs and the promotion of a tumour promoting microenvironment (He et al. 2010). Therefore, although beyond the scope of this study, it is possible that the increased sensitivity to doxorubicin in EC-FAK KD animals is due to changes in the innate immune response caused by angiocrine signalling of endothelial cells in response to doxorubicin.

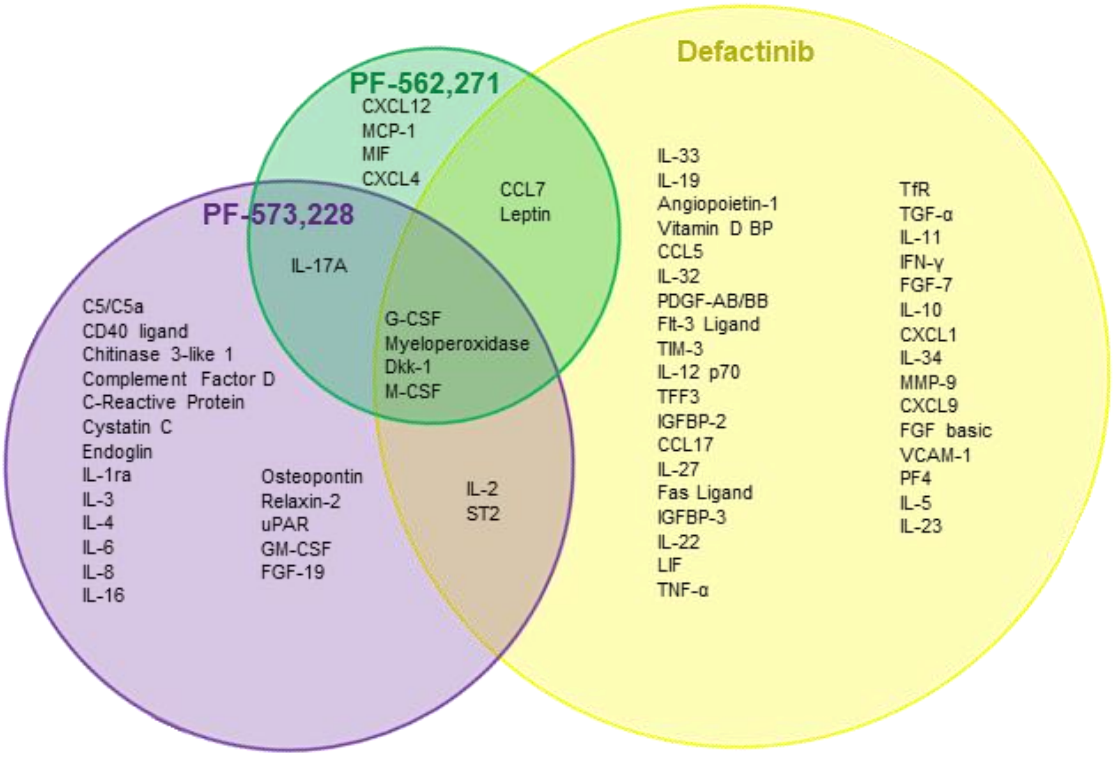

Figure 13.11 Venn diagram of the cytokines whose response to doxorubicin was significantly downregulated by FAK kinase inhibition demonstrating the commonly changed cytokines between treatments with different inhibitors.

13.14 Cytokine array raw data demonstrate a trend towards reduced cytokine production in response to doxorubicin in cells genetically or pharmacologically rendered kinase-dead

The raw data for these cytokine arrays, which includes all cytokines, not just those that were significantly regulated, demonstrates a trend towards reduced cytokine production with doxorubicin treatment in both genetically and all pharmacologically kinase-dead cells **(Figure 13.12)**. However, this was most prominent in the defactinib treated cells, where there was a downregulation in the majority of cytokines with doxorubicin treatment compared to baseline **(Figure 13.12 D)**. This may be because defactinib has the lowest IC_{50} for FAK of all of the inhibitors.

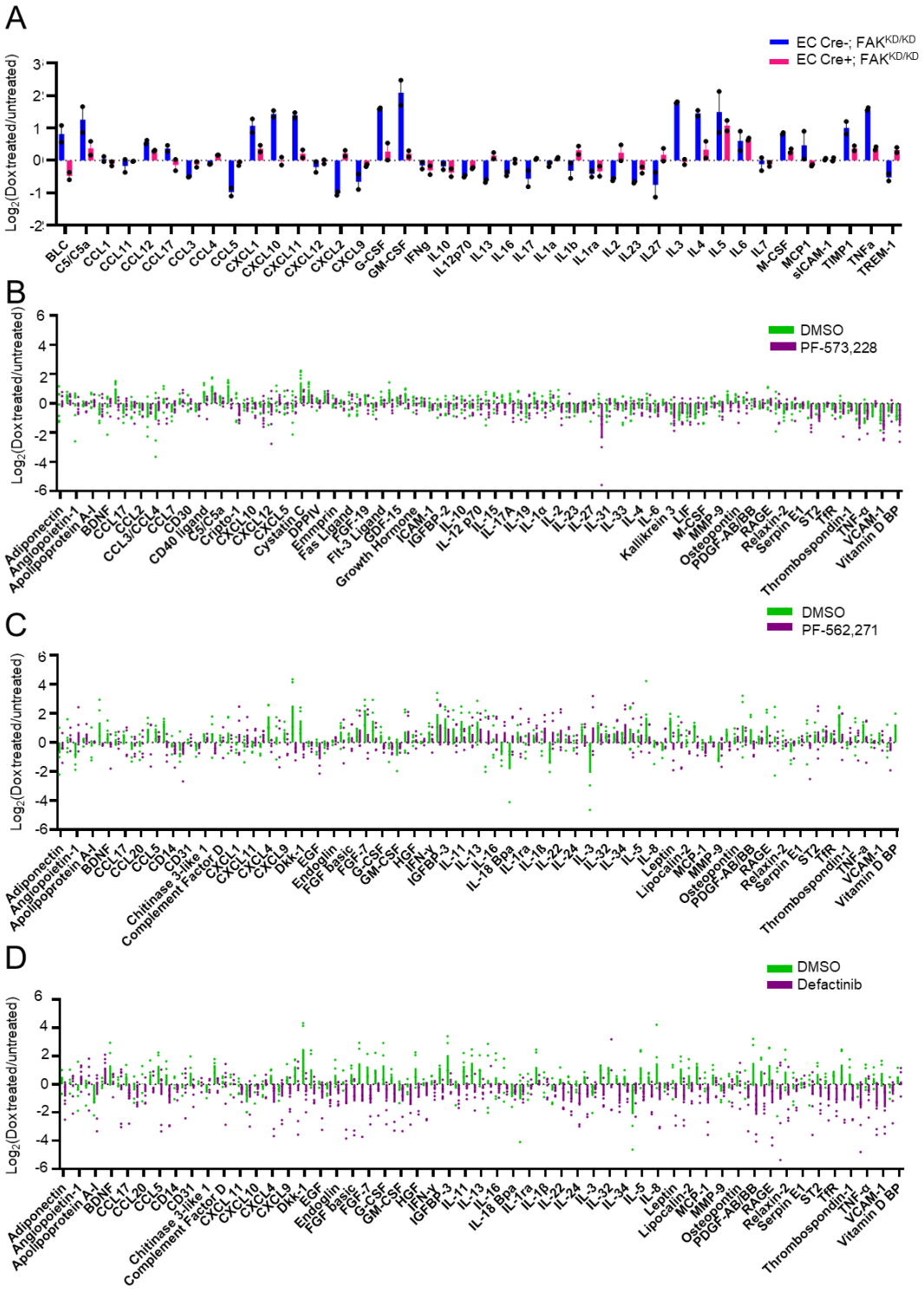
A
EC Cre-; FAK^KD/KD
EC Cre+; FAK^KD/KD
Log2(Dox treated/untreated)
BLC
C5/C5a
CCL1
CCL11
CCL12
CCL17
CCL3
CCL4
CCL5
CXCL1
CXCL10
CXCL11
CXCL12
CXCL2
CXCL9
G-CSF
GM-CSF
IFNg
IL10
IL12p70
IL13
IL16
IL17
IL1a
IL1b
IL1ra
IL2
IL23
IL27
IL3
IL4
IL5
IL6
IL7
M-CSF
MCP1
sICAM-1
TIMP1
TNFa
TREM-1
B
DMSO
PF-573,228
Log2(Dox treated/untreated)
Adiponectin
Angiopoietin-1
Apolipoprotein A-I
BDNF
CCL17
CCL2
CCL3/CCL4
CCL7
CD30
CD40 ligand
C5/C5a
Cripto-1
CXCL10
CXCL12
CXCL5
Cystatin C
DPPIV
Emmprin
Fas Ligand
FGF-19
Flt-3 Ligand
GDF-15
Growth Hormone
ICAM-1
IGFBP-2
IL-10
IL-12 P70
IL-15
IL-17A
IL-1a
IL-2
IL-23
IL-27
IL-31
IL-33
IL-4
IL-6
Kallikrein 3
LIF
M-CSF
MMP-9
Osteopontin
PDGF-AB/BB
RAGE
Relaxin-2
Serpin E1
ST2
TIR
Thrombospondin-1
TNF-a
VCAM-1
Vitamin D BP
C
DMSO
PF-562,271
Log2(Dox treated/untreated)
Adiponectin
Angiopoietin-1
Apolipoprotein A-I
BDNF
CCL17
CCL20
CCL5
CD14
CD31
Chitinase 3-like 1
Complement Factor D
CXCL1
CXCL11
CXCL4
CXCL9
Dkk-1
EGF
Endoglin
FGF basic
FGF-7
G-CSF
GM-CSF
HGF
IFNγ
IGFBP-3
IL-11
IL-13
IL-16
IL-18 Bpa
IL-1ra
IL-1ß
IL-22
IL-24
IL-3
IL-32
IL-34
IL-5
IL-8
Leptin
Lipocalin-2
MCP-1
MMP-9
Osteopontin
PDGF-AB/BB
RAGE
Relaxin-2
Serpin E1
ST2
TIR
Thrombospondin-1
TNF-a
VCAM-1
Vitamin D BP
D
DMSO
Defactinib
Log2(Dox treated/untreated)
Adiponectin
Angiopoietin-1
Apolipoprotein A-I
BDNF
CCL17
CCL20
CCL5
CD14
CD31
Chitinase 3-like 1
Complement Factor D
CXCL1
CXCL11
CXCL4
CXCL9
Dkk-1
EGF
Endoglin
FGF basic
FGF-7
G-CSF
GM-CSF
HGF
IFNγ
IGFBP-3
IL-11
IL-13
IL-16
IL-18 Bpa
IL-1ra
IL-1ß
IL-22
IL-24
IL-3
IL-32
IL-34
IL-5
IL-8
Leptin
Lipocalin-2
MCP-1
MMP-9
Osteopontin
PDGF-AB/BB
RAGE
Relaxin-2
Serpin E1
ST2
TIR
Thrombospondin-1
TNF-a
VCAM-1
Vitamin D BP

Figure 13.12 Raw data for cytokine arrays of genetic and pharmacological FAK kinase domain inhibition show a similar trend with doxorubicin treatment.

Bar charts the fold-change expression of all cytokines identified represented as log_2(doxorubicin treated/untreated) for (A) WT and FAK KD MLECs (B) PF-573,228 treated and control HPMECs. For PF-573,228 cytokine arrays, n=3 control and 3 treated cytokine array membranes (6 dots per condition) each membrane represents an independent cell sample. (C) PF-562,271 treated and control HPMECs. For PF-573,271 n=2 control and PF-573, 271 treated and 3 doxorubicin treated cytokine array membranes (4, 4 and 6 dots per condition respectively). (D) Defactinib treated and control HPMECs. For defactinib n=2 control and defactinib treated and 3 doxorubicin treated cytokine array membranes (4, 4 and 6 dots per condition respectively).

14 Discussion I: Targeting angiocrine signalling to enhance chemosensitivity

The primary aim of the work presented in this chapter was to establish whether the kinase activity of EC FAK is involved in doxorubicin induced angiocrine signalling and chemosensitisation cancer.

Previous work has demonstrated that the deletion of EC-FAK sensitises tumours to DNA damaging therapy (Tavora, Reynolds, et al. 2014). Proteomic, phosphoproteomic and secretomic studies further contributed to our understanding of the molecular changes that doxorubicin triggers within endothelial cells. In each of the three analyses, we see a strong signature in response to doxorubicin in WT cells which is significantly reduced in FAK-KO endothelial cells. Understanding the role of the kinase domain in this altered response to doxorubicin is clinically important as FAK inhibition is typically specific to a single FAK function, most commonly the kinase function through ATP competitive inhibition. FAK is known to exhibit scaffolding and nuclear functions in addition to its kinase functions. It therefore expected, that there may be some phenotypic differences between animals that are endothelial cell specific FAK knockout and endothelial cell specific FAK kinase dead. It was previously unknown how much the kinase domain of FAK was responsible for the endothelial cell FAK mediated sensitivity to doxorubicin. I have shown through tumour growth curves that rendering the endothelial cells of mice with established tumours FAK kinase-dead sensitises the tumours to doxorubicin, although the effect is more subtle than that observed for complete FAK ablation in endothelial cells (Tavora, Reynolds, et al. 2014). Also similar to the FAK-KO model, this sensitisation happens not through changes in blood vessel density, perfusion or doxorubicin delivery but through changes in the tumour cell response to doxorubicin in terms of apoptosis, proliferation and DNA damage. In addition, I have shown that the cytokine production in response to doxorubicin is altered by inhibition of the FAK kinase domain by three different inhibitors, PF-573,228 (*Pfizer*), PF-562,271 (*Pfizer*) or defactinib (*Verastem*). All three inhibitors have a similar trend in reducing cytokine production of HPMECs in response to doxorubicin compared to control HPMECs. This suggests that targeting the kinase domain of endothelial cell FAK through pharmacological inhibition may lead to a clinical benefit in sensitising tumours to doxorubicin.

14.1 The modest sensitisation of kinase-dead mice to doxorubicin suggests that the kinase domain is partially responsible for the sensitising effect of endothelial cell FAK

While the deletion of endothelial cell FAK clearly sensitises subcutaneous B16-F0 melanoma tumours to doxorubicin, deletion of the kinase domain only modestly does so. This suggests some role of the kinase domain in the sensitisation role of FAK, but it is not exclusively responsible.

We have shown previously that FAK is responsible for tumour angiogenesis, and FAK deletion causes an alteration in endothelial cell signalling as well as a reduction in proliferation and migration (Tavora et al. 2010). Loss of the kinase activity of FAK in endothelial cells causes a similar phenotype to endothelial cell FAK KO with regards to the formation of the tumour, tumour angiogenesis and hypoxia when the kinase domain is inactivated prior to tumour induction (Alexopoulou et al. 2017). However, while FAK deletion is known to be embryonic lethal (e10.5-11.5) due to increased endothelial cell retraction and apoptotic death (Braren et al. 2006), in adult mice, initiation of an *EC FAK-KO* mutation does not result in endothelial cell apoptosis, partly due to compensation by Pyk2 allowing cell survival (Sulzmaier, Jean, and Schlaepfer 2014; Lim, Miller, et al. 2010; Weis et al. 2008). Therefore, in adult mice, endothelial cell FAK mutations can be induced with little impact on health.

In the case of cancer models, most tumours rely on angiogenesis once their volume has exceeded 1-2 mm^3 (Bergers and Benjamin 2003; Deshpande et al. 2011). Therefore, tumours above this size are likely to have already established angiogenesis. FAK is necessary for the initiation of angiogenesis but not blood vessel maintenance. Hence, the effect of endothelial cell FAK deletion in established tumours is somewhat different and occurs without affecting blood delivery by the blood vessels (Tavora, Reynolds, et al. 2014). Similarly, in the present study, the kinase-dead mutation was not activated until the tumours were established and had reached 100 mm^3. These tumours were therefore likely to have already established angiogenesis and, as in the case of EC-FAK KO in established tumours, there is no change in blood vessel density, perfusion or doxorubicin delivery with the onset of this mutation. While the kinase domain is required absolutely for FAK function in initiation and growth of tumours and appears important in doxorubicin resistance in established tumours, it may not be entirely responsible for the role of endothelial cell FAK in doxorubicin sensitivity. As the sensitisation to doxorubicin

appears more modest with an endothelial cell FAK kinase-dead mutation than endothelial cell FAK knockout, it is likely that the kinase domain is supported, to some extent, by scaffolding or nuclear functions of FAK. However, with this model, we are not able to dissect the importance of either the scaffolding or nuclear functions of FAK.

14.2 Tumour cells response to doxorubicin is endothelial cell FAK kinase dead mutation

The effect of EC-FAK KD mutation in established tumours on perivascular proliferation, tumour cell apoptosis and tumour cell DNA damage was also similar to that of the EC-FAK KO mutation (Tavora, Reynolds, et al. 2014). *EC Cre+; FAK$^{KD/KD}$* mice treated with doxorubicin showed less perivascular proliferation, more tumour cell apoptosis and tumour cell DNA damage per blood vessel than similarly treated *EC Cre-; FAK$^{KD/KD}$* mice. This, coupled with the observations in vascular histology, suggested that the change in tumour growth was not due to changes in blood vessel development but to an altered response of the tumour cells to doxorubicin caused by changes in angiogenic signalling.

14.3 Endothelial cells produce a protumorigenic microenvironment in response to doxorubicin which is moderated by genetic inactivation of the kinase domain or FAK kinase inhibition

Tumour growth curves and tumour cell histology demonstrated that the kinase domain of FAK is at least in part responsible for the sensitisation to doxorubicin observed in EC FAK^{KO} mice (Tavora, Reynolds, et al. 2014). Tavora et al. demonstrated that DNA damaging therapies stimulate endothelial cells to provide protective paracrine signals, and endothelial cell FAK is an essential component of this process; in its absence, this protective signalling is much reduced. The present study suggests that the kinase domain of FAK is involved in the sensitisation of tumours to doxorubicin.

Therefore, to characterise these paracrine signals, we performed a cytokine array on WT and FAK-KD endothelial cells treated with or without doxorubicin. This array confirmed that WT endothelial cells upregulated expression of many cytokines in response to doxorubicin, but this effect was lost in FAK KD cells. Some of the cytokines whose response to doxorubicin was downregulated by FAK KD mutation were common to those observed in FAK-KO cells, for example, granulocyte-macrophage colony-stimulating factor (GM-CSF), interleukin 4 (IL-4) and complement component 5 (C5)/C5a. GM-CSF is

a monomeric glycoprotein cytokine that is secreted by macrophages, T cells, mast cells, natural killer cells and fibroblasts, as well as endothelial cells. It promotes the maturation of dendritic cells, monocytes and macrophages (Root and Dale 1999) and is often upregulated in human cancer. In addition to its role in the immune system, it is also known to promoting a pro-tumourigenic microenvironment, increasing tumour growth and frequency of metastasis (Hong 2016). IL-4 is involved in regulating cytokine production in the TME; it activates TAMs and MDSCs, promoting tumour development (Wang and Joyce 2010). Therefore, it is considered a possible target for cancer therapy (Suzuki et al. 2015). C5 is an important component of the complement system; it is cleaved to C5a and C5b. C5a has roles in mediating the chemotaxis of inflammatory myeloid cells microbial killing (Langley, Fraser, and Proft 2015).

The complement system is also known to be involved in cancer; it has immunoregulatory functions in activating the TME, promoting tumour development, progression, metastasis and recurrence through interaction with stromal cells. Additionally, direct interaction of the complement system with tumour cells promotes tumour cell proliferation, EMT, migration and invasion (Zhang et al. 2019). However, C5 can also have antitumour properties; in Ewing's Sarcoma, which, unlike many adult cancers, is non-inflammatory in origin, there is still a macrophage-enriched TME, and increased levels of C5 correlate with improved survival (Savola et al. 2011). These cytokines, whose production by endothelial cells in response to doxorubicin is downregulated by both the FAK KO and FAK KD mutations, are broadly cancer-causing. They have roles in regulating the immune system creating a protumorigenic microenvironment. Therefore, this suggests a link between both mechanisms, as knockout of FAK in endothelial cells reduces the protective cytokine profile produced by endothelial cells in response to doxorubicin, so does rendering the endothelial cells FAK kinase-dead. The change in cytokine profile appears to be particularly similar in regulation of the immune system.

The three cytokines most strongly upregulated by WT MLECs in response to doxorubicin were GM-CSF, IL-3 and G-CSF. In each case, the doxorubicin-induced production of these cytokines was reduced to a level close to baseline in FAK-KD MLECs. All three cytokines are involved in inflammation (Dougan, Dranoff, and Dougan 2019; Liu et al. 2020). As previously discussed, GM-CSF induces maturation of dendritic cells, monocytes and macrophage, making it a critical cytokine in the innate immune response (Root and Dale 1999). IL-3 to is critical to the innate immune system, stimulating bone marrow precursors to differentiate into granulocytes, monocytes, macrophages, eosinophils,

basophils, and mast cells (Dougan, Dranoff, and Dougan 2019). Finally, following the trend of innate immune regulators, the primary function of G-CSF is in granulocyte production (Turner et al. 2014). G-CSF has also been shown to upregulated in many cancers and to be involved in cancer progression (Liu et al. 2020).

Together, these data suggest that endothelial cells produce an inflammatory cytokine response to doxorubicin treatment, which is much reduced by either FAK ablation or rendering FAK kinase-dead. There seems to be a commonality in the modulation of the innate immune for cancer progression in the most affected cytokines.

To establish whether FAK kinase inhibition in human endothelial cells could have the same effect as genetic inactivation of the kinase domain in mouse endothelial cells, we performed cytokine arrays with HPMECs treated with and without PF-573,228, PF-562,271 or defactinib and doxorubicin. Indeed, the main effects of the kinase-dead mutation were recapitulated in these arrays with broad downregulation in cytokine production in response to doxorubicin and cytokines of the innate immune system commonly affected. There was an evident change in cytokine production for each inhibitor in response to doxorubicin with fewer cytokines upregulated and more downregulate. Notably, of the cytokines whose regulation was significantly altered in response to more than one inhibitor, several are involved in inflammation and the innate immune system, as discussed for the FAK-KD mouse endothelial cells. They are also broadly tumour promoting in their action. For example, chemokine (C-C motif) ligand 7 (CCL7) is a chemoattractant for leukocytes, including monocytes and neutrophils; it promotes a protumorigenic microenvironment allowing invasion and metastasis of tumour cells (Liu et al. 2018). G-CSF, which was highly regulated in FAK-KD and has roles in the innate immune system and cancer progression, is also downregulated by all three of the inhibitors in response to doxorubicin.

In addition, one of the cytokines whose production in response to doxorubicin is downregulated by all three of the inhibitors is Dkk-1 which is known to inhibit the Wnt signalling pathway. Wnt signalling has important roles in tumorigenesis and embryogenesis through the β-catenin/TCF transcription complex and downstream regulation of genes. It is, however, also involved in a negative feedback loop with Dkk-1, increased Wnt activity increases the activity of Dkk-1 (Niida et al. 2004). It is interesting that the production of Dkk-1 by endothelial cells in response to doxorubicin is reduced by all three inhibitors, as this may suggest an increase in Wnt activity and possible

increased tumorigenesis. However, increased expression of Dkk-1 is also associated with poor prognosis in some cases (Shen et al. 2010; Wei et al. 2020; Gao et al. 2018) so its exact role in this model would require further investigation to determine.

The effect on the innate immune system is also observed in the secretomics data **(Figure 13.1 D).** The secretion of heat shock protein 90-alpha (HS90A), Serum amyloid P component (SAP), Complement Factor H (CFAH), Cathepsin X (CATZ) and beta-hexosaminidase subunit beta (HEXB) were altered by doxorubicin treatment in EC-FAK KO but not in EC-WT cells **(Figure 13.1 D).** Each of these proteins have roles in pathways related to the innate immune system (Zininga, Ramatsui, and Shonhai 2018; Bottazzi et al. 2016; Parente et al. 2017; Perišić Nanut et al. 2014; Koo et al. 2008). For example, HSP90A on the cell surface triggers the action of danger/damage-associated molecular patterns (DAMPs), which in turn activate the innate immune system (Zininga, Ramatsui, and Shonhai 2018; Multhoff et al. 2012). Similarly, the pentraxin, SAP is a humoral component of innate immunity involved in wound repair and regulation of fibrosis. It binds to neutrophils controlling their function, and also prevents monocytes from differentiating into fibroblast-like fibrocytes (Bottazzi et al. 2016; Cox, Pilling, and Gomer 2014).

However, despite many similarities between the responses of FAK-KO MLECs, FAK-KD MLECs and FAK kinase inhibitor-treated HPMECs in response to doxorubicin, one difference is that FAK inhibition induced a downregulation in cytokine response to doxorubicin whereas the response was neutral in the FAK KO and FAK KD MLECs. Although beyond the scope of the work included in this thesis, this may be due to off-target effects of FAK kinase inhibitors (Roh et al. 2013) or compensatory mechanisms in FAK-KD MLECs (Sulzmaier, Jean, and Schlaepfer 2014). It is known that the effects of FAK kinase inhibitors can have off-target effects. For example, platelet aggregation in response to thrombin, ADP, or collagen is not significantly altered in FAK KO mice compared to WT animals. However, in vitro, the inhibitors PF-573,228 and PF-562,271 both significantly inhibited platelet aggregation in response to thrombin, ADP, and collagen in isolated platelets from either FAK-KO or WT animals. This demonstrates that the inhibitors must have an off-target effect outside of FAK inhibition as their effect on platelet aggregation is present even in the absence of FAK (Roh et al. 2013).

Although the effect of the three kinase inhibitors was broadly consistent, inducing a downregulation rather than upregulation in cytokine production in response to

doxorubicin, the effect of defactinib appeared to be the strongest. This is perhaps unsurprising as defactinib is the most potent inhibitor of both FAK and Pyk2 with IC_{50}s of 0.6nM for both kinases (4nM FAK and >1000 nM Pyk2 for PF-573,228; 1.5 nM FAK and 14 nM Pyk2 for PF-562,271) (Slack-Davis et al. 2007; Shimizu et al. 2016; Chauhan and Khan 2021). Defactinib is also the inhibitor that has progressed furthest through clinical trials of the three (Gerber et al. 2020; Jones et al. 2015), and there are still trials running using it (ICR 2021; Currie 2021). Defactinib is, therefore, a promising drug for use in combination with chemotherapy and may regulate chemosensitisation through its effects on endothelial cell angiocrine signalling.

14.4 Conclusions

In summary, the kinase domain of FAK is involved in regulating chemosensitisation *in vivo*, although it may be supported by other functions of FAK. This sensitization in vivo correlates with altered angiocrine signalling in vivo, especially affecting cytokines involved in regulating the innate immune system. The pharmacological inhibition of FAK in human endothelial cells recapitulates a similar effect to the genetically FAK-KD murine endothelial cells. However, rather than neutralising cytokine production in response to doxorubicin, inhibition appears to cause a downregulation in doxorubicin-induced cytokine production.

15 Results II: Testing the effect of low dose of the vascular promotion agent *29P* in enhancing chemosensitisation in pancreatic ductal adenocarcinoma.

15.1 Vascular promotion as a method for enhancing tumour therapy

Our previous research demonstrates that vascular promotion with low dose Cilengitide in combination with the vasodilator verapamil can be used as a method to enhance response to chemotherapy (Wong et al. 2015). In both spontaneous pancreatic tumours in the KPC mouse and orthotopically injected pancreatic cancer cells (DT6066), ldCil/Ver/Gem treated animals had increased blood vessel density and reduced tumour growth in comparison to gemcitabine alone **(published work panel of Figure 15.1)**.

However, ldCil is not orally available and therefore less convenient for use in the clinic; additionally, it has limited commercial viability as it is off-patent. Therefore, there is a need to develop novel, orally available, vascular promoting agents such as ***29P***. Herein we test ***29P*** as a vascular promoting agent in murine models of pancreatic cancer. Moreover, vascular promotion has the potential to reduce the levels of hypoxia in tumour tissue. As hypoxia shifts immune cell infiltration towards tolerance (Vito, El-Sayes, and Mossman 2020) and hinders immunotherapy (Noman et al. 2019), we initially aimed to investigate the potential to combine vascular promotion with immunotherapy.

Graphical abstract

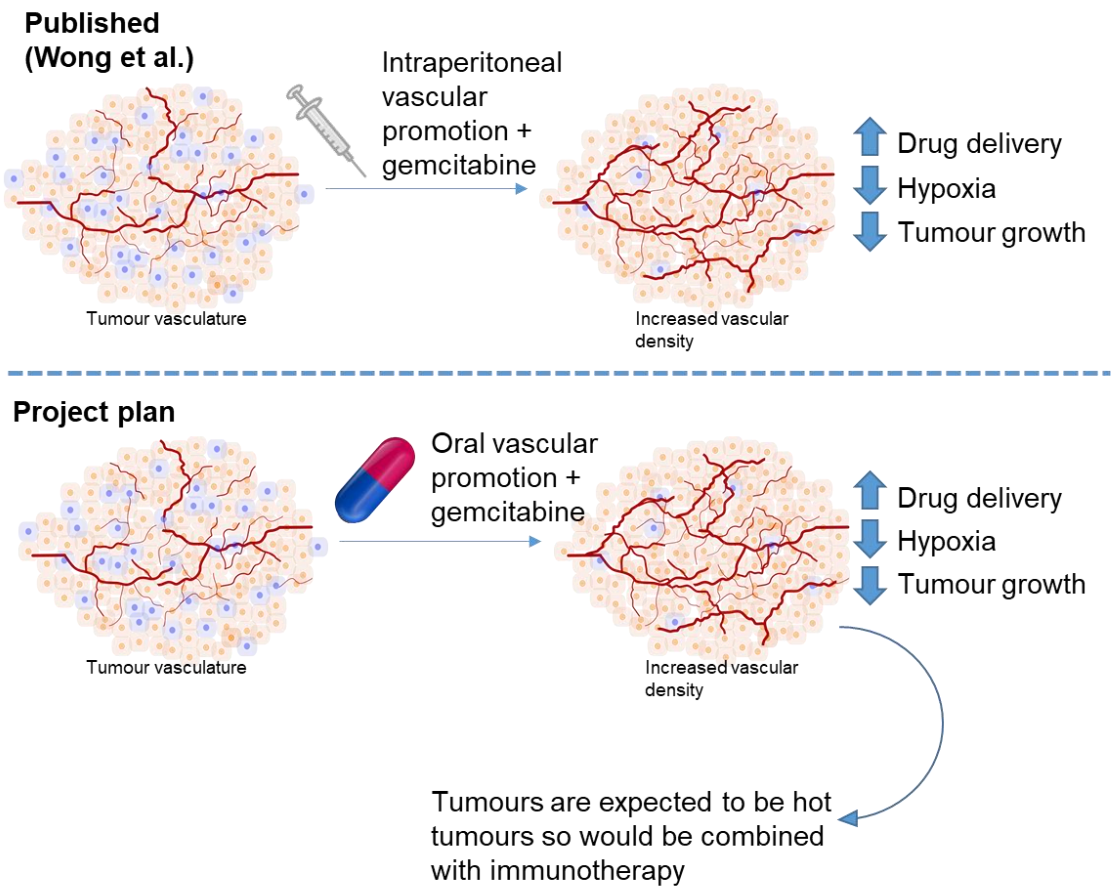

Figure 15.1 Graphical abstract 29P

In previously published work, it was shown that combination of the intraperitoneal vascular promotor low dose Cilengitide with vasodilator Verapamil and gemcitabine increases drug delivery, reduces hypoxia (represented by blue cells) and reduces tumour growth. Therefore, it was hoped that by using the oral vascular promotor, ***29P***, the blood vessel density could similarly be increased, reducing hypoxia and tumour growth. This reduction in hypoxia was expected to make tumours 'hot', having an immune-inflamed phenotype which is more sensitive to immunotherapy. However, there were problems with the oral vascular promotion strategy.

15.2 Cells were sensitised to gemcitabine by *29* treatment *in vitro*

In addition to enhancing gemcitabine delivery to tumours by increasing blood vessel density, low dose Cilengitide also had direct effects on enhancing gemcitabine sensitivity. Therefore, to see whether there was a similar sensitisation effect with ***29P***, the effects of ***29*** in combination with gemcitabine on cell survival was tested on cancer cell lines. The human non-small-cell lung cancer cell line A549 was tested by MTT assay for its relative survival at gemcitabine concentrations 0-100 nM in combination with ***29*** doses of 0.2, 2 and 20 nM compared to no ***29*** treatment **(Figure 15.2 A, B and C)**. There was no difference in response to gemcitabine between 0.2 nM 29 treatment and placebo in this cell line (**Figure 15.2 A)**. However, with 2 nM ***29***, there was significantly more cell death with 25, 50 and 75 nM gemcitabine treatment (**Figure 15.2 B)**. With 20 nM ***29***, there was increased cell death with 50 or 75 nM ***29*** compared to placebo (**Figure 15.2 C)**. This result suggests that, in the case of the A549 cell line, ***29*** may enhance gemcitabine delivery to the cells.

In the TB32048 KPC pancreatic cancer cell line, there was significantly more cell death in cells treated with 25 nM or 50 nM gemcitabine when treated with 20 nM ***29P*** compared to placebo. There were, however, no differences in cell death in response to gemcitabine with 2 nM ***29*** treatment or to 75 or 100 nM gemcitabine treatment with 20 nM ***29*** **(Figure 15.2 D)**. In DT60066 cells at low passage, cells were significantly more sensitive to 50 nM gemcitabine when treated with 20 nM ***29,*** but at all other doses of ***29*** and gemcitabine, there were no differences in sensitivity **(Figure 15.2 E)**. It is noteworthy that these low pass DT6066 cells appeared to be less resistant to Gemcitabine treatment overall. In contrast, high passage DT6066 cells were sensitised to 50 nM gemcitabine treatment by 2 nM ***29*** and to 100 nM gemcitabine treatment by 20 nM ***29*** **(Figure 15.2 F)**. Therefore, in the pancreatic cancer cells (TB32048 and DT6066), there was a sensitisation to gemcitabine at certain doses, but the sensitisation was not as consistent as in the A549 line. Additionally, it was unexpected that high passage DT6066 cells were less gemcitabine sensitive overall than low passage.

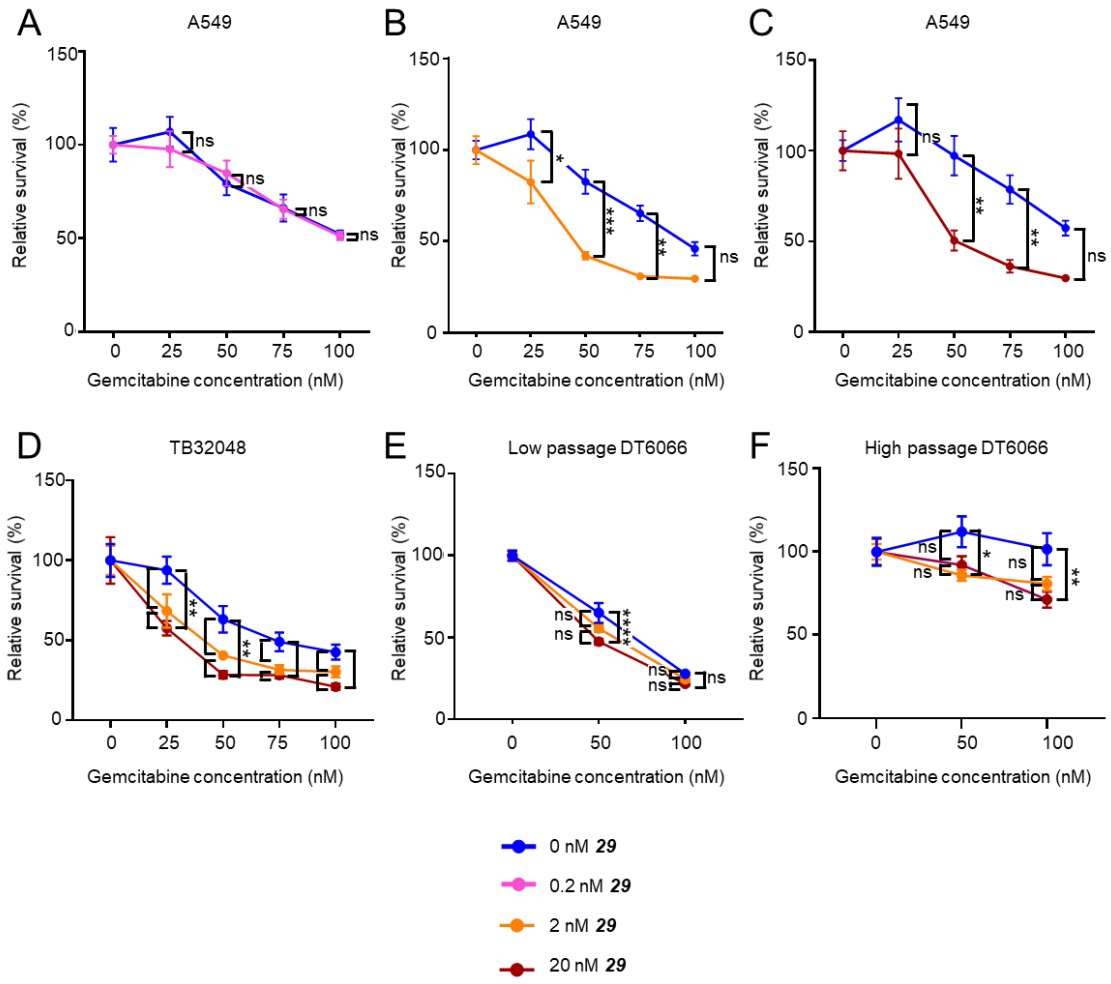

Figure 15.2 Cell sensitivity to gemcitabine is affected by *29 in vitro*

A-C on A549 cells, data kindly provided by Dr José Manuel Muñoz Félix, Barts Cancer Institute. Relative cell survival of A549 cells treated with 0-100 nM gemcitabine and (A) 0.2 nM ***29*** vs placebo, (B) 2 nM ***29*** vs placebo or (C) 20 nM ***29*** vs placebo. (D) Relative cell survival of TB32058 cells treated with 0-100 nM gemcitabine and 0, 2 or 20 nM ***29***, all differences not labelled were not significantly different (E) Relative cell survival of low passage DT6066 cells treated with 0-100 nM gemcitabine and 0, 2 or 20 nM ***29*** (F) Relative cell survival of high passage DT6066 cells treated with 0-100 nM gemcitabine and 0, 2 or 20 nM ***29***. N=6 wells of a 96 well plate for A, B and C, N=10 wells for D, N=30 wells of a 96 well plate for E, N=18 wells of a 96 well plate for F. Analysed by 2-way ANOVA, ns, not significant (P>0.05), **P ≤ 0.01, ***P ≤ 0.001, **** P <0.0001.

15.3 *29P* does not alter tumour volume or in TB32048 orthotopically injected tumours compared to gemcitabine treatment alone

The initial experimental aim was to establish whether the triple combination of ldCil/Ver/Gem75 could be simplified to ***29P*** and gemcitabine giving a similar level of vascular promotion and tumour growth reduction. Verapamil is a vasodilator, so it may enhance the drug delivery but does not directly contribute to vascular promotion. Therefore, we removed verapamil from the dosing strategy and compared ***29P*** and gemcitabine once or twice per week to gemcitabine once or twice per week or placebo.

The orthotopic model of pancreatic cancer used by Wong et al. was DT6066 cells injected into the pancreas. The DT6066 cell line is derived from a mouse harbouring *Kras* and *P53* mutations (KP mouse) where a tumour arose in the pancreas by chance rather than the KPC model where the mutations are driven to the pancreas by *Pdx-1-Cre* mutation. The cells grow poorly in females and were derived from mixed background (C57bl6/129sv), so they must be injected into male WT mix animals. Therefore, as a newer cell line (TB32048) was available, which was derived from a true KPC animal and could be injected into C57 females, we began using orthotopically injected TB32048 cells as a model of pancreatic cancer.

1000 TB32048 cells were injected orthotopically into the pancreas of female wildtype C57bl6J mice. After 20 days of treatment, tumours were imaged by MRI and treated for 19 days before harvesting for IHC or FACs analysis **(Figure 15.3 A**). MRI showed tumours at 20 days were similar volumes (mean volume of 163.5mm^3, sem 20.12) **(Figure 15.3 B)**. To determine the optimum dosing strategy of ***29P*** and gemcitabine, mice were given 75 mg/kg gemcitabine once or twice per week either as a monotherapy or in combination with 250 µg/kg ***29P***. It was expected that gemcitabine would have little effect on tumour volumes as pancreatic tumours are typically gemcitabine resistant (Olive, Jacobetz, Davidson, Gopinathan, McIntyre, Honess, Madhu, Goldgraben, Caldwell, Allard, Frese, Denicola, et al. 2009). ***29P*** was expected to increase blood vessel density and possibly reduce tumour volume. We have previously shown that ***29P*** is vascular promoting (Weinmuller et al. 2017), and the vascular promoting agent Cilengitide increases chemotherapy delivery to tumours reducing their volume (Wong et al. 2015).

After 19 days of treatment, mice were culled, and tumours harvested. Final tumour volumes were significantly smaller in mice treated with gemcitabine **(Figure 15.3 C and D)** once per week compared with mice treated with placebo. This does not accurately

model clinical data as only 5-10 % of patients respond to Gemcitabine (Olive, Jacobetz, Davidson, Gopinathan, McIntyre, Honess, Madhu, Goldgraben, Caldwell, Allard, Frese, Denicola, et al. 2009). Although there were significant differences between placebo and gemcitabine treated mice, ***29P*** conferred no additional tumour reduction, and ***29P*** treatment did not produce significantly different tumour volumes to gemcitabine alone. Necropsies revealed metastases and abnormalities in all treatment groups but most frequently in mice treated with gemcitabine **(Figure 15.3 E)**. Overall, this schedule of ***29P*** had no significant effect on tumour growth.

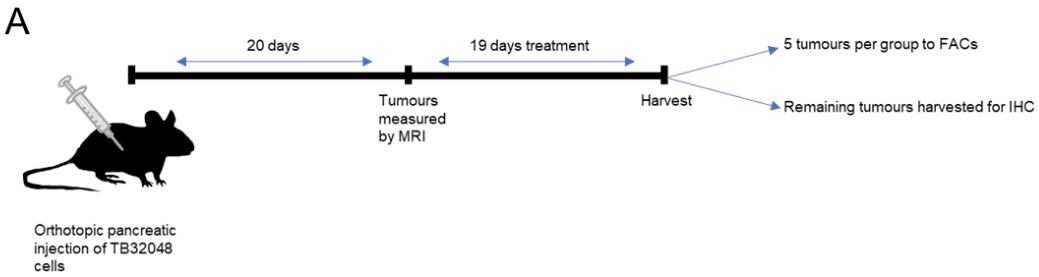
A
20 days
19 days treatment
5 tumours per group to FACs
Tumours measured by MRI
Harvest
Remaining tumours harvested for IHC
Orthotopic pancreatic injection of TB32048 cells

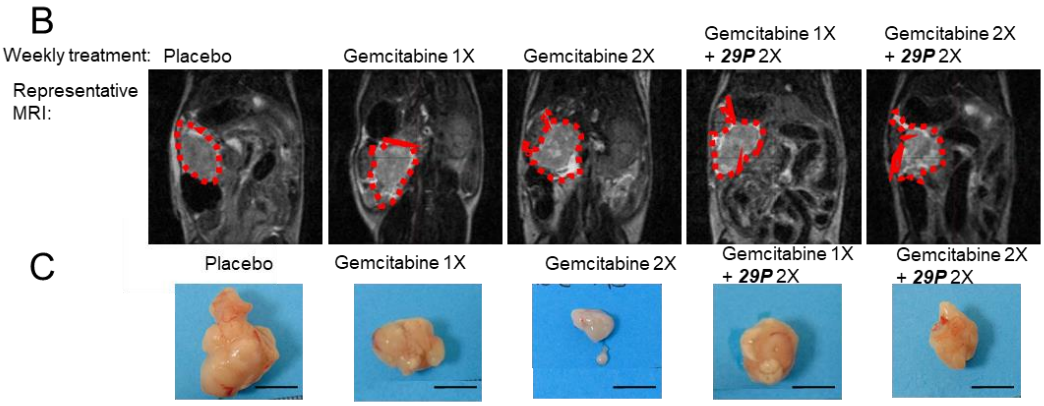
B
Weekly treatment:
Placebo
Gemcitabine 1X
Gemcitabine 2X
Gemcitabine 1X + 29P 2X
Gemcitabine 2X + 29P 2X
Representative MRI:
C
Placebo
Gemcitabine 1X
Gemcitabine 2X
Gemcitabine 1X + 29P 2X
Gemcitabine 2X + 29P 2X

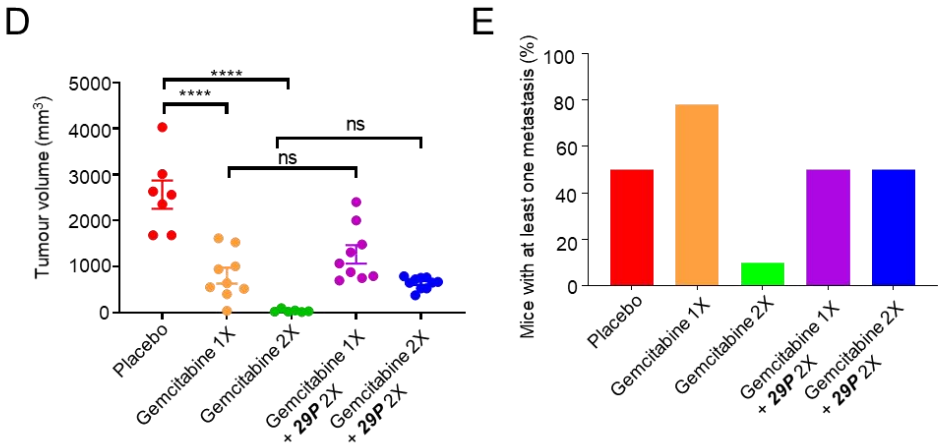
D
Tumour volume (mm3)
5000
4000
3000
2000
1000
0
****
****
ns
ns
Placebo
Gemcitabine 1X
Gemcitabine 2X
Gemcitabine 1X + 29P 2X
Gemcitabine 2X + 29P 2X
E
Mice with at least one metastasis (%)
100
80
60
40
20
0
Placebo
Gemcitabine 1X
Gemcitabine 2X
Gemcitabine 1X + 29P 2X
Gemcitabine 2X + 29P 2X

Figure 15.3 The volume of pancreatic orthotopically injected TB32048 cells was reduced by gemcitabine but the addition of 29P did not further reduce the volume.

(A) Schematic of the experimental design. Placebo animals were treated with saline gavage (200 µl) twice per week and saline IP (100 µl) twice per week. Gemcitabine animals were treated with saline gavage (200 µl) twice per week and gemcitabine in saline, 75 mg/kg IP (100 µl) once or twice per week. Gemcitabine + ***29P*** animals were treated with ***29P*** gavage, 250 µg/kg (200 µl) twice per week and gemcitabine in saline, 75 mg/kg IP (100 µl) once or twice per week. (B) Tumours were confirmed and their volumes estimated on day 20 by MRI with a T2 scan confirming consistent tumour sizes across groups before treatment. (C) After 19 days treatment, animals were culled and tumours weighed showing significantly smaller tumours in Gemcitabine treated mice than placebo but no further change with ***29P***. N numbers were 7, 9, 8 (reduced to 6 by exclusion of outliers by ROUT, Q=1 %) 9 and 10 for placebo, gemcitabine 1X, gemcitabine 2X, gemcitabine 1X + ***29P*** 2X and gemcitabine 2X + ***29P*** 2X respectively. (D) Representative tumours from each treatment group. (E) Percentage of mice with at least one metastasis visible at necropsy. Tumour volume analysed with a one-way ANOVA. ns, not significant (P>0.05), **** P <0.0001. Scale bar represents 1cm.

15.4 Blood vessel quantification

Previously published work demonstrated a vascular promotion effect of ***29P*** on both *ex vivo* aortic ring assays and an *in vivo* subcutaneous LLC model (Weinmuller et al. 2017). In addition, unpublished data in our group has shown that ***29P*** has vascular promoting effects on KP lung tumours, in this model, it has also been shown to enhance checkpoint blockade immunotherapy. It therefore was expected that ***29P*** would increase the number of tumour blood vessels, and analysis of blood vessels was performed by endomucin staining of tumour sections from each treatment group **(Figure 15.4 A)**. Total vessels were counted **(Figure 15.4 A and B),** showing no significant differences between treatment groups suggesting that in this model, using this dosing strategy, ***29P*** treatment did not work successfully as a vascular promotor.

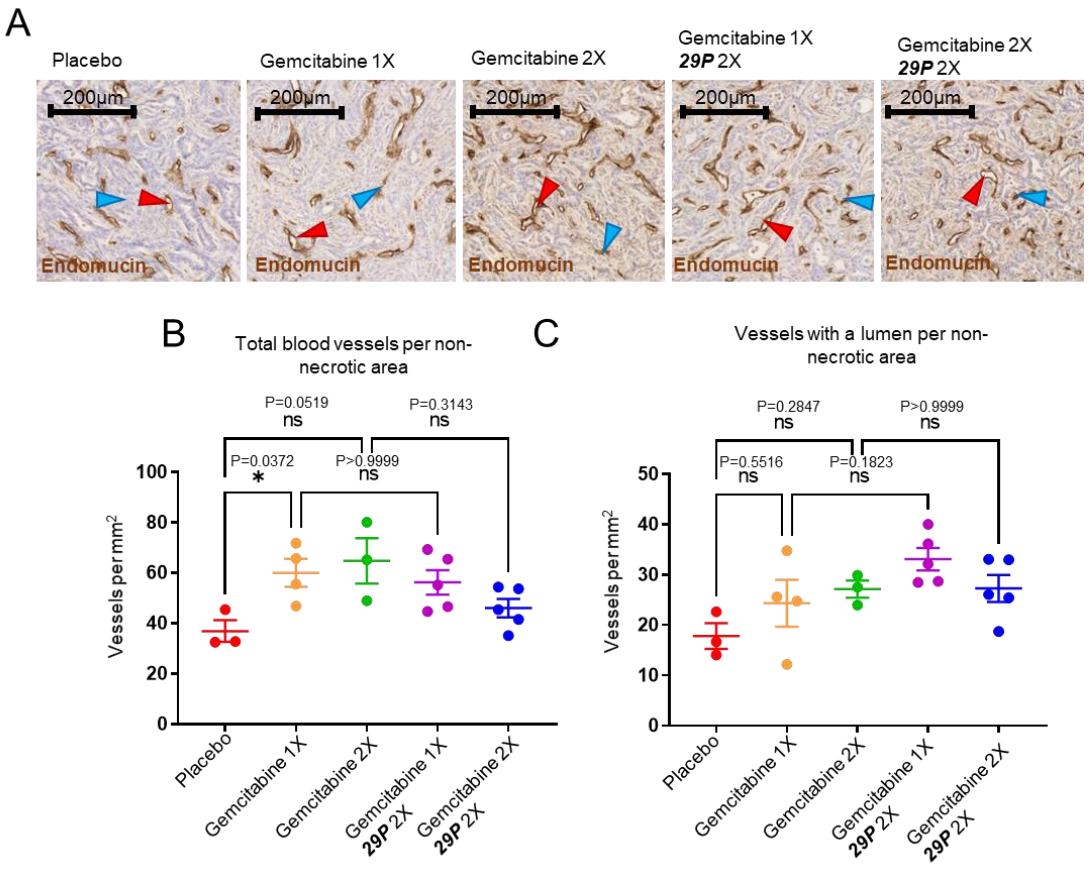
A
Placebo
Gemcitabine 1X
Gemcitabine 2X
Gemcitabine 1X
29P 2X
Gemcitabine 2X
29P 2X
200µm
Endomucin
B
Total blood vessels per non-necrotic area
Vessels per mm2
P=0.0519
ns
P=0.3143
ns
P=0.0372
*
P>0.9999
ns
C
Vessels with a lumen per non-necrotic area
P=0.2847
ns
P>0.9999
ns
P=0.5516
ns
P=0.1823
ns
Placebo
Gemcitabine 1X
Gemcitabine 2X
Gemcitabine 1X 29P 2X
Gemcitabine 2X 29P 2X

Figure 15.4 The blood vessel density was not affected but the treatment regime.

(A) Endomucin staining was used to stain blood vessels and those with a visible lumen (red arrowheads) and without (blue arrowheads) were quantified for each treatment group. (B) There was no significant difference between treatment groups for the total number of blood vessels per non-necrotic area with the exception of increased blood vessel density in gemcitabine treated tumours compared to placebo. (C) There were also no significant differences in the density of lumenated vessels. Total vessels analysed with Kruskal-Wallis, vessels with a visible lumen analysed with a one-way ANOVA. * $P < 0.05$ ns, not significant. For B and C, N=3, 4, 3, 5 and 5 for placebo, gemcitabine 1X, gemcitabine 2X, gemcitabine 1X + ***29P*** 2X and gemcitabine 2X + ***29P*** 2X respectively.

15.5 TB32048 vs DT6066 and gemcitabine sensitivity

Although the TB32048 model was chosen as it is a KPC cell line and can be orthotopically injected into C57bl6 mice of either sex, the TB32048 cells grew much more rapidly *in vivo* than the DT6066 cells used by Wong et al. (Wong et al. 2015). Therefore, the choice of cell line may justify the lack of reduction in tumour weight or increase in blood vessel density with vascular promotion in TB32048 tumours compared to DT6066 tumours. In addition, the TB32048 tumour weights were significantly reduced by gemcitabine treatment alone, whereas Wong et al. (Wong et al. 2015) demonstrate that the DT6066 line was not gemcitabine sensitive. This suggested greater gemcitabine sensitivity in TB32048 than DT6066. As gemcitabine sensitivity is low in patients (Olive, Jacobetz, Davidson, Gopinathan, McIntyre, Honess, Madhu, Goldgraben, Caldwell, Allard, Frese, Denicola, et al. 2009), DT6066 may better model the clinical situation.

15.6 Mice injected with DT6066 cells did not have significant differences in tumour volumes between treatment groups; however, the treatment was poorly tolerated and therefore had to be stopped early.

As ***29P*** in combination with gemcitabine in the TB32048 model of pancreatic cancer did not appear to have induced vascular promotion or enhanced gemcitabine response, we decided to more directly compare the experimental scheme with the work of Wong et al. Therefore, WT mix male animals were orthotopically injected with $1X10^6$ DT6066 tumour cells as published (Wong et al. 2015). Treatment began, in cohorts, two days after tumours were palpable (9-16 days post-injection). One cohort of animals was treated with the triple combination used by Wong et al. (3 treatments per week of gemcitabine + IdCil + verapamil) to try to recapitulate the vascular promotion demonstrated. For comparison, other treatment groups of animals were with gemcitabine + ***29P*** + verapamil, gemcitabine + ***29P***, gemcitabine alone or placebo. In each group, the treatment was administered three times per week. We planned to treat animals for three weeks (9 treatments in total), but as mice became sick, were found dead and losing weight, treatment was ceased after seven treatments and tumours harvested three weeks after the start of treatment **(Figure 15.5 A)**. With this dosing strategy and shortened treatment regime, there was no significant difference in tumour weight **(Figure 15.5 B)** between groups. It is noteworthy that the average tumour weight

in the placebo treated mice and Gemcitabine treated mice was approximately 400mg and 250mg, respectively, whereas it was approximately 3000mg and 2500mg in the experiments from Wong et al., 2015, suggesting that in my experiments that tumours had not had the chance to grow enough to see any possible difference after treatment with gemcitabine and ***29P***.

A

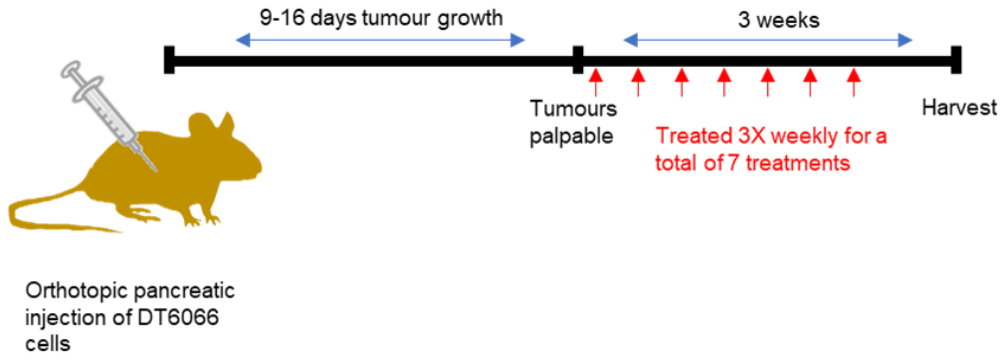

Orthotopic pancreatic injection of DT6066 cells

B

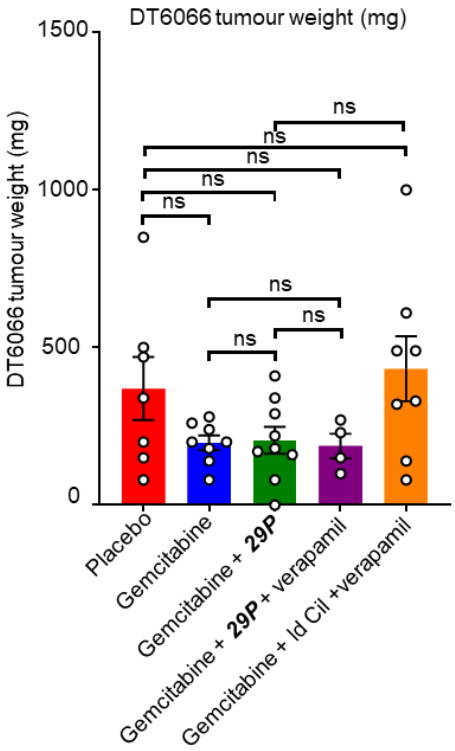

Figure 15.5 No treatment schedule significantly altered the tumour weight but treatment had to be stopped early due to poor toleration in the Gemcitabine, 29P and verapamil combination treatment.

(A) Schematic diagram of experimental design and dosing strategy. Placebo animals were treated with saline gavage (200 µl) and two saline IP injections (100 µl each), they also had sucrose water 2 % w/v. Gemcitabine animals were treated with saline gavage (200 µl), gemcitabine in saline, 75 mg/kg IP (100 µl) and a saline IP (100 µl) they also had sucrose water 2 % w/v. Gemcitabine + ***29P*** animals were treated with ***29P*** gavage, 250 µg/kg (200 µl), gemcitabine in saline, 75 mg/kg IP (100 µl) and a saline IP (100 µl) they also had sucrose water 2 % w/v. Gemcitabine + ***29P*** + verapamil animals were treated with ***29P*** gavage, 250 µg/kg (200 µl) and gemcitabine in saline, 75 mg/kg IP (100 µl) and a saline IP (100 µl) they also had 0.3 % Verapamil v/v in sucrose water 2 % w/v (protected from light). Gemcitabine + ldCil + Verapamil animals were treated with saline gavage (200 µl), gemcitabine in saline, 75 mg/kg IP (100 µl) and a ldCil IP, 50 µg/kg in saline (100 µl) they also had 0.3 % Verapamil v/v in sucrose water 2 % w/v (protected from light). All treatments were given 3 times per week with the exception of sucrose/verapamil water which was constantly available. (B) There was no difference in tumour weight between treatment groups. Tumour weight comparisons by one way ANOVA with Tukey's multiple comparisons ns, not significant ($P > 0.05$). N numbers were 7, 8, 9, 4 and 8 for placebo, gemcitabine, gemcitabine + ***29P***, gemcitabine + ***29P*** + verapamil, gemcitabine + ld Cil + verapamil respectively. No outliers excluded by ROUT, Q=1 %.

15.6.1 Blood vessel density was not impacted by either the triple combination developed by Wong et al. or equivalent 29P treatments with a shortened treatment regime

We quantified the blood vessel density and found no differences between treatment groups **(Figure 15.6)** in contrast to Wong et al. (Wong et al. 2015). However, the poor tolerance of the gemcitabine + ***29P*** + verapamil combination meant that the treatment schedule was shorter than that used by Wong et al. Therefore, the schedule needed to be optimised to demonstrate whether the effects of ***29P*** with gemcitabine is equivalent to ldCil and verapamil. Placebo (sucrose drinking water, 200 µl saline gavage, 100 µl saline IP), gemcitabine alone (sucrose drinking water, 200 µl saline gavage, 100 µl gemcitabine 75mg/kg IP), and gemcitabine + ***29P*** treatments (sucrose drinking water, 200 µl, 250 µg/kg ***29P*** gavage, 100 µl gemcitabine 75mg/kg IP) were all well-tolerated in both models used. Therefore, we were confident that animals could tolerate a schedule of one gavage and one IP three times per week in addition to sucrose water **(Figure 15.7 A)**. In addition, Wong et al. showed good toleration of the gemcitabine + ldCil + verapamil combination, which was moderately well tolerated in our hands. However, in the DT6066 model, and gemcitabine + ***29P*** + verapamil which was very poorly tolerated **(Figure 15.7 A and B)**. Therefore, we inferred that there may have been an adverse drug effect between ***29P*** and verapamil, so this treatment group was removed from future experiments.

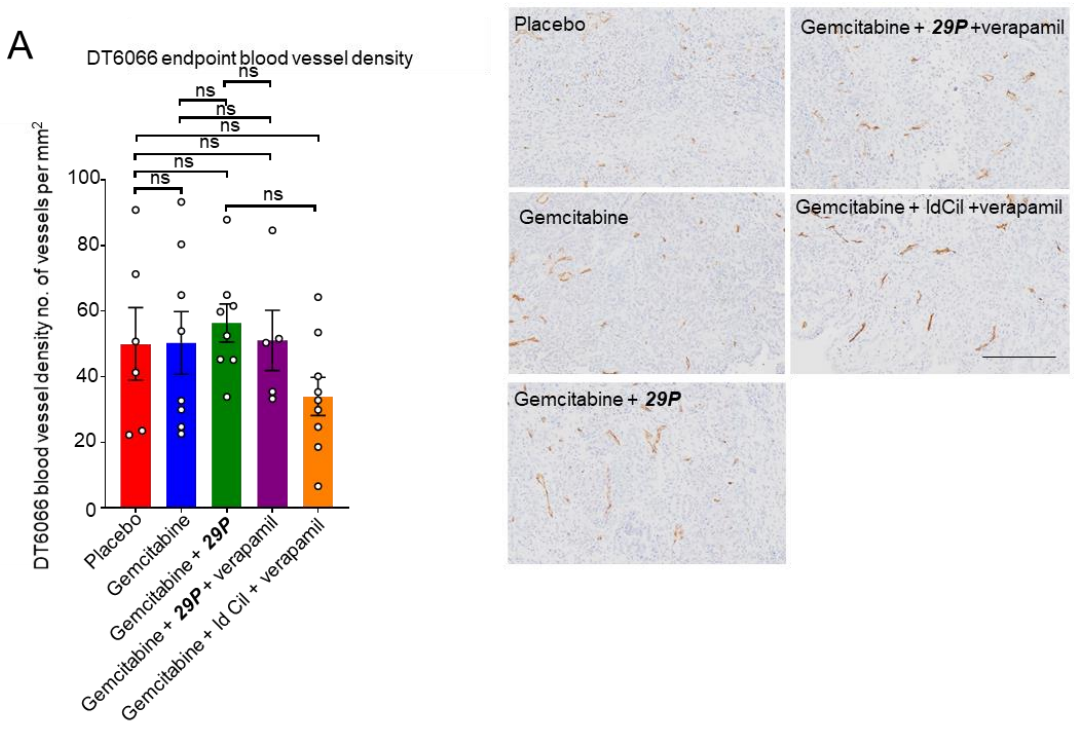

Figure 15.6 Blood vessel density delivery was not affected by any of the treatment schedules.

Animals were treated as described for figure 16.4. (A) Blood vessel density at endpoint. Bar chart shows mean number of blood vessels per mm^2 ± s.e.m, n= 6, 8, 8, 5 and 9 (no values were excluded by ROUT, Q=1 %) tumours from independent mice, for each tumour, 10 fields from one section were quantified. Images show representative fields of endomucin staining (DAB) with Hematoxylin as a nuclear marker. NS, not significant ($P > 0.05$) analysed by one way ANOVA. Scale bar 200 µm.

A

	C57Bl6J with TB32048	C57Bl6J/129 mixed background mice with DT6066
Saline IP (100 µl) + saline gavage (200 µl)	Well tolerated	Well tolerated
Gemcitabine IP (75 mg/kg, 100 µl) + saline gavage (200 µl)	Well tolerated	Well tolerated
Gemcitabine IP (75 mg/kg, 100 µl) + ***29P*** gavage (250 µg/kg, 200 µl)	Well tolerated	Well tolerated
Gemcitabine IP (75 mg/kg, 100 µl) + low dose Cilengitide IP (50 µg/kg, 100 µl) + verapamil water (0.3% in sucrose water) + saline gavage (200 µl)	Unknown	Tolerated
Gemcitabine IP (75 mg/kg, 100 µl) + ***29P*** (250 µg/kg, 200µl) + verapamil water (0.3% in sucrose water)	Unknown	Not tolerated

B

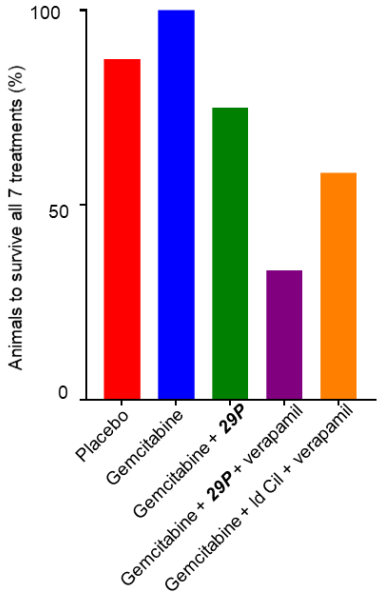

Figure 15.7 Gemcitabine + 29P + verapamil were not tolerated when given in combination.

(A) Table of known drug tolerances (B) percentage of experimental animals to reach the harvest date in the experiment described in figure 16.4 without having to be culled early or being found dead.

15.7 Longer time course experiment: DT6066 tumours showed no difference in volume and had poor tolerance of the treatment schedule.

As no vascular promotion had been demonstrated with the triple combination treatment or comparative ***29P*** treatments, when a shorter treatment schedule was used, we aimed to treat the animals for longer to establish vascular promotion. Previous experiments had suggested an adverse reaction between ***29P*** and verapamil which may necessitate a shorter treatment schedule. Therefore, we compared the gemcitabine + ld Cilengitide + verapamil triple combination with placebo, gemcitabine alone or ***29P*** and gemcitabine without verapamil.

WT mix male mice were orthotopically injected with 1 $X10^6$ DT6066 cells. 16 days after tumour cell injection, the presence of tumours was confirmed by ultrasound **(Figure 15.8 A)**. All but two of the 60 mice had tumours confirmed by ultrasound, so treatment was started two days later, and the animals without tumour were excluded. Mice were treated three times per week with i) placebo or ii) gemcitabine or iii) gemcitabine + ***29P*** or iv) gemcitabine, ldCil and verapamil as described in **Figure 15.8 A** and legend. They were treated for two weeks on, two weeks off, one week on, one week off and then harvested. The treatment was poorly tolerated, with 19 mice having to be culled or being found dead over the first two weeks due to weight loss. At harvest, there were some tumours in each group that had regressed **(Figure 15.8 B)**. However, quantifying the volume at harvest of either all tumour volumes **(Figure 15.8 C)** or tumour volumes excluding those that had regressed **(Figure 15.8 D)**, the only significant difference was a reduced tumour weight with gemcitabine compared to placebo.

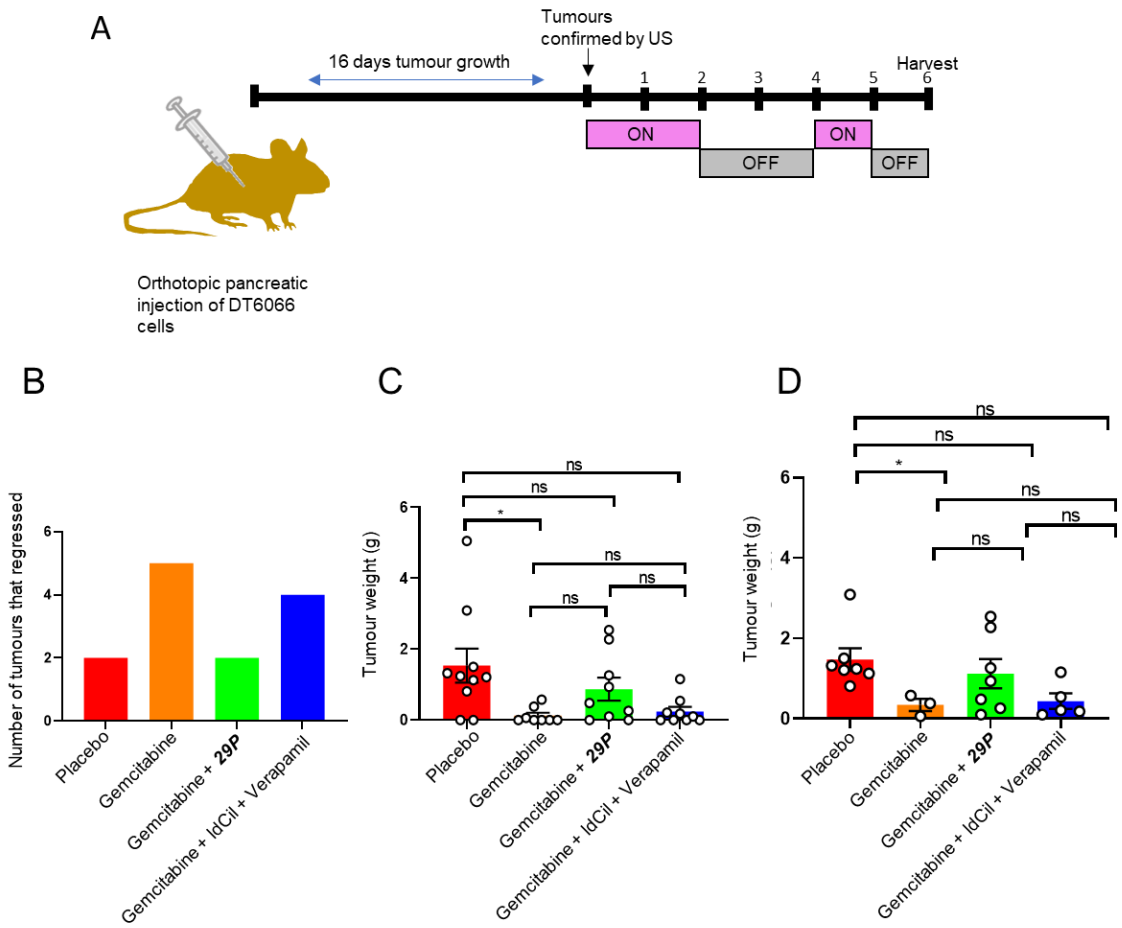
A
Tumours
confirmed by US
16 days tumour growth
Harvest
1
2
3
4
5
6
ON
OFF
ON
OFF
Orthotopic pancreatic
injection of DT6066
cells
B
Number of tumours that regressed
0
2
4
6
Placebo
Gemcitabine
Gemcitabine + 29P
Gemcitabine + IdCil + Verapamil
C
Tumour weight (g)
0
2
4
6
ns
ns
*
ns
ns
ns
Placebo
Gemcitabine
Gemcitabine + 29P
Gemcitabine + IdCil + Verapamil
D
Tumour weight (g)
0
2
4
6
ns
ns
*
ns
ns
ns
Placebo
Gemcitabine
Gemcitabine + 29P
Gemcitabine + IdCil + Verapamil

Figure 15.8 Tumour weight was reduced by gemcitabine treatment alone but not vascular promotion strategies in combination with gemcitabine.

(A) Schematic of the experimental design. Placebo animals were treated with saline gavage (200 µl) and saline IP (100 µl), they also had sucrose water 2 % w/v. Gemcitabine animals were treated with saline gavage (200 µl) and gemcitabine in saline, 75 mg/kg IP (100 µl) and they also had sucrose water 2 % w/v. Gemcitabine + ***29P*** animals were treated with ***29P*** gavage, 250 µg/kg (200 µl) and gemcitabine in saline, 75 mg/kg IP (100 µl) and they also had sucrose water 2 w/v. Gemcitabine + ldCil + Verapamil animals were treated with saline gavage (200 µl), gemcitabine in saline, 75 mg/kg IP (100 µl) and a ldCil IP, 50 µg/kg in saline (100 µl) they also had 0.3 % Verapamil v/v in sucrose water 2 % w/v (protected from light). All treatments were given 3 times per week with the exception of sucrose/verapamil water which was constantly available. All treatments were given two weeks on, two weeks off, one week on, one week off. (B) Number of tumours in each group that regressed. (C) Tumour weight at harvest was reduced by gemcitabine alone but not in combination with vascular promotion when compared to placebo. N=10, 10 (reduced to 8 by exclusion of outliers by ROUT, Q=1 %), 9 and 10 (reduced to 9 by exclusion of outliers by ROUT, Q=1 %) for placebo, gemcitabine, gemcitabine + ***29P*** and gemcitabine + ldCil + verapamil respectively (D) Tumour weight at harvest excluding animals with no tumour was reduced by gemcitabine alone but not in combination with vascular promotion when compared to placebo. By exclusion of zero values, the n numbers were reduced to 8 (further reduced to 7 by exclusion of outliers by ROUT, Q=1 %) , 3, 7 and 5 for placebo, gemcitabine, gemcitabine + ***29P*** and gemcitabine + ldCil + verapamil respectively. C and D are analysed with a one-way ANOVA. ns, not significant ($P > 0.05$), *$P < 0.05$.

15.7.1 Survival was not significantly reduced by treatment, but the animal weight was significantly reduced by gemcitabine treatment in all combinations

As detailed in the previous section, treatment using was poorly tolerated, with 19 mice having to be culled due to weight loss or being found dead over the first two weeks. There was no significant difference in survival between the groups by log-rank (mantel-cox) test with Bonferroni correction **(Figure 15.9 A)**. However, the weight of the animals throughout treatment was reduced in all treatment groups compared to placebo **(Figure 15.9 B)**. Each of these animals was treated with gemcitabine (75mg/kg 100µl IP) three times per week in addition to sucrose water (with or without verapamil) and 200µl gavage (saline or 250 µg/kg ***29P***). This suggests that the tolerance of gemcitabine was poor. This was unexpected as it appeared to be well tolerated in Wong et al.'s triple combination. However, we added a saline gavage to this group due to the comparison with the ***29P*** treated group, which required gavage. In some animals, gavage is associated with increased stress and weight loss (Jones, Boyd, and Wallace 2016). Therefore, it is possible that serial gavages in combination with gemcitabine treatment increased stress and led to poor toleration of the treatment regimes.

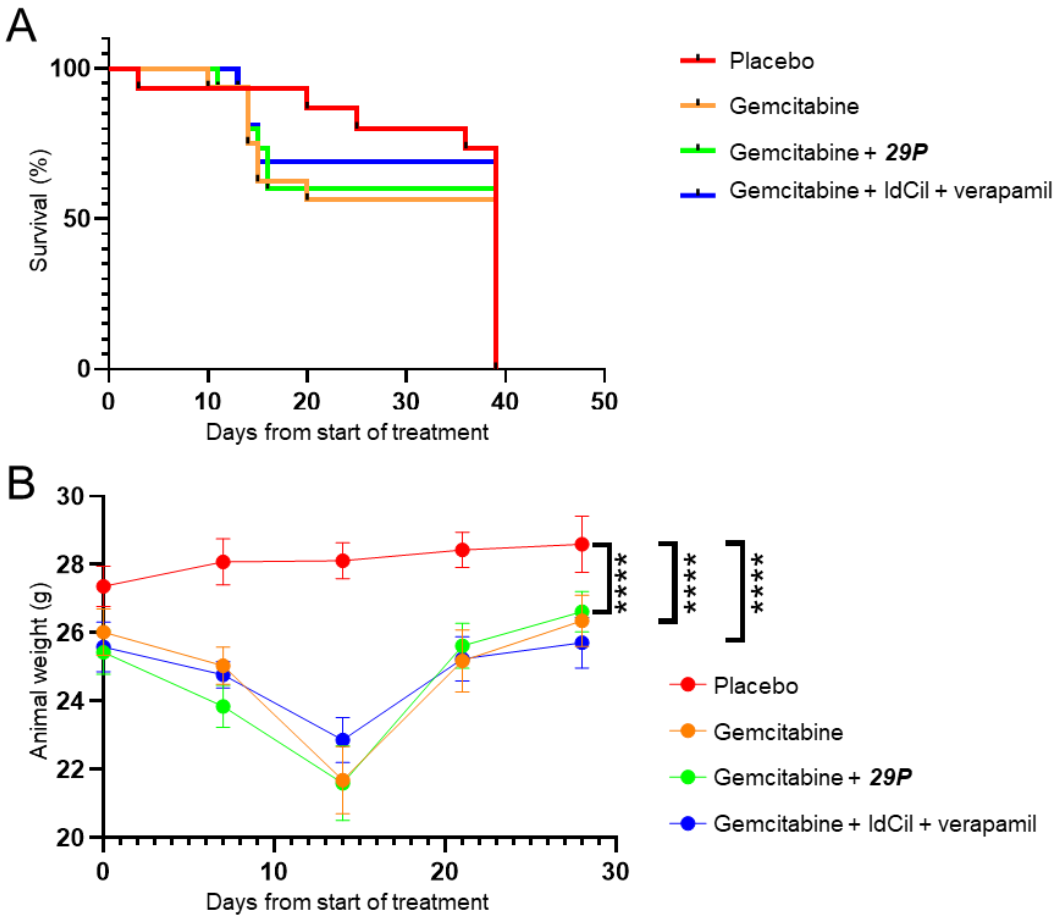

Figure 15.9 Survival was not significantly reduced by treatment but the animal weight was significantly reduced by gemcitabine treatment in all combinations.

(A) Survival was not significantly different between groups analysed by log-rank (mantel-cox) test with Bonferroni correction. The initial number of animals in each group was 15, 16, 15 and 16 for placebo, gemcitabine, gemcitabine + ***29P*** and gemcitabine + IdCil + verapamil respectively. (B) Animal weight was significantly lower in all treatment groups compared to placebo analysed with 2-way ANOVA ****P<0.00001. The n number was reduced with time as animals had to be culled as indicated in 16.8 A.

15.8 Tumour volume was reduced by gemcitabine treatment but not further reduced by combination with *29P* given two or three times per week

It seemed possible that the stress of being gavaged three times per week was causing animals too much stress for them to tolerate gemcitabine treatment. Therefore, we compared animals with two or three ***29P*** gavages per week in combination with gemcitabine to animals treated with gemcitabine or placebo in addition to saline gave twice per week. Animals were orthotopically implanted with DT6066 cells and tumours confirmed by US after 14 days. Following tumour confirmation, animals were treated three times per week for three weeks, imaged by US again, and all mice culled at 21 days when tumours were harvested for volume analysis. Doses and dosing strategy are detailed in **Figure 15.10 A** and legend.

The percentage change in tumour volume by US imaging was significantly lower in the gemcitabine and gemcitabine + ***29P*** twice per week groups compared to placebo **(Figure 15.10 B)**. However, there was no reduction in tumour growth in animals treated with either ***29P*** dosing strategy in combination with gemcitabine compared to gemcitabine alone. This suggested that tumours responded to gemcitabine, but 29P treatment did not appear to further enhance gemcitabine response. This response to gemcitabine was not expected as both in published use of this model (Wong et al. 2015) and in pancreatic cancer in the clinic (Olive, Jacobetz, Davidson, Gopinathan, McIntyre, Honess, Madhu, Goldgraben, Caldwell, Allard, Frese, DeNicola, et al. 2009) minimal response to gemcitabine is recorded.

However, the tolerance of the treatment was good, with the majority of animals being culled due to the tumour in the placebo group rather than the treatment. Animals treated with ***29P*** three times and gemcitabine had increased survival compared to placebo **(Figure 15.10 C)**.

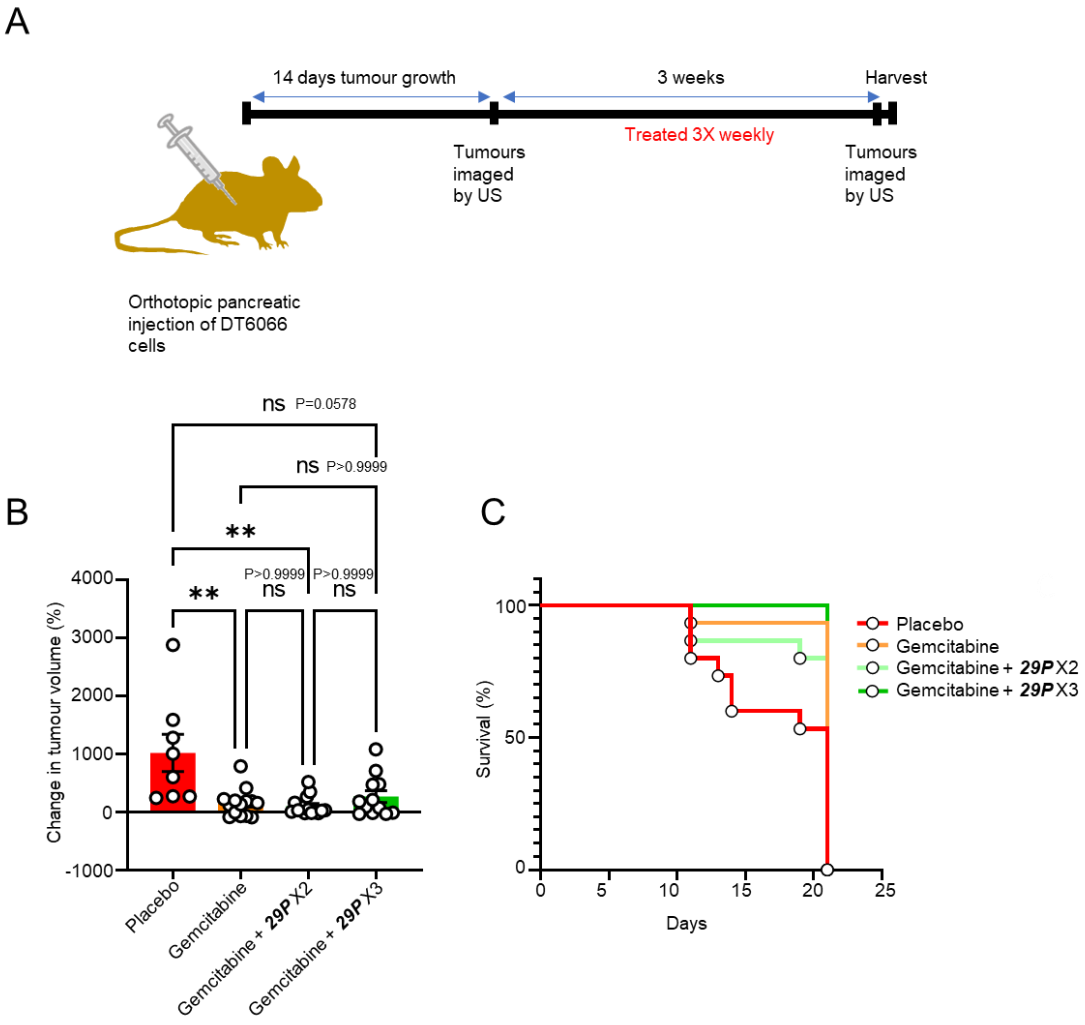
A
14 days tumour growth
3 weeks
Harvest
Treated 3X weekly
Tumours imaged by US
Tumours imaged by US
Orthotopic pancreatic injection of DT6066 cells
B
ns P=0.0578
ns P>0.9999
**
**
P>0.9999
ns
P>0.9999
ns
Change in tumour volume (%)
4000
3000
2000
1000
0
-1000
Placebo
Gemcitabine
Gemcitabine + 29P X2
Gemcitabine + 29P X3
C
Survival (%)
100
50
0
0
5
10
15
20
25
Days
Placebo
Gemcitabine
Gemcitabine + 29P X2
Gemcitabine + 29P X3

Figure 15.10 Tumour volume was reduced by gemcitabine but not 29P treatment and survival was increased by 29P three times per week and Gemcitabine.

(A) Schematic diagram of experimental design and dosing strategy. Placebo animals were treated with saline gavage (200 µl) twice per week and saline IP (100 µl) three times per week. Gemcitabine animals were treated with saline gavage (200 µl) twice per week and gemcitabine in saline, 75 mg/kg IP (100 µl) three times per week. Gemcitabine + ***29P*** X2 animals were treated with ***29P*** gavage, 250 µg/kg (200 µl) twice per week and gemcitabine in saline, 75 mg/kg IP (100 µl) three times per week. Gemcitabine + ***29P*** X3 animals were treated with ***29P*** gavage, 250 µg/kg (200 µl) three times per week and gemcitabine in saline, 75 mg/kg IP (100 µl) three times per week. (B) Tumour volume was reduced in animals treated with gemcitabine or ***29P*** twice and gemcitabine compared to placebo. (C) Survival was significantly longer in animals treated with ***29P*** X3 and gemcitabine compared to placebo. Tumour volume analysis, n=8, 14, 16 (reduced to 14 by exclusion of outliers by ROUT, Q=1 %) and 12 independent mice, one tumour per animal for placebo, Gemcitabine, Gemcitabine + ***29P*** X2 and gemcitabine + ***29P*** X3 treated animals respectively. Tumour volume compared by Kruskal-Wallis, ns, not significant ($P > 0.05$), **$P \leq 0.01$. Survival analysed by log-rank (mantel-cox) test with Bonferroni correction. Animals treated with gemcitabine + ***29P*** X3 survived significantly longer than placebo with a family-wise significance level over 5 %, all other treatment groups were not significantly different to placebo.

15.8.1 Tumour blood vessel density and perfusion were not impacted by treatment with *29P* twice or three times per week

Animals treated as described for **Figure 15.10** were analysed for blood vessel density and perfusion. Tumours harvested two days after the cessation of treatment were sectioned. Tumour sections were stained for endomucin (green) with DAPI as a counterstain **(Figure 15.11 A)**. Total blood vessel density (ie sum of luminated and non-luminated) was not different between the different treatment groups. In addition, 10 minutes before harvest, animals were injected IV with PE-PECAM. Sections from these tumours were stained for endomucin and counterstained with DAPI and imaged as described (methods). Quantification of the percentages of perfused blood vessels showed no differences between treatment groups **(Figure 15.11 B)**.

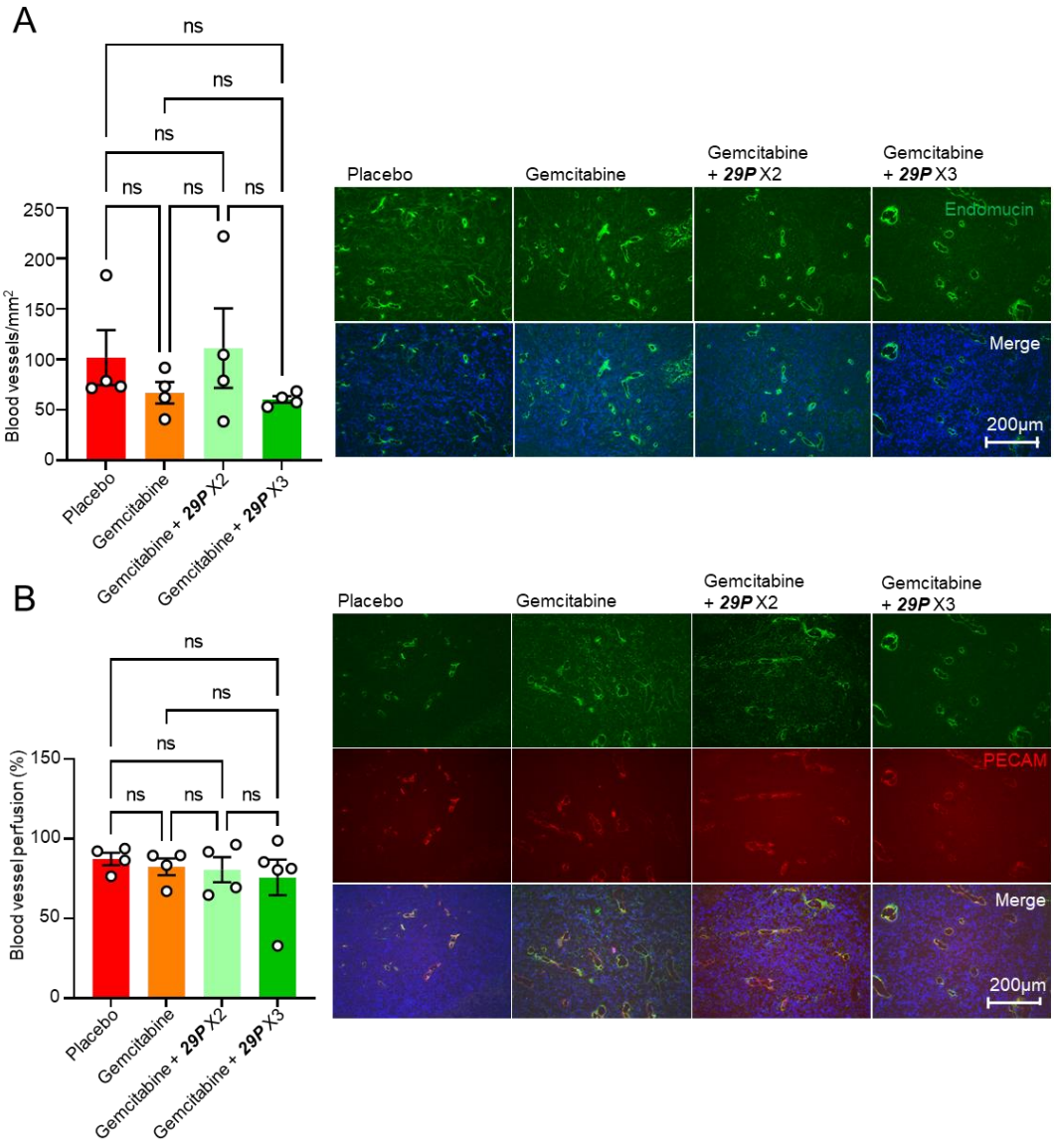
A
ns
ns
ns
ns
ns
ns
250
200
150
100
50
0
Blood vessels/mm2
Placebo
Gemcitabine
Gemcitabine + 29P X2
Gemcitabine + 29P X3
Placebo
Gemcitabine
Gemcitabine + 29P X2
Gemcitabine + 29P X3
Endomucin
Merge
200µm
B
ns
ns
ns
ns
ns
ns
150
100
50
0
Blood vessel perfusion (%)
Placebo
Gemcitabine
Gemcitabine + 29P X2
Gemcitabine + 29P X3
Placebo
Gemcitabine
Gemcitabine + 29P X2
Gemcitabine + 29P X3
PECAM
Merge
200µm

Figure 15.11 Blood vessel density and perfusion were not affected by gemcitabine or 29P treatment.

Animals were treated as described for figure 16.8. (A) Blood vessel density of tumours harvested two days after the last treatment. Bar chart shows mean number of blood vessels per mm^2 ± s.e.m, n= 4, 4, 4 and 5 (reduced to 4 by exclusion of outliers by ROUT, Q=1 %) for placebo, gemcitabine, gemcitabine + ***29P*** X 2 and gemcitabine + ***29P*** X 3 respectively, tumours from independent mice, for each tumour, 10 fields from one section were quantified. Images show representative fields of endomucin staining (green) with DAPI as a nuclear marker. (B) Blood vessel perfusion. Bar chart shows the percentage perfused blood vessels ± s.e.m, n= 4, 4, 4 and 5 tumours from independent mice. No values were excluded by exclusion of outliers by ROUT, Q=1 %. For each tumour, 10 fields from one section were quantified. Images show representative fields of endomucin (green) and PECAM (red) with DAPI as a nuclear marker. NS, not significant ($P > 0.05$) analysed by Kruskal-Wallis test. Scale bar 200 μm.

15.9 Gemcitabine resistant cells gifted to us were significantly more gemcitabine resistant *in vitro* than either TB32048 or our original stock of DT6066 cells

In our hands, it appeared that the DT6066 cells were responding to gemcitabine at 75 mg/kg when grown *in vivo*. This was in contrast to the both the clinical setting (Olive, Jacobetz, Davidson, Gopinathan, McIntyre, Honess, Madhu, Goldgraben, Caldwell, Allard, Frese, DeNicola, et al. 2009) and the work of Wong et al. (Wong et al. 2015). In addition, the strong response to gemcitabine may prevent any vascular promotion from further enhancing the drug response. Therefore, we needed to adapt the model to better recapitulate the clinical response. We received some gemcitabine resistant DT6066 cells as a gift from Dr Lewis Stevens and Dr Ping Pui Wong.

After 48 h treatment with gemcitabine concentrations (0 to 100 nM), the reduction in cell number with gemcitabine treatment was significantly more in TB32048 and our original DT6066 stock than in the gemcitabine resistant cells **(Figure 15.12)**. This suggested that the new DT6066 line gifted to us was truly gemcitabine resistant in comparison to previously used cell lines and may better model the clinical setting.

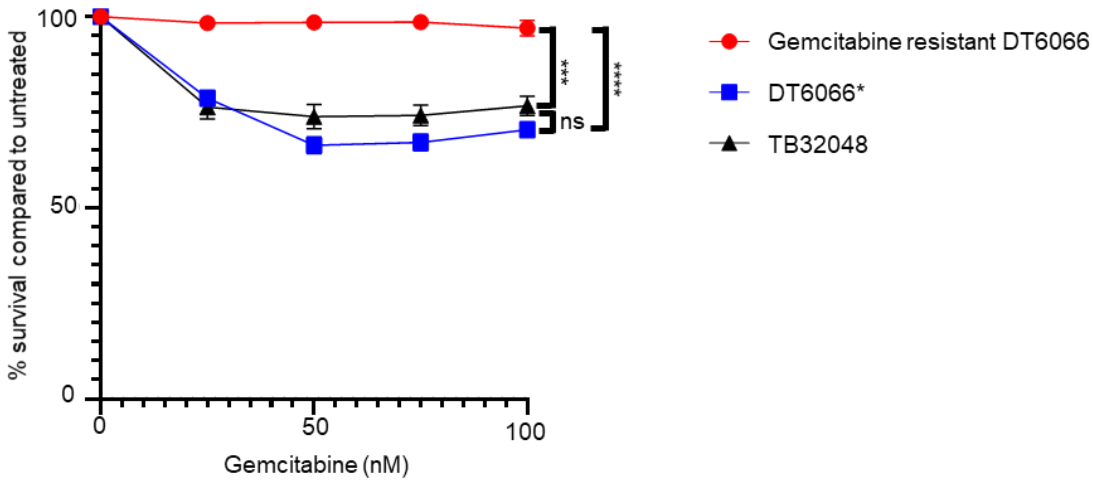

Figure 15.12 Cell death was greater in DT6066* cells and TB32048 cells than in gemcitabine resistant DT6066 cells.

Line graph of cell survival relative to total cell number analysed by intensity measures of crystal violet stains. Analysed by two-way ANOVA N=250 wells of a 24 well plate. ns, not significant ($P > 0.05$), ***$P \leq 0.001$, ****$P<0.00001$. DT6066* cells were the cells used previously in Figure 15.2 and Figures 15.5-15.11.

15.10 The weight and blood vessel density of orthotopically implanted gemcitabine resistant DT6066 tumour cells at harvest were not impacted by treatment with different doses of *29P*

Using ***29P*** at 250 µg/kg, we had not observed vascular promotion. This dose was used due to recommendations based on unpublished work in a lung tumour model in our group. However, the published dose used in subcutaneous models was 50 µg/kg (Weinmuller et al. 2017). However, as the response may be different in a pancreatic model to either the lung or subcutaneous model, we hypothesised that the dose may have needed to be adjusted to induce vascular promotion.

Therefore, we orthotopically injected animals with gemcitabine resistant DT6066 cells and confirmed tumour initiation by US after 14 days. Animals were treated three times per week with ***29P*** at 250, 150 or 50 µg/kg or placebo saline gavage **(Figure 15.13 A)**. Mice were culled 12 days after the start of treatment. However, neither the tumour volume **(Figure 15.13 B)** or the blood vessel density **(Figure 15.13 C)** were significantly changed by any of the ***29P*** doses compared to placebo at this stage.

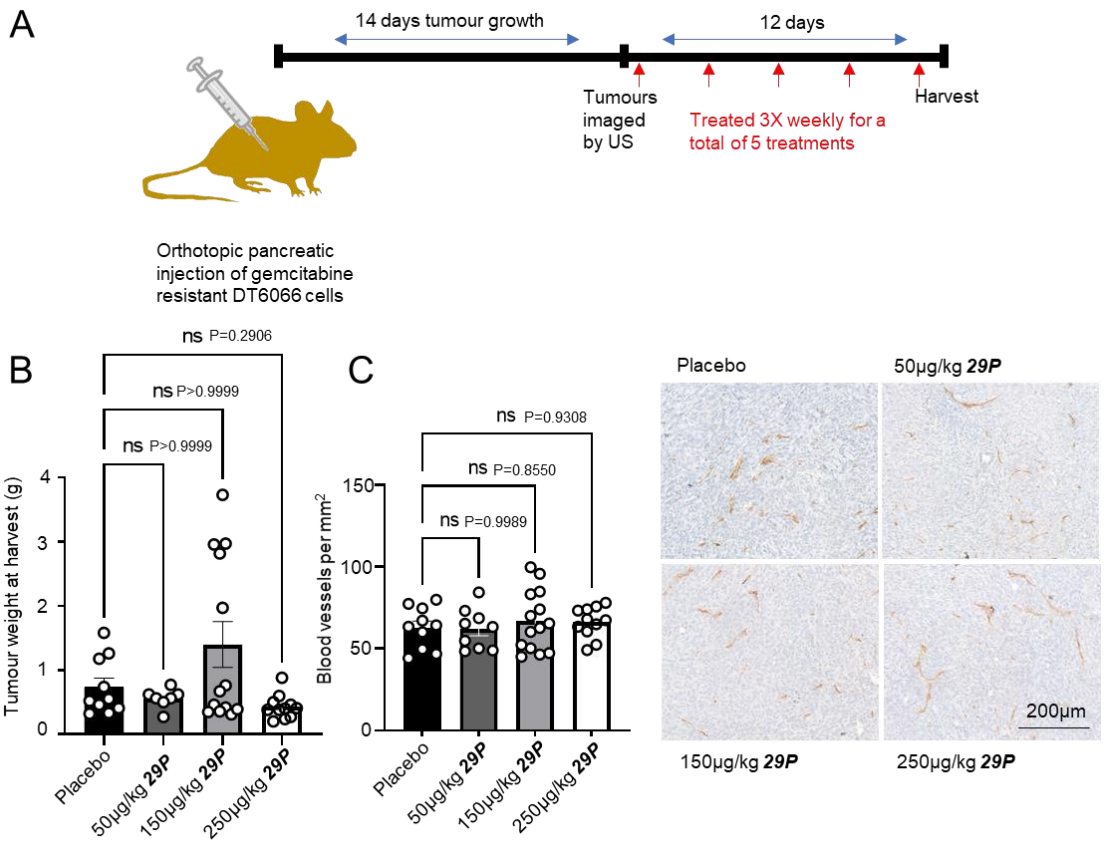

Figure 15.13 Tumour volume and blood vessel density were not affected by different doses of *29P*.

(A) Schematic diagram of experimental design and dosing strategy. Placebo animals were treated with saline gavage (200 µl). 50 µg/kg ***29P*** animals were treated with 50 µg/kg ***29P*** in saline by gavage (200 µl). 150 µg/kg ***29P*** animals were treated with 150 µg/kg ***29P*** in saline by gavage (200 µl). 250 µg/kg ***29P*** animals were treated with 250 µg/kg ***29P*** in saline by gavage (200 µl). All treatments were given three times per week. (B) Tumour volume was not affected by different doses of ***29P***, bar chart shows mean tumour weight ± s.e.m, n= 10, 8 (reduced to seven by exclusion of outliers by ROUT, Q=1 %), 13, 12 (reduced to 11 by exclusion of outliers by ROUT, Q=1 %) tumours from independent mice. Analysed by Kruskal-Wallis, ns, not significant ($P > 0.05$). (C) Total tumour blood vessel density (ie for both lumenated and closed vessels summed) was not affected by different doses of ***29P***. Bar chart shows mean number of blood vessels per mm^2 ± s.e.m, n= 10, 9, 14 and 11 tumours from independent mice analysed by 1- way ANOVA, ns, not significant ($P > 0.05$).

15.11 *29P* and Gemcitabine treatment did not impact tumour volume or animal survival in the KPC

The KPC model is considered to be the most accurate model of human pancreatic cancer (Lee et al. 2016; Hingorani et al. 2005). Therefore, in parallel to our orthotopic experiments, we also ran a KPC experiment to establish the effects of ***29P*** and gemcitabine alone or in combination on tumour growth in this model. The treatment schedule was based on the published schedule used by Wong et al. (Wong et al. 2015). Animals were treated three times per week for three weeks, followed by three cycles of a week on week off treatment schedule and then five weeks off treatment before harvest **(Figure 15.14 A)** unless they had to be culled early due to sickness.

In animals that were treated for at least seven weeks, there was no difference in tumour volume between treatment groups **(Figure 15.14 B)**. There was also no difference in survival between treatment groups **(Figure 15.14 C).** However, there is considerable variation within the KPC model, and the number of animals is, therefore, likely to be too low to confirm that there is no difference with treatment.

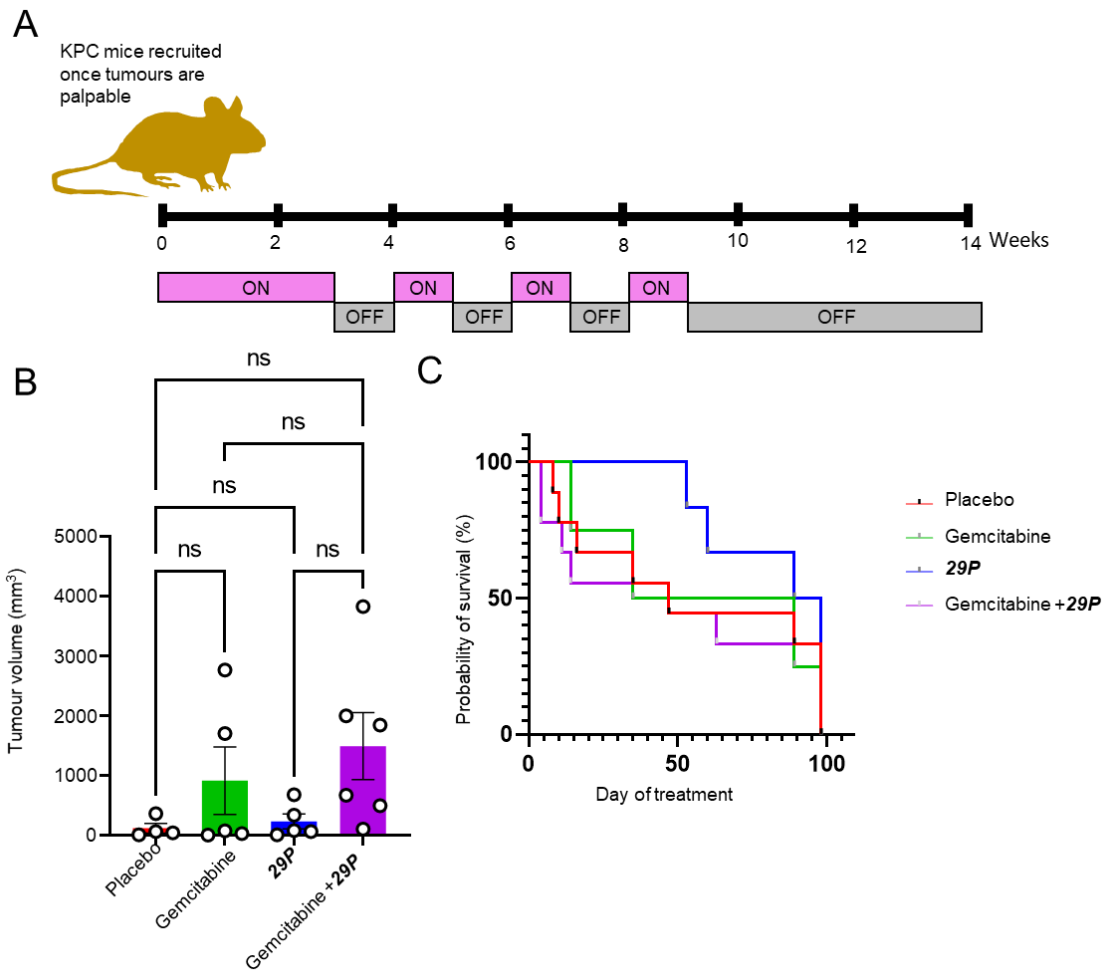

Figure 15.14 KPC tumour volume and survival to the experimental end point were not affected by treatment with gemcitabine or *29P*.

(A) Schematic diagram of experimental design and dosing strategy. Placebo animals were treated with saline gavage (200 µl) and saline IP (100 µl). Gemcitabine animals were treated with saline gavage (200 µl) and gemcitabine in saline, 75 mg/kg IP (100 µl). ***29P*** animals were treated with ***29P*** gavage, 250 µg/kg (200 µl) and saline IP (100 µl). Gemcitabine + ***29P*** animals were treated with ***29P*** gavage, 250 µg/kg (200 µl) and gemcitabine in saline, 75 mg/kg IP (100 µl). (B) Tumour volume with placebo, ***29P***, gemcitabine or combination treatment for 7-14 weeks. Analysed by 1-way ANOVA, not significant ($P > 0.05$). N= 5 (reduced to 4 by exclusion of outliers by ROUT, Q=1 %), 5, 5 and 6 for placebo, gemcitabine, ***29P*** and gemcitabine + ***29P*** respectively. (C) Survival curve. No significant differences analysed by log-rank (Mantel-Cox) test.

15.11.1 Blood vessel density is not impacted by treatment with *29P* or gemcitabine in the KPC model of pancreatic cancer

Sections of tumours from animals treated for at least seven weeks were stained for endomucin and the blood vessel density calculated. There was no significant difference in blood vessel density between treatment groups with this number of animals **(Figure 15.15)**. However, due to the variation in the KPC model and the poor survival in this experiment, this is too few animals to confirm that there was no vascular promotion effect in these animals.

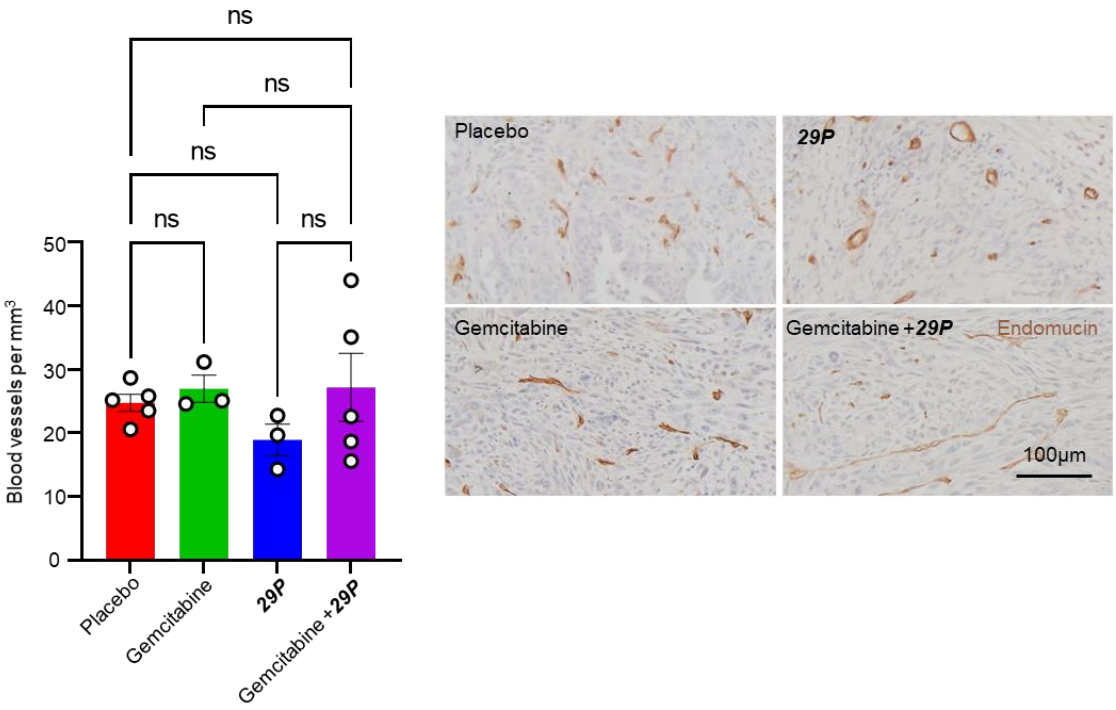

Figure 15.15 Tumour blood vessel density is not affected by treatment strategy in the KPC model.

Bar chart shows blood vessel density per mm3. Representative images show endomucin (DAB) with haematoxylin counterstain. One-way ANOVA with Šidák's multiple comparison. ns, not significant ($P > 0.05$). N= 5, 3, 3, 5 for placebo, gemcitabine, ***29P*** and gemcitabine + ***29P*** respectively. Scale bar = 100 µm.

16 Discussion II: Testing the effect of vascular promotion agent low dose *29P* in enhancing chemosensitisation in pancreatic ductal adenocarcinoma.

16.1 A major problem in this project has been optimising the right treatment model.

The KPC model, harbouring the mutations *Trp53*^{R172H}, *Kras*^{G12D} and *Pdx-1-cre*, is the most commonly used mouse model of pancreatic cancer and is widely considered to be the most accurate model of human disease (Lee et al. 2016; Hingorani et al. 2005). It is typical of human disease in terms of ascites and cachexia development (Hingorani et al. 2005), cellular morphology, poor vascularity (Jacobetz et al. 2013), fibrosis, and metastatic spread (Hingorani et al. 2005). Tumours are also immunocompetent and accurately model the immunosuppressive microenvironment of human PDAC tumours (Beatty et al. 2011). However, the model is expensive and slow to breed enough animals for large experiments. Therefore, orthotopically implanted pancreatic tumours are a good alternative, but there are variations between cell lines, and they are known to differ considerably from the KPC model in several aspects. While the KPC model spontaneously develops tumours and has a median age of five months, orthotopically injected models typically grow much faster and form tumours in around one month (Tseng et al. 2010; Spear et al. 2019). As they are faster growing, they are less stroma rich and have more tumour cells due to more rapid tumour progression, leading to more differences in structure and infiltration. The KPC model has high levels of collagen and vimentin immune infiltration and stellate cells, whereas orthotopic models typically have much lower levels (Majumder et al. 2016). Similarly, while KPC tumours are comparable to human disease in that they are well infiltrated with B cells correlating with their T cell infiltration, orthotopic TB32048 tumours have little B cell infiltration (Spear et al. 2019).

16.2 In vitro sensitisation of cancer cells to gemcitabine with *29*

Low dose Cilengitide was shown to sensitise tumour cells to gemcitabine, not just by increased delivery but also through mechanisms altering its transport and metabolism in

cancer cells (Wong et al. 2015). ***29P*** was developed based on the structure of Cilengitide and has similar properties (Weinmuller et al. 2017). Therefore, it was important to establish whether ***29P*** would directly affect tumour cell response to gemcitabine. To this end, we produced dose-response curves of cell death at different gemcitabine doses in combination with the deprotected version of ***29P***, ***29***. In the lung cancer cell line, A549, cells were sensitised to gemcitabine treatment when treated with 2 nM or 20 nM ***29*** treatment, although doses were not significant for all gemcitabine doses. In the pancreatic cancer cells TB32048 and DT6066, too, ***29*** treatment sensitised the cells to some, but not all, doses of gemcitabine. This may suggest a direct effect on gemcitabine response in pancreatic cancer cells.

Interestingly, low passage DT6066 cells were not sensitised to gemcitabine treatment at any dose tested by 2 nM ***29***, the only cell line not to be sensitised by this dose. These low passage DT6066 cells were also the most gemcitabine sensitive of the limited cell lines tested, with the number of cells surviving treatment with 100 nM gemcitabine and no ***29*** treatment, only 28 % of the number that survived with no treatment. It is not clear why there were differences in gemcitabine sensitivity between high and low passage DT6066 cells, however, it is possible this is an indication of genetic drift in the cells (Ben-David et al. 2018). Therefore, it may be that in these gemcitabine sensitive cells, the ***29*** treatment could not confer any further advantage in response to gemcitabine. Overall, there was some sensitisation to gemcitabine with ***29*** treatment, and therefore, it was hoped that ***29*** would enhance gemcitabine treatment in vivo, both through vascular promotion and direct effects.

16.3 *29P* did not impact the tumour volume or blood vessel density in TB32048 tumours. this may be due to fast-growing cells producing tumours that do not accurately mimic human PDAC.

In orthotopically injected TB32048 pancreatic tumours, 29P did not reduce tumour growth in combination with gemcitabine compared to gemcitabine alone (**Figure 15.3)**. This was unexpected as it was hoped that the 29P would act as a vascular promoter, increasing delivery of gemcitabine to the tumour and reducing tumour growth. However, blood vessel density was also not affected by 29P treatment suggesting that it did not act as a vascular promotor in the model and treatment regime used **(Figure 15.3)**. However, in this experiment, animals were only treated for 19 days which was

considerably shorter than the two months that orthotopic tumours were treated by Wong et al. (Wong et al. 2015). However, as, in our experiment, there were tumours above the home office limit at harvest, it would not have been possible to treat the animals for longer. A slower growing tumour model would be required in order to be able to treat the animals for longer.

In addition, the blood vessel density in this model was higher than in the KPC. The blood vessel density of placebo-treated TB32048 tumours in our hands was approximately 40 vessels per mm^2**,** whereas placebo-treated KPC tumours have a much lower blood vessel density of approximately ten vessels per mm^2. As human PDAC is characteristically hypovascularized (Olive, Jacobetz, Davidson, Gopinathan, McIntyre, Honess, Madhu, Goldgraben, Caldwell, Allard, Frese, Denicola, et al. 2009), the highly vascular, fast-growing TB32048 model may not be an accurate model. This may explain the lack of vascular promotion in the TB32048 model. While Wong et al. (Wong et al. 2015) only show slightly lower blood vessel density in placebo-treated DT6066 tumours than my TB32048 tumours, approximately 30 vessels per mm^2, they demonstrate successful vascular promotion in the DT6066 model, and I, therefore, moved to this slower growing tumour model.

16.4 Mice had poor tolerance of *29P* in combination with verapamil, possibly showing an adverse drug effect

When WT mix mice implanted with DT6066 tumours were treated with 250 µg/kg ***29P*** and verapamil in combination, eight of the 12 animals were found dead or had to be culled sick within two weeks of treatment and the following two weeks off treatment **(Figure 15.7)**. Similarly, four animals treated with IdCil and verapamil had to be culled within the same timeframe. The animals culled were thin with very pale liver and kidneys. This suggests poor tolerance of the drugs, which was unexpected since the treatment regime was similar to previously used regimes. I had not treated the TB32048 mice with verapamil, so I did not know how this reacted with ***29P,*** but as my mice had responded well to ***29P*** with gemcitabine and Wong et al. had a good response with IdCil, verapamil and gemcitabine treated animals, it was unexpected that the treatment was so poorly tolerated. However, there were some differences compared to previous work; as ***29P*** is oral, it was given by gavage.

Similarly, IdCil, verapamil, gemcitabine animals were given a placebo gavage three times weekly. This was more gavages than in my TB32048 experiment, where mice only received two gavages per week and Wong et al.'s DT6066 experiment where the mice were not gavaged. In addition, while both ***29P*** and verapamil have been used without adverse effects in previous experiments, they have not been used in combination, and we had never used ***29P*** in mixed background mice. It is possible that there was an adverse drug interaction between ***29P*** and verapamil; although most adverse drug interactions merely reduce the effect of one or both of the drugs (Becker 2011), there are cases where adverse drug interactions being fatal (Kraft and Waldman 2001). For example, in the early 1990s, there were fatal cases of treatment with the antihistamine Terfenadine. Like ***29P***, Terfenadine is a prodrug; it is rapidly metabolised in the liver by cytochrome P450 3A4 to its active form fexofenadine, so it is undetectable in plasma. However, in combination with the antifungal ketoconazole or antibiotic erythromycin, the metabolism of Terfenadine is inhibited and enters the bloodstream, in its unmetabolised form, and causes Torsades de Pointes, a form of tachycardia most commonly a response to adverse drug effects that can be fatal (Monahan et al. 1990). There are many challenges associated with prediction of adverse drug interaction *in vitro*; while screens for cytochrome P450 are well established to prevent adverse drug reactions, and more metabolic tests are being developed, there is still much uncertainty in how drugs will interact *in vivo* (Wienkers and Heath 2005). Verapamil has previously been reported to have adverse drug interactions as it inhibits the transport of digoxin through the P-glycoprotein (Pgp) (Ledwitch, Barnes, and Roberts 2016) transporter, increasing the serum concentration of digoxin (Klein et al. 1982). However, as we intend to use ***29P*** without verapamil eventually, we removed the ***29P*** with verapamil and gemcitabine combination from any further experiments. We had also not previously used ***29P*** in mixed background mice. While an adverse drug reaction is unlikely to be due to genetic background, however, there are some effects that are different between background, such as susceptibility to certain diseases(Simpson et al. 1997), different fear responses (Radulovic, Kammermeier, and Spiess 1998; Stiedl et al. 1999) as well as some differing responses to drugs (Dockstader and van der Kooy 2001; Roth et al. 2002).

16.5 Mice implanted with DT6066 tumours poorly tolerated treatment even without the combination of *29P* with verapamil, suggesting an additional effect

As animals appeared to have a poor tolerance of ***29P*** in combination with verapamil, mice implanted with DT6066 tumours were treated with gemcitabine + ***29P*** and, the gemcitabine + ld Cilengitide + verapamil combination used by Wong et al., gemcitabine alone or placebo without the gemcitabine + ***29P*** + verapamil + gemcitabine combination. Animals were treated three times per week for two weeks on, two weeks off, one week on, one week off as described in **(Figure 15.8 A)**.

Despite not combining ***29P*** and verapamil, the tolerance was still poor in this experiment. Survival to the experimental endpoint was not significantly impacted, but the animal weight was significantly reduced in all treatment groups compared to placebo **(Figure 15.9)**. This was unexpected as gemcitabine at 75 mg/kg is generally well tolerated. However, one possible cause for this was the stress caused by gavage; in the experiments performed by Wong et al., none of the animals were gavaged. In this experiment, animals treated with ***29P*** were gavaged three times per week with 250 µg/kg ***29P,*** and all other groups were gavaged with an equivalent volume of saline. Oral gavage is well known to be stressful for mice (Balcombe, Barnard, and Sandusky 2004; Walker et al. 2012). Although the placebo animals were also given a saline gavage three times per week, gemcitabine treatment adds an additional stress that placebo animals were not exposed to. Therefore, it is possible that high gavage frequency in combination with gemcitabine in post-surgery animals may have contributed to the poor tolerance. Weight loss is a known side effect of the stress of gavage (Arantes-Rodrigues et al. 2012; Jones, Boyd, and Wallace 2016).

16.6 DT6066 tumours were highly sensitive to gemcitabine

As we had hypothesised that the frequency of gavages might have contributed to poor drug tolerance, I aimed to assess whether the gavage frequency could be reduced. Therefore, dosing strategies of gemcitabine + ***29P*** three times or twice per week were compared with gemcitabine alone or placebo for their effect on implanted DT6066 tumours as described in **Figure 15.10**. However, in this experiment, the tumours appeared to be highly sensitive to gemcitabine. There was a trend towards smaller

tumours for all gemcitabine treated animals than gemcitabine, which was significant in gemcitabine and gemcitabine + ***29P*** treated animals compared to placebo. However, 29P did not confer any additional benefit compared to gemcitabine alone. In these tumours, too, there was no difference in blood vessel density **(Figure 15.11),** so it was not expected that ***29P*** would improve response to gemcitabine. However, the sensitivity to gemcitabine was not representative of patients (Olive, Jacobetz, Davidson, Gopinathan, McIntyre, Honess, Madhu, Goldgraben, Caldwell, Allard, Frese, DeNicola, et al. 2009) and meant that it would be challenging to improve response with combination therapy. Therefore, we needed a more resistant model. To this end, I began using a gemcitabine resistant DT6066 line, which was considerably less sensitive to gemcitabine than either DT6066 I had been using or TB32048 **(Figure 15.12)**.

16.7 *29P* dose-response

Up to this point, we had not demonstrated vascular promotion with ***29P*** treatment, but each experiment had had problems that may have impaired the ability to show vascular promotion. In addition, the DT6066 tumours had appeared highly sensitive to gemcitabine. Therefore, we tested the response of implanted gemcitabine resistant tumours to a range of ***29P*** doses three times per week as described in **Figure 15.13 B**. ***29P*** doses 50 to 250 µg/kg did not enhance blood vessel density when used as a monotherapy. However, all of the animals in this experiment were treated three times per week for 12 days. It is possible that this was not long enough for a vascular promotion effect or that a different dosing strategy may have been required for vascular promotion. The experiment was terminated because several of the tumours were reaching the legal limit on our animal licence. Therefore, with this model, the tumours could not be treated long term, and a slower growing tumour model may be required in order to show the long-term effects of ***29P***.

16.8 *29P* treatment in the KPC model

There were problems with the treatment of orthotopic models of pancreatic cancer with ***29P***. We hypothesised that one of the reasons that there was no vascular promotion in the orthotopics might have been that the tumours were fast-growing. Fast-growing tumours cannot be treated for as long as the animals have to be culled at the legal limit, and the vascularity may be higher (Folkman 1971; Lugano, Ramachandran, and Dimberg 2020). KPC tumours are slow growing, poorly vascularized and gemcitabine resistant

(Olive, Jacobetz, Davidson, Gopinathan, McIntyre, Honess, Madhu, Goldgraben, Caldwell, Allard, Frese, DeNicola, et al. 2009); therefore, they better model pancreatic cancer and it was hoped that they would overcome some of these challenges. However, the disadvantage of the KPC model is that the model is expensive and time-consuming to breed; there is considerable variation between animals, and animals may need to be culled due to off-target reasons such as papillomas (Gades et al. 2008). Therefore, the n-number of this experiment was low. In this small n number experiment, the KPC tumour volume and survival to the experimental endpoint and blood vessel density were not affected by treatment with gemcitabine or ***29P*** **(Figure 15.14 and Figure 15.15)**. A larger n-number would be required to draw firm conclusions from this experiment; however, the trends from these data may be informative for future studies. Whereas in the orthotopic models, the tumours were highly sensitive to gemcitabine, there was no indication from these data that the gemcitabine treated tumours had reduced growth compared to other treatment groups. In addition, there was no trend towards increased blood vessel density in the 29P treated groups. While the n-number was too small to draw conclusions from this and the data were not statistically significant, it may imply that the dose and dosing strategy for ***29P*** required optimisation for this study.

16.9 Conclusions

The results of this study remain inconclusive. While we have not demonstrated vascular promotion with *29P* treatment in any of the models presented, each model had problems outside of the vascular promotion strategy. In order to effectively test *29P* as a vascular promotor in pancreatic cancer, we would require a model that:

- Accurately models human PDAC in terms of vascularity, gemcitabine sensitivity, growth dynamics and microenvironment features
- Is slow-growing enough to allow long term treatment and accurate modelling of hypovacularised pancreatic tumours
- Can be reproduced sufficiently to have a large n number and statistically significant data.

For this reason, I have produced pancreatic cancer organoids from KPC tumours. As described in the following chapters, it is hoped that these organoids may be useful in recapitulating features of the KPC colony while allowing large n numbers and reproducibility.

17 Results III Organoids

17.1 Modelling pancreatic cancer

There is a great clinical need for new therapies for pancreatic cancer due to its notoriously poor survival (Rahib et al. 2014). The KPC model of pancreatic cancer is widely considered the most clinically relevant model with transition through the stages of PanIn to PDAC, closely following clinical cases.

However, the breeding strategy for KPC animals is time-consuming, expensive and involves culling many animals of the wrong genotype. Initially, animals heterozygous for both *Kras* $^{KO(LSL\text{-}G12D)}$ and *Trp53*^{R172H} mutations. *Kras* $^{KO(LSL\text{-}G12D)}$ homozygotes die *in utero*, so two-thirds of the animals born alive are heterozygous for *Kras* $^{KO(LSL\text{-}G12D),}$ and the remaining one third are homozygous *Kras* WTs. One-third *Trp53*^{R172H} animals are homozygous mutant, one-third homozygous WT and half of the animals are heterozygous for the *Trp53*^{R172H} mutation. Therefore, in combination, one-third of the animals born are heterozygous for both the *Kras* $^{KO(LSL\text{-}G12D)}$ and *Trp53*^{R172H} mutations, and the remaining two-thirds of the animals are euthanised. These heterozygote animals are crossed with *Pdx-1-Cre* animals to drive the mutation to the pancreas and give the *LSL-Kras*$^{G12D/+}$*;LSL-Trp53*$^{R172H/+}$*;Pdx-1-Cre* (KPC) genotype. In this second cross, one-quarter of the animals born will genotype as KPC, so the majority of the animals in the breeding strategy must be euthanised, making it a wasteful, costly and time-consuming process. In addition, tumours do not develop until approximately 16 weeks of age (Lee et al. 2016), further adding to the timescale and housing costs. Therefore, quicker, less wasteful methods are required for the modelling of pancreatic cancer.

Organoid production is a promising method. Tumours can be taken from KPC animals and grown in 3-D as organoids before implanting into a wild-type animal, forming a tumour that better recapitulates clinical PDAC development than the implant of 2-D cell cultures does (Kim et al. 2009).

A line of organoids can be produced from one KPC animal, which can be passaged, frozen, and implanted into several animals that will all produce tumours that model human pancreatic cancer development. This process is less wasteful as the majority of animals used can be included in experiments; from one KPC tumour, several experiments can be performed **(Figure 17.1)**.

Therefore, during my PhD, I travelled to the Tuveson lab (Cold Spring Harbor, USA) to learn their method of KPC organoid production to develop the model within the lab.

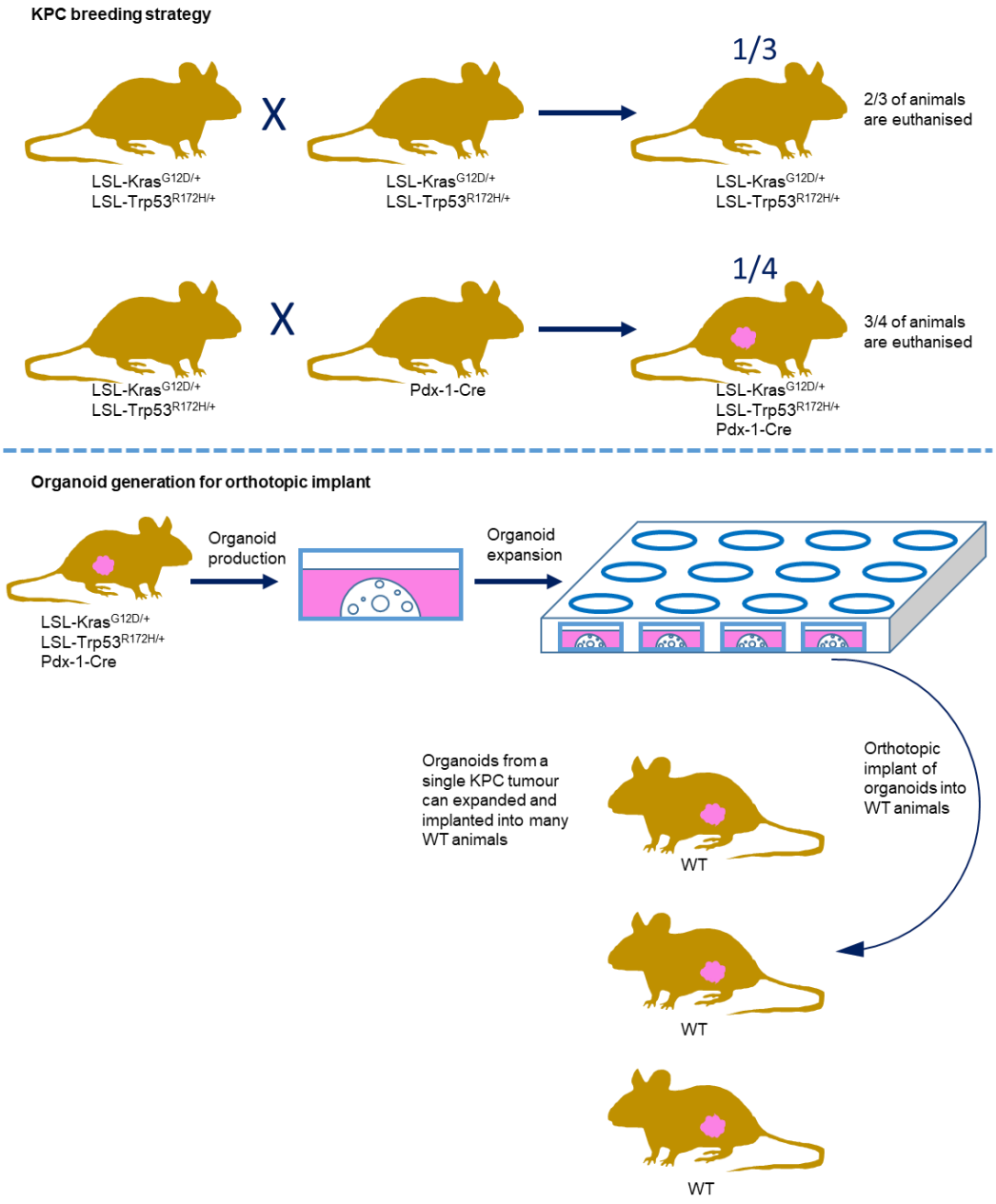

Figure 17.1 Graphical abstract on the organoid production.

When KPC mice are bred, the majority of litters born are not a complete KPC genotype, therefore, the breeding of KPCs is expensive and time consuming. However, organoids can be produced from KPC mice, these organoids can be passaged continuously and can be implanted into wildtype animals. Therefore, many tumour bearing animals can be produced from one KPC.

17.2 Preparation of media for organoid production

17.2.1 Media required for organoid isolation and passage

In preparation for organoid isolation and passage, there are several different mediums that must be produced **(Figure 17.2)**. For organoid isolation, the tumour is placed in mouse wash medium and digested in mouse digestion medium (see *Materials and methods* 12.13.8.2). Mouse splitting medium (described in *Materials and methods 12.13.8.3*) is required for passage. In addition, the Matrigel dome of organoids must be coated with a mouse organoid feeding medium containing all the nutrients and growth factors required by the organoids.

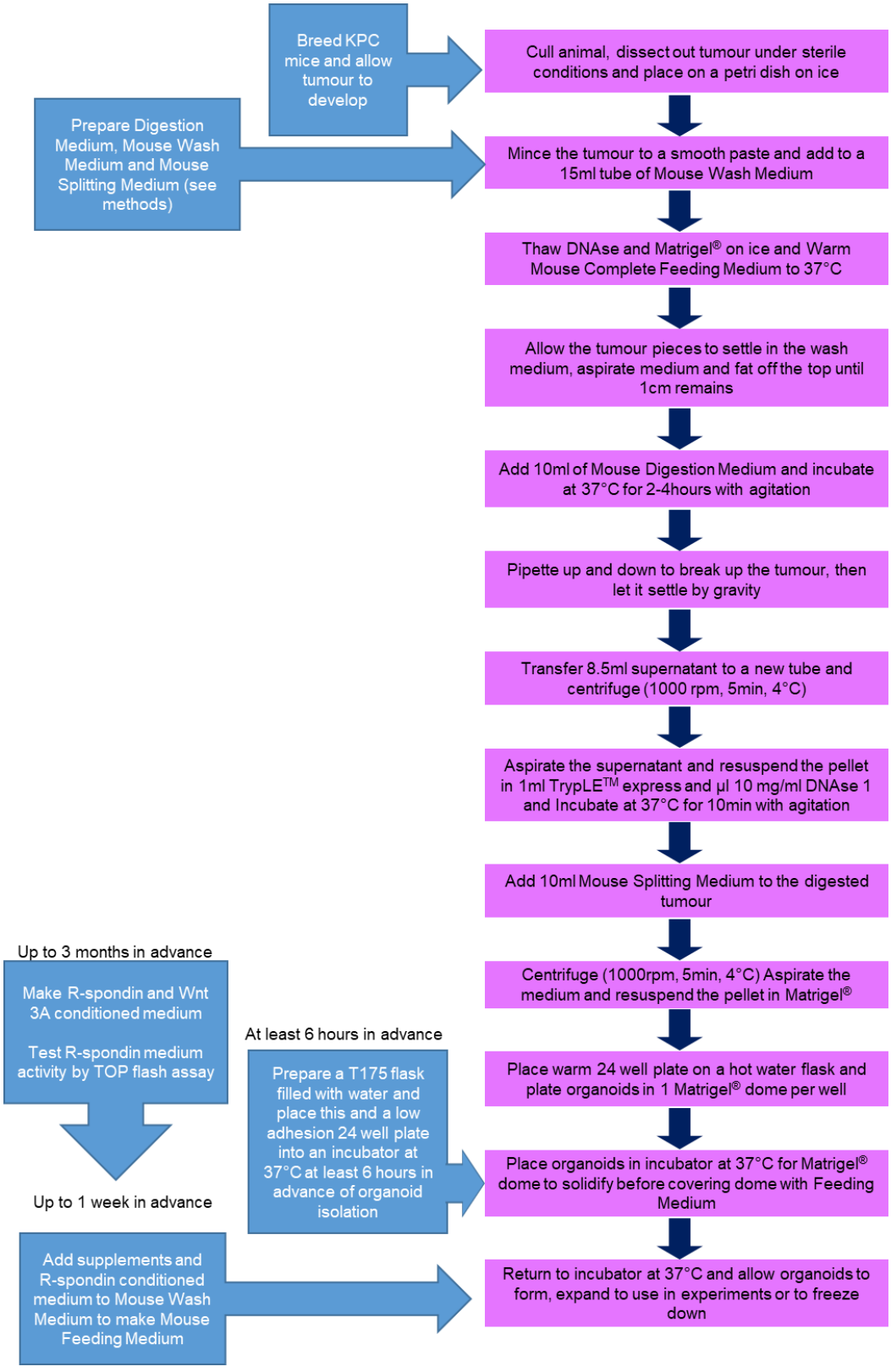

Figure 17.2 Flow diagram of organoid isolation.

17.2.1.1 Mouse organoid feeding medium

17.2.1.1.1 Mouse organoid feeding medium components

Organoids are suspended in a Matrigel® dome surrounded by a mouse organoid feeding medium supplemented with growth factors and hormones to allow continuous passage. Media production is described in *Materials and Methods* (12.13.8.4) and the role of each feeding medium component in **(Figure 17.3)**.

Media component	Function in medium
Advanced DMEM/F-12	Base for media; this contains BSA which prevents organoids and growth factors for sticking to plasticware
HEPES	Buffering agent, maintains the pH of the medium
GlutaMAX	Glutamine supplement
Penicillin/Streptomycin	Antibiotics
A 83-01	Inhibits the downstream effects of transforming growth factor beta (TGF-β) through inhibition of its receptor activin receptor-like kinase (ALK)5
mEGF	Growth factor that stimulates cell growth and differentiation, essential to maintaining organoids over 2–5 weeks
hFGF-10	Growth factor promoting cell survival, essential to maintaining organoids over 2–5 weeks
hGastrin I	Hormone pancreatic growth factor which stimulates pancreatic acinar cells to secrete digestive enzymes
mNoggin	Inhibits bone morphogenetic protein (BMP)4, chordin, follistatin, leading to TGF beta inhibition. TGF-β pathway inhibitors required for propagation essential to maintain the cultures >2 months
N-acetylcysteine	Antioxidant, replenishes glutathione stores
Nicotinamide	B vitamin, Inhibits poly(ADP-ribose) polymerases (PARP-1), promotes endocrine lineage; essential to maintain organoid cultures >2 months
R-Spondin 1 Conditioned medium	Activates Wnt pathway triggering the regenerative response in duct cells allowing unlimited expansion essential to maintaining organoids over 2–5 weeks
B27 supplement	Contains the hormones insulin and progesterone. Insulin and progesterone. Lead to retinoic acid activation Full formulation: Biotin, DL Alpha tocopherol acetate, DL Alpha tocopherol, vitamin A, BSA (fatty acid free fraction V), Catalase, Human recombinant insulin, human transferrin, superoxide dismutase, corticosterone, D-Galactose, ethanolamine HCL, Glutathione (reduced), L-Carnitine HCL, linoleic acid, progesterone, putrescine 2HCL, Sodium Selenite, T3(trido-l-thyronine)
Y-27632*	Rho kinase inhibitor helps cells cope with stress, required for initial isolation and thawing of organoids

Figure 17.3 Mouse organoid feeding medium component functions.

Taken from (Boj et al. 2015; Huch et al. 2013) *Y-27632 is only required in mouse organoid feeding medium when organoids are initially isolated or thawed.

17.2.1.1.2 R-spondin conditioned medium

One of the mouse organoid feeding medium components is R-spondin conditioned medium produced from Cultrex® R-spondin1 Cells (Trevigen 3710-001-K) as described in *materials and methods* (12.13.2) and **Figure 17.4**.

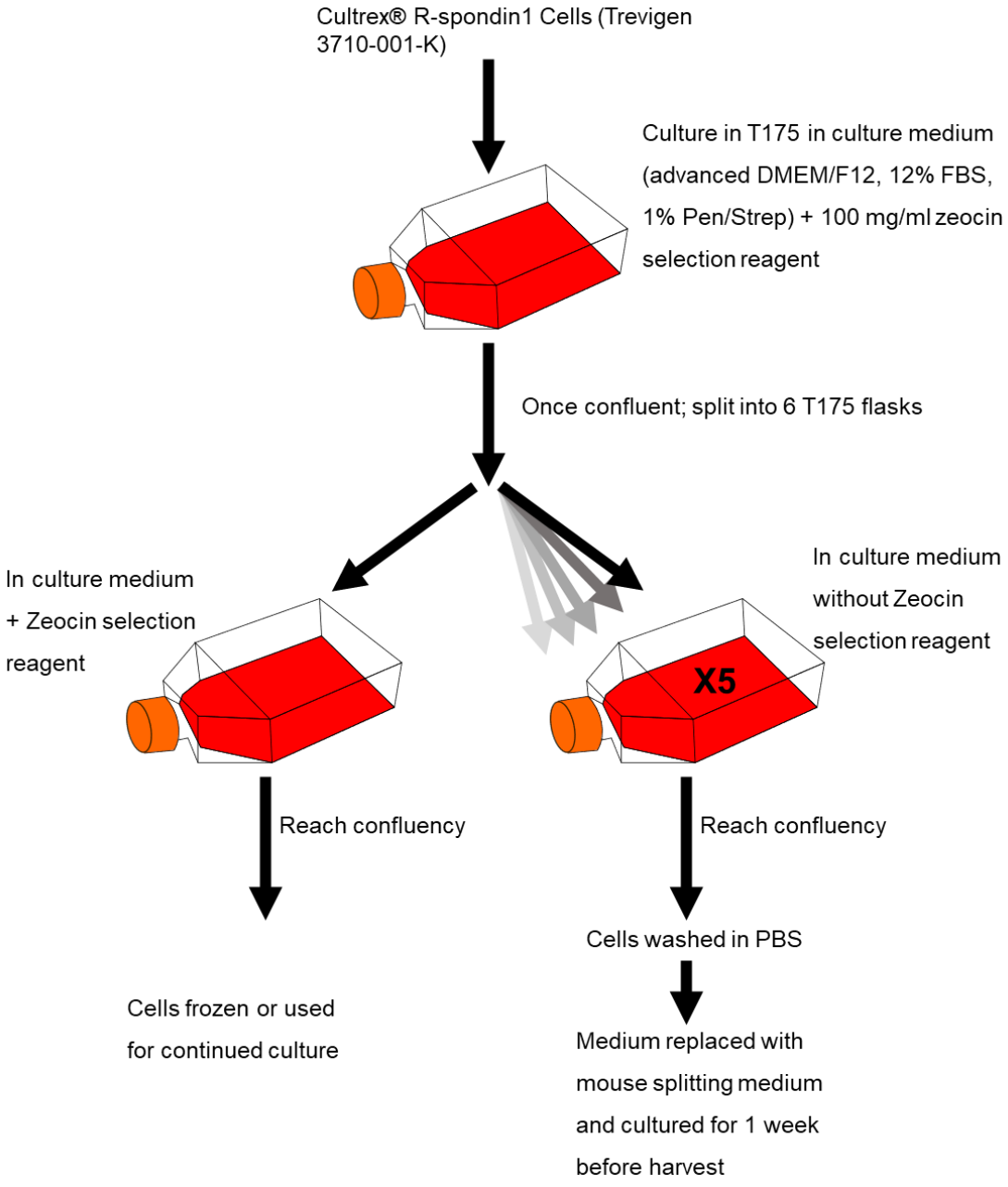

Figure 17.4 Cultrex® R-spondin1 Cells (Trevigen 3710-001-K) culture for R-Spondin conditioned medium production.

17.2.1.1.3 Wnt-3A conditioned medium

The R-Spondin in the conditioned medium functions to make Wnt-3A stable and therefore potentiates its signal. Therefore, to test R-Spondin activity, testing the activity of a Wnt-3A sample with and without R-Spondin can be confirmed. Wnt-3A conditioned medium is therefore required to confirm the activity of R-Spondin.

Wnt-3A conditioned medium can be produced from L-Wnt-3A cells (ATCC CRL-2647) as described in *materials and methods* (12.13.3). This medium can be stored at -20 °C.

17.2.1.1.4 Testing of medium

In order to test the R-Spondin activity of the conditioned medium, the Wnt-3A activity of Wnt-3A conditioned medium with and without R-Spondin conditioned medium was tested by a TOPFLASH assay as described in *materials and methods* (12.13.7). In order to do this, TOPflash (12456) and FOPflash (12457) plasmids are required and were purchased from Addgene **(Figure 17.5)** and were expanded in a miniprep as described in *materials and methods* (12.13.4).

A

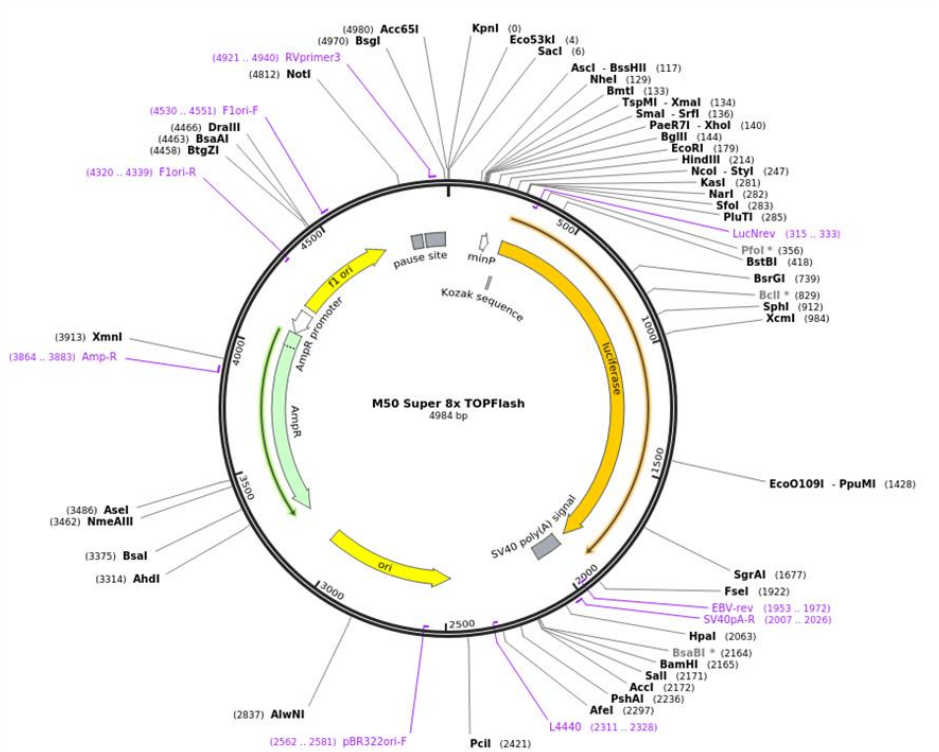

B

Figure 17.5 Testing of R-spondin level in conditioned medium.

(A) TOP Plasmid (B) FOP plasmid

17.2.1.1.4.1 Confirmation of correct plasmid sequence

Once plasmids had been expanded in a miniprep, the correct sequence was confirmed by cutting at restriction sites. Bam HI, Eco RI and Xmn I restriction sites are present in both plasmids; therefore, by cutting the plasmids at the restriction sites, the sequence can be confirmed as mapped. The mapped plasmid sized were 4984 bp (TOP plasmid) and 4973 bp (FOP plasmid). Each plasmid was cut once with each restriction enzyme to produce linear DNA of 4984 bp and 4973 bp for TOP and FOP plasmids, respectively. Both plasmids were also cut at each combination of two restriction sites. The predicted sizes of the cut fragments were based on the plasmid maps **(Figure 17.5)** as listed in **Figure 17.6 A**.

The plasmids were run, uncut, on a gel, and were predicted to run faster than linear DNA. The singly cut plasmids were run next to these, and as predicted, plasmids once cut at each restriction site ran at the same size on the gel, which was slightly behind the uncut sample. This confirmed that each plasmid had one of each restriction site, and each restriction enzyme had successfully cut at this site **(Figure 17.6 A)**. Following each of the single cuts, each of the double cuts were run on the gel showing two fragments in each case. The relative sizes were as expected, with fragments formed from cuts at Eco RI and Bam HI the closest together in size and the DNA cut at Eco RI and Xmn I forming the largest and smallest fragments from both plasmids.

17.2.1.1.4.2 Testing of R-spondin conditioned medium by TOPFLASH assay

Once the plasmids were confirmed, they were used to perform a TOPFlash assay to measure Wnt-3A activity as described in *materials and methods* (12.13.7). HEK cells were transfected with both the TOP plasmid and a *renilla luciferase* plasmid. The TOP plasmid has T-cell factor/lymphoid enhancer factor (TCF/LEF) binding sites for Wnt upstream of the *Firefly Luciferase* gene. When cells transfected with the TOP plasmid are exposed to conditioned medium, Wnt will drive expression of firefly *luciferase*. In all cells where the transfection was successful, there will also be *renilla luciferase* expression. Therefore, in TOP transfected cells, the level of *luciferase* expression corrected to the level of *renilla* expression indicates the Wnt activity of the medium. The FOP plasmid is similar to the TOP plasmid, but with a mutated TCF/LEF binding site, so it is expected to be unresponsive to Wnt activity and was used as a negative control; any luminescence in cells transfected with this plasmid was background.

Therefore, for each medium condition, the *luciferase* value for cells transfected with TOP and *FOP* plasmids was divided by the *renilla* expression in these cells, giving the amount of luminescence normalised to the number of transfected cells. The *luciferase/renilla* value for *TOP* was then divided by the *luciferase/renilla* value for *FOP*, giving the luminescence value normalised to the background signal.

Normal, unconditioned mouse splitting medium was tested against 50 % Wnt conditioned medium, 50 % mouse splitting medium, and 50 % Wnt conditioned medium, 50 % R-Spondin conditioned medium **(Figure 17.6 B)**. Wnt conditioned medium activity alone was low and did not enhance *luciferase* expression compared to mouse splitting medium alone. However, with R-Spondin conditioned medium, the Wnt activity was significantly higher. This confirmed that the R-spondin conditioned medium was active and could be used in mouse organoid feeding medium.

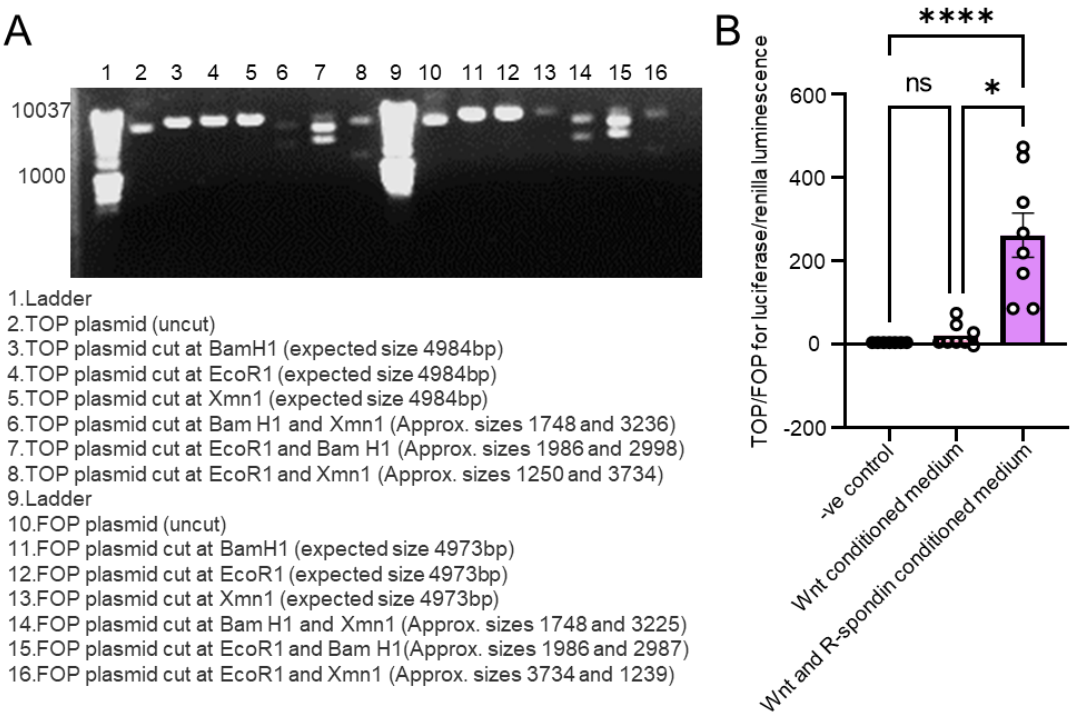

Figure 17.6 Testing R-spondin levels in conditioned medium.

(A) DNA gel of restriction digests of TOP and FOP plasmids to confirm the correct sequence (B) TOPflash assay of Wnt activity demonstrating R-spondin increasing Wnt activity. Bar chart shows *luciferase* luminescence per transfected cells normalised to the background signal mean ±s.e.m, analysed by Kruskal-Wallis ns, not significant ($P > 0.05$) ****$P<0.00001$. N=8 in each group, reduced to seven in the negative control group by exclusion of outliers by ROUT, Q=1 %.

17.3 Organoid isolation

Once the medium was prepared, organoids were digested from KPC tumours as described in *materials and methods* (12.13.9) and **Figure 17.2**. They were resuspended in Matrigel® and plated one dome per well into a 24 well plate. They were placed in an incubator at 37 °C to allow the Matrigel® to harden before covering in feeding medium supplemented with Y-27632 Rho kinase inhibitor (changing to medium without Y-27632 once media began to yellow). After 2-3 days, the organoids began to form into small spheres **(Figure 17.7 A)** and, with further culture, grew into larger organoids **(Figure 17.7 B)**.

In order to culture organoids for biotherapeutics experiments, they were plated into 96 well plates as described in *materials and methods* (12.13.15). Organoids from both WT mix and C57Bl6 KPC mice were plated like this with many small spheres forming in each well **(Figure 17.7 C)**. 24 hours after plating into the 96 well plate; cells were treated with gemcitabine by addition of gemcitabine containing medium on top of the current culture medium. After 48 hours treatment with gemcitabine, an MTT assay was performed and the cell number corrected to the number of cells in the untreated samples. After 48 hours culture with gemcitabine, the number of organoids from both WT mix **(Figure 17.7 D)** and C57Bl6 **(Figure 17.7 E)** KPC mice was reduced.

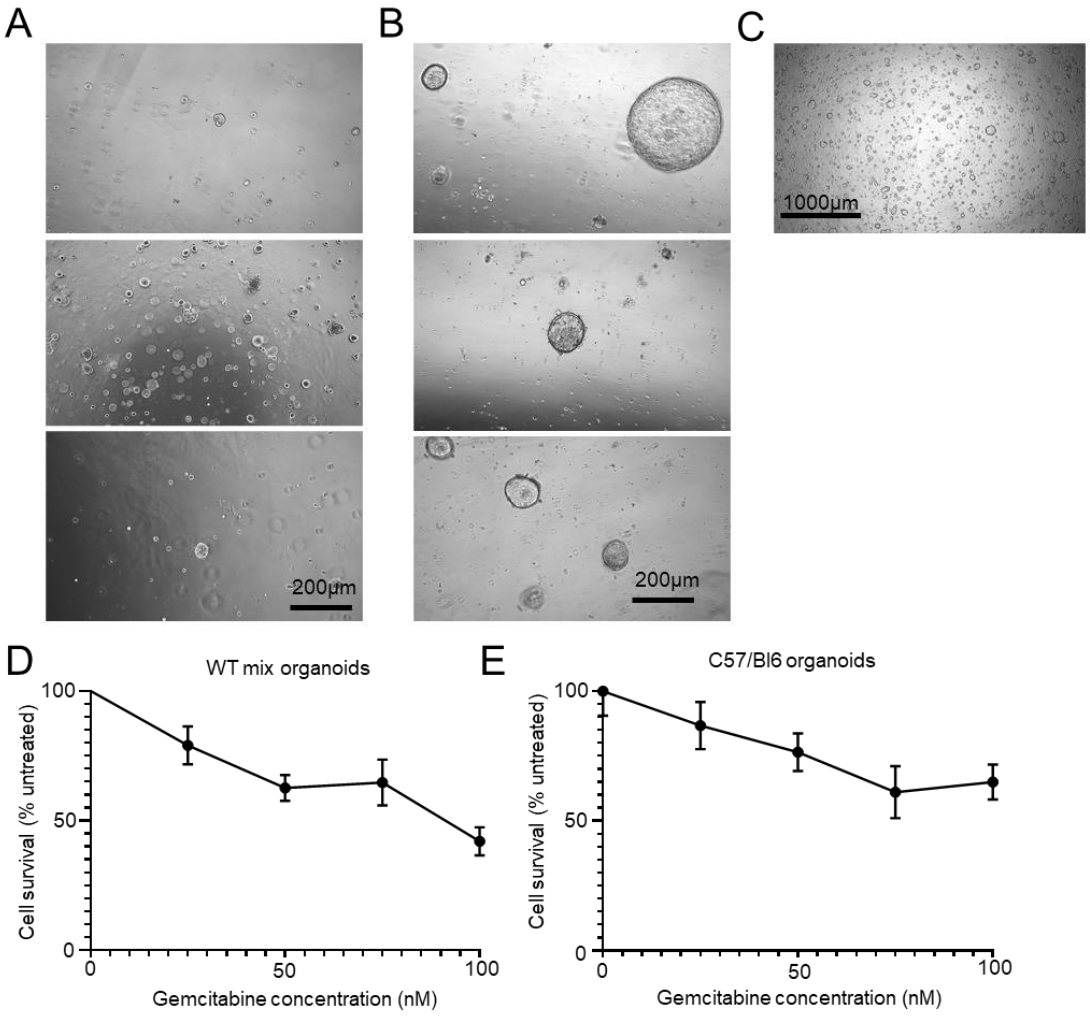

Figure 17.7 Organoid growth *in vitro*.

(A) Early-stage organoid growth (roughly 2-3 days after plating) and (B) late-stage organoid growth in Matrigel® domes *in vitro* (roughly 5-7 days after plating). (C) Growth of organoids in Matrigel® and medium in 96 well plate format for biotherapeutics experiments. (D) Cell survival with gemcitabine treatment in organoids derived from WT mix (C57bl6/129sv) KPC tumours. (E) Cell survival with gemcitabine treatment in organoids derived fromC57bl6 KPC tumours. For C and D, n=12 wells for each gemcitabine concentration, no values were excluded by ROUT, Q=1 %.

17.4 In vivo organoid growth pilot

Organoids from WT mix KPC mice were digested to a single cell suspension and 250, 000 single cells implanted into the pancreas of eight WT mix animals. At implant, the organoids had been freeze-thawed three times and had been passaged four times since thawing. Two weeks after they were implanted, tumours had established, they were imaged by MRI and a tumour volume estimated by segmentation. Following MRI imaging, four of the animals were culled and the tumours harvested. The remaining animals were imaged two weeks later, the tumour volumes quantified, and the tumours harvested **(Figure 17.8 A)**. In all four animals that were imaged twice, the tumours increased in size from two to four weeks post-implantation **(Figure 17.8 B)**.

The tumours harvested at two and four weeks were sectioned and stained for H and E **(Figure 17.8 C and D)**. In both cases, there were large areas of high-grade tumour with mitotic cells visible. In addition, there were areas of necrosis in the tumours harvested at each time point.

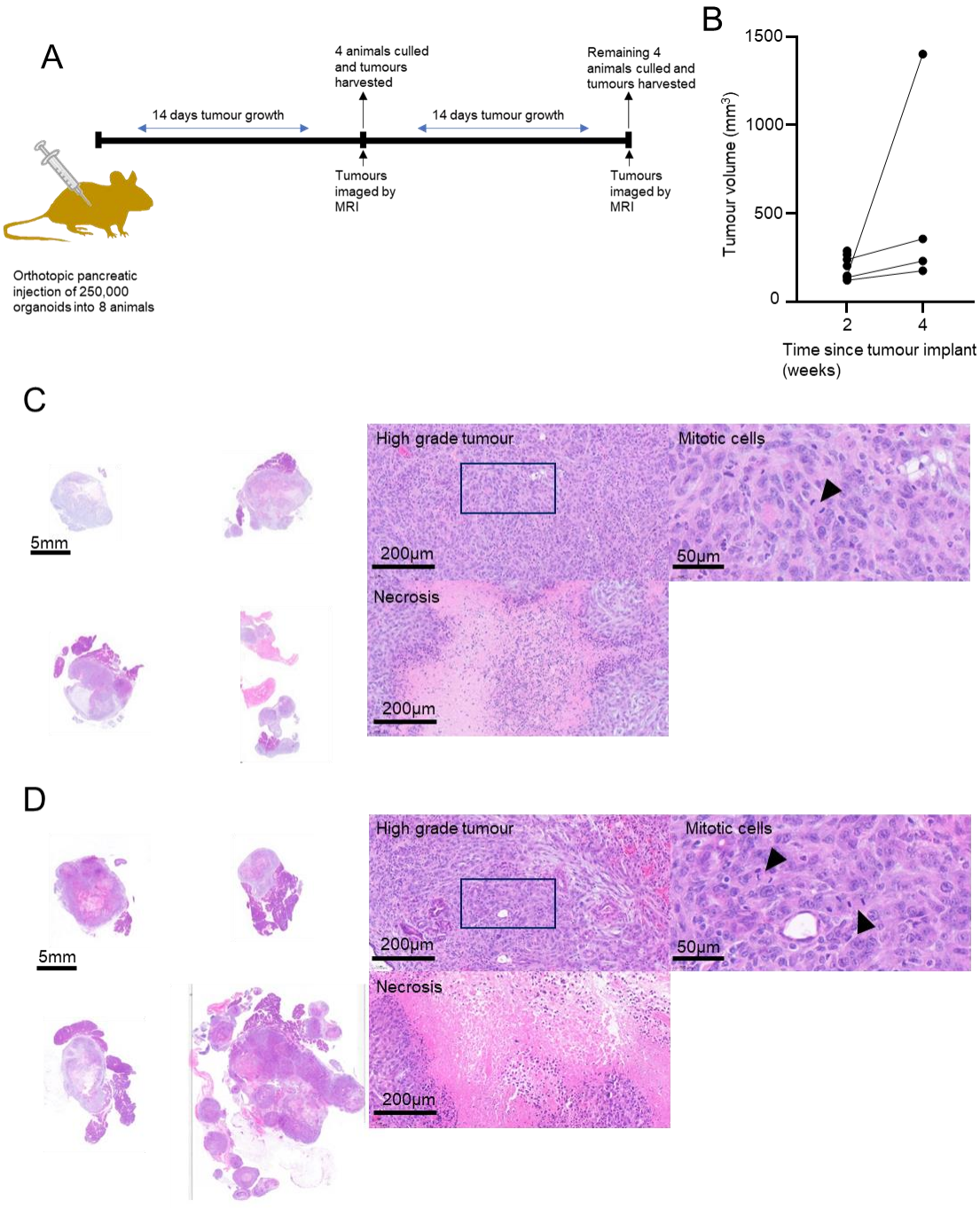

Figure 17.8 Organoid growth *in vitro*.

(A) Schematic diagram of experimental design and dosing strategy showing organoids from mixed (C57bl6 / 129sv) implanted into mixed (C57bl6 / 129sv) mice. (B) Tumour volume measured by MRI at two and four weeks. (C) H and E staining of tumours harvested at 2 weeks after implant of organoids showing high grade tumour, mitotic cells and areas of necrosis. (D) H and E images of tumours harvested at four weeks after organoid implant.

18 Discussion III Organoids

Novel pancreatic cancer therapies represent a considerable clinical need due to their poor prognosis and challenges to treatment (Orth et al. 2019; Siegel, Miller, and Jemal 2015). The tumour microenvironment of pancreatic cancer is a major contributor to the challenges in its treatment, and it is therefore important to be able to accurately model the microenvironment in order to be able to test novel therapies. Organoid models may offer a useful compromise between the clinical relevance of the KPC model and the ease, cost-effectiveness and reproducibility of orthotopically injected 2D cell lines.

I have presented an explanation of how organoids were produced using the Tuveson method. I have shown data from pilot studies testing their gemcitabine sensitivity *in vitro* and orthotopic growth *in vivo*. We hope that these organoids may become a useful model for testing therapies for pancreatic cancer, including vascular protocols such as ***29P***, at BCI.

Organoids from both C57bl6 and mixed background C57bl6/129sv KPCs were isolated. The lines formed organoids successfully in Matrigel® and could be passaged multiple times; lines were also frozen and thawed successfully, demonstrating that a bank of these organoids can be produced from the KPC colony for future use.

The *in vitro* organoid experiments suggested that the gemcitabine sensitivity was comparable to normal DT6066 cells and TB32048 cells **(Figure 15.12 and Figure 17.7)**; however, this was a higher level of sensitivity than the gemcitabine resistant DT6066 cells. As PDAC tumours are not generally considered to be gemcitabine sensitive, this may pose a problem to the modelling of PDAC (Olive, Jacobetz, Davidson, Gopinathan, McIntyre, Honess, Madhu, Goldgraben, Caldwell, Allard, Frese, DeNicola, et al. 2009). However, it is plausible that to create gemcitabine resistant organoids that KPC mice could be treated with gemcitabine and tumour harvested from the mice with the biggest tumours. These organoids could be derived from these gemcitabine resistant tumours. Repeats with additional replicates are also recommended.

Organoids from mixed background animals were implanted orthotopically into WT mixed background (C57bl6/129sv) animals. All eight animals implanted developed tumours, and at the two-week time point, the volumes were fairly comparable (122-288mm^3) **(Figure 17.8 B)**. There was variation in the tumour growth from two to four weeks, with one tumour reaching 1402 mm^3, while the remaining three animals in the experiment

had tumours with volumes ranging from 176-357 mm^3. However, as only four animals remained in the experiment to four weeks, this is not a great enough n-number to draw conclusions about the variation of tumour growth in this model.

In addition, several of the tumours appeared to have large areas of necrosis visible in their H and E histology. Again, since this experiment represented a small pilot, a larger sample size would be needed to determine whether the necrosis is unusually high. However, it is also possible that there may have been increased necrosis due to the implant of mixed background organoids into WT mix animals. This runs the risk of producing an immune response to the organoids as the genetic variation in outbred colonies leads to a variation in response to a graft (Reichenbach et al. 2013). Therefore, it will be useful to perform a similar experiment with C57bl6 organoids implanted into pure background C57bl6 to see whether there are any differences in the level of necrosis.

The experiment should be repeated with a larger n-number, but this pilot was encouraging in that organoids, originally derived from a single KPC mouse and passaged multiple times, can produce a tumour in the pancreas of a WT animal.

Overall, I have successfully isolated, passaged and freeze-thawed organoids from C57b6 and C57bl6/129sv. I have also implanted organoids from C57bl6/129sv KPCs into eight C57bl6/129sv, which grew successfully. Further experiments are required to determine their level of gemcitabine sensitivity and their growth pattern *in vivo*.

19 General conclusions

While historically cancer therapies focused on targeting tumour cells, it is now widely accepted that the tumour microenvironment has an essential role to play in chemotherapy resistance, drug delivery and the immune response and, as such, represents a valuable drug target. The tumour vasculature has roles in angiogenesis, creating a pro-tumorigenic vascular niche and chemotherapy resistance, but vasculature is also essential in drug delivery and the creation of a normoxic immunopermissive tumour microenvironment.

Here, I investigated two strategies to exploit the vasculature for better therapies. I have investigated the effects of the kinase domain of FAK in chemotherapy resistance and demonstrated that by inactivating the kinase domain, doxorubicin stimulated angiocrine signalling of FAK is reduced. Although the effects are modest, there is a sensitisation of *EC Cre+; FAK$^{KD/KD}$* mice to doxorubicin compared to controls. This sensitisation is observed in reduced tumour growth through increases in apoptosis and DNA damage, and decreased proliferation. In addition, pharmacological inhibition of the FAK kinase domain with three different kinase inhibitors caused a downregulation in cytokine production in response to doxorubicin. The FAK and Pyk2 dual inhibitor was particularly effective in altering the cytokine profile and may be useful clinically, combined with DNA damaging therapy to reduce resistance.

In addition, I worked on the development of a dosing strategy for the use of vascular promotion drug, ***29P***, in models of pancreatic cancer. Unfortunately, this data remains inconclusive; however, our published data demonstrate that vascular promotion can improve the delivery of chemotherapy, reducing tumour size and improving survival. As PDAC is typically poorly vascularized, the use of ***29P*** to enhance the blood vessel density and ultimately enhance the delivery of chemotherapeutics and the action of checkpoint blockade immunotherapy is a goal of the lab.

Although I was not able to optimise a dosing strategy for ***29P*** as a vascular promotor within the scope of my thesis, I have produced a number of pancreatic cancer organoid lines from KPCs. We hope that this bank of organoids can be expanded and used *in vivo* to further test the use of ***29P*** and alternative vascular promotors. Using a model that can be reproduced more quickly than the KPC but better recapitulates the clinical setting

than 2-D cell line injection does, we hope to test dosing strategies quickly and with large n-numbers while ensuring as accurate modelling as possible.

20 Future work

Having addressed all of the reviewer's comments, I hope to resubmit my paper 'Elucidating the role of the kinase activity of endothelial cell focal adhesion kinase in angiocrine signalling and tumour growth' to the Journal of Pathology in the next few weeks.

In addition to this, I will return to the lab for a few months, during which time I intend to make a bank of organoid lines from both WT mix and C57bl6 KPC tumours. I will test the growth of these organoids *in vivo* and *in vitro* so that they can be used for future projects within the lab. Eventually, we aim to have a database of organoids with histology of the original tumour, gemcitabine sensitivity data *in vitro*, histology of the tumours produced by organoid implantation and tumour growth curves for the implanted tumours. We expect some variation between organoid lines, and therefore, this bank will help inform future experiments.

For future experiments on the use of ***29P*** as a vascular promotor, it will be important to find a slow-growing tumour model. We hope that this may be achieved through the use of KPC organoids, as they are expected to grow slower *in vivo* than 2-D cell lines. In addition, we hypothesised that repeated gavage may have caused stress to the animals. Therefore, it may be useful to perform experiments with IP injection of the deprotected form of ***29P***, ***29***. We had avoided this as a major advantage of ***29P*** is its oral availability, but this may be of value in separating the vascular promotion effect from any gavage stress. Another problem faced within this thesis was the sensitivity to gemcitabine. We may, therefore, produce gemcitabine resistant organoids, either by producing organoids from gemcitabine treated KPC mice or by continuously treating organoids with low dose gemcitabine *in vitro* before implantation.

By using these adaptations to the orthotopic model, we hope to be able to optimise a dosing strategy of ***29P*** (or ***29***) with gemcitabine. Once a dose and dosing strategy have been optimised and repeated in an orthotopically implanted organoid model, this will inform the best doses to use for a longer-term KPC study. We hope that, once the model is optimised, 29P may still be effective as a vascular promotor. If this is the case, then future work in the lab will use ***29P*** in combination with checkpoint blockade immunotherapy. It is hoped that this may improve the efficacy of immunotherapy in

pancreatic cancer due to reduced levels of hypoxia and improved drug delivery to the tumour.

21 References

Abdollahi, Amir, Kenneth E. Lipson, Axel Sckell, Heike Zieher, Frank Klenke, Daniel Poerschke, Alexandra Roth, Xiaohong Han, Martin Krix, Marc Bischof, Philip Hahnfeldt, Hermann-Josef Grone, Juergen Debus, Lynn Hlatky, and Peter E. Huber. 2003. 'Combined Therapy with Direct and Indirect Angiogenesis Inhibition Results in Enhanced Antiangiogenic and Antitumor Effects', *Cancer Research*, 63: 8890.

Abremski, K., and R. Hoess. 1984. 'Bacteriophage P1 site-specific recombination. Purification and properties of the Cre recombinase protein', *J Biol Chem*, 259: 1509-14.

Acosta, J. C., A. O'Loghlen, A. Banito, M. V. Guijarro, A. Augert, S. Raguz, M. Fumagalli, M. Da Costa, C. Brown, N. Popov, Y. Takatsu, J. Melamed, F. d'Adda di Fagagna, D. Bernard, E. Hernando, and J. Gil. 2008. 'Chemokine signaling via the CXCR2 receptor reinforces senescence', *Cell*, 133: 1006-18.

Adair, TH, and JP Montani. 2010. "Angiogenesis." In. https://www.ncbi.nlm.nih.gov/books/NBK53242/: Morgan & Claypool Life Sciences.

Adamis, Anthony P., and Adrienne J. Berman. 2010. 'Chapter 70 - Inhibition of angiogenesis.' in Leonard A. Levin and Daniel M. Albert (eds.), *Ocular Disease* (W.B. Saunders: Edinburgh).

Adams, R. H., and K. Alitalo. 2007. 'Molecular regulation of angiogenesis and lymphangiogenesis', *Nat Rev Mol Cell Biol*, 8: 464-78.

Aird, W. C. 2012. 'Endothelial cell heterogeneity', *Cold Spring Harb Perspect Med*, 2: a006429.

Akwii, Racheal G., Md S. Sajib, Fatema T. Zahra, and Constantinos M. Mikelis. 2019. 'Role of Angiopoietin-2 in Vascular Physiology and Pathophysiology', *Cells*, 8: 471.

Alanko, J., and J. Ivaska. 2016. 'Endosomes: Emerging Platforms for Integrin-Mediated FAK Signalling', *Trends Cell Biol*, 26: 391-98.

Alanko, J., A. Mai, G. Jacquemet, K. Schauer, R. Kaukonen, M. Saari, B. Goud, and J. Ivaska. 2015. 'Integrin endosomal signalling suppresses anoikis', *Nat Cell Biol*, 17: 1412-21.

Alday-Parejo, Begoña, Roger Stupp, and Curzio Rüegg. 2019. 'Are Integrins Still Practicable Targets for Anti-Cancer Therapy?', *Cancers*, 11: 978.

Alexopoulou, Annika N., Colan M. Ho-Yen, Vassilis Papalazarou, George Elia, J. Louise Jones, and Kairbaan Hodivala-Dilke. 2014. 'Tumour-associated endothelial-FAK correlated with molecular sub-type and prognostic factors in invasive breast cancer', *BMC Cancer*, 14: 237.

Alexopoulou, Annika N., Delphine M. Lees, Natalia Bodrug, Tanguy Lechertier, Isabelle Fernandez, Gabriela D'Amico, Matthew Dukinfield, Silvia Batista, Bernardo Tavora, Bryan Serrels, and Kairbaan Hodivala-Dilke. 2017. 'Focal Adhesion Kinase (FAK) tyrosine 397E mutation restores the vascular leakage defect in endothelium-specific FAK-kinase dead mice', *J Pathol*, 242: 358-70.

Algire, G. H., H. W. Chalkley, W. E. Earle, F. Y. Legallais, H. D. Park, E. Shelton, and E. L. Schilling. 1950. 'Vascular reactions of normal and malignant tissues in vivo. III. Vascular reactions' of mice to fibroblasts treated in vitro with methylcholanthrene', *J Natl Cancer Inst*, 11: 555-80.

Algire, Glenn H., Harold W. Chalkley, Frances Y. Legallais, and Helen D. Park. 1945. 'Vasculae Reactions of Normal and Malignant Tissues in Vivo. I. Vascular

Reactions of Mice to Wounds and to Normal and Neoplastic Transplants', *JNCI: Journal of the National Cancer Institute*, 6: 73-85.
Aliper, Alexander M., Victoria P. Frieden-Korovkina, Anton Buzdin, Sergey A. Roumiantsev, and Alex Zhavoronkov. 2014. 'A role for G-CSF and GM-CSF in nonmyeloid cancers', *Cancer medicine*, 3: 737-46.
Alonso, J. L., M. Essafi, J. P. Xiong, T. Stehle, and M. A. Arnaout. 2002. 'Does the integrin alphaA domain act as a ligand for its betaA domain?' in, *Curr Biol* (England).
Anthis, N. J., K. L. Wegener, F. Ye, C. Kim, B. T. Goult, E. D. Lowe, I. Vakonakis, N. Bate, D. R. Critchley, M. H. Ginsberg, and I. D. Campbell. 2009. 'The structure of an integrin/talin complex reveals the basis of inside-out signal transduction', *Embo j*, 28: 3623-32.
Arantes-Rodrigues, Regina, Andreia Henriques, Rosário Pinto-Leite, Ana Faustino-Rocha, Jacinta Pinho-Oliveira, Catarina Teixeira-Guedes, Fernanda Seixas, Adelina Gama, Bruno Colaço, Aura Colaço, and Paula A. Oliveira. 2012. 'The effects of repeated oral gavage on the health of male CD-1 mice', *Lab Animal*, 41: 129-34.
Armulik, Annika, Guillem Genové, and Christer Betsholtz. 2011. 'Pericytes: Developmental, Physiological, and Pathological Perspectives, Problems, and Promises', *Developmental Cell*, 21: 193-215.
Astier, Anne, Hava Avraham, Serge N. Manie, Jerome Groopman, Timothy Canty, Shalom Avraham, and Arnold S. Freedman. 1997. 'The Related Adhesion Focal Tyrosine Kinase Is Tyrosine-phosphorylated after β1-Integrin Stimulation in B Cells and Binds to p130cas*', *Journal of Biological Chemistry*, 272: 228-32.
Augustin, H. G., G. Y. Koh, G. Thurston, and K. Alitalo. 2009. 'Control of vascular morphogenesis and homeostasis through the angiopoietin-Tie system', *Nat Rev Mol Cell Biol*, 10: 165-77.
Aumailley, M., M. Gurrath, G. Muller, J. Calvete, R. Timpl, and H. Kessler. 1991. 'Arg-Gly-Asp constrained within cyclic pentapeptides. Strong and selective inhibitors of cell adhesion to vitronectin and laminin fragment P1', *FEBS Lett*, 291: 50-4.
Ausprunk, D. H., D. R. Knighton, and J. Folkman. 1974. 'Differentiation of vascular endothelium in the chick chorioallantois: a structural and autoradiographic study', *Dev Biol*, 38: 237-48.
———. 1975. 'Vascularization of normal and neoplastic tissues grafted to the chick chorioallantois. Role of host and preexisting graft blood vessels', *Am J Pathol*, 79: 597-618.
Avraamides, Christie J., Barbara Garmy-Susini, and Judith A. Varner. 2008. 'Integrins in angiogenesis and lymphangiogenesis', *Nature reviews. Cancer*, 8: 604-17.
Avraham, H., S. Y. Park, K. Schinkmann, and S. Avraham. 2000. 'RAFTK/Pyk2-mediated cellular signalling', *Cell Signal*, 12: 123-33.
Avraham, Shalom, Roanna London, Yigong Fu, Setsuo Ota, Dan Hiregowdara, Junzhi Li, Shuxian Jiang, Linda M. Pasztor, Robert A. White, Jerome E. Groopman, and Hava Avraham. 1995. 'Identification and Characterization of a Novel Related Adhesion Focal Tyrosine Kinase (RAFTK) from Megakaryocytes and Brain (*)', *Journal of Biological Chemistry*, 270: 27742-51.
Bagher, P., and S. S. Segal. 2011. 'Regulation of blood flow in the microcirculation: role of conducted vasodilation', *Acta physiologica (Oxford, England)*, 202: 271-84.
Balcombe, J. P., N. D. Barnard, and C. Sandusky. 2004. 'Laboratory routines cause animal stress', *Contemp Top Lab Anim Sci*, 43: 42-51.
Balkwill, F. 2009. 'Tumour necrosis factor and cancer', *Nat Rev Cancer*, 9: 361-71.
Balkwill, Frances R., Melania Capasso, and Thorsten Hagemann. 2012. 'The tumor microenvironment at a glance', *Journal of Cell Science*, 125: 5591.

Baluk, Peter, Hiroya Hashizume, and Donald M. McDonald. 2005. 'Cellular abnormalities of blood vessels as targets in cancer', *Current Opinion in Genetics & Development*, 15: 102-11.

Baluk, Peter, Shunichi Morikawa, Amy Haskell, Michael Mancuso, and Donald M. McDonald. 2003. 'Abnormalities of basement membrane on blood vessels and endothelial sprouts in tumors', *The American journal of pathology*, 163: 1801-15.

Bandyopadhyay, A., and S. Raghavan. 2009. 'Defining the role of integrin alphavbeta6 in cancer', *Current drug targets*, 10: 645-52.

Bates, G. J., S. B. Fox, C. Han, R. D. Leek, J. F. Garcia, A. L. Harris, and A. H. Banham. 2006. 'Quantification of regulatory T cells enables the identification of high-risk breast cancer patients and those at risk of late relapse', *J Clin Oncol*, 24: 5373-80.

Beatty, Gregory L., Elena G. Chiorean, Matthew P. Fishman, Babak Saboury, Ursina R. Teitelbaum, Weijing Sun, Richard D. Huhn, Wenru Song, Dongguang Li, Leslie L. Sharp, Drew A. Torigian, Peter J. O'Dwyer, and Robert H. Vonderheide. 2011. 'CD40 agonists alter tumor stroma and show efficacy against pancreatic carcinoma in mice and humans', *Science*, 331: 1612-16.

Becker, Daniel E. 2011. 'Adverse drug interactions', *Anesthesia progress*, 58: 31-41.

Beinke, S., H. Phee, J. M. Clingan, J. Schlessinger, M. Matloubian, and A. Weiss. 2010. 'Proline-rich tyrosine kinase-2 is critical for CD8 T-cell short-lived effector fate', *Proc Natl Acad Sci U S A*, 107: 16234-9.

Belcik, J. Todd, Yue Qi, Beat A. Kaufmann, Aris Xie, Sherry Bullens, Terry K. Morgan, Susan P. Bagby, Ganesh Kolumam, Joe Kowalski, Jon A. Oyer, Stuart Bunting, and Jonathan R. Lindner. 2012. 'Cardiovascular and systemic microvascular effects of anti-vascular endothelial growth factor therapy for cancer', *Journal of the American College of Cardiology*, 60: 618-25.

Ben-David, Uri, Benjamin Siranosian, Gavin Ha, Helen Tang, Yaara Oren, Kunihiko Hinohara, Craig A. Strathdee, Joshua Dempster, Nicholas J. Lyons, Robert Burns, Anwesha Nag, Guillaume Kugener, Beth Cimini, Peter Tsvetkov, Yosef E. Maruvka, Ryan O'Rourke, Anthony Garrity, Andrew A. Tubelli, Pratiti Bandopadhayay, Aviad Tsherniak, Francisca Vazquez, Bang Wong, Chet Birger, Mahmoud Ghandi, Aaron R. Thorner, Joshua A. Bittker, Matthew Meyerson, Gad Getz, Rameen Beroukhim, and Todd R. Golub. 2018. 'Genetic and transcriptional evolution alters cancer cell line drug response', *Nature*, 560: 325-30.

Bergers, G., and L. E. Benjamin. 2003. 'Tumorigenesis and the angiogenic switch', *Nat Rev Cancer*, 3: 401-10.

Bergers, Gabriele, Rolf Brekken, Gerald McMahon, Thiennu H. Vu, Takeshi Itoh, Kazuhiko Tamaki, Kazuhiko Tanzawa, Philip Thorpe, Shigeyoshi Itohara, Zena Werb, and Douglas Hanahan. 2000. 'Matrix metalloproteinase-9 triggers the angiogenic switch during carcinogenesis', *Nature Cell Biology*, 2: 737-44.

Bergers, Gabriele, and Steven Song. 2005. 'The role of pericytes in blood-vessel formation and maintenance', *Neuro-oncology*, 7: 452-64.

Bergman, A. M., H. M. Pinedo, I. Talianidis, G. Veerman, W. J. P. Loves, C. L. van der Wilt, and G. J. Peters. 2003. 'Increased sensitivity to gemcitabine of P-glycoprotein and multidrug resistance-associated protein-overexpressing human cancer cell lines', *British Journal Of Cancer*, 88: 1963.

Bingle, L., N. J. Brown, and C. E. Lewis. 2002. 'The role of tumour-associated macrophages in tumour progression: implications for new anticancer therapies', *J Pathol*, 196: 254-65.

Bochen, Alexander, Udaya Kiran Marelli, Elke Otto, Diego Pallarola, Carlos Mas-Moruno, Francesco Saverio Di Leva, Heike Boehm, Joachim P. Spatz, Ettore Novellino, Horst Kessler, and Luciana Marinelli. 2013. 'Biselectivity of isoDGR Peptides for Fibronectin Binding Integrin Subtypes α5β1 and αvβ6: Conformational Control through Flanking Amino Acids', *Journal of Medicinal Chemistry*, 56: 1509-19.

Boj, Sylvia F., Chang-Il Hwang, Lindsey A. Baker, Iok In Christine Chio, Dannielle D. Engle, Vincenzo Corbo, Myrthe Jager, Mariano Ponz-Sarvise, Hervé Tiriac, Mona S. Spector, Ana Gracanin, Tobiloba Oni, Kenneth H. Yu, Ruben van Boxtel, Meritxell Huch, Keith D. Rivera, John P. Wilson, Michael E. Feigin, Daniel Öhlund, Abram Handly-Santana, Christine M. Ardito-Abraham, Michael Ludwig, Ela Elyada, Brinda Alagesan, Giulia Biffi, Georgi N. Yordanov, Bethany Delcuze, Brianna Creighton, Kevin Wright, Youngkyu Park, Folkert H. M. Morsink, I. Quintus Molenaar, Inne H. Borel Rinkes, Edwin Cuppen, Yuan Hao, Ying Jin, Isaac J. Nijman, Christine Iacobuzio-Donahue, Steven D. Leach, Darryl J. Pappin, Molly Hammell, David S. Klimstra, Olca Basturk, Ralph H. Hruban, George Johan Offerhaus, Robert G. J. Vries, Hans Clevers, and David A. Tuveson. 2015. 'Organoid Models of Human and Mouse Ductal Pancreatic Cancer', *Cell*, 160: 324-38.

Borst, P., R. Evers, M. Kool, and J. Wijnholds. 1999. 'The multidrug resistance protein family', *Biochim Biophys Acta*, 1461: 347-57.

Bottazzi, Barbara, Antonio Inforzato, Massimo Messa, Marialuisa Barbagallo, Elena Magrini, Cecilia Garlanda, and Alberto Mantovani. 2016. 'The pentraxins PTX3 and SAP in innate immunity, regulation of inflammation and tissue remodelling', *Journal of hepatology*, 64: 1416-27.

Bourguignon, L. Y., K. Peyrollier, W. Xia, and E. Gilad. 2008. 'Hyaluronan-CD44 interaction activates stem cell marker Nanog, Stat-3-mediated MDR1 gene expression, and ankyrin-regulated multidrug efflux in breast and ovarian tumor cells', *J Biol Chem*, 283: 17635-51.

Brahmer, J. R., C. G. Drake, I. Wollner, J. D. Powderly, J. Picus, W. H. Sharfman, E. Stankevich, A. Pons, T. M. Salay, T. L. McMiller, M. M. Gilson, C. Wang, M. Selby, J. M. Taube, R. Anders, L. Chen, A. J. Korman, D. M. Pardoll, I. Lowy, and S. L. Topalian. 2010. 'Phase I study of single-agent anti-programmed death-1 (MDX-1106) in refractory solid tumors: safety, clinical activity, pharmacodynamics, and immunologic correlates', *J Clin Oncol*, 28: 3167-75.

Brami-Cherrier, Karen, Nicolas Gervasi, Diana Arsenieva, Katarzyna Walkiewicz, Marie-Claude Boutterin, Alvaro Ortega, Paul G. Leonard, Bastien Seantier, Laila Gasmi, Tahar Bouceba, Gress Kadaré, Jean-Antoine Girault, and Stefan T. Arold. 2014. 'FAK dimerization controls its kinase-dependent functions at focal adhesions', *The EMBO Journal*, 33: 356-70.

Braren, Rickmer, Huiqing Hu, Yung Hae Kim, Hilary E. Beggs, Louis F. Reichardt, and Rong Wang. 2006. 'Endothelial FAK is essential for vascular network stability, cell survival, and lamellipodial formation', *The Journal of Cell Biology*, 172: 151-62.

Brem, S., H. Brem, J. Folkman, D. Finkelstein, and A. Patz. 1976. 'Prolonged tumor dormancy by prevention of neovascularization in the vitreous', *Cancer Res*, 36: 2807-12.

Bridgeman, V. L., P. B. Vermeulen, S. Foo, A. Bilecz, F. Daley, E. Kostaras, M. R. Nathan, E. Wan, S. Frentzas, T. Schweiger, B. Hegedus, K. Hoetzenecker, F. Renyi-Vamos, E. A. Kuczynski, N. S. Vasudev, J. Larkin, M. Gore, H. F. Dvorak, S. Paku, R. S. Kerbel, B. Dome, and A. R. Reynolds. 2017. 'Vessel co-option is common in

human lung metastases and mediates resistance to anti-angiogenic therapy in preclinical lung metastasis models', *J Pathol*, 241: 362-74.
Bridgewater, R. E., J. C. Norman, and P. T. Caswell. 2012. 'Integrin trafficking at a glance', *J Cell Sci*, 125: 3695-701.
Brinkmann, Volker, Ulrike Reichard, Christian Goosmann, Beatrix Fauler, Yvonne Uhlemann, David S. Weiss, Yvette Weinrauch, and Arturo Zychlinsky. 2004. 'Neutrophil Extracellular Traps Kill Bacteria', *Science*, 303: 1532.
Brooks, P. C., S. Strömblad, R. Klemke, D. Visscher, F. H. Sarkar, and D. A. Cheresh. 1995. 'Antiintegrin alpha v beta 3 blocks human breast cancer growth and angiogenesis in human skin', *J Clin Invest*, 96: 1815-22.
Brooks, PC, RA Clark, and DA Cheresh. 1994. 'Requirement of vascular integrin alpha v beta 3 for angiogenesis', *Science*, 264: 569-71.
Brooks, Peter C., Anthony M. P. Montgomery, Mauricio Rosenfeld, Ralph A. Reisfeld, Tianhua Hu, George Klier, and David A. Cheresh. 1994. 'Integrin αvβ3 antagonists promote tumor regression by inducing apoptosis of angiogenic blood vessels', *Cell*, 79: 1157-64.
Brooks, Peter C., Staffan Strömblad, Luraynne C. Sanders, Tami L. von Schalscha, Ronald T. Aimes, William G. Stetler-Stevenson, James P. Quigley, and David A. Cheresh. 1996. 'Localization of Matrix Metalloproteinase MMP-2 to the Surface of Invasive Cells by Interaction with Integrin αvβ3', *Cell*, 85: 683-93.
Brown, J. M. 2014. 'Vasculogenesis: a crucial player in the resistance of solid tumours to radiotherapy', *The British journal of radiology*, 87: 20130686-86.
Brufsky, A. M., S. Hurvitz, E. Perez, R. Swamy, V. Valero, V. O'Neill, and H. S. Rugo. 2011. 'RIBBON-2: a randomized, double-blind, placebo-controlled, phase III trial evaluating the efficacy and safety of bevacizumab in combination with chemotherapy for second-line treatment of human epidermal growth factor receptor 2-negative metastatic breast cancer', *J Clin Oncol*, 29: 4286-93.
Buerkle, M. A., S. A. Pahernik, A. Sutter, A. Jonczyk, K. Messmer, and M. Dellian. 2002. 'Inhibition of the alpha-nu integrins with a cyclic RGD peptide impairs angiogenesis, growth and metastasis of solid tumours in vivo', *Br J Cancer*, 86: 788-95.
Burri, P. H., R. Hlushchuk, and V. Djonov. 2004. 'Intussusceptive angiogenesis: its emergence, its characteristics, and its significance', *Dev Dyn*, 231: 474-88.
Cabrita, Rita, Martin Lauss, Adriana Sanna, Marco Donia, Mathilde Skaarup Larsen, Shamik Mitra, Iva Johansson, Bengt Phung, Katja Harbst, Johan Vallon-Christersson, Alison van Schoiack, Kristina Lövgren, Sarah Warren, Karin Jirström, Håkan Olsson, Kristian Pietras, Christian Ingvar, Karolin Isaksson, Dirk Schadendorf, Henrik Schmidt, Lars Bastholt, Ana Carneiro, Jennifer A. Wargo, Inge Marie Svane, and Göran Jönsson. 2020. 'Tertiary lymphoid structures improve immunotherapy and survival in melanoma', *Nature*, 577: 561-65.
Calderwood, D. A., V. Tai, G. Di Paolo, P. De Camilli, and M. H. Ginsberg. 2004. 'Competition for talin results in trans-dominant inhibition of integrin activation', *J Biol Chem*, 279: 28889-95.
Calderwood, D. A., B. Yan, J. M. de Pereda, B. G. Alvarez, Y. Fujioka, R. C. Liddington, and M. H. Ginsberg. 2002. 'The phosphotyrosine binding-like domain of talin activates integrins', *J Biol Chem*, 277: 21749-58.
Calderwood, David A., Sanford J. Shattil, and Mark H. Ginsberg. 2000. 'Integrins and Actin Filaments: Reciprocal Regulation of Cell Adhesion and Signaling *', *Journal of Biological Chemistry*, 275: 22607-10.
Campbell, D. J., and M. A. Koch. 2011. 'Treg cells: patrolling a dangerous neighborhood.' in, *Nat Med* (United States).

Campbell, Iain D., and Martin J. Humphries. 2011. 'Integrin structure, activation, and interactions', *Cold Spring Harbor perspectives in biology*, 3: a004994.
Campochiaro, Peter A. 2013. 'Ocular neovascularization', *Journal of molecular medicine (Berlin, Germany)*, 91: 311-21.
Cance, William G., and Vita M. Golubovskaya. 2008. 'Focal Adhesion Kinase Versus p53: Apoptosis or Survival?', *Science Signaling*, 1: pe22.
Canel, Marta, Alan Serrels, Derek Miller, Paul Timpson, Bryan Serrels, Margaret C. Frame, and Valerie G. Brunton. 2010. 'Quantitative In vivo Imaging of the Effects of Inhibiting Integrin Signaling via Src and FAK on Cancer Cell Movement: Effects on E-cadherin Dynamics', *Cancer Research*, 70: 9413.
Cao, Renhai, Anna Eriksson, Hajime Kubo, Kari Alitalo, Yihai Cao, and Johan Thyberg. 2004. 'Comparative Evaluation of FGF-2–, VEGF-A–, and VEGF-C–Induced Angiogenesis, Lymphangiogenesis, Vascular Fenestrations, and Permeability', *Circulation Research*, 94: 664-70.
Cao, Yihai, and Robert Langer. 2008. 'A review of Judah Folkman's remarkable achievements in biomedicine', *Proc Natl Acad Sci U S A*, 105: 13203-05.
Cao, Zhongwei, Bi-Sen Ding, Peipei Guo, Sharrell B Lee, Jason M Butler, Stephanie C Casey, Michael Simons, Wayne Tam, Dean W Felsher, Koji Shido, Arash Rafii, Joseph M Scandura, and Shahin Rafii. 2014. 'Angiocrine Factors Deployed by Tumor Vascular Niche Induce B Cell Lymphoma Invasiveness and Chemoresistance', *Cancer Cell*, 25: 350-65.
Carmeliet, Peter. 2000. 'Mechanisms of angiogenesis and arteriogenesis', *Nature Medicine*, 6: 389-95.
Carmeliet, Peter, and Rakesh K. Jain. 2000. 'Angiogenesis in cancer and other diseases', *Nature*, 407: 249-57.
Casado, P., and P. R. Cutillas. 2011. 'A self-validating quantitative mass spectrometry method for assessing the accuracy of high-content phosphoproteomic experiments', *Mol Cell Proteomics*, 10: M110.003079.
Caswell, P. T., and J. C. Norman. 2006. 'Integrin trafficking and the control of cell migration', *Traffic*, 7: 14-21.
Cedervall, Jessica, Yanyu Zhang, and Anna-Karin Olsson. 2016. 'Tumor-Induced NETosis as a Risk Factor for Metastasis and Organ Failure', *Cancer Research*, 76: 4311.
Chauhan, Akshita, and Tabassum Khan. 2021. 'Focal adhesion kinase—An emerging viable target in cancer and development of focal adhesion kinase inhibitors', *Chemical Biology & Drug Design*, 97: 774-94.
Chauhan, Vikash P., Triantafyllos Stylianopoulos, John D. Martin, Zoran Popović, Ou Chen, Walid S. Kamoun, Moungi G. Bawendi, Dai Fukumura, and Rakesh K. Jain. 2012. 'Normalization of tumour blood vessels improves the delivery of nanomedicines in a size-dependent manner', *Nature nanotechnology*, 7: 383-88.
Chen, H. X., and J. N. Cleck. 2009. 'Adverse effects of anticancer agents that target the VEGF pathway', *Nat Rev Clin Oncol*, 6: 465-77.
Chen, Xiao Lei, Ju-Ock Nam, Christine Jean, Christine Lawson, Colin T Walsh, Erik Goka, Ssang-Taek Lim, Alok Tomar, Isabelle Tancioni, Sean Uryu, Jun-Lin Guan, Lisette M Acevedo, Sara M Weis, David A Cheresh, and David D Schlaepfer. 2012. 'VEGF-Induced Vascular Permeability Is Mediated by FAK', *Developmental Cell*, 22: 146-57.
Chen, Z., X. H. Xu, and J. Hu. 2016. 'Role of pericytes in angiogenesis: focus on cancer angiogenesis and anti-angiogenic therapy', *Neoplasma*, 63: 173-82.
Chiang, Anne C., and Joan Massagué. 2008. 'Molecular basis of metastasis', *N Engl J Med*, 359: 2814-23.

Chien, S. 2007. 'Mechanotransduction and endothelial cell homeostasis: the wisdom of the cell', *Am J Physiol Heart Circ Physiol*, 292: H1209-24.
Chinot, O. L. 2014. 'Cilengitide in glioblastoma: when did it fail?', *Lancet Oncol*, 15: 1044-5.
Claxton, S., V. Kostourou, S. Jadeja, P. Chambon, K. Hodivala-Dilke, and M. Fruttiger. 2008. 'Efficient, inducible Cre-recombinase activation in vascular endothelium', *Genesis*, 46: 74-80.
Cohen, M. H., J. Gootenberg, P. Keegan, and R. Pazdur. 2007. 'FDA drug approval summary: bevacizumab plus FOLFOX4 as second-line treatment of colorectal cancer', *Oncologist*, 12: 356-61.
Coller, B. S., U. Seligsohn, and P. A. Little. 1987. 'Type I Glanzmann thrombasthenia patients from the Iraqi-Jewish and Arab populations in Israel can be differentiated by platelet glycoprotein IIIa immunoblot analysis', *Blood*, 69: 1696-703.
Conroy, T., F. Desseigne, M. Ychou, O. Bouche, R. Guimbaud, Y. Becouarn, A. Adenis, J. L. Raoul, S. Gourgou-Bourgade, C. de la Fouchardiere, J. Bennouna, J. B. Bachet, F. Khemissa-Akouz, D. Pere-Verge, C. Delbaldo, E. Assenat, B. Chauffert, P. Michel, C. Montoto-Grillot, and M. Ducreux. 2011. 'FOLFIRINOX versus gemcitabine for metastatic pancreatic cancer', *N Engl J Med*, 364: 1817-25.
Cooke, V. G., V. S. LeBleu, D. Keskin, Z. Khan, J. T. O'Connell, Y. Teng, M. B. Duncan, L. Xie, G. Maeda, S. Vong, H. Sugimoto, R. M. Rocha, A. Damascena, R. R. Brentani, and R. Kalluri. 2012. 'Pericyte depletion results in hypoxia-associated epithelial-to-mesenchymal transition and metastasis mediated by met signaling pathway', *Cancer Cell*, 21: 66-81.
Cools-Lartigue, Jonathan, Jonathan Spicer, Braedon McDonald, Stephen Gowing, Simon Chow, Betty Giannias, France Bourdeau, Paul Kubes, and Lorenzo Ferri. 2013. 'Neutrophil extracellular traps sequester circulating tumor cells and promote metastasis', *The Journal of Clinical Investigation*, 123: 3446-58.
Coppé, J. P., C. K. Patil, F. Rodier, Y. Sun, D. P. Muñoz, J. Goldstein, P. S. Nelson, P. Y. Desprez, and J. Campisi. 2008. 'Senescence-associated secretory phenotypes reveal cell-nonautonomous functions of oncogenic RAS and the p53 tumor suppressor', *PLoS Biol*, 6: 2853-68.
Coronella, J. A., P. Telleman, G. A. Kingsbury, T. D. Truong, S. Hays, and R. P. Junghans. 2001. 'Evidence for an antigen-driven humoral immune response in medullary ductal breast cancer', *Cancer Res*, 61: 7889-99.
Corsi, J. M., C. Houbron, P. Billuart, I. Brunet, K. Bouvrée, A. Eichmann, J. A. Girault, and H. Enslen. 2009. 'Autophosphorylation-independent and -dependent functions of focal adhesion kinase during development', *J Biol Chem*, 284: 34769-76.
Corsi, J. M., E. Rouer, J. A. Girault, and H. Enslen. 2006. 'Organization and post-transcriptional processing of focal adhesion kinase gene', *BMC Genomics*, 7: 198.
Cox, N., D. Pilling, and R. H. Gomer. 2014. 'Serum amyloid P: a systemic regulator of the innate immune response', *J Leukoc Biol*, 96: 739-43.
Craig, David, Mu Gao, Klaus Schulten, and Viola Vogel. 2004. 'Structural Insights into How the MIDAS Ion Stabilizes Integrin Binding to an RGD Peptide under Force', *Structure*, 12: 2049-58.
Criscuoli, M. L., M. Nguyen, and B. P. Eliceiri. 2005. 'Tumor metastasis but not tumor growth is dependent on Src-mediated vascular permeability', *Blood*, 105: 1508-14.
Critchley, David R., and Alexandre R. Gingras. 2008. 'Talin at a glance', *Journal of Cell Science*, 121: 1345.

CRUK. 2019. 'Bevacizumab (Avastin)', CRUK, Accessed 07/07/2021. https://www.cancerresearchuk.org/about-cancer/cancer-in-general/treatment/cancer-drugs/drugs/bevacizumab.

Curiel, T. J., G. Coukos, L. Zou, X. Alvarez, P. Cheng, P. Mottram, M. Evdemon-Hogan, J. R. Conejo-Garcia, L. Zhang, M. Burow, Y. Zhu, S. Wei, I. Kryczek, B. Daniel, A. Gordon, L. Myers, A. Lackner, M. L. Disis, K. L. Knutson, L. Chen, and W. Zou. 2004. 'Specific recruitment of regulatory T cells in ovarian carcinoma fosters immune privilege and predicts reduced survival', *Nat Med*, 10: 942-9.

Curley, G. P., H. Blum, and M. J. Humphries. 1999. 'Integrin antagonists', *Cell Mol Life Sci*, 56: 427-41.

Currie. 2021. "Study of FAK (Defactinib) and PD-1 (Pembrolizumab) Inhibition in Advanced Solid Malignancies (FAK-PD1)." In.: https://ClinicalTrials.gov/show/NCT02758587.

Cutillas, P. R., and B. Vanhaesebroeck. 2007. 'Quantitative profile of five murine core proteomes using label-free functional proteomics', *Mol Cell Proteomics*, 6: 1560-73.

Daldrup, H., D. M. Shames, M. Wendland, Y. Okuhata, T. M. Link, W. Rosenau, Y. Lu, and R. C. Brasch. 1998. 'Correlation of dynamic contrast-enhanced MR imaging with histologic tumor grade: comparison of macromolecular and small-molecular contrast media', *AJR Am J Roentgenol*, 171: 941-9.

Dallinga, Marchien, Sonja Boas, Ingeborg Klaassen, Roeland Merks, Cornelis van Noorden, and Reinier Schlingemann. 2015. "Tip Cells in Angiogenesis." In, edited by Ltd John Wiley & Sons. https://doi.org/10.1002/9780470015902.a0025977.

Danen, Erik. 2000. 'Integrins: An Overview of Structural and Functional Aspects'.

De Franceschi, N., H. Hamidi, J. Alanko, P. Sahgal, and J. Ivaska. 2015. 'Integrin traffic - the update', *J Cell Sci*, 128: 839-52.

De Palma, M., M. A. Venneri, R. Galli, L. Sergi Sergi, L. S. Politi, M. Sampaolesi, and L. Naldini. 2005. 'Tie2 identifies a hematopoietic lineage of proangiogenic monocytes required for tumor vessel formation and a mesenchymal population of pericyte progenitors', *Cancer Cell*, 8: 211-26.

De Palma, M., M. A. Venneri, C. Roca, and L. Naldini. 2003. 'Targeting exogenous genes to tumor angiogenesis by transplantation of genetically modified hematopoietic stem cells', *Nat Med*, 9: 789-95.

De Palma, Michele, and Luigi Naldini. 2011. 'Angiopoietin-2 TIEs Up Macrophages in Tumor Angiogenesis', *Clinical Cancer Research*, 17: 5226.

De Val, S., and B. L. Black. 2009. 'Transcriptional control of endothelial cell development', *Dev Cell*, 16: 180-95.

DeClerck, Yves A. 2012. 'Desmoplasia: A Response or a Niche?', *Cancer Discovery*, 2: 772.

Deshpande, Nirupama, Ying Ren, Kira Foygel, Jarrett Rosenberg, and Jürgen K. Willmann. 2011. 'Tumor angiogenic marker expression levels during tumor growth: longitudinal assessment with molecularly targeted microbubbles and US imaging', *Radiology*, 258: 804-11.

Di Paolo, G., L. Pellegrini, K. Letinic, G. Cestra, R. Zoncu, S. Voronov, S. Chang, J. Guo, M. R. Wenk, and P. De Camilli. 2002. 'Recruitment and regulation of phosphatidylinositol phosphate kinase type 1 gamma by the FERM domain of talin', *Nature*, 420: 85-9.

Diaz, Roberto Jose, Sheikh Ali, Mehreen Gull Qadir, Macarena I. De La Fuente, Michael E. Ivan, and Ricardo J. Komotar. 2017. 'The role of bevacizumab in the treatment of glioblastoma', *Journal of Neuro-Oncology*, 133: 455-67.

Diggle, Peter, Patrick Heagerty, K. Y. Liang, and Scott Zeger. 2002. *The Analysis of Longitudinal Data*.

Dikic, I., G. Tokiwa, S. Lev, S. A. Courtneidge, and J. Schlessinger. 1996. 'A role for Pyk2 and Src in linking G-protein-coupled receptors with MAP kinase activation', *Nature*, 383: 547-50.

Dimberg, A., and M. Sund. 2014. 'Cancer Angiogenesis and Vasculogenesis.' in Linda M. McManus and Richard N. Mitchell (eds.), *Pathobiology of Human Disease* (Academic Press: San Diego).

Dockstader, Colleen L., and Derek van der Kooy. 2001. 'Mouse Strain Differences in Opiate Reward Learning Are Explained by Differences in Anxiety, Not Reward or Learning', *The Journal of Neuroscience*, 21: 9077-81.

Donaldson, J. G., and C. L. Jackson. 2011. 'ARF family G proteins and their regulators: roles in membrane transport, development and disease', *Nat Rev Mol Cell Biol*, 12: 362-75.

Dong, Daoyin, and Peixin Yang. 2018. 'Yolk Sac.' in Michael K. Skinner (ed.), *Encyclopedia of Reproduction (Second Edition)* (Academic Press: Oxford).

Dormond, Olivier, Ferdy J. Lejeune, and Curzio Ruegg. 2002. 'Modulation of cdk2, cyclin D1, p16INK4a, p21WAF and p27Kip1 expression in endothelial cells by TNF/IFN gamma', *Anticancer research*, 22: 3159-63.

Dougan, M., G. Dranoff, and S. K. Dougan. 2019. 'GM-CSF, IL-3, and IL-5 Family of Cytokines: Regulators of Inflammation', *Immunity*, 50: 796-811.

Dozynkiewicz, M. A., N. B. Jamieson, I. Macpherson, J. Grindlay, P. V. van den Berghe, A. von Thun, J. P. Morton, C. Gourley, P. Timpson, C. Nixon, C. J. McKay, R. Carter, D. Strachan, K. Anderson, O. J. Sansom, P. T. Caswell, and J. C. Norman. 2012. 'Rab25 and CLIC3 collaborate to promote integrin recycling from late endosomes/lysosomes and drive cancer progression', *Dev Cell*, 22: 131-45.

Dranoff, Glenn. 2004. 'Cytokines in cancer pathogenesis and cancer therapy', *Nature Reviews Cancer*, 4: 11-22.

Dudley, A. C. 2012. 'Tumor endothelial cells', *Cold Spring Harb Perspect Med*, 2: a006536.

Dukinfield, Matthew, Eleni Maniati, Louise E. Reynolds, Aisah Aubdool, Reshma S. Baliga, Gabriela D'Amico, Oscar Maiques, Jun Wang, Kenneth C. Bedi, Jr., Kenneth B. Margulies, Victoria Sanz-Moreno, Adrian Hobbs, and Kairbaan Hodivala-Dilke. 2019. 'Repurposing an anti-cancer agent for the treatment of hypertrophic heart disease', *The Journal of pathology*, 249: 523-35.

Durand, Nisha, Ligia I. Bastea, Jason Long, Heike Döppler, Kun Ling, and Peter Storz. 2016. 'Protein Kinase D1 regulates focal adhesion dynamics and cell adhesion through Phosphatidylinositol-4-phosphate 5-kinase type-l γ', *Scientific Reports*, 6: 35963.

Dvorak, H. F. 1986. 'Tumors: wounds that do not heal. Similarities between tumor stroma generation and wound healing', *N Engl J Med*, 315: 1650-9.

Dvorak, H. F., L. F. Brown, M. Detmar, and A. M. Dvorak. 1995. 'Vascular permeability factor/vascular endothelial growth factor, microvascular hyperpermeability, and angiogenesis', *Am J Pathol*, 146: 1029-39.

Díaz-González, F., J. Forsyth, B. Steiner, and M. H. Ginsberg. 1996. 'Trans-dominant inhibition of integrin function', *Mol Biol Cell*, 7: 1939-51.

Edwardson, D. W., A. M. Parissenti, and A. T. Kovala. 2019. 'Chemotherapy and Inflammatory Cytokine Signalling in Cancer Cells and the Tumour Microenvironment', *Adv Exp Med Biol*, 1152: 173-215.

Eliceiri, B. P., R. Klemke, S. Strömblad, and D. A. Cheresh. 1998. 'Integrin αvβ3 requirement for sustained mitogen-activated protein kinase activity during angiogenesis', *Journal of Cell Biology*, 140: 1255-63.

Eltzschig, H. K., P. Abdulla, E. Hoffman, K. E. Hamilton, D. Daniels, C. Schönfeld, M. Löffler, G. Reyes, M. Duszenko, J. Karhausen, A. Robinson, K. A. Westerman, I. R. Coe, and S. P. Colgan. 2005. 'HIF-1-dependent repression of equilibrative nucleoside transporter (ENT) in hypoxia', *J Exp Med*, 202: 1493-505.

Emsley, J., C. G. Knight, R. W. Farndale, M. J. Barnes, and R. C. Liddington. 2000. 'Structural basis of collagen recognition by integrin alpha2beta1', *Cell*, 101: 47-56.

Erkan, Mert, Carolin Reiser-Erkan, Christoph W. Michalski, Stefanie Deucker, Danguole Sauliunaite, Sylvia Streit, Irene Esposito, Helmut Friess, and Jörg Kleeff. 2009. 'Cancer-stellate cell interactions perpetuate the hypoxia-fibrosis cycle in pancreatic ductal adenocarcinoma', *Neoplasia (New York, N.Y.)*, 11: 497-508.

Errasti-Murugarren, E., P. Fernández-Calotti, M. Veyhl-Wichmann, M. Diepold, I. Pinilla-Macua, S. Pérez-Torras, H. Kipp, H. Koepsell, and M. Pastor-Anglada. 2012. 'Role of the transporter regulator protein (RS1) in the modulation of concentrative nucleoside transporters (CNTs) in epithelia', *Mol Pharmacol*, 82: 59-67.

Falcón, Beverly L., Hiroya Hashizume, Petros Koumoutsakos, Jeyling Chou, James V. Bready, Angela Coxon, Jonathan D. Oliner, and Donald M. McDonald. 2009. 'Contrasting actions of selective inhibitors of angiopoietin-1 and angiopoietin-2 on the normalization of tumor blood vessels', *The American journal of pathology*, 175: 2159-70.

Feletou, M., E. H. Tang, and P. M. Vanhoutte. 2008. 'Nitric oxide the gatekeeper of endothelial vasomotor control', *Front Biosci*, 13: 4198-217.

Fennell, D. A., P. Baas, P. Taylor, A. K. Nowak, D. Gilligan, T. Nakano, J. A. Pachter, D. T. Weaver, A. Scherpereel, N. Pavlakis, J. P. van Meerbeeck, S. Cedres, L. Nolan, H. Kindler, and Jgjv Aerts. 2019. 'Maintenance Defactinib Versus Placebo After First-Line Chemotherapy in Patients With Merlin-Stratified Pleural Mesothelioma: COMMAND-A Double-Blind, Randomized, Phase II Study', *J Clin Oncol*, 37: 790-98.

Fernández-Sánchez, María Elena, Sandrine Barbier, Joanne Whitehead, Gaëlle Béalle, Aude Michel, Heldmuth Latorre-Ossa, Colette Rey, Laura Fouassier, Audrey Claperon, Laura Brullé, Elodie Girard, Nicolas Servant, Thomas Rio-Frio, Hélène Marie, Sylviane Lesieur, Chantal Housset, Jean-Luc Gennisson, Mickaël Tanter, Christine Ménager, Silvia Fre, Sylvie Robine, and Emmanuel Farge. 2015. 'Mechanical induction of the tumorigenic β-catenin pathway by tumour growth pressure', *Nature*, 523: 92-95.

Folkman, J, and M Klagsbrun. 1987. 'Angiogenic factors', *Science*, 235: 442-47.

Folkman, J. 2006. 'Antiangiogenesis in cancer therapy--endostatin and its mechanisms of action', *Exp Cell Res*, 312: 594-607.

Folkman, J., and M. Hochberg. 1973. 'Self-regulation of growth in three dimensions', *J Exp Med*, 138: 745-53.

Folkman, J., D. M. Long, Jr., and F. F. Becker. 1963. 'Growth and metastasis of tumor in organ culture', *Cancer*, 16: 453-67.

Folkman, Judah. 1971. 'Tumor Angiogenesis: Therapeutic Implications', *New England Journal of Medicine*, 285: 1182-86.

Forster, Jake C., Wendy M. Harriss-Phillips, Michael Jj Douglass, and Eva Bezak. 2017. 'A review of the development of tumor vasculature and its effects on the tumor microenvironment', *Hypoxia (Auckland, N.Z.)*, 5: 21-32.

Fozza, C., and M. Longinotti. 2011. 'T-Cell Traffic Jam in Hodgkin's Lymphoma: Pathogenetic and Therapeutic Implications', *Adv Hematol*, 2011: 501659.
Francavilla, Chiara, Luigi Maddaluno, and Ugo Cavallaro. 2009. 'The functional role of cell adhesion molecules in tumor angiogenesis', *Seminars in Cancer Biology*, 19: 298-309.
Frantz, Christian, Kathleen M. Stewart, and Valerie M. Weaver. 2010. 'The extracellular matrix at a glance', *Journal of Cell Science*, 123: 4195.
Fridman, W. H., F. Pagès, C. Sautès-Fridman, and J. Galon. 2012. 'The immune contexture in human tumours: impact on clinical outcome.' in, *Nat Rev Cancer* (England).
Friedlander, M., P. C. Brooks, R. W. Shaffer, C. M. Kincaid, J. A. Varner, and D. A. Cheresh. 1995. 'Definition of two angiogenic pathways by distinct alpha v integrins', *Science*, 270: 1500-2.
Fuchs, Tobias A., Ulrike Abed, Christian Goosmann, Robert Hurwitz, Ilka Schulze, Volker Wahn, Yvette Weinrauch, Volker Brinkmann, and Arturo Zychlinsky. 2007. 'Novel cell death program leads to neutrophil extracellular traps', *Journal of Cell Biology*, 176: 231-41.
Gabrilovich, Dmitry I., and Srinivas Nagaraj. 2009. 'Myeloid-derived suppressor cells as regulators of the immune system', *Nature reviews. Immunology*, 9: 162-74.
Gades, Naomi M., Akihiro Ohash, Lisa D. Mills, Matt A. Rowley, Kelly S. Predmore, Ronald J. Marler, and Fergus J. Couch. 2008. 'Spontaneous vulvar papillomas in a colony of mice used for pancreatic cancer research', *Comparative medicine*, 58: 271-75.
Galdiero, Maria Rosaria, Gianni Marone, and Alberto Mantovani. 2018. 'Cancer Inflammation and Cytokines', *Cold Spring Harbor Perspectives in Biology*, 10.
Ganss, R. 2015. 'Keeping the Balance Right: Regulator of G Protein Signaling 5 in Vascular Physiology and Pathology', *Prog Mol Biol Transl Sci*, 133: 93-121.
Gao, Haihe, Lisha Li, Mang Xiao, Yongwei Guo, Yi Shen, Lixin Cheng, and Ming Tang. 2018. 'Elevated DKK1 expression is an independent unfavorable prognostic indicator of survival in head and neck squamous cell carcinoma', *Cancer management and research*, 10: 5083-89.
Geiger, Benjamin, Joachim P. Spatz, and Alexander D. Bershadsky. 2009. 'Environmental sensing through focal adhesions', *Nature Reviews Molecular Cell Biology*, 10: 21-33.
Gerber, David E., D. Ross Camidge, Daniel Morgensztern, Jeremey Cetnar, Ronan J. Kelly, Suresh S. Ramalingam, David R. Spigel, Woondong Jeong, Pier P. Scaglioni, Song Zhang, Marilyn Li, David T. Weaver, Louis Vaikus, Mitchell Keegan, Joanna C. Horobin, and Timothy F. Burns. 2020. 'Phase 2 study of the focal adhesion kinase inhibitor defactinib (VS-6063) in previously treated advanced KRAS mutant non-small cell lung cancer', *Lung Cancer*, 139: 60-67.
Gilbert, L. A., and M. T. Hemann. 2010. 'DNA damage-mediated induction of a chemoresistant niche', *Cell*, 143: 355-66.
Gilbert, SF, and MA Sunderland. 2000. *Developmental Biology. 6th edition.* (Sinauer Associates: Online).
Gillen, S., T. Schuster, C. Meyer Zum Buschenfelde, H. Friess, and J. Kleeff. 2010. 'Preoperative/neoadjuvant therapy in pancreatic cancer: a systematic review and meta-analysis of response and resection percentages', *PLoS Med*, 7: e1000267.

Gimbrone, M. A., Jr., R. S. Cotran, S. B. Leapman, and J. Folkman. 1974. 'Tumor growth and neovascularization: an experimental model using the rabbit cornea', *J Natl Cancer Inst*, 52: 413-27.

Gimbrone, M. A., Jr., S. B. Leapman, R. S. Cotran, and J. Folkman. 1973. 'Tumor angiogenesis: iris neovascularization at a distance from experimental intraocular tumors', *J Natl Cancer Inst*, 50: 219-28.

Ginsberg, Mark H. 2014. 'Integrin activation', *BMB reports*, 47: 655-59.

Ginsberg, Mark H., Anthony Partridge, and Sanford J. Shattil. 2005. 'Integrin regulation', *Current Opinion in Cell Biology*, 17: 509-16.

Gogineni, A., M. Caunt, A. Crow, C. V. Lee, G. Fuh, N. van Bruggen, W. Ye, and R. M. Weimer. 2013. 'Inhibition of VEGF-C modulates distal lymphatic remodeling and secondary metastasis', *PLoS One*, 8: e68755.

Goldmann, E. 1907. 'THE GROWTH OF MALIGNANT DISEASE IN MAN AND THE LOWER ANIMALS,: WITH SPECIAL REFERENCE TO THE VASCULAR SYSTEM', *The Lancet*, 170: 1236-40.

Golombek, Susanne K., Jan-Niklas May, Benjamin Theek, Lia Appold, Natascha Drude, Fabian Kiessling, and Twan Lammers. 2018. 'Tumor targeting via EPR: Strategies to enhance patient responses', *Advanced drug delivery reviews*, 130: 17-38.

Golubovskaya, Vita M., Sheila Figel, Baotran T. Ho, Christopher P. Johnson, Michael Yemma, Grace Huang, Min Zheng, Carl Nyberg, Andrew Magis, David A. Ostrov, Irwin H. Gelman, and William G. Cance. 2012. 'A small molecule focal adhesion kinase (FAK) inhibitor, targeting Y397 site: 1-(2-hydroxyethyl)-3, 5, 7-triaza-1-azoniatricyclo [3.3.1.1(3,7)]decane; bromide effectively inhibits FAK autophosphorylation activity and decreases cancer cell viability, clonogenicity and tumor growth in vivo', *Carcinogenesis*, 33: 1004-13.

Gottschalk, Kay-Eberhard, and Horst Kessler. 2004. 'A Computational Model of Transmembrane Integrin Clustering', *Structure*, 12: 1109-16.

Gourgou-Bourgade, S., C. Bascoul-Mollevi, F. Desseigne, M. Ychou, O. Bouche, R. Guimbaud, Y. Becouarn, A. Adenis, J. L. Raoul, V. Boige, J. Berille, and T. Conroy. 2013. 'Impact of FOLFIRINOX compared with gemcitabine on quality of life in patients with metastatic pancreatic cancer: results from the PRODIGE 4/ACCORD 11 randomized trial', *J Clin Oncol*, 31: 23-9.

Granot, Z., E. Henke, E. A. Comen, T. A. King, L. Norton, and R. Benezra. 2011. 'Tumor entrained neutrophils inhibit seeding in the premetastatic lung', *Cancer Cell*, 20: 300-14.

Grant, D. S., K. Tashiro, B. Segui-Real, Y. Yamada, G. R. Martin, and H. K. Kleinman. 1989. 'Two different laminin domains mediate the differentiation of human endothelial cells into capillary-like structures in vitro', *Cell*, 58: 933-43.

Grant, Roger I., David A. Hartmann, Robert G. Underly, Andrée-Anne Berthiaume, Narayan R. Bhat, and Andy Y. Shih. 2019. 'Organizational hierarchy and structural diversity of microvascular pericytes in adult mouse cortex', *Journal of cerebral blood flow and metabolism : official journal of the International Society of Cerebral Blood Flow and Metabolism*, 39: 411-25.

Guan, Jun-Lin. 1997. 'Role of focal adhesion kinase in integrin signaling', *The International Journal of Biochemistry & Cell Biology*, 29: 1085-96.

Guerra, Liliana, Teresa Odorisio, Giovanna Zambruno, and Daniele Castiglia. 2017. 'Stromal microenvironment in type VII collagen-deficient skin: The ground for squamous cell carcinoma development', *Matrix Biology*, 63: 1-10.

Hamzah, Juliana, Manfred Jugold, Fabian Kiessling, Paul Rigby, Mitali Manzur, Hugo H. Marti, Tamer Rabie, Sylvia Kaden, Hermann-Josef Gröne, Günter J.

Hämmerling, Bernd Arnold, and Ruth Ganss. 2008. 'Vascular normalization in Rgs5-deficient tumours promotes immune destruction', *Nature*, 453: 410-14.
Hanahan, Douglas, and Robert A Weinberg. 2011. 'Hallmarks of Cancer: The Next Generation', *Cell*, 144: 646-74.
Hansen, Elsa, Robert J. Woods, and Andrew F. Read. 2017. 'How to Use a Chemotherapeutic Agent When Resistance to It Threatens the Patient', *PLOS Biology*, 15: e2001110.
Harburger, David S., and David A. Calderwood. 2009. 'Integrin signalling at a glance', *Journal of Cell Science*, 122: 159.
Hashizume, H., P. Baluk, S. Morikawa, J. W. McLean, G. Thurston, S. Roberge, R. K. Jain, and D. M. McDonald. 2000. 'Openings between defective endothelial cells explain tumor vessel leakiness', *Am J Pathol*, 156: 1363-80.
Haskell, H., M. Natarajan, T. P. Hecker, Q. Ding, J. Stewart, Jr., J. R. Grammer, and C. L. Gladson. 2003. 'Focal adhesion kinase is expressed in the angiogenic blood vessels of malignant astrocytic tumors in vivo and promotes capillary tube formation of brain microvascular endothelial cells', *Clin Cancer Res*, 9: 2157-65.
He, D., H. Li, N. Yusuf, C. A. Elmets, J. Li, J. D. Mountz, and H. Xu. 2010. 'IL-17 promotes tumor development through the induction of tumor promoting microenvironments at tumor sites and myeloid-derived suppressor cells', *J Immunol*, 184: 2281-8.
Heil, Matthias, and Wolfgang Schaper. 2004. 'Influence of Mechanical, Cellular, and Molecular Factors on Collateral Artery Growth (Arteriogenesis)', *Circulation Research*, 95: 449-58.
Heim, J. B., E. J. Squirewell, A. Neu, G. Zocher, S. Sominidi-Damodaran, S. P. Wyles, E. Nikolova, N. Behrendt, D. M. Saunte, J. Lock-Andersen, K. S. Gaonkar, H. Yan, J. N. Sarkaria, M. Krendel, J. van Deursen, R. Sprangers, T. Stehle, R. T. Böttcher, J. H. Lee, T. Ordog, and A. Meves. 2017. 'Myosin-1E interacts with FAK proline-rich region 1 to induce fibronectin-type matrix', *Proc Natl Acad Sci U S A*, 114: 3933-38.
Heldin, C. H., K. Rubin, K. Pietras, and A. Ostman. 2004. 'High interstitial fluid pressure - an obstacle in cancer therapy', *Nat Rev Cancer*, 4: 806-13.
Hellstrom, M., M. Kalen, P. Lindahl, A. Abramsson, and C. Betsholtz. 1999. 'Role of PDGF-B and PDGFR-beta in recruitment of vascular smooth muscle cells and pericytes during embryonic blood vessel formation in the mouse', *Development*, 126: 3047-55.
Helmink, Beth A., Sangeetha M. Reddy, Jianjun Gao, Shaojun Zhang, Rafet Basar, Rohit Thakur, Keren Yizhak, Moshe Sade-Feldman, Jorge Blando, Guangchun Han, Vancheswaran Gopalakrishnan, Yuanxin Xi, Hao Zhao, Rodabe N. Amaria, Hussein A. Tawbi, Alex P. Cogdill, Wenbin Liu, Valerie S. LeBleu, Fernanda G. Kugeratski, Sapna Patel, Michael A. Davies, Patrick Hwu, Jeffrey E. Lee, Jeffrey E. Gershenwald, Anthony Lucci, Reetakshi Arora, Scott Woodman, Emily Z. Keung, Pierre-Olivier Gaudreau, Alexandre Reuben, Christine N. Spencer, Elizabeth M. Burton, Lauren E. Haydu, Alexander J. Lazar, Roberta Zapassodi, Courtney W. Hudgens, Deborah A. Ledesma, SuFey Ong, Michael Bailey, Sarah Warren, Disha Rao, Oscar Krijgsman, Elisa A. Rozeman, Daniel Peeper, Christian U. Blank, Ton N. Schumacher, Lisa H. Butterfield, Monika A. Zelazowska, Kevin M. McBride, Raghu Kalluri, James Allison, Florent Petitprez, Wolf Herman Fridman, Catherine Sautès-Fridman, Nir Hacohen, Katayoun Rezvani, Padmanee Sharma, Michael T. Tetzlaff, Linghua Wang, and Jennifer A. Wargo. 2020. 'B cells and tertiary lymphoid structures promote immunotherapy response', *Nature*, 577: 549-55.

Henderson, N. C., F. Rieder, and T. A. Wynn. 2020. 'Fibrosis: from mechanisms to medicines', *Nature*, 587: 555-66.
Herbert, Shane P., and Didier Y. R. Stainier. 2011. 'Molecular control of endothelial cell behaviour during blood vessel morphogenesis', *Nature reviews. Molecular cell biology*, 12: 551-64.
Hildebrand, J D, M D Schaller, and J T Parsons. 1993. 'Identification of sequences required for the efficient localization of the focal adhesion kinase, pp125FAK, to cellular focal adhesions', *The Journal of Cell Biology*, 123: 993-1005.
Hillen, Femke, and Arjan W. Griffioen. 2007. 'Tumour vascularization: sprouting angiogenesis and beyond', *Cancer and Metastasis Reviews*, 26: 489-502.
Hingorani, S. R., L. Wang, A. S. Multani, C. Combs, T. B. Deramaudt, R. H. Hruban, A. K. Rustgi, S. Chang, and D. A. Tuveson. 2005. 'Trp53R172H and KrasG12D cooperate to promote chromosomal instability and widely metastatic pancreatic ductal adenocarcinoma in mice', *Cancer Cell*, 7: 469-83.
Hiraoka, N., K. Onozato, T. Kosuge, and S. Hirohashi. 2006. 'Prevalence of FOXP3+ regulatory T cells increases during the progression of pancreatic ductal adenocarcinoma and its premalignant lesions', *Clin Cancer Res*, 12: 5423-34.
Hiratsuka, Sachie, Shom Goel, Walid S. Kamoun, Yoshiro Maru, Dai Fukumura, Dan G. Duda, and Rakesh K. Jain. 2011. 'Endothelial focal adhesion kinase mediates cancer cell homing to discrete regions of the lungs via E-selectin up-regulation', *Proceedings of the National Academy of Sciences*, 108: 3725.
Hodivala-Dilke, Kairbaan M., Kevin P. McHugh, Dimitrios A. Tsakiris, Helen Rayburn, Denise Crowley, Mollie Ullman-Culleré, F. Patrick Ross, Barry S. Coller, Steven Teitelbaum, and Richard O. Hynes. 1999. 'β3-integrin–deficient mice are a model for Glanzmann thrombasthenia showing placental defects and reduced survival', *The Journal of Clinical Investigation*, 103: 229-38.
Hong, In-Sun. 2016. 'Stimulatory versus suppressive effects of GM-CSF on tumor progression in multiple cancer types', *Experimental & molecular medicine*, 48: e242-e42.
Hong, S. P., J. Wen, S. Bang, S. Park, and S. Y. Song. 2009. 'CD44-positive cells are responsible for gemcitabine resistance in pancreatic cancer cells', *Int J Cancer*, 125: 2323-31.
Hood, J. D., R. Frausto, W. B. Kiosses, M. A. Schwartz, and D. A. Cheresh. 2003. 'Differential alphav integrin-mediated Ras-ERK signaling during two pathways of angiogenesis', *J Cell Biol*, 162: 933-43.
Hoshida, T., N. Isaka, J. Hagendoorn, E. di Tomaso, Y. L. Chen, B. Pytowski, D. Fukumura, T. P. Padera, and R. K. Jain. 2006. 'Imaging steps of lymphatic metastasis reveals that vascular endothelial growth factor-C increases metastasis by increasing delivery of cancer cells to lymph nodes: therapeutic implications', *Cancer Res*, 66: 8065-75.
Hruban, Ralph H., Anirban Maitra, and Michael Goggins. 2008. 'Update on pancreatic intraepithelial neoplasia', *International journal of clinical and experimental pathology*, 1: 306-16.
Hsu, V. W., M. Bai, and J. Li. 2012. 'Getting active: protein sorting in endocytic recycling.' in, *Nat Rev Mol Cell Biol* (England).
Hu, B., and S. Y. Cheng. 2009. 'Angiopoietin-2: development of inhibitors for cancer therapy', *Curr Oncol Rep*, 11: 111-6.
Huang, B., P. Y. Pan, Q. Li, A. I. Sato, D. E. Levy, J. Bromberg, C. M. Divino, and S. H. Chen. 2006. 'Gr-1+CD115+ immature myeloid suppressor cells mediate the development of tumor-induced T regulatory cells and T-cell anergy in tumor-bearing host', *Cancer Res*, 66: 1123-31.

Huang, Y. Q., J. J. Li, L. Hu, M. Lee, and S. Karpatkin. 2002. 'Thrombin induces increased expression and secretion of angiopoietin-2 from human umbilical vein endothelial cells', *Blood*, 99: 1646-50.

Huang, Y., J. Yuan, E. Righi, W. S. Kamoun, M. Ancukiewicz, J. Nezivar, M. Santosuosso, J. D. Martin, M. R. Martin, F. Vianello, P. Leblanc, L. L. Munn, P. Huang, D. G. Duda, D. Fukumura, R. K. Jain, and M. C. Poznansky. 2012. 'Vascular normalizing doses of antiangiogenic treatment reprogram the immunosuppressive tumor microenvironment and enhance immunotherapy', *Proc Natl Acad Sci U S A*, 109: 17561-6.

Huch, Meritxell, Paola Bonfanti, Sylvia F. Boj, Toshiro Sato, Cindy J. M. Loomans, Marc van de Wetering, Mozhdeh Sojoodi, Vivian S. W. Li, Jurian Schuijers, Ana Gracanin, Femke Ringnalda, Harry Begthel, Karien Hamer, Joyce Mulder, Johan H. van Es, Eelco de Koning, Robert G. J. Vries, Harry Heimberg, and Hans Clevers. 2013. 'Unlimited in vitro expansion of adult bi-potent pancreas progenitors through the Lgr5/R-spondin axis', *The EMBO Journal*, 32: 2708-21.

Hui, L., and Y. Chen. 2015. 'Tumor microenvironment: Sanctuary of the devil', *Cancer Lett*, 368: 7-13.

Humphries, M. J., E. J. Symonds, and A. P. Mould. 2003. 'Mapping functional residues onto integrin crystal structures', *Curr Opin Struct Biol*, 13: 236-43.

Hung, Y. Y., Y. C. Fu, H. J. Wei, I. C. Tsai, and C. C. Chen. 2013. 'Multi-detector row computed tomographic evaluation of a rare type of complete vascular ring: double aortic arch with atretic left arch distal to the origin of left subclavian artery', *Korean J Radiol*, 14: 845-8.

Huth, J. R., E. T. Olejniczak, R. Mendoza, H. Liang, E. A. Harris, M. L. Lupher, Jr., A. E. Wilson, S. W. Fesik, and D. E. Staunton. 2000. 'NMR and mutagenesis evidence for an I domain allosteric site that regulates lymphocyte function-associated antigen 1 ligand binding', *Proc Natl Acad Sci U S A*, 97: 5231-6.

Hynes, R. O. 2002. 'Integrins: bidirectional, allosteric signaling machines', *Cell*, 110: 673-87.

Hynes, Richard O. 2009. 'The Extracellular Matrix: Not Just Pretty Fibrils', *Science*, 326: 1216.

ICR. 2021. "Phase I Trial of VS-6063 and RO5126766." In.: https://ClinicalTrials.gov/show/NCT03875820.

International Consensus Group for Hepatocellular, Neoplasia. 2009. 'Pathologic diagnosis of early hepatocellular carcinoma: A report of the international consensus group for hepatocellular neoplasia', *Hepatology*, 49: 658-64.

Jabbari, K., and G. Bernardi. 2004. 'Cytosine methylation and CpG, TpG (CpA) and TpA frequencies', *Gene*, 333: 143-9.

Jacobetz, Michael A., Derek S. Chan, Albrecht Neesse, Tashinga E. Bapiro, Natalie Cook, Kristopher K. Frese, Christine Feig, Tomoaki Nakagawa, Meredith E. Caldwell, Heather I. Zecchini, Martijn P. Lolkema, Ping Jiang, Anne Kultti, Curtis B. Thompson, Daniel C. Maneval, Duncan I. Jodrell, Gregory I. Frost, H. M. Shepard, Jeremy N. Skepper, and David A. Tuveson. 2013. 'Hyaluronan impairs vascular function and drug delivery in a mouse model of pancreatic cancer', *Gut*, 62: 112-20.

Jain, R. K., T. Snyders, L. Nandgoapal, R. Garje, Y. Zakharia, and S. Gupta. 2018. 'Immunotherapy Advances in Urothelial Carcinoma', *Curr Treat Options Oncol*, 19: 79.

Jain, Rakesh K. 2005. 'Normalization of Tumor Vasculature: An Emerging Concept in Antiangiogenic Therapy', *Science*, 307: 58-62.

———. 2013. 'Normalizing tumor microenvironment to treat cancer: bench to bedside to biomarkers', *Journal of clinical oncology : official journal of the American Society of Clinical Oncology*, 31: 2205-18.
Jain, Rakesh K., and Triantafyllos Stylianopoulos. 2010. 'Delivering nanomedicine to solid tumors', *Nat Rev Clin Oncol*, 7: 653-64.
Jayadev, Ranjay, and David R. Sherwood. 2017. 'Basement membranes', *Current Biology*, 27: R207-R11.
Jean, Christine, Xiao Lei Chen, Ju-Ock Nam, Isabelle Tancioni, Sean Uryu, Christine Lawson, Kristy K. Ward, Colin T. Walsh, Nichol L.G. Miller, Majid Ghassemian, Patric Turowski, Elisabetta Dejana, Sara Weis, David A. Cheresh, and David D. Schlaepfer. 2014. 'Inhibition of endothelial FAK activity prevents tumor metastasis by enhancing barrier function', *The Journal of Cell Biology*, 204: 247-63.
Jing, X., F. Yang, C. Shao, K. Wei, M. Xie, H. Shen, and Y. Shu. 2019. 'Role of hypoxia in cancer therapy by regulating the tumor microenvironment', *Mol Cancer*, 18: 157.
Jones, Carissa P., Kelli L. Boyd, and Jeanne M. Wallace. 2016. 'Evaluation of Mice Undergoing Serial Oral Gavage While Awake or Anesthetized', *Journal of the American Association for Laboratory Animal Science : JAALAS*, 55: 805-10.
Jones, Matthew L., Amelia J. Shawe-Taylor, Christopher M. Williams, and Alastair W. Poole. 2009. 'Characterization of a novel focal adhesion kinase inhibitor in human platelets', *Biochemical and Biophysical Research Communications*, 389: 198-203.
Jones, S. F., L. L. Siu, J. C. Bendell, J. M. Cleary, A. R. Razak, J. R. Infante, S. S. Pandya, P. L. Bedard, K. J. Pierce, B. Houk, W. G. Roberts, S. M. Shreeve, and G. I. Shapiro. 2015. 'A phase I study of VS-6063, a second-generation focal adhesion kinase inhibitor, in patients with advanced solid tumors', *Invest New Drugs*, 33: 1100-7.
Kaelin, William G., Shashi Shrivastav, David G. Shand, and Randy L. Jirtie. 1982. 'Effect of Verapamil on Malignant Tissue Blood Flow in SMT-2A Tumor-bearing Rats', *Cancer Res*, 42: 3944-49.
Kalluri, R., and M. Zeisberg. 2006. 'Fibroblasts in cancer', *Nat Rev Cancer*, 6: 392-401.
Kanner, S. B., A. Aruffo, and P. Y. Chan. 1994. 'Lymphocyte antigen receptor activation of a focal adhesion kinase-related tyrosine kinase substrate', *Proceedings of the National Academy of Sciences*, 91: 10484.
Kapp, Tobias G., Maximilian Fottner, Oleg V. Maltsev, and Horst Kessler. 2016. 'Small Cause, Great Impact: Modification of the Guanidine Group in the RGD Motif Controls Integrin Subtype Selectivity', *Angewandte Chemie International Edition*, 55: 1540-43.
Kapp, Tobias G., Florian Rechenmacher, Stefanie Neubauer, Oleg V. Maltsev, Elisabetta A. Cavalcanti-Adam, Revital Zarka, Ute Reuning, Johannes Notni, Hans-Jürgen Wester, Carlos Mas-Moruno, Joachim Spatz, Benjamin Geiger, and Horst Kessler. 2017. 'A Comprehensive Evaluation of the Activity and Selectivity Profile of Ligands for RGD-binding Integrins', *Scientific Reports*, 7: 39805.
Karampitsakos, Theodoros, Vasilios Tzilas, Rodoula Tringidou, Paschalis Steiropoulos, Vasilis Aidinis, Spyros A. Papiris, Demosthenes Bouros, and Argyris Tzouvelekis. 2017. 'Lung cancer in patients with idiopathic pulmonary fibrosis', *Pulmonary Pharmacology & Therapeutics*, 45: 1-10.
Katsuta, Eriko, Qianya Qi, Xuan Peng, Steven N. Hochwald, Li Yan, and Kazuaki Takabe. 2019. 'Pancreatic adenocarcinomas with mature blood vessels have better overall survival', *Scientific Reports*, 9: 1310.

Kelly, B. D., S. F. Hackett, K. Hirota, Y. Oshima, Z. Cai, S. Berg-Dixon, A. Rowan, Z. Yan, P. A. Campochiaro, and G. L. Semenza. 2003. 'Cell type-specific regulation of angiogenic growth factor gene expression and induction of angiogenesis in nonischemic tissue by a constitutively active form of hypoxia-inducible factor 1', *Circ Res*, 93: 1074-81.

Kim, M. P., D. B. Evans, H. Wang, J. L. Abbruzzese, J. B. Fleming, and G. E. Gallick. 2009. 'Generation of orthotopic and heterotopic human pancreatic cancer xenografts in immunodeficient mice', *Nat Protoc*, 4: 1670-80.

Kim, Semi, Kelly Bell, Shaker A. Mousa, and Judith A. Varner. 2000. 'Regulation of Angiogenesis in Vivo by Ligation of Integrin α5β1 with the Central Cell-Binding Domain of Fibronectin', *The American Journal of Pathology*, 156: 1345-62.

Kim, Y. N., K. H. Koo, J. Y. Sung, U. J. Yun, and H. Kim. 2012. 'Anoikis resistance: an essential prerequisite for tumor metastasis', *Int J Cell Biol*, 2012: 306879.

Kisucka, Janka, Catherine E. Butterfield, Dan G. Duda, Sarah C. Eichenberger, Simin Saffaripour, Jerry Ware, Zaverio M. Ruggeri, Rakesh K. Jain, Judah Folkman, and Denisa D. Wagner. 2006. 'Platelets and platelet adhesion support angiogenesis while preventing excessive hemorrhage', *Proceedings of the National Academy of Sciences of the United States of America*, 103: 855.

Kita, Keiji, Tatsuya Itoshima, and Takao Tsuji. 1991. 'Observation of microvascular casts of human hepatocellular carcinoma by scanning electron microscopy', *Gastroenterologia Japonica*, 26: 319-28.

Klein, H. O., R. Lang, E. Weiss, E. Di Segni, C. Libhaber, J. Guerrero, and E. Kaplinsky. 1982. 'The influence of verapamil on serum digoxin concentration', *Circulation*, 65: 998-1003.

Knighton, D., D. Ausprunk, D. Tapper, and J. Folkman. 1977. 'Avascular and vascular phases of tumour growth in the chick embryo', *Br J Cancer*, 35: 347-56.

Kollmannsberger, Philip, Cécile M. Bidan, John W. C. Dunlop, Peter Fratzl, and Viola Vogel. 2018. 'Tensile forces drive a reversible fibroblast-to-myofibroblast transition during tissue growth in engineered clefts', *Science Advances*, 4: eaao4881.

Konerding, M. A., W. Malkusch, B. Klapthor, C. van Ackern, E. Fait, S. A. Hill, C. Parkins, D. J. Chaplin, M. Presta, and J. Denekamp. 1999. 'Evidence for characteristic vascular patterns in solid tumours: quantitative studies using corrosion casts', *Br J Cancer*, 80: 724-32.

Koo, Ingrid Chou, Yamini M. Ohol, Ping Wu, J. Hiroshi Morisaki, Jeffery S. Cox, and Eric J. Brown. 2008. 'Role for lysosomal enzyme beta-hexosaminidase in the control of mycobacteria infection', *Proceedings of the National Academy of Sciences of the United States of America*, 105: 710-15.

Koreishi, A. F., A. J. Saenz, D. O. Persky, H. Cui, A. Moskowitz, C. H. Moskowitz, and J. Teruya-Feldstein. 2010. 'The role of cytotoxic and regulatory T cells in relapsed/refractory Hodgkin lymphoma', *Appl Immunohistochem Mol Morphol*, 18: 206-11.

Kostourou, Vassiliki, Tanguy Lechertier, Louise E. Reynolds, Delphine M. Lees, Marianne Baker, Dylan T. Jones, Bernardo Tavora, Antoine R. Ramjaun, Graeme M. Birdsey, Stephen D. Robinson, Maddy Parsons, Anna M. Randi, Ian R. Hart, and Kairbaan Hodivala-Dilke. 2013. 'FAK-heterozygous mice display enhanced tumour angiogenesis', *Nature Communications*, 4: 2020.

Kraft, Walter K., and Scott A. Waldman. 2001. 'Manufacturer's Drug Interaction and Postmarketing Adverse Event Data', *Drug Safety*, 24: 637-43.

Kuczynski, E. A., and A. R. Reynolds. 2020. 'Vessel co-option and resistance to anti-angiogenic therapy', *Angiogenesis*, 23: 55-74.

Kuczynski, Elizabeth A., Peter B. Vermeulen, Francesco Pezzella, Robert S. Kerbel, and Andrew R. Reynolds. 2019. 'Vessel co-option in cancer', *Nature Reviews Clinical Oncology*, 16: 469-93.

Kuilman, T., C. Michaloglou, L. C. Vredeveld, S. Douma, R. van Doorn, C. J. Desmet, L. A. Aarden, W. J. Mooi, and D. S. Peeper. 2008. 'Oncogene-induced senescence relayed by an interleukin-dependent inflammatory network', *Cell*, 133: 1019-31.

Kurmasheva, R. T., R. Gorlick, E. A. Kolb, S. T. Keir, J. M. Maris, R. B. Lock, H. Carol, M. Kang, C. P. Reynolds, J. Wu, P. J. Houghton, and M. A. Smith. 2017. 'Initial testing of VS-4718, a novel inhibitor of focal adhesion kinase (FAK), against pediatric tumor models by the Pediatric Preclinical Testing Program', *Pediatr Blood Cancer*, 64.

Kusmartsev, Sergei, Srinivas Nagaraj, and Dmitry I. Gabrilovich. 2005. 'Tumor-associated CD8+ T cell tolerance induced by bone marrow-derived immature myeloid cells', *Journal of immunology (Baltimore, Md. : 1950)*, 175: 4583-92.

Laki, K. 1972. 'Our ancient heritage in blood clotting and some of its consequences', *Ann N Y Acad Sci*, 202: 297-307.

Langley, Ries J., John D. Fraser, and Thomas Proft. 2015. '32 - Bacterial superantigens and superantigen-like toxins.' in Joseph Alouf, Daniel Ladant and Michel R. Popoff (eds.), *The Comprehensive Sourcebook of Bacterial Protein Toxins (Fourth Edition)* (Academic Press: Boston).

Larson, R. S., A. L. Corbi, L. Berman, and T. Springer. 1989. 'Primary structure of the leukocyte function-associated molecule-1 alpha subunit: an integrin with an embedded domain defining a protein superfamily', *J Cell Biol*, 108: 703-12.

Lasky, Joseph L., and Hong Wu. 2005. 'Notch Signaling, Brain Development, and Human Disease', *Pediatric Research*, 57: 104-09.

Lauro, Salvatore, Concetta Elisa Onesti, Riccardo Righini, and Paolo Marchetti. 2014. 'The Use of Bevacizumab in Non-Small Cell Lung Cancer: An Update', *Anticancer Research*, 34: 1537.

Lawson, Christine, and David D Schlaepfer. 2013. *pHocal adhesion kinase regulation is on a FERM foundation*.

Lawson, M. A., and F. R. Maxfield. 1995. 'Ca(2+)- and calcineurin-dependent recycling of an integrin to the front of migrating neutrophils', *Nature*, 377: 75-9.

Lebrun, Patricia, Véronique Baron, Christof R. Hauck, David D. Schlaepfer, and Emmanuel Van Obberghen. 2000. 'Cell Adhesion and Focal Adhesion Kinase Regulate Insulin Receptor Substrate-1 Expression *', *Journal of Biological Chemistry*, 275: 38371-77.

Lechertier, T., and K. Hodivala-Dilke. 2012. 'Focal adhesion kinase and tumour angiogenesis', *J Pathol*, 226: 404-12.

Ledwitch, Kaitlyn V., Robert W. Barnes, and Arthur G. Roberts. 2016. 'Unravelling the complex drug-drug interactions of the cardiovascular drugs, verapamil and digoxin, with P-glycoprotein', *Bioscience reports*, 36: e00309.

Lee, Jae W., Chad A. Komar, Fee Bengsch, Kathleen Graham, and Gregory L. Beatty. 2016. 'Genetically Engineered Mouse Models of Pancreatic Cancer: The KPC Model (LSL-Kras(G12D/+) ;LSL-Trp53(R172H/+) ;Pdx-1-Cre), Its Variants, and Their Application in Immuno-oncology Drug Discovery', *Current protocols in pharmacology*, 73: 14.39.1-14.39.20.

Legate, K. R., S. A. Wickström, and R. Fässler. 2009. 'Genetic and cell biological analysis of integrin outside-in signaling', *Genes Dev*, 23: 397-418.

Levin, Victor A., Nancy D. Mendelssohn, James Chan, Mady C. Stovall, Scott J. Peak, Jennie L. Yee, Rita L. Hui, and David M. Chen. 2015. 'Impact of bevacizumab

administered dose on overall survival of patients with progressive glioblastoma', *Journal of Neuro-Oncology*, 122: 145-50.
Ley, K., J. Rivera-Nieves, W. J. Sandborn, and S. Shattil. 2016. 'Integrin-based therapeutics: biological basis, clinical use and new drugs', *Nat Rev Drug Discov*, 15: 173-83.
Li, S., Q. Zhang, and Y. Hong. 2020. 'Tumor Vessel Normalization: A Window to Enhancing Cancer Immunotherapy', *Technol Cancer Res Treat*, 19: 1533033820980116.
Lim, S. T., N. L. Miller, J. O. Nam, X. L. Chen, Y. Lim, and D. D. Schlaepfer. 2010. 'Pyk2 inhibition of p53 as an adaptive and intrinsic mechanism facilitating cell proliferation and survival', *J Biol Chem*, 285: 1743-53.
Lim, Ssang-Taek, Xiao Lei Chen, Yangmi Lim, Dan A. Hanson, Thanh-Trang Vo, Kyle Howerton, Nicholas Larocque, Susan J. Fisher, David D. Schlaepfer, and Dusko Ilic. 2008. 'Nuclear FAK promotes cell proliferation and survival through FERM-enhanced p53 degradation', *Molecular cell*, 29: 9-22.
Lim, Ssang-Taek, Xiao Lei Chen, Alok Tomar, Nichol L. G. Miller, Jiyeon Yoo, and David D. Schlaepfer. 2010. 'Knock-in Mutation Reveals an Essential Role for Focal Adhesion Kinase Activity in Blood Vessel Morphogenesis and Cell Motility-Polarity but Not Cell Proliferation', *Journal of Biological Chemistry*, 285: 21526-36.
Ling, K., R. L. Doughman, A. J. Firestone, M. W. Bunce, and R. A. Anderson. 2002. 'Type I gamma phosphatidylinositol phosphate kinase targets and regulates focal adhesions', *Nature*, 420: 89-93.
Liu, Li, Yangyang Liu, Xiaohua Yan, Chong Zhou, and Xiangyang Xiong. 2020. 'The role of granulocyte colony-stimulating factor in breast cancer development: A review', *Molecular medicine reports*, 21: 2019-29.
Liu, X., S. Wu, Y. Yang, M. Zhao, G. Zhu, and Z. Hou. 2017. 'The prognostic landscape of tumor-infiltrating immune cell and immunomodulators in lung cancer', *Biomed Pharmacother*, 95: 55-61.
Liu, Y., Y. Cai, L. Liu, Y. Wu, and X. Xiong. 2018. 'Crucial biological functions of CCL7 in cancer', *PeerJ*, 6: e4928.
Lobert, Viola Hélène, Andreas Brech, Nina Marie Pedersen, Jørgen Wesche, Angela Oppelt, Lene Malerød, and Harald Stenmark. 2010. 'Ubiquitination of α5β1 Integrin Controls Fibroblast Migration through Lysosomal Degradation of Fibronectin-Integrin Complexes', *Developmental Cell*, 19: 148-59.
Lorgis, V., G. Maura, G. Coppa, K. Hassani, L. Taillandier, B. Chauffert, L. Apetoh, S. Ladoire, and F. Ghiringhelli. 2012. 'Relation between bevacizumab dose intensity and high-grade glioma survival: a retrospective study in two large cohorts', *J Neurooncol*, 107: 351-8.
Lu, C., A. V. Paschall, H. Shi, N. Savage, J. L. Waller, M. E. Sabbatini, N. H. Oberlies, C. Pearce, and K. Liu. 2017. 'The MLL1-H3K4me3 Axis-Mediated PD-L1 Expression and Pancreatic Cancer Immune Evasion', *J Natl Cancer Inst*, 109.
Lu, Chunhua, Tomas Bonome, Yang Li, Aparna A. Kamat, Liz Y. Han, Rosemarie Schmandt, Robert L. Coleman, David M. Gershenson, Robert B. Jaffe, Michael J. Birrer, and Anil K. Sood. 2007. 'Gene Alterations Identified by Expression Profiling in Tumor-Associated Endothelial Cells from Invasive Ovarian Carcinoma', *Cancer Research*, 67: 1757.
Lu, Shaoying, and Yingxiao Wang. 2014. 'Chapter Two - Single-Cell Imaging of Mechanotransduction in Endothelial Cells.' in Adam J. Engler and Sanjay Kumar (eds.), *Progress in Molecular Biology and Translational Science* (Academic Press).

Lugano, R., M. Ramachandran, and A. Dimberg. 2020. 'Tumor angiogenesis: causes, consequences, challenges and opportunities', *Cell Mol Life Sci*, 77: 1745-70.
Luo, B. H., C. V. Carman, and T. A. Springer. 2007. 'Structural basis of integrin regulation and signaling', *Annu Rev Immunol*, 25: 619-47.
Luo, Ming, Xiaofeng Zhao, Song Chen, Suling Liu, Max S. Wicha, and Jun-Lin Guan. 2013. 'Distinct FAK activities determine progenitor and mammary stem cell characteristics', *Cancer research*, 73: 5591-602.
Lutz, Eric R., Annie A. Wu, Elaine Bigelow, Rajni Sharma, Guanglan Mo, Kevin Soares, Sara Solt, Alvin Dorman, Anthony Wamwea, Allison Yager, Daniel Laheru, Christopher L. Wolfgang, Jiang Wang, Ralph H. Hruban, Robert A. Anders, Elizabeth M. Jaffee, and Lei Zheng. 2014. 'Immunotherapy converts nonimmunogenic pancreatic tumors into immunogenic foci of immune regulation', *Cancer immunology research*, 2: 616-31.
Ma, Jianguo, Sharon Pulfer, Shaolan Li, Jianxiong Chu, Karin Reed, and James M. Gallo. 2001. 'Pharmacodynamic-mediated Reduction of Temozolomide Tumor Concentrations by the Angiogenesis Inhibitor TNP-470', *Cancer Res*, 61: 5491-98.
Mabeta, P. 2016. 'PF573,228 inhibits vascular tumor cell growth, migration as well as angiogenesis, induces apoptosis and abrogates PRAS40 and S6RP phosphorylation', *Acta Pharm*, 66: 399-410.
Maeda, H., H. Nakamura, and J. Fang. 2013. 'The EPR effect for macromolecular drug delivery to solid tumors: Improvement of tumor uptake, lowering of systemic toxicity, and distinct tumor imaging in vivo', *Adv Drug Deliv Rev*, 65: 71-9.
Majumder, Kaustav, Nivedita Arora, Shrey Modi, Rohit Chugh, Alice Nomura, Bhuwan Giri, Rajinder Dawra, Sundaram Ramakrishnan, Sulagna Banerjee, Ashok Saluja, and Vikas Dudeja. 2016. 'A Novel Immunocompetent Mouse Model of Pancreatic Cancer with Robust Stroma: a Valuable Tool for Preclinical Evaluation of New Therapies', *Journal of gastrointestinal surgery : official journal of the Society for Surgery of the Alimentary Tract*, 20: 53-65.
Manninen, Aki. 2015. 'Epithelial polarity – Generating and integrating signals from the ECM with integrins', *Experimental Cell Research*, 334: 337-49.
Manzur, Mitali, Juliana Hamzah, and Ruth Ganss. 2009. 'Modulation of G Protein Signaling Normalizes Tumor Vessels', *Cancer Research*, 69: 396.
Mas-Moruno, C., R. Fraioli, F. Rechenmacher, S. Neubauer, T. G. Kapp, and H. Kessler. 2016. 'αvβ3- or α5β1-Integrin-Selective Peptidomimetics for Surface Coating', *Angew Chem Int Ed Engl*, 55: 7048-67.
Mas-Moruno, Carlos, Florian Rechenmacher, and Horst Kessler. 2010. 'Cilengitide: the first anti-angiogenic small molecule drug candidate design, synthesis and clinical evaluation', *Anti-Cancer Agents in Medicinal Chemistry*, 10: 753-68.
Matsumura, Y., and H. Maeda. 1986. 'A new concept for macromolecular therapeutics in cancer chemotherapy: mechanism of tumoritropic accumulation of proteins and the antitumor agent smancs', *Cancer Res*, 46: 6387-92.
Maubant, S., D. Saint-Dizier, M. Boutillon, F. Perron-Sierra, P. J. Casara, J. A. Hickman, G. C. Tucker, and E. Van Obberghen-Schilling. 2006. 'Blockade of alpha v beta3 and alpha v beta5 integrins by RGD mimetics induces anoikis and not integrin-mediated death in human endothelial cells', *Blood*, 108: 3035-44.
Mauri, C., and A. Bosma. 2012. 'Immune regulatory function of B cells', *Annu Rev Immunol*, 30: 221-41.
May, T., P. P. Mueller, H. Weich, N. Froese, U. Deutsch, D. Wirth, A. Kroger, and H. Hauser. 2005. 'Establishment of murine cell lines by constitutive and conditional immortalization', *J Biotechnol*, 120: 99-110.

Maybin, Jacqueline A., and Hilary O. D. Critchley. 2015. 'Menstrual physiology: implications for endometrial pathology and beyond', *Human reproduction update*, 21: 748-61.
Mazzieri, R., F. Pucci, D. Moi, E. Zonari, A. Ranghetti, A. Berti, L. S. Politi, B. Gentner, J. L. Brown, L. Naldini, and M. De Palma. 2011. 'Targeting the ANG2/TIE2 axis inhibits tumor growth and metastasis by impairing angiogenesis and disabling rebounds of proangiogenic myeloid cells', *Cancer Cell*, 19: 512-26.
McCloskey, K. E. 2011. '1.46 - Effects of Shear Stress on Cells.' in Murray Moo-Young (ed.), *Comprehensive Biotechnology (Second Edition)* (Academic Press: Burlington).
McDonald, Braedon, Rossana Urrutia, Bryan G Yipp, Craig N Jenne, and Paul Kubes. 2012. 'Intravascular Neutrophil Extracellular Traps Capture Bacteria from the Bloodstream during Sepsis', *Cell Host & Microbe*, 12: 324-33.
McLean, G. W., N. H. Komiyama, B. Serrels, H. Asano, L. Reynolds, F. Conti, K. Hodivala-Dilke, D. Metzger, P. Chambon, S. G. Grant, and M. C. Frame. 2004. 'Specific deletion of focal adhesion kinase suppresses tumor formation and blocks malignant progression', *Genes Dev*, 18: 2998-3003.
Medici, D., and R. Kalluri. 2012. 'Endothelial-mesenchymal transition and its contribution to the emergence of stem cell phenotype', *Semin Cancer Biol*, 22: 379-84.
Meng, M. B., N. G. Zaorsky, L. Deng, H. H. Wang, J. Chao, L. J. Zhao, Z. Y. Yuan, and W. Ping. 2015. 'Pericytes: a double-edged sword in cancer therapy', *Future Oncol*, 11: 169-79.
Merwin, R. M., and G. H. Algire. 1956. 'The role of graft and host vessels in the vascularization of grafts of normal and neoplastic tissue', *J Natl Cancer Inst*, 17: 23-33.
Michael, Magdalene, and Maddy Parsons. 2020. 'New perspectives on integrin-dependent adhesions', *Current opinion in cell biology*, 63: 31-37.
Milne, K., M. Köbel, S. E. Kalloger, R. O. Barnes, D. Gao, C. B. Gilks, P. H. Watson, and B. H. Nelson. 2009. 'Systematic analysis of immune infiltrates in high-grade serous ovarian cancer reveals CD20, FoxP3 and TIA-1 as positive prognostic factors', *PLoS One*, 4: e6412.
Mitra, S. K., D. A. Hanson, and D. D. Schlaepfer. 2005. 'Focal adhesion kinase: in command and control of cell motility', *Nat Rev Mol Cell Biol*, 6: 56-68.
Mitra, S. K., and D. D. Schlaepfer. 2006. 'Integrin-regulated FAK-Src signaling in normal and cancer cells', *Curr Opin Cell Biol*, 18: 516-23.
Monahan, Brian P., Clifford L. Ferguson, Eugene S. Killeavy, Bruce K. Lloyd, James Troy, and Louis R. Cantilena, Jr. 1990. 'Torsades de Pointes Occurring in Association With Terfenadine Use', *JAMA*, 264: 2788-90.
Monteran, Lea, and Neta Erez. 2019. 'The Dark Side of Fibroblasts: Cancer-Associated Fibroblasts as Mediators of Immunosuppression in the Tumor Microenvironment', *Frontiers in Immunology*, 10: 1835.
Morote-Garcia, J. C., P. Rosenberger, N. M. Nivillac, I. R. Coe, and H. K. Eltzschig. 2009. 'Hypoxia-inducible factor-dependent repression of equilibrative nucleoside transporter 2 attenuates mucosal inflammation during intestinal hypoxia', *Gastroenterology*, 136: 607-18.
Moser, Markus, Bernhard Nieswandt, Siegfried Ussar, Miroslava Pozgajova, and Reinhard Fässler. 2008. 'Kindlin-3 is essential for integrin activation and platelet aggregation', *Nature Medicine*, 14: 325-30.

Motulsky, Harvey J., and Ronald E. Brown. 2006. 'Detecting outliers when fitting data with nonlinear regression – a new method based on robust nonlinear regression and the false discovery rate', *BMC Bioinformatics*, 7: 123.
Multhoff, G., A. G. Pockley, C. Streffer, and U. S. Gaipl. 2012. 'Dual role of heat shock proteins (HSPs) in anti-tumor immunity', *Curr Mol Med*, 12: 1174-82.
Murakami, Takashi, Yukihiko Hiroshima, Ryusei Matsuyama, Yuki Homma, Robert M. Hoffman, and Itaru Endo. 2019. 'Role of the tumor microenvironment in pancreatic cancer', *Annals of gastroenterological surgery*, 3: 130-37.
Müller, Gerhard, Marion Gurrath, and Horst Kessler. 1994. 'Pharmacophore refinement of gpIIb/IIIa antagonists based on comparative studies of antiadhesive cyclic and acyclic RGD peptides', *Journal of Computer-Aided Molecular Design*, 8: 709-30.
Nabors, L. B., T. Mikkelsen, S. S. Rosenfeld, F. Hochberg, N. S. Akella, J. D. Fisher, G. A. Cloud, Y. Zhang, K. Carson, S. M. Wittemer, A. D. Colevas, and S. A. Grossman. 2007. 'Phase I and correlative biology study of cilengitide in patients with recurrent malignant glioma', *J Clin Oncol*, 25: 1651-7.
Nabors, L. Burt, Thomas Mikkelsen, Monika E. Hegi, Xiaubu Ye, Tracy Batchelor, Glenn Lesser, David Peereboom, Myrna R. Rosenfeld, Jeff Olsen, Steve Brem, Joy D. Fisher, Stuart A. Grossman, and for the New Approaches to Brain Tumor Therapy Central Nervous System Consortium. 2012. 'A safety run-in and randomized phase 2 study of cilengitide combined with chemoradiation for newly diagnosed glioblastoma (NABTT 0306)', *Cancer*, 118: 5601-07.
Nader, G. P., E. J. Ezratty, and G. G. Gundersen. 2016. 'FAK, talin and PIPKIγ regulate endocytosed integrin activation to polarize focal adhesion assembly', *Nat Cell Biol*, 18: 491-503.
Nagae, Masamichi, Suyong Re, Emiko Mihara, Terukazu Nogi, Yuji Sugita, and Junichi Takagi. 2012. 'Crystal structure of α5β1 integrin ectodomain: Atomic details of the fibronectin receptor', *Journal of Cell Biology*, 197: 131-40.
Nagy, Andras. 2000. 'Cre recombinase: The universal reagent for genome tailoring', *genesis*, 26: 99-109.
Nagy, J. A., A. M. Dvorak, and H. F. Dvorak. 2007. 'VEGF-A and the induction of pathological angiogenesis', *Annu Rev Pathol*, 2: 251-75.
Naser, Rayan, Abdullah Aldehaiman, Escarlet Díaz-Galicia, and Stefan T. Arold. 2018. 'Endogenous Control Mechanisms of FAK and PYK2 and Their Relevance to Cancer Development', *Cancers*, 10.
Nguyen, P. D., G. E. Hollway, C. Sonntag, L. B. Miles, T. E. Hall, S. Berger, K. J. Fernandez, D. B. Gurevich, N. J. Cole, S. Alaei, M. Ramialison, R. L. Sutherland, J. M. Polo, G. J. Lieschke, and P. D. Currie. 2014. 'Haematopoietic stem cell induction by somite-derived endothelial cells controlled by meox1', *Nature*, 512: 314-8.
Nieberler, Markus, Ute Reuning, Florian Reichart, Johannes Notni, Hans-Jürgen Wester, Markus Schwaiger, Michael Weinmüller, Andreas Räder, Katja Steiger, and Horst Kessler. 2017. 'Exploring the Role of RGD-Recognizing Integrins in Cancer', *Cancers*, 9: 116.
NIH. 2021. 'Tamoxifen Citrate', NIH, Accessed 8/4/21.
Niida, Atsushi, Takatoshi Hiroko, Mana Kasai, Yoichi Furukawa, Yusuke Nakamura, Yutaka Suzuki, Sumio Sugano, and Tetsu Akiyama. 2004. 'DKK1, a negative regulator of Wnt signaling, is a target of the β-catenin/TCF pathway', *Oncogene*, 23: 8520-26.
Nisato, R. E., J. C. Tille, A. Jonczyk, S. L. Goodman, and M. S. Pepper. 2003a. 'alphav beta 3 and alphav beta 5 integrin antagonists inhibit angiogenesis in vitro', *Angiogenesis*, 6: 105-19.

Nisato, Riccardo E., Jean-Christophe Tille, Alfred Jonczyk, Simon L. Goodman, and Michael S. Pepper. 2003b. 'αvβ3 and αvβ5 integrin antagonists inhibit angiogenesis in vitro', *Angiogenesis*, 6: 105-19.

Nishida, Naoyo, Hirohisa Yano, Takashi Nishida, Toshiharu Kamura, and Masamichi Kojiro. 2006. 'Angiogenesis in cancer', *Vascular health and risk management*, 2: 213-19.

Nolan, E., and I. Malanchi. 2020. 'Neutrophil 'safety net' causes cancer cells to metastasize and proliferate.' in, *Nature* (England).

Noman, Muhammad Zaeem, Meriem Hasmim, Audrey Lequeux, Malina Xiao, Caroline Duhem, Salem Chouaib, Guy Berchem, and Bassam Janji. 2019. 'Improving Cancer Immunotherapy by Targeting the Hypoxic Tumor Microenvironment: New Opportunities and Challenges', *Cells*, 8: 1083.

Noy, R., and J. W. Pollard. 2014. 'Tumor-associated macrophages: from mechanisms to therapy', *Immunity*, 41: 49-61.

Nozawa, Hiroaki, Christopher Chiu, and Douglas Hanahan. 2006. 'Infiltrating neutrophils mediate the initial angiogenic switch in a mouse model of multistage carcinogenesis', *Proceedings of the National Academy of Sciences*, 103: 12493.

Ojalvo, Laureen S., Charles A. Whittaker, John S. Condeelis, and Jeffrey W. Pollard. 2010. 'Gene Expression Analysis of Macrophages That Facilitate Tumor Invasion Supports a Role for Wnt-Signaling in Mediating Their Activity in Primary Mammary Tumors', *The Journal of Immunology*, 184: 702.

Oldberg, A., A. Franzén, and D. Heinegård. 1986. 'Cloning and sequence analysis of rat bone sialoprotein (osteopontin) cDNA reveals an Arg-Gly-Asp cell-binding sequence', *Proc Natl Acad Sci U S A*, 83: 8819-23.

Olive, K. P., M. A. Jacobetz, C. J. Davidson, A. Gopinathan, D. McIntyre, D. Honess, B. Madhu, M. A. Goldgraben, M. E. Caldwell, D. Allard, K. K. Frese, G. Denicola, C. Feig, C. Combs, S. P. Winter, H. Ireland-Zecchini, S. Reichelt, W. J. Howat, A. Chang, M. Dhara, L. Wang, F. Ruckert, R. Grutzmann, C. Pilarsky, K. Izeradjene, S. R. Hingorani, P. Huang, S. E. Davies, W. Plunkett, M. Egorin, R. H. Hruban, N. Whitebread, K. McGovern, J. Adams, C. Iacobuzio-Donahue, J. Griffiths, and D. A. Tuveson. 2009. 'Inhibition of Hedgehog signaling enhances delivery of chemotherapy in a mouse model of pancreatic cancer', *Science*, 324: 1457-61.

Olive, Kenneth P., Michael A. Jacobetz, Christian J. Davidson, Aarthi Gopinathan, Dominick McIntyre, Davina Honess, Basetti Madhu, Mae A. Goldgraben, Meredith E. Caldwell, David Allard, Kristopher K. Frese, Gina DeNicola, Christine Feig, Chelsea Combs, Stephen P. Winter, Heather Ireland-Zecchini, Stefanie Reichelt, William J. Howat, Alex Chang, Mousumi Dhara, Lifu Wang, Felix Rückert, Robert Grützmann, Christian Pilarsky, Kamel Izeradjene, Sunil R. Hingorani, Pearl Huang, Susan E. Davies, William Plunkett, Merrill Egorin, Ralph H. Hruban, Nigel Whitebread, Karen McGovern, Julian Adams, Christine Iacobuzio-Donahue, John Griffiths, and David A. Tuveson. 2009. 'Inhibition of Hedgehog Signaling Enhances Delivery of Chemotherapy in a Mouse Model of Pancreatic Cancer', *Science*, 324: 1457-61.

Orth, Michael, Philipp Metzger, Sabine Gerum, Julia Mayerle, Günter Schneider, Claus Belka, Maximilian Schnurr, and Kirsten Lauber. 2019. 'Pancreatic ductal adenocarcinoma: biological hallmarks, current status, and future perspectives of combined modality treatment approaches', *Radiation Oncology*, 14: 141.

Oxvig, C., and T. A. Springer. 1998. 'Experimental support for a beta-propeller domain in integrin alpha-subunits and a calcium binding site on its lower surface', *Proc Natl Acad Sci U S A*, 95: 4870-5.

Padera, T. P., A. H. Kuo, T. Hoshida, S. Liao, J. Lobo, K. R. Kozak, D. Fukumura, and R. K. Jain. 2008. 'Differential response of primary tumor versus lymphatic metastasis to VEGFR-2 and VEGFR-3 kinase inhibitors cediranib and vandetanib', *Mol Cancer Ther*, 7: 2272-9.

Padera, T. P., B. R. Stoll, J. B. Tooredman, D. Capen, E. di Tomaso, and R. K. Jain. 2004. 'Pathology: cancer cells compress intratumour vessels', *Nature*, 427: 695.

Padera, Timothy P., Eelco F. J. Meijer, and Lance L. Munn. 2016. 'The Lymphatic System in Disease Processes and Cancer Progression', *Annual review of biomedical engineering*, 18: 125-58.

Parente, Paola, Pietro Parcesepe, Claudia Covelli, Nunzio Olivieri, Andrea Remo, Massimo Pancione, Tiziana Pia Latiano, Paolo Graziano, Evaristo Maiello, and Guido Giordano. 2018. 'Crosstalk between the Tumor Microenvironment and Immune System in Pancreatic Ductal Adenocarcinoma: Potential Targets for New Therapeutic Approaches', *Gastroenterology Research and Practice*, 2018: 7530619.

Parente, R., S. J. Clark, A. Inforzato, and A. J. Day. 2017. 'Complement factor H in host defense and immune evasion', *Cell Mol Life Sci*, 74: 1605-24.

Park, J. S., I. K. Kim, S. Han, I. Park, C. Kim, J. Bae, S. J. Oh, S. Lee, J. H. Kim, D. C. Woo, Y. He, H. G. Augustin, I. Kim, D. Lee, and G. Y. Koh. 2016. 'Normalization of Tumor Vessels by Tie2 Activation and Ang2 Inhibition Enhances Drug Delivery and Produces a Favorable Tumor Microenvironment', *Cancer Cell*, 30: 953-67.

Patel, Manish R., Jeffrey R. Infante, Kathleen N. Moore, Mitchell Keegan, Anne Poli, Mahesh Padval, Suzanne Fields Jones, Joanna Horobin, and Howard A. Burris. 2014. 'Phase 1/1b study of the FAK inhibitor defactinib (VS-6063) in combination with weekly paclitaxel for advanced ovarian cancer', *Journal of Clinical Oncology*, 32: 5521-21.

Paul, N. R., G. Jacquemet, and P. T. Caswell. 2015. 'Endocytic Trafficking of Integrins in Cell Migration', *Curr Biol*, 25: R1092-105.

Pedrosa, Ana-Rita, Natalia Bodrug, Jesus Gomez-Escudero, Edward P. Carter, Louise E. Reynolds, Paraskevi Natalia Georgiou, Isabelle Fernandez, Delphine M. Lees, Vassiliki Kostourou, Annika N. Alexopoulou, Silvia Batista, Bernardo Tavora, Bryan Serrels, Maddy Parsons, Thomas Iskratsch, and Kairbaan M. Hodivala-Dilke. 2019. 'Tumor angiogenesis is differentially regulated by phosphorylation of endothelial cell focal adhesion kinase tyrosines-397 and -861', *Cancer Research*: canres.3934.2018.

Pekarek, L. A., B. A. Starr, A. Y. Toledano, and H. Schreiber. 1995. 'Inhibition of tumor growth by elimination of granulocytes', *Journal of Experimental Medicine*, 181: 435-40.

Pellinen, T., and J. Ivaska. 2006. 'Integrin traffic', *J Cell Sci*, 119: 3723-31.

Pellinen, T., S. Tuomi, A. Arjonen, M. Wolf, H. Edgren, H. Meyer, R. Grosse, T. Kitzing, J. K. Rantala, O. Kallioniemi, R. Fässler, M. Kallio, and J. Ivaska. 2008. 'Integrin trafficking regulated by Rab21 is necessary for cytokinesis', *Dev Cell*, 15: 371-85.

Perez-Riverol, Y., A. Csordas, J. Bai, M. Bernal-Llinares, S. Hewapathirana, D. J. Kundu, A. Inuganti, J. Griss, G. Mayer, M. Eisenacher, E. Pérez, J. Uszkoreit, J. Pfeuffer, T. Sachsenberg, S. Yilmaz, S. Tiwary, J. Cox, E. Audain, M. Walzer, A. F. Jarnuczak, T. Ternent, A. Brazma, and J. A. Vizcaíno. 2019. 'The PRIDE database and related tools and resources in 2019: improving support for quantification data', *Nucleic Acids Res*, 47: D442-d50.

Perišić Nanut, Milica, Jerica Sabotič, Anahid Jewett, and Janko Kos. 2014. 'Cysteine Cathepsins as Regulators of the Cytotoxicity of NK and T Cells', *Frontiers in Immunology*, 5: 616.

Petitprez, Florent, Aurélien de Reyniès, Emily Z. Keung, Tom Wei-Wu Chen, Cheng-Ming Sun, Julien Calderaro, Yung-Ming Jeng, Li-Ping Hsiao, Laetitia Lacroix, Antoine Bougoüin, Marco Moreira, Guillaume Lacroix, Ivo Natario, Julien Adam, Carlo Lucchesi, Yec'han Laizet, Maud Toulmonde, Melissa A. Burgess, Vanessa Bolejack, Denise Reinke, Khalid M. Wani, Wei-Lien Wang, Alexander J. Lazar, Christina L. Roland, Jennifer A. Wargo, Antoine Italiano, Catherine Sautès-Fridman, Hussein A. Tawbi, and Wolf H. Fridman. 2020. 'B cells are associated with survival and immunotherapy response in sarcoma', *Nature*, 577: 556-60.

Petrova, Varvara, Margherita Annicchiarico-Petruzzelli, Gerry Melino, and Ivano Amelio. 2018. 'The hypoxic tumour microenvironment', *Oncogenesis*, 7: 10.

Pezzella, F., U. Pastorino, E. Tagliabue, S. Andreola, G. Sozzi, G. Gasparini, S. Menard, K. C. Gatter, A. L. Harris, S. Fox, M. Buyse, S. Pilotti, M. Pierotti, and F. Rilke. 1997. 'Non-small-cell lung carcinoma tumor growth without morphological evidence of neo-angiogenesis', *Am J Pathol*, 151: 1417-23.

Phillips, Phoebe. 2012. *Pancreatic Cancer and Tumor Microenvironment*.

Piera-Velazquez, S., F. A. Mendoza, and S. A. Jimenez. 2016. 'Endothelial to Mesenchymal Transition (EndoMT) in the Pathogenesis of Human Fibrotic Diseases', *J Clin Med*, 5.

Pierini, L. M., M. A. Lawson, R. J. Eddy, B. Hendey, and F. R. Maxfield. 2000. 'Oriented endocytic recycling of alpha5beta1 in motile neutrophils', *Blood*, 95: 2471-80.

Pierschbacher, Michael D., and Erkki Ruoslahti. 1984. 'Cell attachment activity of fibronectin can be duplicated by small synthetic fragments of the molecule', *Nature*, 309: 30-33.

Pilon-Thomas, Shari, Krithika N. Kodumudi, Asmaa E. El-Kenawi, Shonagh Russell, Amy M. Weber, Kimberly Luddy, Mehdi Damaghi, Jonathan W. Wojtkowiak, James J. Mulé, Arig Ibrahim-Hashim, and Robert J. Gillies. 2016. 'Neutralization of Tumor Acidity Improves Antitumor Responses to Immunotherapy', *Cancer Research*, 76: 1381.

Pinedo, H. M., H. M. Verheul, R. J. D'Amato, and J. Folkman. 1998. 'Involvement of platelets in tumour angiogenesis?', *Lancet*, 352: 1775-7.

Plow, E. F., M. D. Pierschbacher, E. Ruoslahti, G. A. Marguerie, and M. H. Ginsberg. 1985. 'The effect of Arg-Gly-Asp-containing peptides on fibrinogen and von Willebrand factor binding to platelets', *Proc Natl Acad Sci U S A*, 82: 8057-61.

Poulos, Michael G., Eric J. Gars, Michael C. Gutkin, Christopher C. Kloss, Michael Ginsberg, Joseph M. Scandura, Shahin Rafii, and Jason M. Butler. 2014. 'Activation of the vascular niche supports leukemic progression and resistance to chemotherapy', *Experimental Hematology*, 42: 976-86.e3.

Pouysségur, J., F. Dayan, and N. M. Mazure. 2006. 'Hypoxia signalling in cancer and approaches to enforce tumour regression', *Nature*, 441: 437-43.

Prabhakar, U., H. Maeda, R. K. Jain, E. M. Sevick-Muraca, W. Zamboni, O. C. Farokhzad, S. T. Barry, A. Gabizon, P. Grodzinski, and D. C. Blakey. 2013. 'Challenges and key considerations of the enhanced permeability and retention effect for nanomedicine drug delivery in oncology.' in, *Cancer Res* (©2013 aacr.).

Presta, Marco, Patrizia Dell'Era, Stefania Mitola, Emanuela Moroni, Roberto Ronca, and Marco Rusnati. 2005. 'Fibroblast growth factor/fibroblast growth factor receptor system in angiogenesis', *Cytokine & Growth Factor Reviews*, 16: 159-78.

Qian, B. Z., and J. W. Pollard. 2010. 'Macrophage diversity enhances tumor progression and metastasis', *Cell*, 141: 39-51.
Qin, Z., G. Richter, T. Schüler, S. Ibe, X. Cao, and T. Blankenstein. 1998. 'B cells inhibit induction of T cell-dependent tumor immunity', *Nat Med*, 4: 627-30.
Quante, A. S., C. Ming, M. Rottmann, J. Engel, S. Boeck, V. Heinemann, C. B. Westphalen, and K. Strauch. 2016. 'Projections of cancer incidence and cancer-related deaths in Germany by 2020 and 2030', *Cancer Med*, 5: 2649-56.
Quick, J., F. Gessler, S. Dutzmann, E. Hattingen, P. N. Harter, L. M. Weise, K. Franz, V. Seifert, and C. Senft. 2014. 'Benefit of tumor resection for recurrent glioblastoma', *J Neurooncol*, 117: 365-72.
Radulovic, J., J. Kammermeier, and J. Spiess. 1998. 'Generalization of fear responses in C57BL/6N mice subjected to one-trial foreground contextual fear conditioning', *Behav Brain Res*, 95: 179-89.
Rafii, Shahin, Jason M. Butler, and Bi-Sen Ding. 2016. 'Angiocrine functions of organ-specific endothelial cells', *Nature*, 529: 316-25.
Rahib, L., B. D. Smith, R. Aizenberg, A. B. Rosenzweig, J. M. Fleshman, and L. M. Matrisian. 2014. 'Projecting cancer incidence and deaths to 2030: the unexpected burden of thyroid, liver, and pancreas cancers in the United States', *Cancer Res*, 74: 2913-21.
Rajabi, Mehdi, and Shaker A. Mousa. 2017. 'The Role of Angiogenesis in Cancer Treatment', *Biomedicines*, 5: 34.
Ramjiawan, Rakesh R., Arjan W. Griffioen, and Dan G. Duda. 2017. 'Anti-angiogenesis for cancer revisited: Is there a role for combinations with immunotherapy?', *Angiogenesis*, 20: 185-204.
Raza, Ahmad, Michael J. Franklin, and Arkadiusz Z. Dudek. 2010. 'Pericytes and vessel maturation during tumor angiogenesis and metastasis', *American Journal of Hematology*, 85: 593-98.
Red-Horse, Kristy, and Arndt F. Siekmann. 2019. 'Veins and Arteries Build Hierarchical Branching Patterns Differently: Bottom-Up versus Top-Down', *BioEssays : news and reviews in molecular, cellular and developmental biology*, 41: e1800198-e98.
Reddig, P. J., and R. L. Juliano. 2005. 'Clinging to life: cell to matrix adhesion and cell survival', *Cancer Metastasis Rev*, 24: 425-39.
Reichenbach, D. K., Q. Li, R. A. Hoffman, A. L. Williams, W. D. Shlomchik, D. M. Rothstein, A. J. Demetris, and F. G. Lakkis. 2013. 'Allograft outcomes in outbred mice', *American journal of transplantation : official journal of the American Society of Transplantation and the American Society of Transplant Surgeons*, 13: 580-88.
Ren, Bo, Ming Cui, Gang Yang, Huanyu Wang, Mengyu Feng, Lei You, and Yupei Zhao. 2018. 'Tumor microenvironment participates in metastasis of pancreatic cancer', *Molecular Cancer*, 17: 108.
Reynolds, Andrew R., Ian R. Hart, Alan R. Watson, Jonathan C. Welti, Rita G. Silva, Stephen D. Robinson, Georges Da Violante, Morgane Gourlaouen, Mishal Salih, Matt C. Jones, Dylan T. Jones, Garry Saunders, Vassiliki Kostourou, Françoise Perron-Sierra, Jim C. Norman, Gordon C. Tucker, and Kairbaan M. Hodivala-Dilke. 2009. 'Stimulation of tumor growth and angiogenesis by low concentrations of RGD-mimetic integrin inhibitors', *Nature Medicine*, 15: 392.
Reynolds, L. E., and K. M. Hodivala-Dilke. 2006. 'Primary mouse endothelial cell culture for assays of angiogenesis', *Methods Mol Med*, 120: 503-9.
Reynolds, Louise E., Lorenza Wyder, Julie C. Lively, Daniela Taverna, Stephen D. Robinson, Xiaozhu Huang, Dean Sheppard, Richard O. Hynes, and Kairbaan M.

Hodivala-Dilke. 2002. 'Enhanced pathological angiogenesis in mice lacking β3 integrin or β3 and β5 integrins', *Nature Medicine*, 8: 27-34.
Ribatti, D. 2013. 'Angiogenesis.' in Stanley Maloy and Kelly Hughes (eds.), *Brenner's Encyclopedia of Genetics (Second Edition)* (Academic Press: San Diego).
Ribatti, Domenico. 2008. 'Judah Folkman, a pioneer in the study of angiogenesis', *Angiogenesis*, 11: 3-10.
Ribeiro, Aline Lopes, and Oswaldo Keith Okamoto. 2015. 'Combined Effects of Pericytes in the Tumor Microenvironment', *Stem Cells International*, 2015: 868475.
Rigamonti, N., E. Kadioglu, I. Keklikoglou, C. Wyser Rmili, C. C. Leow, and M. De Palma. 2014. 'Role of angiopoietin-2 in adaptive tumor resistance to VEGF signaling blockade', *Cell Rep*, 8: 696-706.
Roberts, W. G., E. Ung, P. Whalen, B. Cooper, C. Hulford, C. Autry, D. Richter, E. Emerson, J. Lin, J. Kath, K. Coleman, L. Yao, L. Martinez-Alsina, M. Lorenzen, M. Berliner, M. Luzzio, N. Patel, E. Schmitt, S. LaGreca, J. Jani, M. Wessel, E. Marr, M. Griffor, and F. Vajdos. 2008. 'Antitumor activity and pharmacology of a selective focal adhesion kinase inhibitor, PF-562,271', *Cancer Res*, 68: 1935-44.
Robinson, S. D., and K. M. Hodivala-Dilke. 2011. 'The role of β3-integrins in tumor angiogenesis: context is everything', *Curr Opin Cell Biol*, 23: 630-7.
Roh, M. E., M. Cosgrove, K. Gorski, and I. S. Hitchcock. 2013. 'Off-targets effects underlie the inhibitory effect of FAK inhibitors on platelet activation: studies using Fak-deficient mice', *Journal of thrombosis and haemostasis : JTH*, 11: 1776-78.
Root, Richard K., and David C. Dale. 1999. 'Granulocyte Colony-Stimulating Factor and Granulocyte-Macrophage Colony-Stimulating Factor: Comparisons and Potential for Use in the Treatment of Infections in Nonneutropenic Patients', *The Journal of Infectious Diseases*, 179: S342-S52.
Ross, Tyler D., Brian G. Coon, Sanguk Yun, Nicolas Baeyens, Keiichiro Tanaka, Mingxing Ouyang, and Martin A. Schwartz. 2013. 'Integrins in mechanotransduction', *Current opinion in cell biology*, 25: 613-18.
Roth, D. M., J. S. Swaney, N. D. Dalton, E. A. Gilpin, and J. Ross, Jr. 2002. 'Impact of anesthesia on cardiac function during echocardiography in mice', *Am J Physiol Heart Circ Physiol*, 282: H2134-40.
Roy-Luzarraga, M., T. Abdel-Fatah, L. E. Reynolds, A. Clear, J. G. Taylor, J. G. Gribben, S. Chan, L. Jones, and K. Hodivala-Dilke. 2020. 'Association of Low Tumor Endothelial Cell pY397-Focal Adhesion Kinase Expression With Survival in Patients With Neoadjuvant-Treated Locally Advanced Breast Cancer', *JAMA Netw Open*, 3: e2019304.
Roy-Luzarraga, M., and K. Hodivala-Dilke. 2016. 'Molecular Pathways: Endothelial Cell FAK-A Target for Cancer Treatment', *Clin Cancer Res*, 22: 3718-24.
Ruggeri, Z. M. 2002. 'Platelets in atherothrombosis', *Nat Med*, 8: 1227-34.
Ruoslahti, E. 1996. 'RGD and other recognition sequences for integrins', *Annu Rev Cell Dev Biol*, 12: 697-715.
Sahai, Erik, Igor Astsaturov, Edna Cukierman, David G. DeNardo, Mikala Egeblad, Ronald M. Evans, Douglas Fearon, Florian R. Greten, Sunil R. Hingorani, Tony Hunter, Richard O. Hynes, Rakesh K. Jain, Tobias Janowitz, Claus Jorgensen, Alec C. Kimmelman, Mikhail G. Kolonin, Robert G. Maki, R. Scott Powers, Ellen Puré, Daniel C. Ramirez, Ruth Scherz-Shouval, Mara H. Sherman, Sheila Stewart, Thea D. Tlsty, David A. Tuveson, Fiona M. Watt, Valerie Weaver, Ashani T. Weeraratna, and Zena Werb. 2020. 'A framework for advancing our understanding of cancer-associated fibroblasts', *Nature Reviews Cancer*, 20: 174-86.

Saltel, F., E. Mortier, V. P. Hytönen, M. C. Jacquier, P. Zimmermann, V. Vogel, W. Liu, and B. Wehrle-Haller. 2009. 'New PI(4,5)P2- and membrane proximal integrin-binding motifs in the talin head control beta3-integrin clustering', *J Cell Biol*, 187: 715-31.

Sandler, Vladislav M., Raphael Lis, Ying Liu, Alon Kedem, Daylon James, Olivier Elemento, Jason M. Butler, Joseph M. Scandura, and Shahin Rafii. 2014. 'Reprogramming human endothelial cells to haematopoietic cells requires vascular induction', *Nature*, 511: 312-18.

Sasaki, Hiroko, Kazuko Nagura, Masaho Ishino, Hirotoshi Tobioka, Kiyoshi Kotani, and Terukatsu Sasaki. 1995. 'Cloning and Characterization of Cell Adhesion Kinase β, a Novel Protein-tyrosine Kinase of the Focal Adhesion Kinase Subfamily (∗)', *Journal of Biological Chemistry*, 270: 21206-19.

Sasich, Larry D., and Sana Rikabi Sukkari. 2012. 'The US FDAs withdrawal of the breast cancer indication for Avastin (bevacizumab)', *Saudi pharmaceutical journal : SPJ : the official publication of the Saudi Pharmaceutical Society*, 20: 381-85.

Savola, Suvi, Arto Klami, Samuel Myllykangas, Cristina Manara, Katia Scotlandi, Piero Picci, Sakari Knuutila, and Jukka Vakkila. 2011. 'High Expression of Complement Component 5 (C5) at Tumor Site Associates with Superior Survival in Ewing's Sarcoma Family of Tumour Patients', *ISRN Oncology*, 2011: 168712.

Sawhney, R., and F. Kabbinavar. 2008. 'Angiogenesis and angiogenic inhibitors in renal cell carcinoma', *Curr Urol Rep*, 9: 26-33.

Scatena, M., M. Almeida, M. L. Chaisson, N. Fausto, R. F. Nicosia, and C. M. Giachelli. 1998. 'NF-κB mediates αvβ3 integrin-induced endothelial cell survival', *Journal of Cell Biology*, 141: 1083-93.

Schioppa, T., R. Moore, R. G. Thompson, E. C. Rosser, H. Kulbe, S. Nedospasov, C. Mauri, L. M. Coussens, and F. R. Balkwill. 2011. 'B regulatory cells and the tumor-promoting actions of TNF-α during squamous carcinogenesis', *Proc Natl Acad Sci U S A*, 108: 10662-7.

Schittenhelm, J., A. Klein, M. S. Tatagiba, R. Meyermann, F. Fend, S. L. Goodman, and B. Sipos. 2013. 'Comparing the expression of integrins αvβ3, αvβ5, αvβ6, αvβ8, fibronectin and fibrinogen in human brain metastases and their corresponding primary tumors', *Int J Clin Exp Pathol*, 6: 2719-32.

Schultze, A., and W. Fiedler. 2011. 'Clinical importance and potential use of small molecule inhibitors of focal adhesion kinase', *Anticancer Agents Med Chem*, 11: 593-9.

Sciarra, A., V. Gentile, S. Salciccia, A. Alfarone, and F. Di Silverio. 2008. 'New anti-angiogenic targeted therapy in advanced renal cell carcinoma (RCC): current status and future prospects', *Rev Recent Clin Trials*, 3: 97-103.

Senger, Donald R., and Carole A. Perruzzi. 1996. 'Cell migration promoted by a potent GRGDS-containing thrombin-cleavage fragment of osteopontin', *Biochimica et Biophysica Acta (BBA) - Molecular Cell Research*, 1314: 13-24.

Serrels, A., T. Lund, B. Serrels, A. Byron, R. C. McPherson, A. von Kriegsheim, L. Gómez-Cuadrado, M. Canel, M. Muir, J. E. Ring, E. Maniati, A. H. Sims, J. A. Pachter, V. G. Brunton, N. Gilbert, S. M. Anderton, R. J. Nibbs, and M. C. Frame. 2015. 'Nuclear FAK controls chemokine transcription, Tregs, and evasion of anti-tumor immunity', *Cell*, 163: 160-73.

Serrels, Alan, and Margaret C. Frame. 2016. 'FAK goes nuclear to control antitumor immunity—a new target in cancer immuno-therapy', *OncoImmunology*, 5: e1119356.

Serrels, Bryan, Niamh McGivern, Marta Canel, Adam Byron, Sarah C. Johnson, Henry J. McSorley, Niall Quinn, David Taggart, Alex Von Kreigsheim, Stephen M.

Anderton, Alan Serrels, and Margaret C. Frame. 2017. 'IL-33 and ST2 mediate FAK-dependent antitumor immune evasion through transcriptional networks', *Science signaling*, 10: eaan8355.

Sfiligoi, C., A. de Luca, I. Cascone, V. Sorbello, L. Fuso, R. Ponzone, N. Biglia, E. Audero, R. Arisio, F. Bussolino, P. Sismondi, and M. De Bortoli. 2003. 'Angiopoietin-2 expression in breast cancer correlates with lymph node invasion and short survival', *Int J Cancer*, 103: 466-74.

Shah, Sunil, Anjali Chandra, Amanjot Kaur, Nirupama Sabnis, Andras Lacko, Zygmunt Gryczynski, Rafal Fudala, and Ignacy Gryczynski. 2017. 'Fluorescence properties of doxorubicin in PBS buffer and PVA films', *Journal of photochemistry and photobiology. B, Biology*, 170: 65-69.

Shattil, S. J., H. Kashiwagi, and N. Pampori. 1998. 'Integrin signaling: the platelet paradigm', *Blood*, 91: 2645-57.

Shattil, Sanford J., Chungho Kim, and Mark H. Ginsberg. 2010. 'The final steps of integrin activation: the end game', *Nature Reviews Molecular Cell Biology*, 11: 288-300.

Shen, Bo, M. Keegan Delaney, and Xiaoping Du. 2012. 'Inside-out, outside-in, and inside–outside-in: G protein signaling in integrin-mediated cell adhesion, spreading, and retraction', *Current Opinion in Cell Biology*, 24: 600-06.

Shen, Cheng-Huang, Hsiao-Yen Hsieh, Yuan-Hung Wang, Syue-Yi Chen, Chun-Liang Tung, Jiann- D. E. R. Wu, Chang-Te Lin, Michael W. Y. Chan, Cheng- D. A. Hsu, and Deching Chang. 2010. 'High Dickkopf-1 expression is associated with poor prognosis in patients with advanced urothelial carcinoma', *Experimental and therapeutic medicine*, 1: 893-98.

Shimaoka, M., C. Lu, A. Salas, T. Xiao, J. Takagi, and T. A. Springer. 2002. 'Stabilizing the integrin alpha M inserted domain in alternative conformations with a range of engineered disulfide bonds', *Proc Natl Acad Sci U S A*, 99: 16737-41.

Shimaoka, Motomu, Azucena Salas, Wei Yang, Gabriele Weitz-Schmidt, and Timothy A. Springer. 2003. 'Small Molecule Integrin Antagonists that Bind to the β2 Subunit I-like Domain and Activate Signals in One Direction and Block Them in the Other', *Immunity*, 19: 391-402.

Shimizu, Toshio, Kazuya Fukuoka, Masayuki Takeda, Tutomu Iwasa, Takeshi Yoshida, Joanna Horobin, Mitchell Keegan, Lou Vaickus, Ajit Chavan, Mahesh Padval, and Kazuhiko Nakagawa. 2016. 'A first-in-Asian phase 1 study to evaluate safety, pharmacokinetics and clinical activity of VS-6063, a focal adhesion kinase (FAK) inhibitor in Japanese patients with advanced solid tumors', *Cancer chemotherapy and pharmacology*, 77: 997-1003.

Shimshek, D. R., J. Kim, M. R. Hübner, D. J. Spergel, F. Buchholz, E. Casanova, A. F. Stewart, P. H. Seeburg, and R. Sprengel. 2002. 'Codon-improved Cre recombinase (iCre) expression in the mouse', *Genesis*, 32: 19-26.

Sieg, David J., Duško Ilić, K. C. Jones, Caroline H. Damsky, Tony Hunter, and David D. Schlaepfer. 1998. 'Pyk2 and Src-family protein-tyrosine kinases compensate for the loss of FAK in fibronectin-stimulated signaling events but Pyk2 does not fully function to enhance FAK− cell migration', *The EMBO Journal*, 17: 5933-47.

Siegel, R. L., K. D. Miller, and A. Jemal. 2015. 'Cancer statistics, 2015', *CA Cancer J Clin*, 65: 5-29.

Siegel, Rebecca L., Kimberly D. Miller, and Ahmedin Jemal. 2019. 'Cancer statistics, 2019', *CA: A Cancer Journal for Clinicians*, 69: 7-34.

Simpson, E. M., C. C. Linder, E. E. Sargent, M. T. Davisson, L. E. Mobraaten, and J. J. Sharp. 1997. 'Genetic variation among 129 substrains and its importance for targeted mutagenesis in mice', *Nat Genet*, 16: 19-27.

Sinha, P., V. K. Clements, S. K. Bunt, S. M. Albelda, and S. Ostrand-Rosenberg. 2007. 'Cross-talk between myeloid-derived suppressor cells and macrophages subverts tumor immunity toward a type 2 response', *J Immunol*, 179: 977-83.

Slack-Davis, Jill K., Karen H. Martin, Robert W. Tilghman, Marcin Iwanicki, Ethan J. Ung, Christopher Autry, Michael J. Luzzio, Beth Cooper, John C. Kath, W. Gregory Roberts, and J. Thomas Parsons. 2007. 'Cellular Characterization of a Novel Focal Adhesion Kinase Inhibitor *', *Journal of Biological Chemistry*, 282: 14845-52.

Small, J. Victor, Theresia Stradal, Emmanuel Vignal, and Klemens Rottner. 2002. 'The lamellipodium: where motility begins', *Trends in Cell Biology*, 12: 112-20.

Solocinski, Kristen, Michelle R. Padget, Kellsye P. Fabian, Benjamin Wolfson, Fabiola Cecchi, Todd Hembrough, Stephen C. Benz, Shahrooz Rabizadeh, Patrick Soon-Shiong, Jeffrey Schlom, and James W. Hodge. 2020. 'Overcoming hypoxia-induced functional suppression of NK cells', *Journal for ImmunoTherapy of Cancer*, 8: e000246.

Spear, Sarah, Juliana B. Candido, Jacqueline R. McDermott, Cristina Ghirelli, Eleni Maniati, Stephen A. Beers, Frances R. Balkwill, Hemant M. Kocher, and Melania Capasso. 2019. 'Discrepancies in the Tumor Microenvironment of Spontaneous and Orthotopic Murine Models of Pancreatic Cancer Uncover a New Immunostimulatory Phenotype for B Cells', *Frontiers in Immunology*, 10.

Sprinzak, D., A. Lakhanpal, L. Lebon, L. A. Santat, M. E. Fontes, G. A. Anderson, J. Garcia-Ojalvo, and M. B. Elowitz. 2010. 'Cis-interactions between Notch and Delta generate mutually exclusive signalling states', *Nature*, 465: 86-90.

Srigley, John R., and Brett Delahunt. 2009. 'Uncommon and recently described renal carcinomas', *Modern Pathology*, 22: S2-S23.

Stacker, Steven A., Carol Caesar, Megan E. Baldwin, Gillian E. Thornton, Richard A. Williams, Remko Prevo, David G. Jackson, Shin-ichi Nishikawa, Hajime Kubo, and Marc G. Achen. 2001. 'VEGF-D promotes the metastatic spread of tumor cells via the lymphatics', *Nature Medicine*, 7: 186-91.

Sternberg, N. 1990. 'Bacteriophage P1 cloning system for the isolation, amplification, and recovery of DNA fragments as large as 100 kilobase pairs', *Proc Natl Acad Sci U S A*, 87: 103-7.

Steven, Antonius, Scott A. Fisher, and Bruce W. Robinson. 2016. 'Immunotherapy for lung cancer', *Respirology*, 21: 821-33.

Stiedl, Oliver, Jelena Radulovic, Ragna Lohmann, Karin Birkenfeld, Markki Palve, Jens Kammermeier, Farahnaz Sananbenesi, and Joachim Spiess. 1999. 'Strain and substrain differences in context- and tone-dependent fear conditioning of inbred mice', *Behav Brain Res*, 104: 1-12.

Stockis, J., S. Liénart, D. Colau, A. Collignon, S. L. Nishimura, D. Sheppard, P. G. Coulie, and S. Lucas. 2017. 'Blocking immunosuppression by human Tregs in vivo with antibodies targeting integrin αVβ8', *Proc Natl Acad Sci U S A*, 114: E10161-e68.

Stokes, J. B., S. J. Adair, J. K. Slack-Davis, D. M. Walters, R. W. Tilghman, E. D. Hershey, B. Lowrey, K. S. Thomas, A. H. Bouton, R. F. Hwang, E. B. Stelow, J. T. Parsons, and T. W. Bauer. 2011. 'Inhibition of focal adhesion kinase by PF-562,271 inhibits the growth and metastasis of pancreatic cancer concomitant with altering the tumor microenvironment', *Mol Cancer Ther*, 10: 2135-45.

Stone, R. L., K. A. Baggerly, G. N. Armaiz-Pena, Y. Kang, A. M. Sanguino, D. Thanapprapasr, H. J. Dalton, J. Bottsford-Miller, B. Zand, R. Akbani, L. Diao, A. M. Nick, K. DeGeest, G. Lopez-Berestein, R. L. Coleman, S. Lutgendorf, and A. K. Sood. 2014. 'Focal adhesion kinase: an alternative focus for anti-angiogenesis therapy in ovarian cancer', *Cancer Biol Ther*, 15: 919-29.

Stupp, R., M. E. Hegi, T. Gorlia, S. C. Erridge, J. Perry, Y. K. Hong, K. D. Aldape, B. Lhermitte, T. Pietsch, D. Grujicic, J. P. Steinbach, W. Wick, R. Tarnawski, D. H. Nam, P. Hau, A. Weyerbrock, M. J. Taphoorn, C. C. Shen, N. Rao, L. Thurzo, U. Herrlinger, T. Gupta, R. D. Kortmann, K. Adamska, C. McBain, A. A. Brandes, J. C. Tonn, O. Schnell, T. Wiegel, C. Y. Kim, L. B. Nabors, D. A. Reardon, M. J. van den Bent, C. Hicking, A. Markivskyy, M. Picard, and M. Weller. 2014. 'Cilengitide combined with standard treatment for patients with newly diagnosed glioblastoma with methylated MGMT promoter (CENTRIC EORTC 26071-22072 study): a multicentre, randomised, open-label, phase 3 trial', *Lancet Oncol*, 15: 1100-8.

Sturtzel, Caterina. 2017. 'Endothelial Cells.' in Susanne Sattler and Teresa Kennedy-Lydon (eds.), *The Immunology of Cardiovascular Homeostasis and Pathology* (Springer International Publishing: Cham).

Stylianopoulos, T., J. D. Martin, V. P. Chauhan, S. R. Jain, B. Diop-Frimpong, N. Bardeesy, B. L. Smith, C. R. Ferrone, F. J. Hornicek, Y. Boucher, L. L. Munn, and R. K. Jain. 2012. 'Causes, consequences, and remedies for growth-induced solid stress in murine and human tumors', *Proc Natl Acad Sci U S A*, 109: 15101-8.

Sukriti, Sukriti, Mohammad Tauseef, Pascal Yazbeck, and Dolly Mehta. 2014. 'Mechanisms regulating endothelial permeability', *Pulmonary circulation*, 4: 535-51.

Sulzmaier, Florian J., Christine Jean, and David D. Schlaepfer. 2014. 'FAK in cancer: mechanistic findings and clinical applications', *Nature Reviews Cancer*, 14: 598.

Sun, Y., J. Wang, Y. Liu, X. Song, Y. Zhang, K. Li, Y. Zhu, Q. Zhou, L. You, and C. Yao. 2005. 'Results of phase III trial of rh-endostatin (YH-16) in advanced non-small cell lung cancer (NSCLC) patients', *Journal of Clinical Oncology*, 23: 7138-38.

Sun, Yue, Narendra Thapa, Andrew C. Hedman, and Richard A. Anderson. 2013. 'Phosphatidylinositol 4,5-bisphosphate: targeted production and signaling', *BioEssays : news and reviews in molecular, cellular and developmental biology*, 35: 513-22.

Sunshine, Joel, and Janis M. Taube. 2015. 'PD-1/PD-L1 inhibitors', *Current opinion in pharmacology*, 23: 32-38.

Suzuki, Akiko, Pamela Leland, Bharat H. Joshi, and Raj K. Puri. 2015. 'Targeting of IL-4 and IL-13 receptors for cancer therapy', *Cytokine*, 75: 79-88.

Suzuki, S., A. Oldberg, E. G. Hayman, M. D. Pierschbacher, and E. Ruoslahti. 1985. 'Complete amino acid sequence of human vitronectin deduced from cDNA. Similarity of cell attachment sites in vitronectin and fibronectin', *Embo j*, 4: 2519-24.

Tachibana, T., H. Onodera, T. Tsuruyama, A. Mori, S. Nagayama, H. Hiai, and M. Imamura. 2005. 'Increased intratumor Valpha24-positive natural killer T cells: a prognostic factor for primary colorectal carcinomas', *Clin Cancer Res*, 11: 7322-7.

Tadokoro, S., S. J. Shattil, K. Eto, V. Tai, R. C. Liddington, J. M. de Pereda, M. H. Ginsberg, and D. A. Calderwood. 2003. 'Talin binding to integrin beta tails: a final common step in integrin activation', *Science*, 302: 103-6.

Tahergorabi, Zoya, and Majid Khazaei. 2012. 'A review on angiogenesis and its assays', *Iranian journal of basic medical sciences*, 15: 1110-26.

Tai, Yu-Ling, Lih-Chyang Chen, and Tang-Long Shen. 2015. 'Emerging roles of focal adhesion kinase in cancer', *BioMed research international*, 2015: 690690-90.

Takada, Yoshikazu, Xiaojing Ye, and Scott Simon. 2007. 'The integrins', *Genome biology*, 8: 215-15.

Tang, Hao-Sha, You-Ji Feng, and Liang-Qing Yao. 2009. 'Angiogenesis, Vasculogenesis, and Vasculogenic Mimicry in Ovarian Cancer', *International Journal of Gynecologic Cancer*, 19: 605-10.

Tavora, B., S. Batista, A. N. Alexopoulou, V. Kostourou, I. Fernandez, S. D. Robinson, D. M. Lees, B. Serrels, and K. Hodivala-Dilke. 2014. 'Generation of point-mutant FAK knockin mice', *genesis*, 52: 907-15.

Tavora, B., S. Batista, L. E. Reynolds, S. Jadeja, S. Robinson, V. Kostourou, I. Hart, M. Fruttiger, M. Parsons, and K. M. Hodivala-Dilke. 2010. 'Endothelial FAK is required for tumour angiogenesis', *EMBO Mol Med*, 2: 516-28.

Tavora, Bernardo, Louise E. Reynolds, Silvia Batista, Fevzi Demircioglu, Isabelle Fernandez, Tanguy Lechertier, Delphine M. Lees, Ping-Pui Wong, Annika Alexopoulou, George Elia, Andrew Clear, Adeline Ledoux, Jill Hunter, Neil Perkins, John G. Gribben, and Kairbaan M. Hodivala-Dilke. 2014. 'Endothelial-cell FAK targeting sensitizes tumours to DNA-damaging therapy', *Nature*, 514: 112-16.

Teichert, Martin, Laura Milde, Annegret Holm, Laura Stanicek, Nicolas Gengenbacher, Soniya Savant, Tina Ruckdeschel, Zulfiyya Hasanov, Kshitij Srivastava, Junhao Hu, Stella Hertel, Arne Bartol, Katharina Schlereth, and Hellmut G. Augustin. 2017. 'Pericyte-expressed Tie2 controls angiogenesis and vessel maturation', *Nature Communications*, 8: 16106.

Thapa, N., Y. Sun, M. Schramp, S. Choi, K. Ling, and R. A. Anderson. 2012. 'Phosphoinositide signaling regulates the exocyst complex and polarized integrin trafficking in directionally migrating cells', *Dev Cell*, 22: 116-30.

Theisen, U., E. Straube, and A. Straube. 2012. 'Directional persistence of migrating cells requires Kif1C-mediated stabilization of trailing adhesions', *Dev Cell*, 23: 1153-66.

Theocharis, A. D., S. S. Skandalis, C. Gialeli, and N. K. Karamanos. 2016. 'Extracellular matrix structure', *Adv Drug Deliv Rev*, 97: 4-27.

Thomas, Markus, Moritz Felcht, Karoline Kruse, Stella Kretschmer, Carleen Deppermann, Andreas Biesdorf, Karl Rohr, Andrew V. Benest, Ulrike Fiedler, and Hellmut G. Augustin. 2010. 'Angiopoietin-2 Stimulation of Endothelial Cells Induces αvβ3 Integrin Internalization and Degradation *', *Journal of Biological Chemistry*, 285: 23842-49.

Tian, M., L. Yu, Y. Qin, D. Wang, X. Wang, and Y. Li. 2015. '[Correlation between metabolic tumor volume (MTV) and microvessel density (MVD) and blood-borne metastasis in colorectal carcinoma]', *Zhonghua Zhong Liu Za Zhi*, 37: 521-5.

Tiwari, A., J. J. Jung, S. M. Inamdar, C. O. Brown, A. Goel, and A. Choudhury. 2011. 'Endothelial cell migration on fibronectin is regulated by syntaxin 6-mediated alpha5beta1 integrin recycling', *J Biol Chem*, 286: 36749-61.

Tohme, Samer, Hamza O. Yazdani, Ahmed B. Al-Khafaji, Alexis P. Chidi, Patricia Loughran, Kerri Mowen, Yanming Wang, Richard L. Simmons, Hai Huang, and Allan Tsung. 2016. 'Neutrophil Extracellular Traps Promote the Development and Progression of Liver Metastases after Surgical Stress', *Cancer Research*, 76: 1367.

Tonnesen, M. G., X. Feng, and R. A. Clark. 2000. 'Angiogenesis in wound healing', *J Investig Dermatol Symp Proc*, 5: 40-6.

Torchilin, V. 2011. 'Tumor delivery of macromolecular drugs based on the EPR effect', *Adv Drug Deliv Rev*, 63: 131-5.

Tsai, Jeff H., and William M. F. Lee. 2009. 'Tie2 in tumor endothelial signaling and survival: implications for antiangiogenic therapy', *Molecular cancer research : MCR*, 7: 300-10.

Tseng, William W., Daniel Winer, Justin A. Kenkel, Okmi Choi, Alan H. Shain, Jonathan R. Pollack, Randy French, Andrew M. Lowy, and Edgar G. Engleman. 2010. 'Development of an Orthotopic Model of Invasive Pancreatic Cancer in an Immunocompetent Murine Host', *Clinical Cancer Research*, 16: 3684-95.

Tucker, W. D., Y. Arora, and K. Mahajan. 2020. 'Anatomy, Blood Vessels.' in, *StatPearls* (StatPearls Publishing

Turner, M. D., B. Nedjai, T. Hurst, and D. J. Pennington. 2014. 'Cytokines and chemokines: At the crossroads of cell signalling and inflammatory disease', *Biochim Biophys Acta*, 1843: 2563-82.

Tycko, B. 2000. 'Epigenetic gene silencing in cancer', *The Journal of clinical investigation*, 105: 401-07.

Tzankov, A., C. Meier, P. Hirschmann, P. Went, S. A. Pileri, and S. Dirnhofer. 2008. 'Correlation of high numbers of intratumoral FOXP3+ regulatory T cells with improved survival in germinal center-like diffuse large B-cell lymphoma, follicular lymphoma and classical Hodgkin's lymphoma', *Haematologica*, 93: 193-200.

Ucuzian, Areck A., Andrew A. Gassman, Andrea T. East, and Howard P. Greisler. 2010. 'Molecular mediators of angiogenesis', *Journal of burn care & research : official publication of the American Burn Association*, 31: 158-75.

Ursoli Ferreira, Fernanda, Lucas Eduardo Botelho Souza, Carolina Hassibe Thomé, Mariana Tomazini Pinto, Clarice Origassa, Suellen Salustiano, Vitor Marcel Faça, Niels Olsen Câmara, Simone Kashima, and Dimas Tadeu Covas. 2019. 'Endothelial Cells Tissue-Specific Origins Affects Their Responsiveness to TGF-β2 during Endothelial-to-Mesenchymal Transition', *International journal of molecular sciences*, 20: 458.

Ushach, I., and A. Zlotnik. 2016. 'Biological role of granulocyte macrophage colony-stimulating factor (GM-CSF) and macrophage colony-stimulating factor (M-CSF) on cells of the myeloid lineage', *J Leukoc Biol*, 100: 481-9.

Vasey, P. A., S. B. Kaye, R. Morrison, C. Twelves, P. Wilson, R. Duncan, A. H. Thomson, L. S. Murray, T. E. Hilditch, T. Murray, S. Burtles, D. Fraier, E. Frigerio, and J. Cassidy. 1999. 'Phase I clinical and pharmacokinetic study of PK1 [N-(2-hydroxypropyl)methacrylamide copolymer doxorubicin]: first member of a new class of chemotherapeutic agents-drug-polymer conjugates. Cancer Research Campaign Phase I/II Committee', *Clin Cancer Res*, 5: 83-94.

Vermeulen, P. B., C. Colpaert, R. Salgado, R. Royers, H. Hellemans, E. Van Den Heuvel, G. Goovaerts, L. Y. Dirix, and E. Van Marck. 2001. 'Liver metastases from colorectal adenocarcinomas grow in three patterns with different angiogenesis and desmoplasia', *J Pathol*, 195: 336-42.

Vestweber, D. 2012. 'Relevance of endothelial junctions in leukocyte extravasation and vascular permeability', *Ann N Y Acad Sci*, 1257: 184-92.

Vita, M. Golubovskaya. 2010. 'Focal Adhesion Kinase as a Cancer Therapy Target', *Anti-Cancer Agents in Medicinal Chemistry*, 10: 735-41.

Vito, A., N. El-Sayes, and K. Mossman. 2020. 'Hypoxia-Driven Immune Escape in the Tumor Microenvironment', *Cells*, 9.

Vuillefroy de Silly, Romain, Pierre-Yves Dietrich, and Paul R. Walker. 2016. 'Hypoxia and antitumor CD8(+) T cells: An incompatible alliance?', *Oncoimmunology*, 5: e1232236-e36.

Wagner, C. L., M. A. Mascelli, D. S. Neblock, H. F. Weisman, B. S. Coller, and R. E. Jordan. 1996. 'Analysis of GPIIb/IIIa receptor number by quantification of 7E3 binding to human platelets', *Blood*, 88: 907-14.

Wajapeyee, N., R. W. Serra, X. Zhu, M. Mahalingam, and M. R. Green. 2008. 'Oncogenic BRAF induces senescence and apoptosis through pathways mediated by the secreted protein IGFBP7', *Cell*, 132: 363-74.

Walker, Mary K., Jason R. Boberg, Mary T. Walsh, Valerie Wolf, Alisha Trujillo, Melissa Skelton Duke, Rupert Palme, and Linda A. Felton. 2012. 'A less stressful alternative to oral gavage for pharmacological and toxicological studies in mice', *Toxicology and Applied Pharmacology*, 260: 65-69.

Wang, Hao-Wei, and Johanna A. Joyce. 2010. 'Alternative activation of tumor-associated macrophages by IL-4', *Cell Cycle*, 9: 4824-35.

Wang, J. Z., Y. J. Xiong, G. C. W. Man, X. Y. Chen, J. Kwong, and C. C. Wang. 2018. 'Clinicopathological and prognostic significance of blood microvessel density in endometrial cancer: a meta-analysis and subgroup analysis', *Arch Gynecol Obstet*, 297: 731-40.

Wang, Jan, and Richard Milner. 2006. 'Fibronectin promotes brain capillary endothelial cell survival and proliferation through α5β1 and αvβ3 integrins via MAP kinase signalling', *Journal of Neurochemistry*, 96: 148-59.

Wang, Ji, and Chengchu Zhu. 2016. 'Anticoagulation in combination with antiangiogenesis and chemotherapy for cancer patients: evidence and hypothesis', *OncoTargets and therapy*, 9: 4737-46.

Wang, Xiangfei, Xiumin Wang, Yang Liu, Yating Dong, Yanan Wang, Muzaffer Ahmad Kassab, Wufang Fan, Xiaochun Yu, and Chen Wu. 2018. 'LGR5 regulates gastric adenocarcinoma cell proliferation and invasion via activating Wnt signaling pathway', *Oncogenesis*, 7: 57.

Wang, Z. 2017. 'ErbB Receptors and Cancer', *Methods Mol Biol*, 1652: 3-35.

Warren, B. A., P. Shubik, R. Wilson, H. Garcia, and R. Feldman. 1978. 'The microcirculation in two transplantable melanomas of the hamster. I. In vivo observations in transparent chambers', *Cancer Lett*, 4: 109-16.

Watanabe, I., T. Hasebe, S. Sasaki, M. Konishi, K. Inoue, T. Nakagohri, T. Oda, K. Mukai, and T. Kinoshita. 2003. 'Advanced pancreatic ductal cancer: fibrotic focus and beta-catenin expression correlate with outcome', *Pancreas*, 26: 326-33.

Watanabe, N., L. Bodin, M. Pandey, M. Krause, S. Coughlin, V. A. Boussiotis, M. H. Ginsberg, and S. J. Shattil. 2008. 'Mechanisms and consequences of agonist-induced talin recruitment to platelet integrin alphaIIbbeta3', *J Cell Biol*, 181: 1211-22.

Wculek, Stefanie K., and Ilaria Malanchi. 2015. 'Neutrophils support lung colonization of metastasis-initiating breast cancer cells', *Nature*, 528: 413-17.

Wegener, K. L., A. W. Partridge, J. Han, A. R. Pickford, R. C. Liddington, M. H. Ginsberg, and I. D. Campbell. 2007. 'Structural basis of integrin activation by talin', *Cell*, 128: 171-82.

Wei, Ruqiong, Raquel Alarcòn Rodrìguez, Marìa Del Mar Requena Mullor, Zhibiao Tan, Yuchang Gui, Jincui Hu, Tingpei Zhu, Xiaoxiao Huang, Yanyan Zhu, and Jianwen Xu. 2020. 'Analyzing the prognostic value of DKK1 expression in human cancers based on bioinformatics', *Annals of translational medicine*, 8: 552-52.

Weigelt, B., and M. J. Bissell. 2008. 'Unraveling the microenvironmental influences on the normal mammary gland and breast cancer', *Semin Cancer Biol*, 18: 311-21.

Weinmuller, M., F. Rechenmacher, U. Kiran Marelli, F. Reichart, T. G. Kapp, A. F. B. Rader, F. S. Di Leva, L. Marinelli, E. Novellino, J. M. Munoz-Felix, K. Hodivala-Dilke, A. Schumacher, J. Fanous, C. Gilon, A. Hoffman, and H. Kessler. 2017.

'Overcoming the Lack of Oral Availability of Cyclic Hexapeptides: Design of a Selective and Orally Available Ligand for the Integrin alphavbeta3', *Angew Chem Int Ed Engl*, 56: 16405-09.

Weis, S., J. Cui, L. Barnes, and D. Cheresh. 2004. 'Endothelial barrier disruption by VEGF-mediated Src activity potentiates tumor cell extravasation and metastasis', *J Cell Biol*, 167: 223-9.

Weis, S. M., S. T. Lim, K. M. Lutu-Fuga, L. A. Barnes, X. L. Chen, J. R. Gothert, T. L. Shen, J. L. Guan, D. D. Schlaepfer, and D. A. Cheresh. 2008. 'Compensatory role for Pyk2 during angiogenesis in adult mice lacking endothelial cell FAK', *J Cell Biol*, 181: 43-50.

Weis, Sara M., and David A. Cheresh. 2005. 'Pathophysiological consequences of VEGF-induced vascular permeability', *Nature*, 437: 497-504.

———. 2011. 'αV integrins in angiogenesis and cancer', *Cold Spring Harbor perspectives in medicine*, 1: a006478-a78.

Werner, J., S. E. Combs, C. Springfeld, W. Hartwig, T. Hackert, and M. W. Buchler. 2013. 'Advanced-stage pancreatic cancer: therapy options', *Nat Rev Clin Oncol*, 10: 323-33.

Whatcott, C. J., H. Han, and D. D. Von Hoff. 2015. 'Orchestrating the Tumor Microenvironment to Improve Survival for Patients With Pancreatic Cancer: Normalization, Not Destruction', *Cancer J*, 21: 299-306.

Whatcott , Clifford J., Richard G. Posner , Daniel D. Von Hoff, and Haiyong. Han. 2012. *Pancreatic Cancer and Tumor Microenvironment.*

Wienkers, Larry C., and Timothy G. Heath. 2005. 'Predicting in vivo drug interactions from in vitro drug discovery data', *Nature Reviews Drug Discovery*, 4: 825-33.

Wong, P. P., J. M. Muñoz-Félix, M. Hijazi, H. Kim, S. D. Robinson, B. De Luxán-Delgado, I. Rodríguez-Hernández, O. Maiques, Y. M. Meng, Q. Meng, N. Bodrug, M. S. Dukinfield, L. E. Reynolds, G. Elia, A. Clear, C. Harwood, Y. Wang, J. J. Campbell, R. Singh, P. Zhang, T. J. Schall, K. P. Matchett, N. C. Henderson, P. W. Szlosarek, S. A. Dreger, S. Smith, J. L. Jones, J. G. Gribben, P. R. Cutillas, P. Meier, V. Sanz-Moreno, and K. M. Hodivala-Dilke. 2020. 'Cancer Burden Is Controlled by Mural Cell-β3-Integrin Regulated Crosstalk with Tumor Cells', *Cell*, 181: 1346-63.e21.

Wong, Ping-Pui, Natalia Bodrug, and Kairbaan M Hodivala-Dilke. 2016. 'Exploring Novel Methods for Modulating Tumor Blood Vessels in Cancer Treatment', *Current Biology*, 26: R1161-R66.

Wong, Ping-Pui, Fevzi Demircioglu, Essam Ghazaly, Wasfi Alrawashdeh, Michael R L. Stratford, Cheryl L Scudamore, Biancastella Cereser, Tatjana Crnogorac-Jurcevic, Stuart McDonald, George Elia, Thorsten Hagemann, Hemant M Kocher, and Kairbaan M Hodivala-Dilke. 2015. 'Dual-Action Combination Therapy Enhances Angiogenesis while Reducing Tumor Growth and Spread', *Cancer Cell*, 27: 123-37.

Worthington, John J, Aoife Kelly, Catherine Smedley, David Bauché, Simon Campbell, Julien C Marie, and Mark A Travis. 2015. 'Integrin αvβ8-Mediated TGF-β Activation by Effector Regulatory T Cells Is Essential for Suppression of T-Cell-Mediated Inflammation', *Immunity*, 42: 903-15.

Xia, W., and T. A. Springer. 2014. 'Metal ion and ligand binding of integrin α5β1', *Proc Natl Acad Sci U S A*, 111: 17863-8.

Xiao, T., J. Takagi, B. S. Coller, J. H. Wang, and T. A. Springer. 2004. 'Structural basis for allostery in integrins and binding to fibrinogen-mimetic therapeutics', *Nature*, 432: 59-67.

Xie, C., J. Zhu, X. Chen, L. Mi, N. Nishida, and T. A. Springer. 2010. 'Structure of an integrin with an alphaI domain, complement receptor type 4', *Embo j*, 29: 666-79.

Xing, F., J. Saidou, and K. Watabe. 2010. 'Cancer associated fibroblasts (CAFs) in tumor microenvironment', *Front Biosci (Landmark Ed)*, 15: 166-79.

Xiong, J. P., T. Stehle, B. Diefenbach, R. Zhang, R. Dunker, D. L. Scott, A. Joachimiak, S. L. Goodman, and M. A. Arnaout. 2001. 'Crystal structure of the extracellular segment of integrin alpha Vbeta3', *Science*, 294: 339-45.

Xiong, J. P., T. Stehle, R. Zhang, A. Joachimiak, M. Frech, S. L. Goodman, and M. A. Arnaout. 2002. 'Crystal structure of the extracellular segment of integrin alpha Vbeta3 in complex with an Arg-Gly-Asp ligand', *Science*, 296: 151-5.

Yamada, Shinya, Xing-Yao Bu, Vazgen Khankaldyyan, Ignacio Gonzales-Gomez, J. Gordon McComb, and Walter E. Laug. 2006. 'EFFECT OF THE ANGIOGENESIS INHIBITOR CILENGITIDE (EMD 121974) ON GLIOBLASTOMA GROWTH IN NUDE MICE', *Neurosurgery*, 59: 1304-12.

Yang, Linbin, Qiang Liu, Xiaoqian Zhang, Xinwei Liu, Boxuan Zhou, Jianing Chen, Di Huang, Jiaqian Li, Heliang Li, Fei Chen, Jiang Liu, Yue Xing, Xueman Chen, Shicheng Su, and Erwei Song. 2020. 'DNA of neutrophil extracellular traps promotes cancer metastasis via CCDC25', *Nature*, 583: 133-38.

Yao, H., D. M. Veine, and D. L. Livant. 2016. 'Therapeutic inhibition of breast cancer bone metastasis progression and lung colonization: breaking the vicious cycle by targeting α5β1 integrin', *Breast Cancer Res Treat*, 157: 489-501.

Yarmolinsky, M., and R. Hoess. 2015. 'The Legacy of Nat Sternberg: The Genesis of Cre-lox Technology', *Annu Rev Virol*, 2: 25-40.

Yen, T. W., N. P. Aardal, M. P. Bronner, D. R. Thorning, C. E. Savard, S. P. Lee, and R. H. Bell, Jr. 2002. 'Myofibroblasts are responsible for the desmoplastic reaction surrounding human pancreatic carcinomas', *Surgery*, 131: 129-34.

Yoo, So Young, and Sang Mo Kwon. 2013. 'Angiogenesis and Its Therapeutic Opportunities', *Mediators of Inflammation*, 2013: 127170.

Yoon, Hyunho, Joshua P. Dehart, James M. Murphy, and Ssang-Taek Steve Lim. 2015. 'Understanding the roles of FAK in cancer: inhibitors, genetic models, and new insights', *The journal of histochemistry and cytochemistry : official journal of the Histochemistry Society*, 63: 114-28.

Yu, Da-Young, Young-Dong Yu, Wan-Bae Kim, Hyung-Joon Han, Sae-Byul Choi, Dong-Sik Kim, Sang-Yong Choi, Joo-Young Kim, Hyeyoon Chang, and Baek-Hui Kim. 2018. 'Clinical significance of pancreatic intraepithelial neoplasia in resectable pancreatic cancer on survivals', *Annals of surgical treatment and research*, 94: 247-53.

Yuan, Jianling, and Peter M. Glazer. 1998. 'Mutagenesis induced by the tumor microenvironment', *Mutation Research/Fundamental and Molecular Mechanisms of Mutagenesis*, 400: 439-46.

Yuen, Angela, and Begoña Díaz. 2014. 'The impact of hypoxia in pancreatic cancer invasion and metastasis', *Hypoxia (Auckland, N.Z.)*, 2: 91-106.

Zhang, Jun-Ming, and Jianxiong An. 2007. 'Cytokines, inflammation, and pain', *International anesthesiology clinics*, 45: 27-37.

Zhang, Kexiong, and David J. Waxman. 2013. 'Impact of tumor vascularity on responsiveness to antiangiogenesis in a prostate cancer stem cell-derived tumor model', *Molecular cancer therapeutics*, 12: 787-98.

Zhang, Ronghua, Qiaofei Liu, Tong Li, Quan Liao, and Yupei Zhao. 2019. 'Role of the complement system in the tumor microenvironment', *Cancer Cell International*, 19: 300.

Zhen, Y., and H. Stenmark. 2015. 'Cellular functions of Rab GTPases at a glance', *J Cell Sci*, 128: 3171-6.
Zheng, Wei, Aleksanteri Aspelund, and Kari Alitalo. 2014. 'Lymphangiogenic factors, mechanisms, and applications', *The Journal of clinical investigation*, 124: 878-87.
Zhou, Jin, Qian Yi, and Liling Tang. 2019. 'The roles of nuclear focal adhesion kinase (FAK) on Cancer: a focused review', *Journal of Experimental & Clinical Cancer Research*, 38: 250.
Zhou, Jing, Camilo Aponte-Santamaría, Sebastian Sturm, Jakob Tómas Bullerjahn, Agnieszka Bronowska, and Frauke Gräter. 2015. 'Mechanism of Focal Adhesion Kinase Mechanosensing', *PLOS Computational Biology*, 11: e1004593.
Zhu, Jieqing, Jianghai Zhu, and Timothy A. Springer. 2013. 'Complete integrin headpiece opening in eight steps', *Journal of Cell Biology*, 201: 1053-68.
Zininga, Tawanda, Lebogang Ramatsui, and Addmore Shonhai. 2018. 'Heat Shock Proteins as Immunomodulants', *Molecules (Basel, Switzerland)*, 23: 2846.

22 Appendix

22.1 Appendix I:Kinase dead

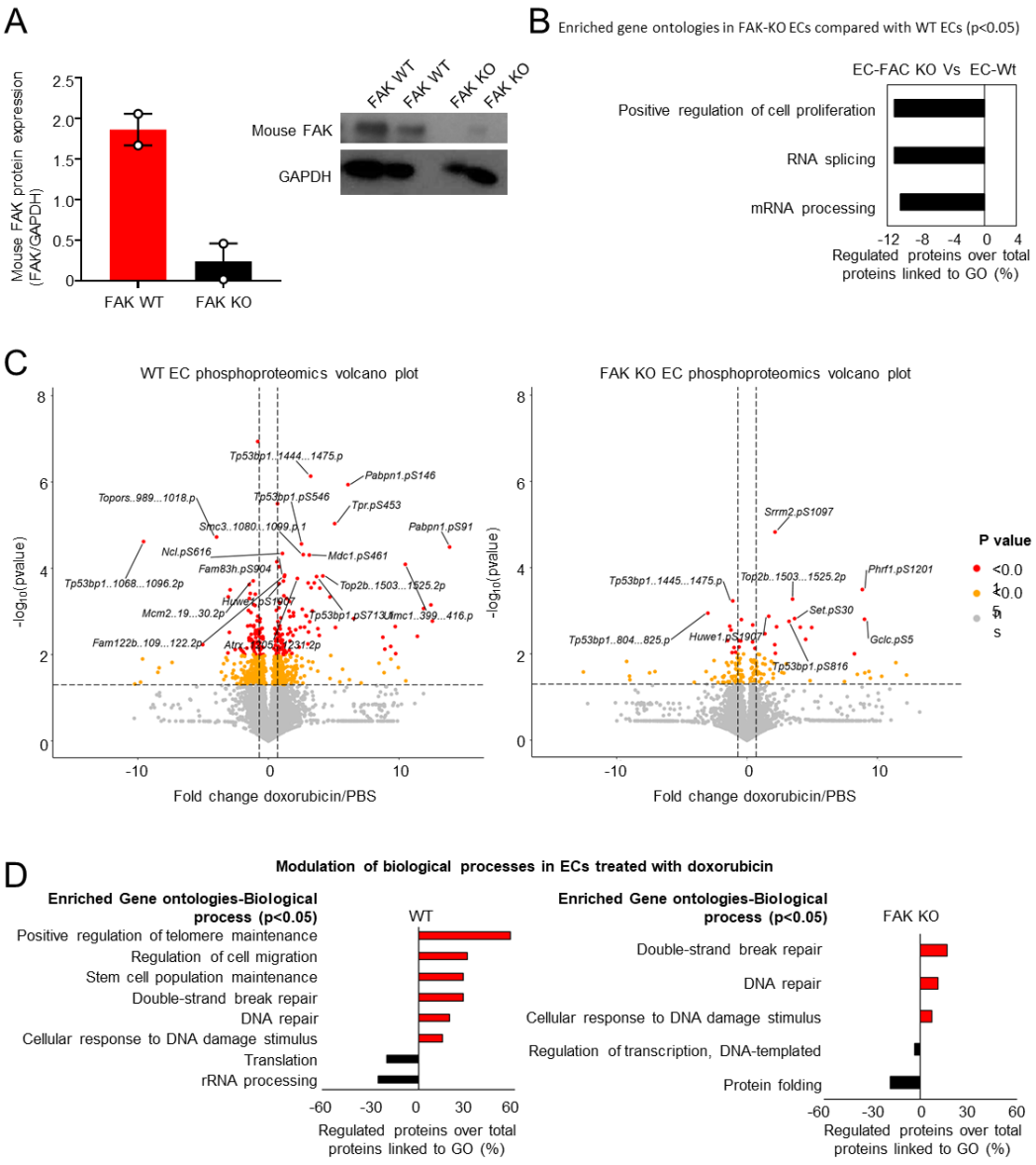

Figure 22.1 Phosphoproteomic changes in response to doxorubicin are greater in WT than FAK-KO endothelial cells.

(A) Western blot showing the level of mouse FAK in typical WT and FAK KO endothelial cell samples with bar chart showing protein levels relative to GAPDH n=2 independent cell preps. (B) Percentage of quantified hits that were significantly different in FAK-KO compared to FAK-WT ECs. Black bars represent down-regulated processes. Biological replicates were performed using 5 independent WT and 4 independent FAK-KO EC cell preps, each prep was produced from 3 mice. (C) Volcano plots showing phosphoproteomic fold-changes upon doxorubicin treatment compared with non-treated controls in FAK-WT (left) and FAK-KO (right) ECs. Red circles represent $p<0.01$, yellow circles represent $p<0.05$ and grey circles non-significant changes proteins. (D) Percentage of quantified hits that were significantly affected by doxorubicin treatment in the mentioned biological processes in FAK-WT (left) and FAK-KO (right). Red bars represent up-regulated processes. Black bars represent down-regulated processes. Biological replicates were performed using 5 independent WT and 4 independent FAK-KO EC cell preps, each prep was produced from 3 mice. Data produced by Dr Rita Pedrosa and Dr Pedro Casado-Izquierdo.

Phosphoproteomics			
Raw file Name	**Genotype**	**Treatment**	**Replicate**
QE1_Rita_Exp1_PP_1.raw	WT	Control	1
QE1_Rita_Exp1_PP_2.raw	WT	Doxorubicin	1
QE1_Rita_Exp1_PP_3.raw	KO	Control	1
QE1_Rita_Exp1_PP_4.raw	KO	Doxorubicin	1
QE1_Rita_Exp1_PP_5.raw	WT	Control	2
QE1_Rita_Exp1_PP_6.raw	WT	Doxorubicin	2
QE1_Rita_Exp1_PP_7.raw	KO	Control	2
QE1_Rita_Exp1_PP_8.raw	KO	Doxorubicin	2
QE1_Rita_Exp1_PP_9.raw	WT	Control	3
QE1_Rita_Exp1_PP_10.raw	WT	Doxorubicin	3
QE1_Rita_Exp1_PP_11.raw	KO	Control	3
QE1_Rita_Exp1_PP_12.raw	KO	Doxorubicin	3
QE1_Rita_Exp1_PP_13.raw	WT	Control	4
QE1_Rita_Exp1_PP_14.raw	WT	Doxorubicin	4
QE1_Rita_Exp1_PP_15.raw	KO	Control	4
QE1_Rita_Exp1_PP_16.raw	KO	Doxorubicin	4
QE1_Rita_Exp1_PP_17.raw	WT	Control	5
QE1_Rita_Exp1_PP_18.raw	WT	Doxorubicin	5
Proteomics			
Raw file Name	**Genotype**	**Treatment**	**Replicate**
QE1_Rita_Exp1_TP_1.raw	WT	Control	1
QE1_Rita_Exp1_TP_2.raw	WT	Doxorubicin	1
QE1_Rita_Exp1_TP_3.raw	KO	Control	1
QE1_Rita_Exp1_TP_4.raw	KO	Doxorubicin	1
QE1_Rita_Exp1_TP_5.raw	WT	Control	2
QE1_Rita_Exp1_TP_6.raw	WT	Doxorubicin	2
QE1_Rita_Exp1_TP_7.raw	KO	Control	2
QE1_Rita_Exp1_TP_8.raw	KO	Doxorubicin	2
QE1_Rita_Exp1_TP_9.raw	WT	Control	3
QE1_Rita_Exp1_TP_10.raw	WT	Doxorubicin	3
QE1_Rita_Exp1_TP_11.raw	KO	Control	3
QE1_Rita_Exp1_TP_12.raw	KO	Doxorubicin	3
QE1_Rita_Exp1_TP_13.raw	WT	Control	4
QE1_Rita_Exp1_TP_14.raw	WT	Doxorubicin	4
QE1_Rita_Exp1_TP_15.raw	KO	Control	4
QE1_Rita_Exp1_TP_16.raw	KO	Doxorubicin	4
QE1_Rita_Exp1_TP_17.raw	WT	Control	5
QE1_Rita_Exp1_TP_18.raw	WT	Doxorubicin	5
Secretomics			
Raw file Name	**Genotype**	**Treatment**	**Replicate**
QE1_Rita_Secretomes_TP_1.raw	WT	Control	1
QE1_Rita_Secretomes_TP_2.raw	WT	Doxorubicin	1
QE1_Rita_Secretomes_TP_3.raw	KO	Control	1
QE1_Rita_Secretomes_TP_4.raw	KO	Doxorubicin	1
QE1_Rita_Secretomes_TP_5.raw	WT	Control	2
QE1_Rita_Secretomes_TP_6.raw	WT	Doxorubicin	2
QE1_Rita_Secretomes_TP_7.raw	KO	Control	2
QE1_Rita_Secretomes_TP_8.raw	KO	Doxorubicin	2
QE1_Rita_Secretomes_TP_9.raw	WT	Control	3
QE1_Rita_Secretomes_TP_1.raw	WT	Doxorubicin	3
QE1_Rita_Secretomes_TP_11.raw	KO	Control	3
QE1_Rita_Secretomes_TP_12.raw	KO	Doxorubicin	3
QE1_Rita_Secretomes_TP_13.raw	WT	Control	4
QE1_Rita_Secretomes_TP_14.raw	WT	Doxorubicin	4
QE1_Rita_Secretomes_TP_15.raw	KO	Control	4
QE1_Rita_Secretomes_TP_16.raw	KO	Doxorubicin	4
QE1_Rita_Secretomes_TP_19.raw	NA	Medium without Cells	1

Table 22.1 Sample details linked to the RAW submitted to PRIDE Mass Spectrometry database.

Data produced by Dr Rita Pedrosa and Dr Pedro Casado-Izquierdo

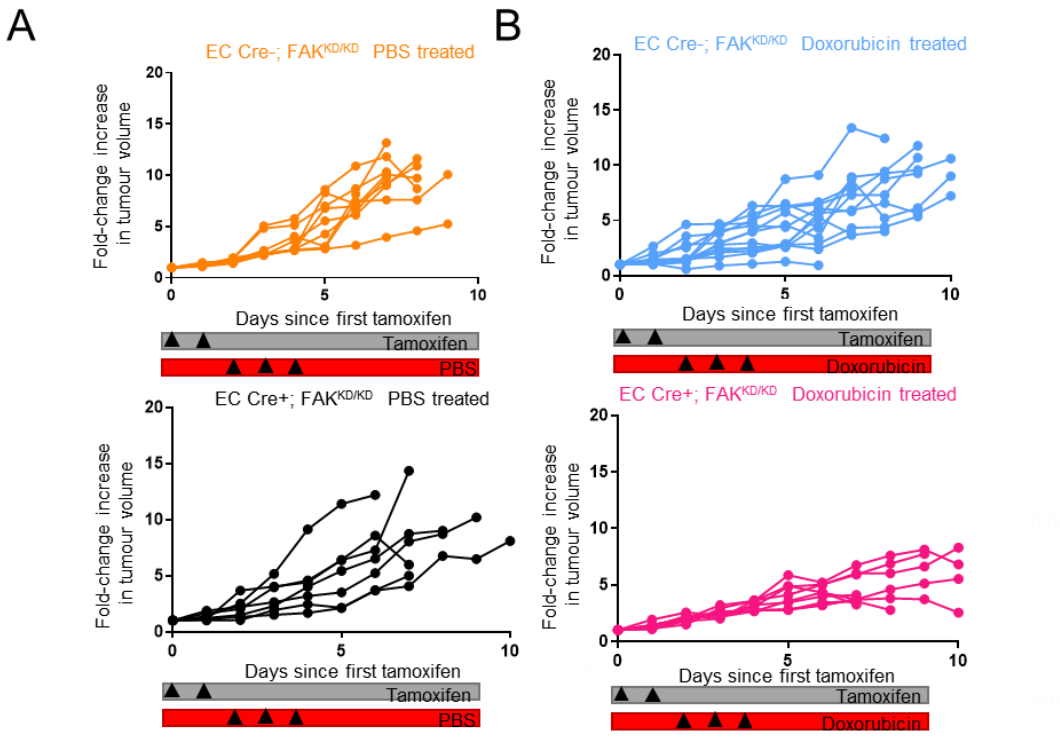

Figure 22.2 Fold-change increase in tumour volume.

(A) Mice were treated as described in the previous figure. Fold-change increase in tumour volume (A) EC Cre-; $FAK^{KD/KD}$ mice and EC Cre+; $FAK^{KD/KD}$ mice treated with PBS (B) EC Cre-; $FAK^{KD/KD}$ mice and EC Cre+; $FAK^{KD/KD}$ mice treated with doxorubicin.

22.2 Appendix II: Observation of the mixed background KPC colony at the time of experimentation

The KPC mouse is a well-established spontaneous model of PDAC. Within this thesis, the model has been used for both testing the efficacy of 29P as a vascular promotor and for the production of PDAC organoids. As in the clinical setting, there is significant variation between animals within this colony. The following histology report some observed features of the KPC colony at the time of experimentation.

22.2.1 General characteristics of tumour progression in the pancreas of KPC colony

In the KPC model of pancreatic cancer, normal pancreatic tissue processes through the stages of PanIn to PDAC. Therefore, in early-stage KPC animals, there are still large regions of the pancreas that have not progressed to PanIn **(Figure 22.3 A)** with examples of acinar cells, ducts and Islets of Langerhans. Pancreatic tissue progresses to regions of PanIN **(Figure 22.3 B)** and eventually to high-grade tumour **(Figure 22.3 C)**. In the highly differentiated tumour, there are mitotic cells **(Figure 22.3 D)**.

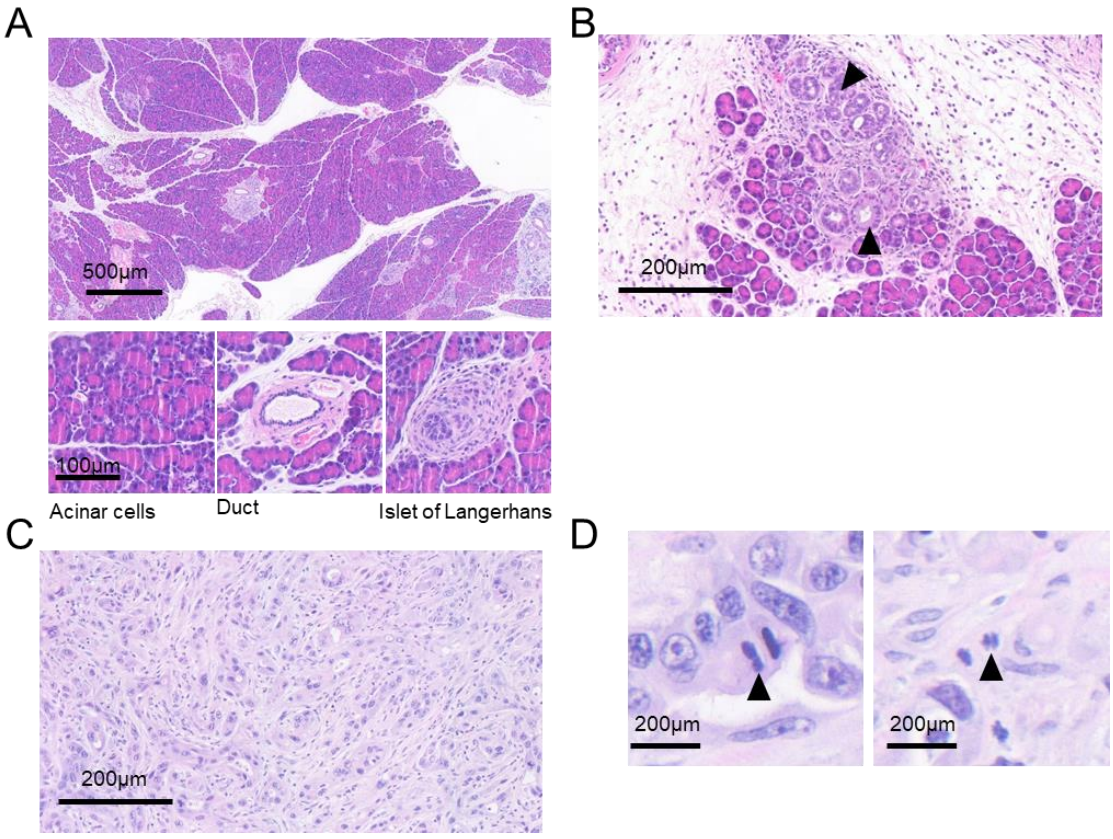

Figure 22.3 General characteristics of the KPC colony in KPC mouse.

(A) Generally normal pancreatic tissue in KPC mouse showing examples of acinar cells, ducts and Islet of Langerhans. (B) PanIN lesions in KPC mouse. (C) High grade pancreatic tumour in KPC mouse. (D) Mitotic cells in high grade pancreatic tumour in KPC mouse.

22.2.2 Additional features of the KPC colony

Even within high-grade PDAC in the KPC model, there are residual areas of PanIN **(Figure 22.4 A)**; they also often contain regions of necrosis **(Figure 22.4 B)**. High-grade PanIN progresses to PDAC at the point that it invades beyond the boundaries of normal pancreatic lobe structure. **Figure 22.4 C** shows early the abnormal pancreatic structure beginning to bulge outside of the normal lobular structure.

In some cases, there are high numbers of mucin cells in PanIN structure as a defence mechanism against proteases that leak from acinar cells **(Figure 22.4 D)**.

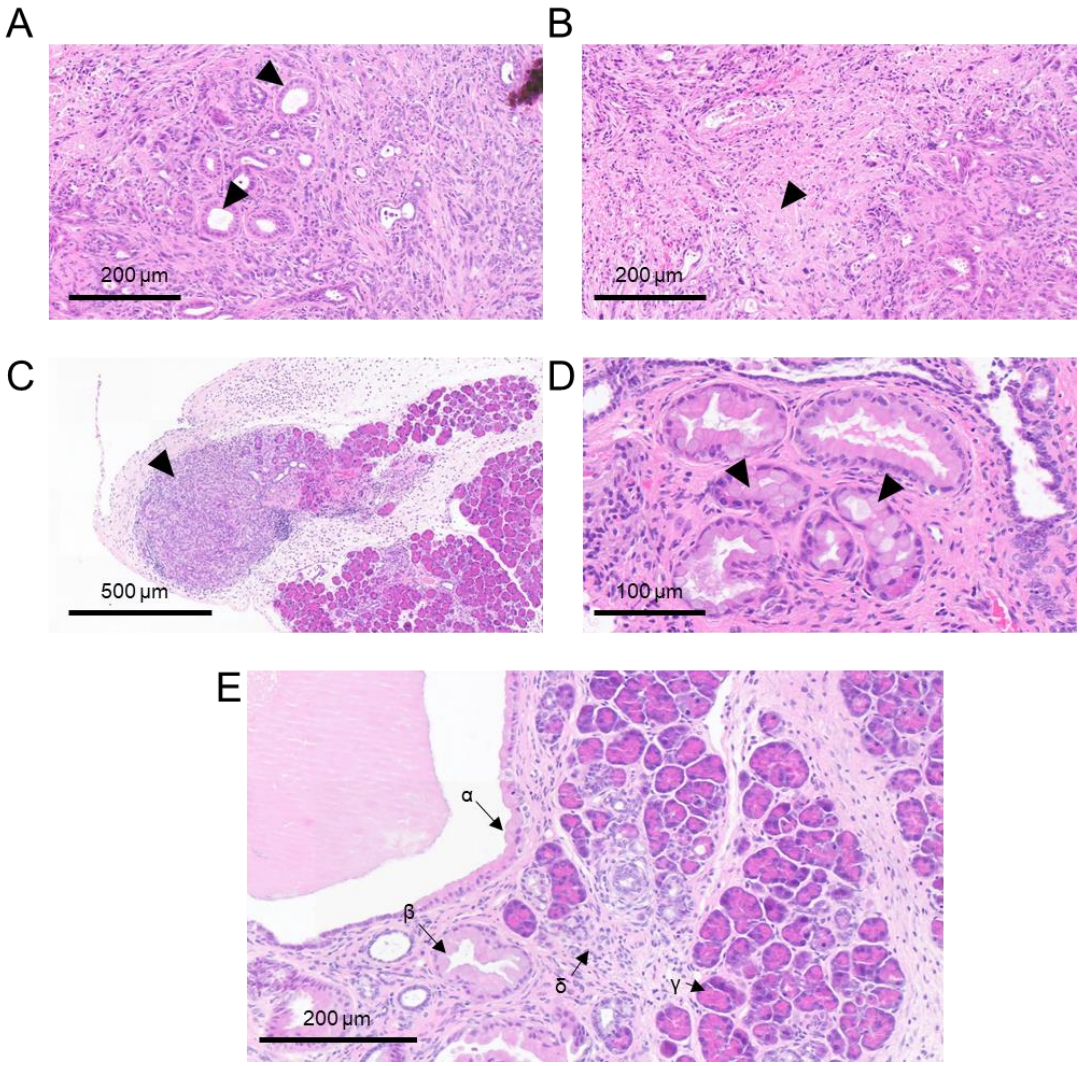

Figure 22.4 Characteristics of tumour development in the KPC colony.

(A) Residual PanIN lesions in high grade tumour. (B) Region of necrosis in high grade tumour. (C) Early invasion of pancreatic tissue. (D) Mucin cells in pancreatic ducts. (E) Progression of PanIN to PDAC showing (α) a large pancreatic duct with PanIN, (β) a smaller pancreatic duct, (γ) relatively undifferentiated pancreatic tissue, (δ) more differentiated tissue with irregular nuclei.

22.2.3 Pancreatic tumours in the KPC mice include examples of lymph nodes and lymph node metastases

Within the pancreatic tumours that form in KPC mice, there are lymph nodes **(Figure 22.5 A)** containing small, dark, circular nuclei characteristic of lymphocytes. In some cases, the tumour metastasises into the lymph node; in **Figure 22.5 B**, the tumour can be seen spreading from the left towards the top right, where lymph node characteristics can be seen. At higher magnification **(Figure 22.5 C)**, the metastasis can be seen as histologically atypical of PDAC. The trabeculations visible in the histology are more typical of neuroendocrine tumour than the irregular structure of PDAC; this may suggest a hybrid tumour.

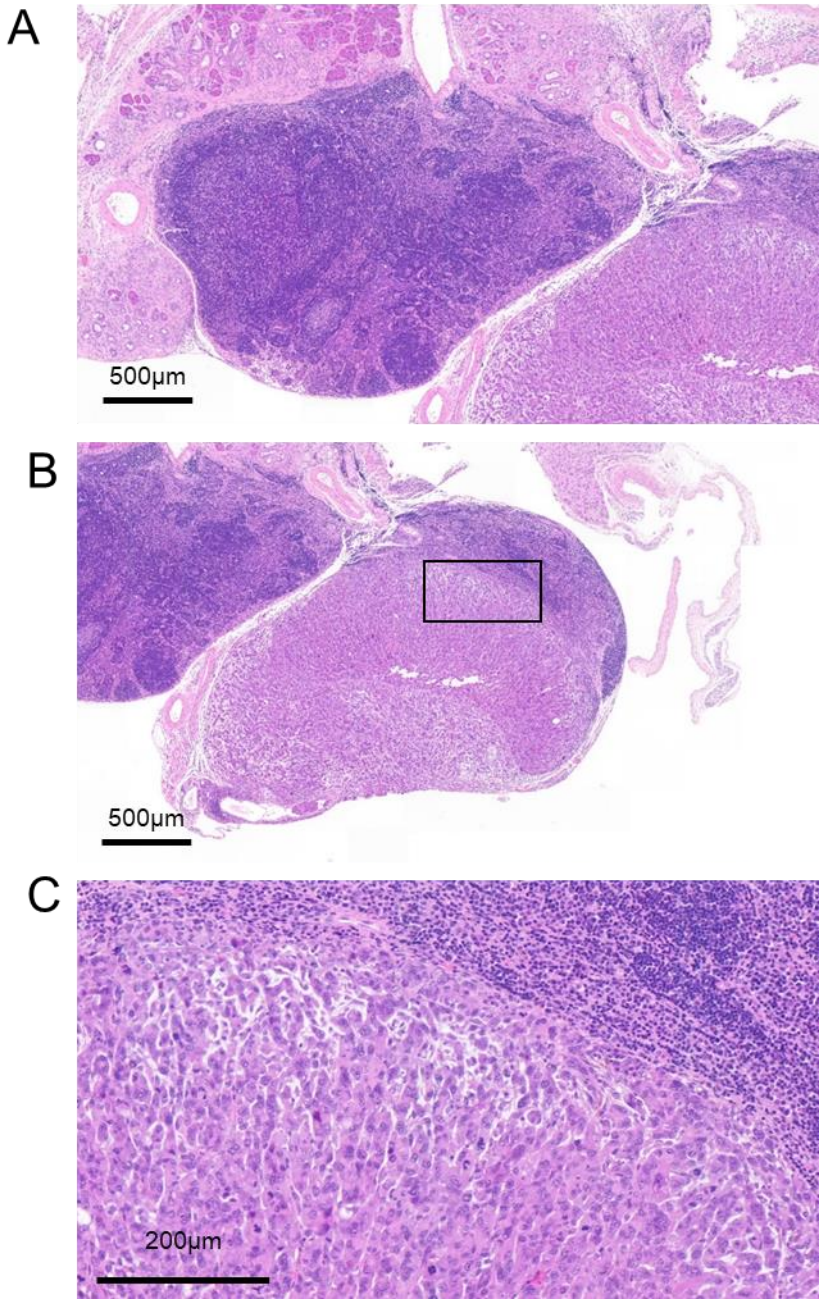

Figure 22.5 Lymph node and lymph node metastases in the pancreas of the KPC mouse.

(A) A lymph node in the pancreatic tumour of a KPC mouse. (B) A lymph node with metastasis invading from left to right. (C) Higher magnification image of metastasis invading lymph node showing trabeculations.

22.2.4 Example of a region of neuroendocrine-like histology within the KPC tumour

Similar to the metastasis into the lymph node, there are regions within the KPC tumour that look more like neuroendocrine than PDAC tumours **(Figure 22.6)**. Whereas PDAC progresses from PanIN, neuroendocrine tumours tend to bulge into the epithelium. Here, the tumour appears to grow into the duct. It has a trabeculated histology (right), similar to the lymph node metastasis. This is not typical of PDAC but may be a hybrid tumour or may have progressed from PDAC to something more neuroendocrine like.

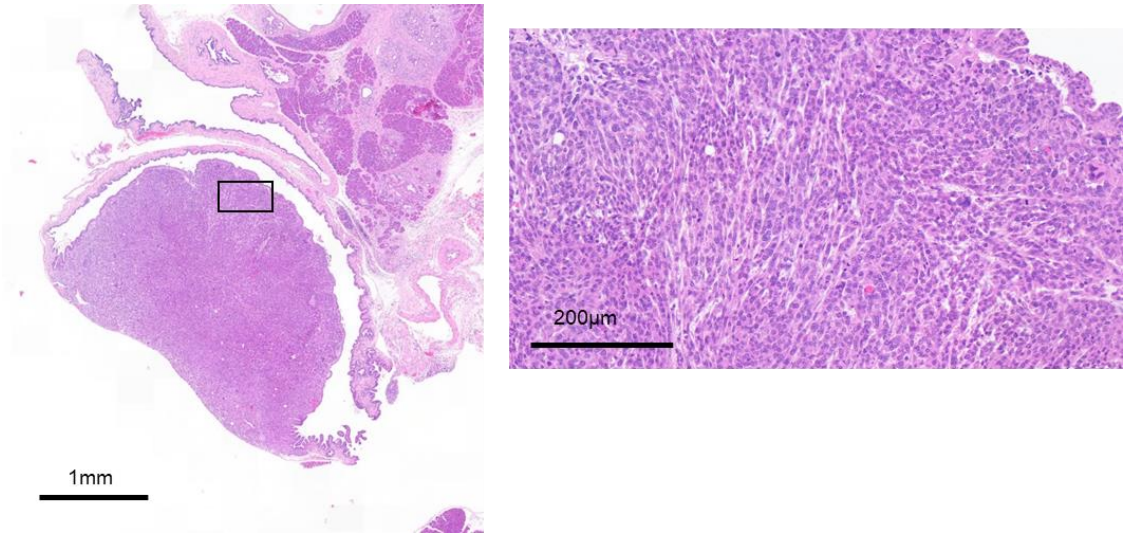

Figure 22.6 Possible neuroendocrine like tumour.

Region of tumour showing more neuroendocrine like tumour at low (left, scale bar = 1 mm) and high (right, scale bar = 200 µm) magnification.